ANALYSIS OF SOIL ERODIBILITY AND RAINFALL EROSIVITY ON THE SOUTPANSBERG RANGE, LIMPOPO PROVINCE, SOUTH AFRICA

By

EDMORE KORI

Student Number: 11606872

A PhD dissertation submitted to the Faculty of Science, Engineering, and Agriculture, Department of Geography and Environmental Sciences, University of Venda

Supervisor: Prof. B. D. O. Odhiambo

Co-Supervisor: Prof H. Chikoore

Co-Supervisor: Prof. S. C. Van den Heever (Colorado State University, USA).

JUNE 2023

DECLARATION

I, **EDMORE KORI,** hereby declare that this dissertation for PhD Degree in Geography at the University of Venda, hereby submitted by me, has not been submitted previously for a degree at this or any other university, that this is my own work in design and execution, and that all reference material contained therein has been duly acknowledged.

Signature: __ 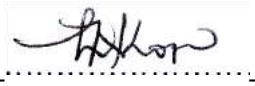 __ Date: 24/06/2023

DEDICATION

To Dumisani, Peace, Vitor and Grace

ABSTRACT

Soil erosion is a global challenge that threatens ecological functionality. The need for better soil conservation practices keeps growing due to the twin challenges of climate change and population growth. However, effective soil erosion management solutions remain elusive to practitioners due to the complexity of the soil erosion process. This is especially true for mountainous tropical regions which experience rainfall as high intensity thunderstorms accompanied by gusts of wind. Therefore, the aim of this research was to analyse soil erodibility and rainfall erosivity on the Soutpansberg range to establish the characteristics of the factors that influence soil erosion. The specific objectives were to classify geomorphic features of the Soutpansberg range; to characterise the spatial-temporal aspects of potentially erosive rainfall; to assess the influence of topography on wind speed and rainfall erosivity; and to compare rainfall erosivity derived from the USLE and the SLEMSA incorporating WDR erosivity.

The classification of geomorphic features needed soil, hydrology, slope, geology and land-use-land-cover data. Soil data were obtained from the Harmonised World Soil Database (HWSD v 1.21) layer downloaded from The International Institute for Applied Systems Analysis (IIASA) online database. Additional soil data were obtained from field samples and splash cups. Hydrological data were downloaded from Department of Water Affairs, Forestry and Fisheries (DWAFF) website. Slope data were derived from the 30m pixel size SRTM DEM obtained from National Geo-Spatial Information (NGI). Geological data were downloaded from South African Geosciences online database. Land-use-land-cover were extracted from the South African National Land Cover 2018 dataset accessed online on the Department of Forestry, Fisheries and Environment website. Rainfall and wind speed data for the spatial-temporal characterisation of rainfall from 2000 to 2019 were obtained from the South African Weather Services.

The data analysis followed different tools. Erodibility was assessed using GIS tools to combine the five factors to create a final soil erodibility map. Potentially erosive rainfall spatial-temporal characterisation section was done using spatial GIS interpolation and spatial autocorrelation. Spatial interpolation was achieved through co-kriging. Spatial autocorrelation was determined by the fusion of the coefficient of variation and the Moran's I. The influence of topography on wind speed and rainfall erosivity was analysed through a Likert scale, simple linear regression and MANOVA. Finally, simple regression analysis and simple comparison were employed to establish the influence of wind on rainfall erosivity. This was treated from the wind free rain (WFR) and wind driven rain (WDR) perspective. The analysis produced the following results.

The geomorphic classification for erodibility was based on intrinsic erodibility, landform position, slope position, geological setting as well as rain exposure. The factors operate on fourteen soil types found on the Soutpansberg range that fall into five granulometric groups. The erodibility maps for both USLE and SLEMSA, a result of a weighted sum overlay of all the erodibility factors, show high to very high erodibility on the south facing slopes of the mountain range. A large part of the range

on the western part of the mountain range is classified as of very low erodibility in the SLEMSA method.

The spatial-temporal characterisation indicates that rainfall on the Soutpansberg Range is very highly variable. The potentially erosive rainfall distribution is spatially dependent on the mountain range and the spatial variation mostly simple. Most rainfall is concentrated in the central areas of the south facing slope. The epicentre is located at elevations above 1200 m.a.s.l. However, rain days are dominated by medium spatial variability.

The spatio-temporal characterisation mapping indicates that flash flood hotspots are in low to very low rainfall regions. This implies that high erosion areas are not defined by total rainfall amounts only because the temporal distribution of the rainfall is also important. Furthermore, the simple linear regression analysis revealed that elevation influences erosivity. In addition, hypothesis tests showed that wind speed and topography increase rainfall erosivity. Empirical data confirm that WFR and WDR erosivity are different. Wind Driven Rain computations where wind is above 2 m/s^{1} produce results similar to samples collected from splash cups.

The research concludes that a deep understanding of the factors controlling soil erodibility is the foundation of effective erosion control. The soils' intrinsic characteristics and raindrop exposure (represented by land use and land cover) explains more of variation in soil loss on the Soutpansberg mountain range. Furthermore, the mountain setting causes rainfall to be concentrated on the central south facing slopes at elevations above 1000 m.a.s.l. sending the very low potentially erosive rain zone to the western region of the mountain range. However, the highest peak of the mountain is in the western region.

Erosion hazard potential is not confined to high rainfall zones only. Potentially erosive rainfall hotspots are located in low and very low rainfall zones. Furthermore, rainfall erosivity is not a function of rainfall amount only because topography increases both wind speed and rainfall erosivity. However, rainfall amount and wind speed are not correlated, and wind speed is not implied in rainfall amount. Nonetheless, wind speed is correlated with rainfall erosivity. Wind speed above $2m/s^{-1}$ increases rainfall erosivity. therefore, wind driven rain (WDR) erosivity is a better representation of rainfall energy than wind free rain (WFR).

The research recommends soil erosion management approaches that also consider rainfall temporal distribution. In addition, further studies on rainfall spatial distribution need to be done using satellite-based rainfall data for more accuracy. Additional research on rainfall erosivity considering rainfall temporal distribution is necessary to identify erosion hazard zones. Intensive and extensive research on incorporating wind speed in the computation of rainfall erosivity can improve soil erosion estimation models.

ACKNOWLEDGEMENTS

I wish to acknowledge the following for their different roles that they played in the production of this document. I thank my wife, Dumisani, for all the support and understanding. I spent long hours working while you took care of the family. Thank you.

I salute my supervisors, Professors B. D. O. Odhiambo, H. Chikoore and S. C, van den Heever for the tireless, heartfelt and courageous leadership. Without you, this document would not have come together. God bless you.

I also want to acknowledge my study buddies, Dr F. Murungweni and Dr W. Tsoriyo for the encouragement. You graduated ahead of me, that made me realise that indeed, this can be done.

I received important technical support to do Hydrometer analysis from Mr T. R. Nkuna. This is greatly appreciated, and God bless you for the good heart.

I also acknowledge funding from Univen RPC and the University Capacity Development Programme (Mountain Research) that made the research smooth. The IAG Working Group on Landform Assessment for Geodiversity also gave me indispensable technical support that literally made this research progress very well.

There are also many friends and relatives who stood by and believed in me through this journey. I acknowledge and thank you all. God abundantly bless you.

TABLE OF CONTENTS

LIST OF FIGURES

LIST OF TABLES

: THE PROBLEM AND ITS SETTING

1.1 Introduction

Soil erosion is a global challenge in both anthropogenic and natural environments. The phenomenon remains a critical and widespread problem in many developing countries (Food and Agriculture Organisation (FAO) and Intergovernmental Technical Panel on Soils (ITPS), 2015; Borrelli *et al.*, 2017), and is especially so for rural agriculture (Ighodaro *et al.*, 2013). Soil erosion is a phenomenon controlled by rainfall and soil factors (Renard *et al.*, 1997; Kinnell, 2010). Soil factors determine erodibility while rainfall characteristics determine erosivity.

Soil erodibility is a measure of the susceptibility of soil particles to detachment and transport by wind, rainfall and runoff (Kinnell, 2010; Kusumandari, 2014). Rainfall erosivity is the energy behind soil detachment and displacement. Knowledge of soil erodibility and rainfall erosivity is an essential requirement for erosion prediction, conservation planning, and the assessment of sediment related environmental effects of watershed land use practices (Wang *et al.*, 2013). Soil erodibility and rainfall erosivity are the main factors that determine the rate of soil erosion and, therefore, need to be comprehensively appreciated (Wischmeier *et al.*, 1958; Stocking *et al.*, 1988; Kusumandari, 2014; Uzun *et al.*, 2017; Food and Agriculture Organisation (FAO), 2019).Therefore, soil erodibility and rainfall erosivity play a dominant role in soil erosion modelling and hence need to be well understood if we are to enhance our comprehension of soil erosion and its impacts on food production. The other factors important to soil erosion are dimensionless multipliers of soil erodibility and rainfall erosivity used to adjust the value to other conditions (Kinnell, 2010). The other factors include geology, slope, land uses and land cover, as well as soil conservation practices (Wischmeier and Smith, 1958; Stocking *et al.*, 1988; FAO, 2019).

Soil erosion is a natural geomorphic surface process that removes soil particles and regolith from their primary location on the Earth's crust and transports them to another location (Zorn and Komac, 2013; Encyclopedia Britannica, 2019; FAO, 2019). The rates of soil formation and removal are emphasised when considering soil erosion. The removal is primarily determined by the soil erodibility and rainfall

erosivity (Renard *et al.*, 1997; Kinnell, 2010). However, other natural agents, including wind, glaciers, snow, sea/lake waves, and gravity can also erode soil.

The soil erosion process varies according to environmental factors because it is a natural geomorphological phenomenon (Xanthakis and Pavlopoulos, 2009; Zorn and Komac, 2013). The interconnected environmental factors are natural and anthropogenic. When anthropogenic factors influence the soil loss process, the phenomenon is termed accelerated soil erosion (Dotterweich, 2013; Zorn and Komac, 2013; Borrelli *et al.*, 2017), which is common in fragile ecosystems (Tse-ring *et al.*, 2010; Kumar *et al.*, 2018; Blanco-Pastor *et al.*, 2019), such as in settled mountainous arid regions in tropical and subtropical regions. Therefore, soil erosion can be approached from an anthropogenic driven or a natural process perspective.

Cognisant of the two perspectives, the research described here approaches soil erosion from a natural process point of view. This is because natural soil erosion is due to various natural regenerative and readjustment processes that are triggered by natural climatic shifts or geomorphological occurrences such as mass wasting (Dotterweich, 2013; Zorn and Komac, 2013; Borrelli *et al.*, 2017). In addition, the primary erosion drivers are natural phenomena - humans only accelerate the natural process (Dotterweich, 2013; Borrelli *et al.*, 2017).

Water and wind can erode independently or in conjunction with each other (Stroosnijder and Gabriels, 2004a; Reis *et al.*, 2010; Erpul, 2013; Marzen *et al.*, 2017). Independent erosion is common with wind than with water. This research focuses on factors that influence soil erosion by water with a special interest in the role played by wind in the concept of Wind Driven Rain (WDR) (Erpul *et al.*, 2013; Marzen, 2017). This builds from the reality that most rainfall in tropical regions is produced through convective storms (Chaudhry *et al.*, 1996; Wu *et al.*, 2020; Muller *et al.*, 2022). The blowing wind during the rain storms causes raindrops to travel through the atmosphere at an oblique angle as they approach the ground surface (Blocken and Carmeliet, 2004) as opposed to perpendicular to the surface in the absence of any wind shear.

The WDR concept is reinforced by the fact that rainfall, especially in tropical climates, is usually produced by high intensity thunderstorms with gusts of winds

(Reis *et al.*, 2010; Sobel, 2012; Zorn and Komac, 2013). Wind Driven Rain considers raindrop characteristics, whose physical properties are easily and significantly affected by wind, as the main eroding agent (Marzen *et al.*, 2015). The intensity of rainfall gives the raindrop its erosive power, technically called the R-factor or energy (E), which initiates the erosion process (Pedersen and Hasholt, 1995; Ritter, 2012; Brodowski, 2013). Cognisant of other research and despite clear connections, there has been a dearth in soil loss estimation models that incorporate the effect of wind on rainfall erosivity (Stroosnijder and Gabriels, 2004c; Erpul, 2013; Marzen, 2017). The wind affects how the raindrop strikes the ground surface, causing rain splash erosion.

The effectiveness of raindrop splash is a function of soil characteristics that determine erodibility and rainfall energy (Torres *et al.*, 1992; Marzen *et al.*, 2017; Fu *et al.*, 2019), among other factors. The influence of the factors is a function of the wind, intrinsic and extrinsic soil erodibility characteristics. Wind influences the raindrop speed, direction, vorticity and vertical velocity (Pedersen and Hasholt, 1995; Brodowski, 2013; Erpul, 2013) and, hence, rainfall erosivity. Intrinsic soil erodibility characteristics are controlled by the soil texture.

1.2 Background to the Research Problem

Soil is the backbone of all biological processes in the ecosystem. It plays a critical role in the production of ecosystem services (Caon and Vargas, 2017; Hill *et al.*, 2019). Hence, soil health is critical for meeting basic food requirements as well as provision of essential ecosystem services (Borrelli *et al.*, 2017). Therefore, soil erosion is a serious issue because soil formation is a slow natural process. The rate of soil removal is, therefore, of importance since soil is a non-renewable resource (Ritter, 2012; Zorn and Komac, 2013; Le Roux and Smith, 2014; FAO, 2015a; Lal, 2015). Soil is considered non-renewable because soil loss and degradation cannot be recovered within a human lifespan (FAO, 2015a; Lal, 2015). Consequently, a lot of research focusing on soil erosion has been done.

However, many knowledge gaps and discrepancies still exist (Lal, 2001; Reis *et al.*, 2010; Poesen, 2018). Specifically, no single soil erosion assessment technique or model can perfectly capture the complex natural process. Hence there is need for

improved understanding of natural soil erosion processes (Reis *et al.*, 2010; Iserloh *et al.*, 2013; Poesen, 2018). As such, the severity, extent and impact of soil erosion cannot be declared with certainty because of the variable assessment techniques and models (Lal, 2001). This exposes the challenges in the recognition, description and quantification of erosion and limited information on the magnitude and frequencies of events that cause erosion (Boardman, 2006).

Soil erosion is a geomorphological process with the ability to create, modify and destroy landforms (Garland *et al.*, 1999). It can cause environmental and property damage, loss of livelihoods and services as well as social and economic disruption (Poesen, 2018). Soil erosion is a threat to agricultural production and food security (FAO and ITPS, 2015). Sediment pollution of water reservoirs reduces water quality and increases purification costs (Rickson, 2014; FAO and ITPS, 2015; Parwada and Van Tol, 2016). As such, soil erosion remains a serious ecological and environmental challenge in developing countries (Xanthakis and Pavlopoulos, 2009; Le Roux and Smith, 2014; Marzen *et al.*, 2015; Borrelli *et al.*, 2017). Therefore, more research still needs to be done in the realm of soil erosion.

A logical starting point for understanding soil erosion is at classifying it. One broad classification is by agent of erosion, resulting in erosion by water (rain), wind and ice. The broad classes have subcategories, as shown by Zachar (1982), who reviewed classification of soil erosion processes by rainfall. The review concludes that most authors consider sheet wash as the first form of erosion.

However, raindrop or splash erosion is the initial loosening or dislodging of soil particles by surface-hitting raindrops that triggers all the soil erosional processes that follow (Zachar, 1982; Pedersen and Hasholt, 1995; Kinnell, 2010; Marzen *et al.*, 2015; Panagos *et al.*, 2015; Fu *et al.*, 2019). The force of a falling raindrop in splash erosion creates a depression in the soil, dislodging soil particles (Panagos *et al.*, 2015). The effectiveness of the raindrop force is determined by the soil erodibility and raindrop erosivity (E).

A soil's erodibility depends on its intrinsic as well as extrinsic characteristics. The intrinsic characteristics are the grain size, shape, and the physical properties of the soil including organic matter content (Bryan, 2000; FAO, 2019). The extrinsic

properties are the characteristics that are not inherent in the soil. Therefore, erodibility is the direct antithesis to erosivity.

Raindrop potential energy (called the R-factor or energy (E)) causes erosion (Zorn and Komac, 2013; Panagos *et al.*, 2015) as a function of several factors (Avwunudiogba and Hudson, 2014). The R-factor is derived from the temporal and spatial characteristics of rainfall. The rainfall characteristics include the amount and intensity, and they are largely influenced by physical factors. Physical factors are the climate-related erosivity factors, such as wind speed in storm events (Pedersen and Hasholt, 1995; Zorn and Komac, 2013). However, the R-factor in classical soil loss estimation models is considered in Wind Free Rain (WFR) conditions.

The WFR concept considers vertically falling raindrop as the erosion driving component under the influence of gravitational and drag forces, without the influence of wind shear forces (Pedersen and Hasholt, 1995; Erpul, 2013; Marzen *et al.*, 2015). In WFR, raindrops fall vertically. In WDR, raindrop paths are oblique. The vertical component is called precipitation and the horizontal component is called wind-driven rain (WDR) (Hens, 2010). The raindrop strike process is considered in view of the physical parameters of a vertically falling raindrop striking a given soil surface, as shown in Figure 1.1. However, the raindrop strike velocity and angle change before the raindrop hits the ground surface due to the shear forces of wind (Marzen *et al.*, 2015). If aspect and slope angle are factored in, then the effect on the raindrop impact is even more significant, depending on the striking angle. This brings into play other factors such as rainfall velocity vector (RVV), raindrop impact velocity vector (RIVV) and angle of rain incidence (ARI) (Erpul, 2013) that need consideration in soil loss modelling. This is because wind considerably increases the kinetic energy of rainfall (Pedersen and Hasholt, 1995).

A further WFR soil erosion assumption is that rain and wind action during a storm are not interrelated (Stroosnijder and Gabriels, 2004b; Reis *et al.*, 2010; Erpul, 2013; Marzen, 2017) and occur in different climates at different temporal and spatial scales. Water erosion is assumed to be confined to the humid zones during the rainy season and wind erosion to the more arid zones during the dry season (Stroosnijder and Gabriels, 2004b). However, natural geomorphological processes are inherently

complex and do not occur in isolation. Winds accompanying rains are sufficient to significantly affect the rain's erosivity (Lyles and Allison, 1976). Wind and rain concurrently occur and erode soil (Reis *et al.*, 2010; Martius *et al.*, 2016; Marzen, 2017). Therefore the classical conceptualisation of water and wind erosion does not represent the natural setting accurately (Erpul, 2013), especially when focusing on mountainous regions.

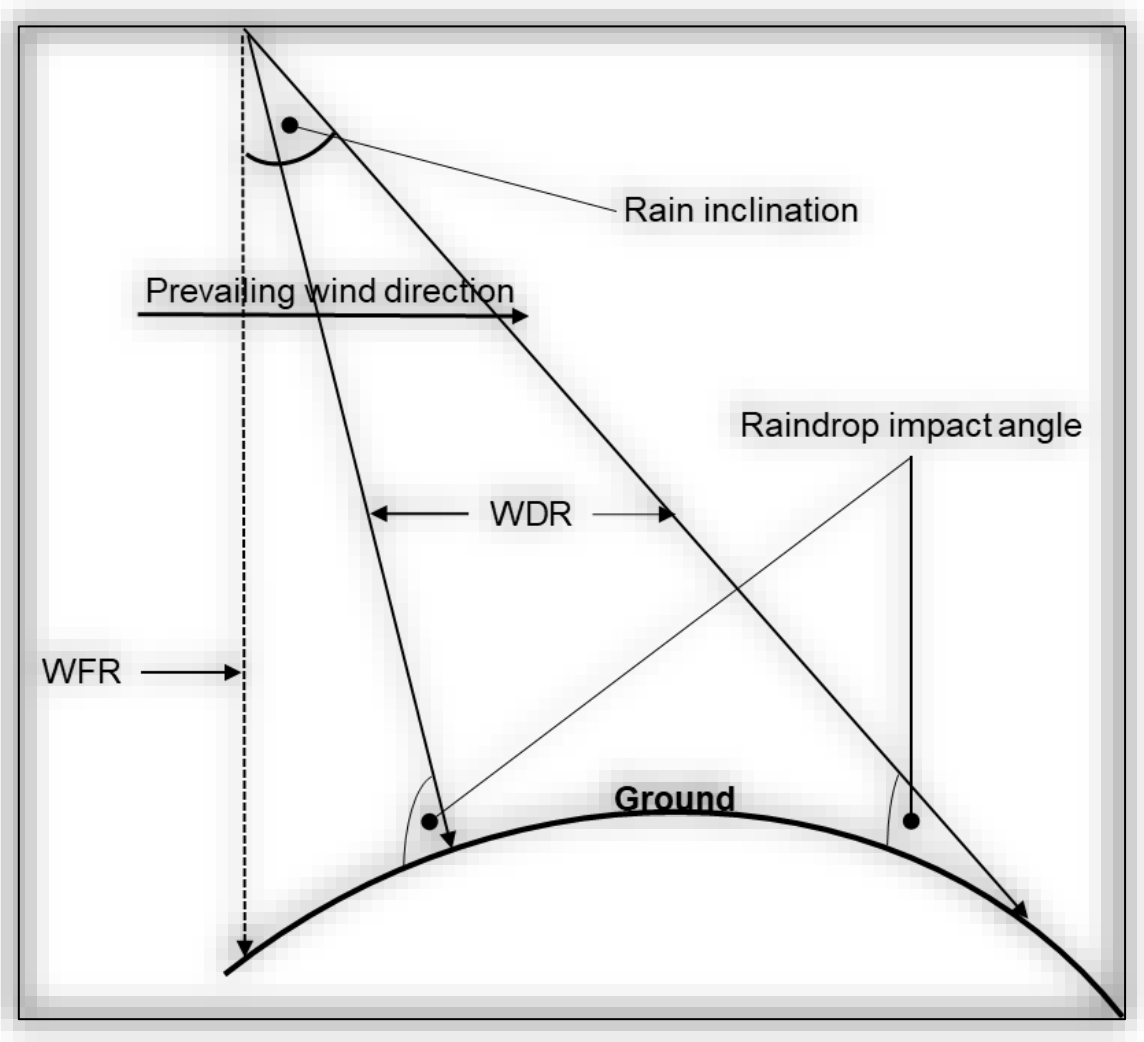

Figure 0.1 : Raindrop Trajectory in WDR and WFR (adapted from Erpul, 2013; Overton, 2013)

Mountainous regions possess unique climatic, geomorphological and environmental characteristics (Beniston, 2003; Mathew, 2006; Sun and Sun, 2015). The uneven mountain terrain creates a surface drag that slows down air flow through frictional resistance (Mathew, 2006). The surface drag is a special connection and interaction

between the Earth's surface and the atmosphere (Mathew, 2006; Barry, 2008) and defines surficial geomorphological processes such as soil erosion. The extent of the boundary layer effect is determined by the surface roughness or ruggedness. The surface drag results in unique mountain weather, creating unique and fragile environments (Barry, 2008) with unique soil erosion processes.

The unique soil erosion processes are primarily driven by water from rainfall. The dynamic and microphysical processes that affect the distribution and intensity of rainfall vary with the dynamics and thermodynamics of airflow as well as the configuration, size and shape of the terrain (Stoelinga *et al.*, 2013). Terrain influences the spatial distribution and physical characteristics of rainfall as it controls wind movements (Mathew, 2006) and the incidence of the sun. The net effect of these factors is captured in the concept of WDR.

In short, the consideration of WDR may be significant in the assessment of soil loss, even when there is no overland flow. The wind effects pertain to raindrop velocity, the deviation from the vertical course of fall and a modification of size and number of raindrops (Iserloh *et al.*, 2013) that significantly affect the raindrop erosivity. Research has shown that such effects are significant (Blocken and Carmeliet, 2010; Erpul, 2013; Iserloh *et al.*, 2013; Marzen *et al.*, 2015; Derome *et al.*, 2017) and deserve attention from researchers. The influence of the wind-driven factors on soil erosion is the subject of the problem statement.

1.3 Problem Statement

Soil is a threatened resource (Borrelli *et al.*, 2017). It is threatened by organic matter loss, contamination, biodiversity loss, compaction, salinisation and erosion, among others (FAO and ITPS, 2015). Erosion is one of the top three threats (FAO and ITPS, 2015; Caon and Vargas, 2017) to soil, together with loss of nutrients and/or organic matter and salinization. Soil erosion by water is recognised as one of the severe environmental problems that can cause ecological collapse (Xanthakis and Pavlopoulos, 2009; Ritter, 2012; Le Roux and Smith, 2014; FAO and ITPS, 2015; Marzen *et al.*, 2015; Global Soil Partnership, 2016; Marzen, 2017; Fu *et al.*, 2019). Erosion has rendered about 30% of the world's cropland unproductive over the past 40 years (FAO and ITPS, 2015). It reduces land productivity and soil fertility,

exacerbates flood disasters which affect land uses as well as the protection and utilization of soil and water resources (Fu *et al.*, 2019). More than 50% of South Africa's land surface faces moderate to severe erosion risk (Stone and Hibron, 2012). The national soil loss is 12.6 t/ha/yr. against the soil formation rate of 5 t/ha/yr. (Le Roux and Smith, 2014). This gives South Africa a net negative soil balance of 7.6 t/ha/yr.

Soil erosion may be a slow natural process that occurs relatively unnoticed, or it may occur at a very fast rate, causing serious loss of topsoil. Combined, wind and water are responsible for three quarters of the global land degradation, making erosion one of the most significant environmental problems worldwide (Toy *et al.*, 2002; FAO and ITPS, 2015; Global Soil Partnership, 2016). Erosion by all agents involves three distinct actions – soil particle detachment, movement and deposition (Choi, 2002; Kinnell, 2005; Ritter, 2012). The soil particle detachment action by raindrop strikes is the focus of this research. Detachment of soil particles caused by raindrop strikes is an initiation process of soil erosion (Pedersen and Hasholt, 1995; Choi, 2002; Blocken and Carmeliet, 2004; Kinnell, 2005; Marzen *et al.*, 2015; Panagos *et al.*, 2015).

Splash erosion is usually more effective and most noticeable during short-duration, high-intensity storms (Ritter, 2012). Short duration, high intensity storms are a common phenomenon of the summer of tropical climates (Sobel, 2012) where the Soutpansberg range is located. Thunderstorms are accompanied by gusts of winds that affect the falling raindrops (Reis *et al.*, 2010; Martius *et al.*, 2016). Wind increases the kinetic energy of rainfall by introducing a horizontal component to drop velocity that changes the angle of impact (Lyles, 1976; Erpul, 2013; Borrelli *et al.*, 2017; Marzen, 2017). Winds accompanying rains usually have sufficient speed to significantly affect the vertical trajectory of a raindrop. The wind imposes a raindrop horizontal velocity component proportional to wind speed (Helming, 1999; Erpul, 2013; Overton, 2013; Marzen *et al.*, 2017) that can result in an increased raindrop kinetic energy by up to three times (Lyles and Allison, 1976; Erpul, 2013; Marzen, 2017) than would be found in "normal" environments. Mountainous environments present a special circumstance to wind behaviour and soil erodibility. Therefore, the

goal of this research is to establish how the mountainous environment affects rainfall erosivity, wind speed as well as soil erodibility.

Raindrop erosivity and soil erodibility are paramount because they determine how fast soil particles are detached. However, soil loss predictions are mostly idealistic because of the methods used to estimate the erosion factors (Marques *et al.*, 2019). There is a lack of soil loss models that capture the contribution of the particle detachment role played by raindrop strike (Stroosnijder and Gabriels, 2004a; Erpul, 2013; Borrelli *et al.*, 2017; Marzen, 2017), let alone the effect of wind on rainfall erosivity. Most soil loss estimates rely on pioneering studies carried out in a wind free environment. The pioneering studies treat water and wind erosion as operating exclusively of one another (Stroosnijder and Gabriels, 2004a; Marzen *et al.*, 2015). However, this is not an accurate representation of the natural processes (Reis *et al.*, 2010; Erpul, 2013; Fister *et al.*, 2014; Marzen, 2017). Splash erosion does not operate exclusively of the effects of wind.

Due to the disjunctive treatment of water and wind action in soil erosion modelling, the recognition, description and quantification of erosion is highly speculative, and inconsistencies persist (Lal, 2001; Boardman, 2006; Borrelli *et al.*, 2017; Marzen, 2017). Pioneering studies deal with soil erosion as a fixed process (Borrelli *et al.*, 2017), categorising soil erosion as occurring under either Wind Free Rain (WFR) or Rain Free Wind (RFW). The highly abstract nature of WFR erosion calls for its revision and is the main basis for the concept of WDR. The concept of WDR is buttressed on the basis that natural rain events often occur as rainstorms, thereby adding a horizontal component to the falling raindrops (Blocken and Carmeliet, 2004; Blocken and Carmeliet, 2010; Reis *et al.*, 2010; Sobel, 2012; Erpul, 2013; Derome *et al.*, 2017). Therefore, the wind effect on raindrops is sufficiently significant and should not to be ignored in erosivity quantification (Reis *et al.*, 2010; Erpul, 2013; Marzen *et al.*, 2015; Marzen, 2017). The wind effect on water erosion is becoming progressively more significant considering the increased frequency of rainstorms due to climate change (Marzen, 2017; Marzen *et al.*, 2017).

1.4 Justification for the Study

Soil erosion by wind and water are the top three threats to soil health (FAO and ITPS, 2015; Caon and Vargas, 2017). The overarching justification for this research is that soil is a vital part of ecosystems and earth system functions that support the delivery of primary ecosystem services (Le Roux and Smith, 2014; FAO and ITPS, 2015; Borrelli *et al.*, 2017; Hill *et al.*, 2019). Soil is humanity's silent ally (FAO, 2015b). As such, the prediction of soil loss is important to establish sustainable land use practices that ensure and guarantee future generations' productive use of soil and water resources (Stanchi *et al.*, 2013; Caon and Vargas, 2017; Marques *et al.*, 2019). In addition, understanding the driving forces behind soil erosion enables easy identification of areas threatened by erosion and hence strategically address the problem (Benavidez *et al.*, 2018). Mountains are catchments of major river basins hence potential sources of downstream sedimentation. Imminently, soil erosion in mountainous areas is a key land use planning issue (Stanchi *et al.*, 2013). This is more so because water erosion affects more than 70% of South Africa's surface area (Garland *et al.*, 1999).

Most South African soils are extremely vulnerable to degradation and have low recovery potential (World Wildlife Fund (WWF)2010a; Parwada and Van Tol, 2016). Mountain soils are even more vulnerable due to shallow depth, more rainfall and steep gradient. Therefore, accurate soil erosion analysis is imperative in unravelling its severity as a pathway to minimisation and rehabilitation of the negative impacts (Le Roux, 2011; Seutloali *et al.*, 2017). Accurate soil erosion analysis begins with the simplification, understanding and control (FAO and ITPS, 2015; Poesen, 2018) of the soil erosion process. The soil erosion process is driven by soil erodibility and rainfall erosivity.

Soil erosion rates are governed by site specific properties. Therefore, generalisation conceals important detail and reduces accuracy. The Limpopo Province is perceived to be one of the most degraded provinces in South Africa (Gibson, 2006). However, this is within a large-scale spatial context that excludes the specific properties of the Soutpansberg range. The specific properties influence erosion process (Parwada and Van Tol, 2016), that is soil erodibility and rainfall erosivity.

Soil erodibility is a function of intrinsic and extrinsic soil erosion resistance factors. The erosive energy is a function of raindrop size, raindrop angle of incidence and raindrop terminal velocity, among other factors. The net effect of the erosivity factors on soil detachment is influenced by wind characteristics (Kusumandari, 2014). Wind influences the raindrop through its speed, direction, vorticity and vertical velocity (Pedersen and Hasholt, 1995; Brodowski, 2013; Erpul, 2013). The challenge to effective and sustainable soil conservation, though, is the disjunctive treatment of water and wind action in soil erosion modelling (Erpul *et al.*, 2003; Stroosnijder and Gabriels, 2004a; Reis *et al.*, 2010; Iserloh *et al.*, 2013; Marzen, 2017).

The disjunctive treatment of water and wind action in soil erosion modelling makes the recognition, description and quantification of erosion highly speculative (Lal, 2001; Marzen, 2017). However, the concept of wind driven rain (WDR) focuses on, and attempts to close, that gap. The concept of WDR recognises the effect of wind on the R-factor of raindrops (Blocken and Carmeliet, 2004; Erpul, 2013; Marzen, 2017). Wind flows in complex natural environments and rain events of various intensities may lead to very different rain deposition distributions in the same locality (Derome *et al.*, 2017). The extent of the influence of WDR on soil particle detachment in a natural landscape is determined by a diversity of parameters. Chief among the parameters is landscape morphology, wind speed, rainfall intensity, raindrop size distribution and rain event duration (Blocken and Carmeliet, 2004; Sun and Sun, 2015; Uzun *et al.*, 2017). The large number of parameters and their variability make the quantification of WDR a highly complex challenge that despite research efforts for a long time, WDR is still an active research subject where a lot of work remains to be done (Blocken and Carmeliet, 2004).

The theory of WDR, as applied in this research, brings in two important interlinked dimensions to the understanding of soil erosion by water. The two dimensions are soil erosion processes and the landscape on which the soil erosion is taking place. As such, this study is significant and justifiable from the two important interlinked dimensions.

1.4.1 The Soil Erosion Process

The raindrop strike initiates soil particle detachment, indicating the first stage in the soil erosion process by water (Pedersen and Hasholt, 1995; Lima *et al.*, 2013; Panagos *et al.*, 2015). The initiation is triggered by the rainfall kinetic energy (KE). Kinetic energy is a crucial indicator of the raindrop potential to dislodge soil particles (Petrů and Kalibová, 2018). The impact of a falling raindrop creates a depression in the soil, dislodging soil particles (Lima *et al.*, 2013; Panagos *et al.*, 2015). Significant to this research is how the kinetic energy of the raindrop is affected by wind in the process of dislodging soil particles. Although KE is a crucial indicator of the raindrop potential to dislodge soil particles, it is not a routinely measured meteorological parameter (Petrů and Kalibová, 2018). This is elaborated in the concept of wind driven rain (WDR).

It is important to highlight that air and water are both fluids and thus, in terms of laws of fluid dynamics, behave in many similar ways. Soil particles are dislodged by the same lift forces and so both fluids must overcome the same forces of resistance. The resistance is significantly influenced by the landscape through the boundary layer effect (Mathew, 2006; Stoelinga *et al.*, 2013; Uzun *et al.*, 2017). That is why the slope component is vital in soil erosion modelling. This brings in the second dimension from which this research is justified.

1.4.2 The Topography

Topography creates a special connection and interaction between the Earth's surface and the atmosphere that defines surficial geomorphological processes. Mountains create the special connection and interaction. They influence rainfall distribution due to their effect on both large and small scale atmospheric circulation systems (Kabanda, 2004; Oettli and Camberlin, 2005; Smith, 2007; Barry, 2008; Zardi and Whiteman, 2013; Sun and Sun, 2015; Rodrigues *et al.*, 2016). However, the meteorological influence of mountains on hydro-geomorphological processes is not well researched.

Generally, mountainous regions experience more precipitation and wind turbulence, affecting the erosive energy of both water and wind (Banta and Cotton, 1981; Barry,

2008; Peattie, 2013; Stoelinga *et al.*, 2013; Sun and Sun, 2015). The topography of the mountainous areas, the fragility of the soils, the absence of vegetation cover and frequent and violent floods (Meghraoui *et al.*, 2017) promote soil erosion. The effectiveness of erosive energy depends on differences in ground surface characteristics such as roughness, topography, vegetation cover, and wind field (Uzun *et al.*, 2017) as well as intrinsic soil characteristics. Wind experiences surface drag or friction from the ground, reducing its energy. The extent of the surface drag depends on the roughness of the surface (Gaberšek and Durran, 2004; Pachauri, 2009). Surfaces with a higher roughness index, such as hills and mountains, create more drag and present an important point of departure for this research.

Soil characteristics determine how the raindrop detaches soil particles. Characteristics such as particle size distribution, soil structure, organic matter content and permeability (Wischmeier and Smith, 1958; Stocking *et al.*, 1988; Breetzke, 2004; O'geen, 2006; Kusumandari, 2014) determine how a soil is affected by rainfall energy. Add to that the effect of land uses, geology, slope and hydrographical factors. This is crucial for targeted erosion control measures. Targeted erosion control measures should position soil erosion management practitioners at a better position to select the most appropriate and effective soil erosion control techniques and strategies which are highly necessary for a sustainable use of soils (Poesen, 2018). This is at the centre of the theoretical framework of this research.

1.5 Theoretical Framework

This research is built on the broad theory of soil erosion prediction. The generic approach is to model soil erosion as water or wind erosion (Stroosnijder and Gabriels, 2004a; Erpul, 2013; Marzen, 2017). The Universal Soil Loss Equation (USLE) is arguably the most widely used soil prediction model (Kinnell, 2010; Avwunudiogba and Hudson, 2014; Marques *et al.*, 2019). The Soil Loss Estimation Model for Southern Africa (SLEMSA) was developed to cater for the weaknesses identified in USLE. Therefore, these two models form the basis of this theoretical framework, and research. Consequently, the theoretical framework begins by outlining the USLE and SLEMSA with special focus on the soil erodibility and climate

elements of both models. The special focus on the climate element directs the theoretical framework to erosivity and the theory of WDR, which is a point of departure for this research.

1.5.1 The Universal Soil Loss Equation (USLE)

The Universal Soil Loss Equation (USLE) is considered as the best model for the estimation of surface erosion that is applicable worldwide (El Jazouli *et al.*, 2017). The USLE is arguably the most widely accepted and used soil loss prediction model worldwide (Kinnell, 2010; Avwunudiogba and Hudson, 2014; Marques *et al.*, 2019). Proposed by Wischmeier and Smith (1958), the model measures annual soil loss resulting from rill and inter rill erosion on slopes in agricultural fields. The USLE is a lumped parameter model (LPM) that predicts soil loss from agricultural land using equation 1.1.

$$A = RKLSCP \qquad \textbf{(0.1)}$$

A = average annual soil loss (Mg ha^{-1} yr^{-1})

R = rainfall erosivity index (MJ mm ha^{-1} hr^{1})

K = soil erodibility factor (Mg ha he ha^{-1} MJ^{-1} mm^{-1})

LS = topographic factor - L is for slope length and S is for slope (dimensionless)

C = cropping factor (dimensionless)

P = conservation practice factor (dimensionless)

The important gap in this theory, which informs this research, is found in rainfall erosivity factor because of its disconnect with the natural rainfall process. The rainfall erosivity factor in USLE is not suited for capturing the erosivity of intense precipitation events, which are common in the humid tropics (Stocking *et al.*, 1988; Lal, 1990). The assumptions regarding the rainfall characteristics of USLE are challenged because the rainfall in temperate regions is significantly different from that of the tropics. Therefore, the use of a single index computed from temperate rainfall properties ignores the rainfall erosivity variation brought by differences in

geographical characteristics (Stocking *et al.*, 1988). In addition, the USLE considers the R-factor in a wind free rain (WFR) environment.

The USLE was developed in the agricultural lands in temperate regions of the northern hemisphere. The climate is significantly different from that of the tropics in general and more particularly in tropical mountainous regions. Rainfall intensities in the tropics exceed the threshold of intensity set for USLE (Chakela and Stocking, 1988; Sobel, 2012). Rainfall erosivity differs with physical characteristics of rainfall, mainly intensity and amount (Wischmeier and Smith, 1958; Elwell, 1976). Rainfall physical characteristics depend on a place's global position as well as the physical landscape of the location.

The most common rainfall characteristics include depth, duration and intensity (Wischmeier and Smith, 1958; Elwell, 1976; Wischmeier and Smith, 1978; Lima *et al.*, 2013). However, an important rainfall characteristic that is overlooked is the driving wind of rain. Considering that most rainfall in mountainous tropical environments in which this study is situated occur as highly intense thunderstorms (Sobel, 2012), applying the WDR perspective to this research becomes ever more critical. However, a look at a tropical environment based soil loss model is necessary before delving into WDR.

1.5.2 The Soil Loss Estimation Model for Southern Africa (SLEMSA)

The SLEMSA is a model to estimate and rank the potential of physical erosion over a specific area (Stocking *et al.*, 1988). It was developed specifically to address the R-factor deficiency of the USLE. The SLEMSA assumes that soil erosion is influenced by a combination of different factors, of which the dominant ones are climate, soil, relief and vegetation cover. Major control variables are selected for each system on the basis of dominance within its system and easy of measurement (Stocking, 1980). The control variables are subsequently combined into three sub-models - the bare soil sub-model, topographical sub-model, and the vegetation sub-model. The multiplication of the sub models then produces the main model.

Soil loss as depicted by SLEMSA is calculated as in equation 1.2:

$$Z = KCX \qquad \textbf{(0.2)}$$

Z = estimated soil loss or erosion hazard (Mg ha^{-1} yr^{-1})

K = soil loss as determined by rainfall erosivity plus soil erodibility (Mg ha hr. ha^{-1} MJ^{-1} mm^{-1})

C = cover determined by vegetation (dimensionless)

X = relief as determined by slope length and steepness (dimensionless) (Stocking, 1980).

As with the USLE, the SLEMSA factors of importance for this research are the rainfall erosivity and soil erodibility. Rainfall erosivity is defined as the mean annual rainfall energy (E) (Morgan, 1995). The mean annual rainfall energy (E) represents the kinetic energy of raindrops as they strike the ground. The kinetic energy for SLEMSA is calculated using the formulae 1.3 or 1.4:

$$E=17.37*P \qquad \textbf{(0.3)}$$

Or

$$E=18.84*P \qquad \textbf{(0.4)}$$

E = kinetic energy (J/m^2/year); and

P = mean annual precipitation (mm/year) for areas experiencing drizzle and aggressive climate, respectively (Stocking *et al.*, 1988). The differentiation between drizzle and “aggressive” climates is an acknowledgement of the variations of the physical characteristics of rainfall brought by various factors such as wind. However, the authors do not define what “aggressive” climates entail. That omission is one of the bases why this research brings in the WDR.

1.5.3 Wind Driven Rain (WDR)

Wind Driven Rain (WDR) is a cross cutting theory that covers areas including Earth Sciences, Meteorology and Building Sciences. It is, however, deeply rooted in the Building Sciences where the theory is used to determine moisture threats on buildings (Gabet and Dunne, 2003; Blocken and Carmeliet, 2004; Blocken and Carmeliet, 2010). The theory is fundamental in soil erosion research because the

obliqueness and increased kinetic energy of raindrops influence the process of soil particle detachment (Gabet and Dunne, 2003; Marzen *et al.*, 2015; Panagos *et al.*, 2015) and causes raindrop splash anisotropy and upslope splash drift (Blocken and Carmeliet, 2004). When wind approaches a relief obstacle, a disturbance in its flow occurs and a specific flow pattern develops around it, including a frontal vortex, separation at obstacle ends, recirculation zones, shear layers and a far wake. When rain is added to the flow field, as a result of the specific flow features, the course of the raindrop trajectory is changed (Blocken and Carmeliet, 2004).

WDR is complex and characterised by a high spatial and temporal variability (Blocken and Carmeliet, 2010). Knowledge of the WDR characteristics is key for adequate planning of practices aimed at soil conservation (Lima *et al.*, 2013). The most important rainfall characteristic for erosion prediction is its erosivity because of its influence on raindrop strike and soil particle detachment (Gabet and Dunne, 2003; Marzen *et al.*, 2015; Panagos *et al.*, 2015). Hence, the following hypotheses are posited for this research.

1.6 Research Hypotheses

This research addresses the following research hypotheses:

a. H_0. Topographical elevation has no effect on rainfall erosivity.

   H_1. Topographical elevation increases rainfall erosivity.

b. H_0. Wind speed has no effect on rainfall erosivity.

   H_1. Wind speed increases rainfall erosivity.

1.7 Objectives

The general objective of this research is to analyse soil erodibility and rainfall erosivity on the Soutpansberg range to establish the characteristics of the factors that influence soil erosion.

The specific objectives are to:

1. classify geomorphic features of the Soutpansberg range to illustrate the erodibility characteristics of the mountain range;
2. characterise the spatial-temporal aspects of potentially erosive rainfall to reveal the distribution of rainfall erosion risk on the mountain range;
3. assess the influence of topography on
    a. wind speed and
    b. rainfall erosivity to establish the effect of topography on wind speed and erosivity;
4. compare rainfall erosivity derived from the USLE and the SLEMSA incorporating WDR erosivity to establish the influence of wind on rainfall erosivity.

1.8 Expected Outputs

Studies that have been carried out in the Soutpansberg range focused mainly on weather and climate change (see Kabanda, 2004; Kabanda and Munyati, 2010; Nenwiini and Kabanda, 2013; Kephe *et al.*, 2016), on ecology (see Mostert, 2006; Kirchhof *et al.*, 2010; Foord *et al.*, 2015), and on geology (Berger *et al.*, 2003). This research analyses the relationship between geomorphological and atmospheric phenomena. Geomorphological factors of interest are topography and soil erosion while wind and rain represent the meteorological factors. The thrust of the research is on the geomorphological analysis of the Soutpansberg region, establishment of the Earth-atmosphere interaction and how they influence soil erosion.

Therefore, the expected outcomes of this research include:

- a soil erodibility map of the Soutpansberg range;
- a spatial temporal map of potentially erosive rainfall on the mountain range;
- a determination of the effect of topography on potentially erosive rain and wind speed distribution;
- a determination of the importance of wind in soil erosion research.

1.9 The Study Area

The Soutpansberg, formerly known as the *Zoutpansberg*, means "Salt Pan Mountain" in Afrikaans. It is a range of mountains in the northern part of South Africa,

Limpopo Province in Vhembe District. The mountain range stretches for approximately 210 km from Punda Maria in Kruger National Park (23º05'S; 29º17'E) in the east to Vivo (22º25'S; 31º20'E) in the west as shown in Figure 1.2. The eastern end of the range is close to the Zimbabwe-Mozambique-South Africa border. The mountain range's highest peak is at Lajuma, reaching the elevation of 1,748 m.a.s.l. The widest part is a 60 km wide north-south axis while the narrowest is 15 km (Berger *et al.*, 2003).

The Soutpansberg range, covering an area of 6 800km^2, was included in the Vhembe Biosphere Reserve by UNESCO since 2009. The Reserve, which also includes the Blouberg Range, the Kruger National Park, the Makgabeng Plateau, the Makuleke Wetlands and the Mapungubwe Cultural Landscape, is a special area for the conservation of a bio-diverse environment and promotion of sustainable development and hence needs protecting from soil erosive forces.

The topography of the mountain range gives rise to orographic rainfall and wind patterns that create a diversity of microclimates (Berger *et al.*, 2003; Kephe *et al.*, 2016). The orographic rainfall forms from the moist south easterly prevailing winds from the Indian Ocean that is forced to rise over the southern scarp of the range (Kabanda, 2004). This results in rainfall on the south facing slopes while the air descends in the north facing slopes, creating dryness. This creates an interesting scenario for soil loss measurement and management.

The topography also creates a huge watershed for many rivers originating from the mountain range. In the central area are Nzhelele and Mutale Rivers flowing to the west and east, respectively. To the far south is Luvuvhu while Mutamba River marks the mountain's northern boundary. Other minor rivers of local importance are also found on the mountain range. Lake Fundudzi, the only lake in South Africa is found on Mutale River. All the rivers drain into Limpopo, making the Soutpansberg range an important catchment area, and erosion studies fundamental to catchment sediment management.

Soutpansberg receives rainfall between October of the previous year and April of the following year. Average rainfall ranges from as low as around 350 mm on the northern slopes, 550 mm in the east to 2000 mm along the central southern slopes

(Berger *et al.*, 2003; Kabanda, 2004; Mostert, 2006). Winds exit the mountain range at Waterpoort, creating the rain shadow effect where rainfall can be as low as 340 mm per year while Entabeni, in the central sections of the mountain, can record as high as 2000 mm of annual precipitation (Kabanda, 2004). The driest areas are the northern slopes, as well as valley floors bordered on either side by mountain ridges.

Kabanda (2004) describes the range as a complex terrain of ridges with various peaks and vast areas characterised by numerous different valley systems separated by elevated areas. Kabanda (2003) further points that the mountain configuration creates funnelling, large scale divergence and convergence of wind. Such observations warrant a detailed analysis of the effect of geomorphological configuration of the mountain range on wind and rainfall characteristics. The geomorphological configuration interrupts the synoptic weather systems to create localised mountain winds such as gap, katabatic and anabatic winds. Therefore, the mountain range is a strong and permanent modifier of the regional climate (Kabanda, 2003).

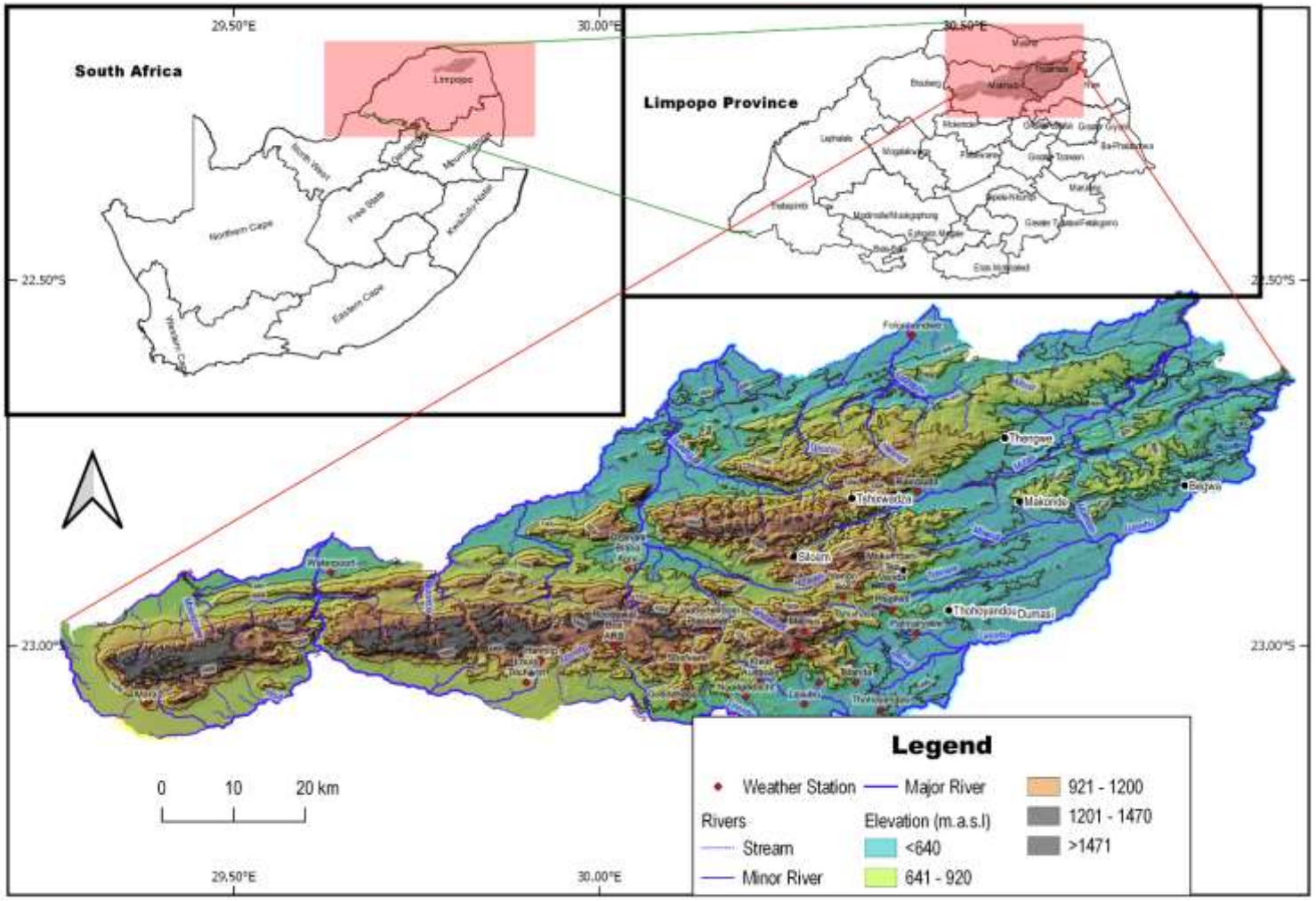

Figure 0.2: Soutpansberg Range

1.10 Operational Definitions of Key Terms and Concepts

Atmospheric circulation – large or small-scale movement of air by which heat is distributed on the surface of the Earth.

Coupling – the link that exists between two or more phenomena.

Geomorphic unit – a landform characterised by a specific origin and geomorphic setting.

Geomorphological – of or relating to the form or surface features of the earth.

Geomorphometry - a sub-discipline of geomorphology focusing on quantitative and qualitative description and measurement of landforms

Landform - morphometrically homogeneous land-surface

Meteorology - the interdisciplinary scientific study of the atmosphere.

Morphodynamic – comprehensive expression for all processes which shape a landform.

Morphogenesis – the regular development of specific landforms which occurs if no climatic accidents or other disturbances arise.

Morphographic – description of the appearance of landforms.

Morphometry – measurements of the geomorphological characteristics of individual landforms.

Mountainous – an area that rises abruptly from the surrounding level and attains a high elevation.

Sedimentation – the natural process by which eroded material settles at the bottom of water bodies to form solid material.

Soil erosion - the wearing away of land's topsoil by the natural physical forces of water and or wind

Spatial scale – the physical extend in terms of space.

Wind driven Rain – rain that has a horizontal velocity component due to wind resulting in drops falling at an oblique angle.

Wind Free Rain - rain that falls in a calm weather where wind effect does not change the vertical trajectory of rain drops.

1.11 Chapter Summary

Soil erosion is a global challenge that threatens ecological functionality. The need for better soil conservation practices keeps growing due to the twin challenges of climate change and population growth. However effective soil management solutions remain elusive to practitioners due to the complexity of the soil erosion process. The complexity of the process is increased by the agents of erosion and their treatment in soil loss estimation models. The major drawback is the disjunct treatment of water and rain. While it is possible to have rainless wind erosion, it is nearly impossible to have windless rain erosion. This is especially true for mountainous tropical regions which experience rainfall as high intensity thunderstorms accompanied by gusts of wind. Therefore, the aim of this research is to analyse soil erodibility and rainfall erosivity on the Soutpansberg range to establish the characteristics of the factors that influence soil erosion. The aim is achieved through four specific objectives. The specific objectives are to classify geomorphic features of the Soutpansberg range to illustrate the erodibility characteristics on the mountain; characterise the spatial-temporal aspects of potentially erosive rainfall to reveal the distribution of rainfall erosion risk on the mountain range; assess the influence of topography on wind speed and rainfall erosivity to establish the effect of topography on wind speed and erosivity; and compare rainfall erosivity derived from the USLE and the SLEMSA incorporating WDR erosivity to establish the influence of wind on rainfall erosivity. The co-occurrence of rain and wind erosion is captured in the concept of WDR as opposed to WFR. The Soutpansberg range of South Africa is chosen for this research because of its influence of the atmospheric dynamics of Vhembe District of South Africa. The situation of the subject matter for this research in literature is further elaborated in the following chapter.

: LITERATURE REVIEW

2.1 Introduction

Soil erosion is estimated to cause between 20 and 200 Gigatons (Gt) of global soil annually (Food and Agriculture Organisation (FAO) and Intergovernmental Technical Panel on Soils (ITPS)2015). However, Caon and Vargas (2017) opine that estimates above 50 Gt are unrealistic. They estimate that water erosion is causing global annual soil loss of between 20 and 30 Gt. Nonetheless, Global Soil Partnership (2016) estimates an annual loss of 75 Gt, globally. Borrelli *et al.* (2017) estimate an annual loss of 35 Gt per annum. The wide range of estimates is indicative of the magnitude of the soil erosion challenge. However, there is no consensus on the exact severity and extent of soil loss. The lack of consensus stems from the heterogenous battery of soil erosion models. FAO and ITPS (2015) agree that there are some conceptual flaws in soil erosion estimation models. Hence, the challenge of soil erosion is still prominent, and soil erosion research is still important.

Soil erosion is important as soil is an incubator to all life forms. All primary ecosystem services are anchored in the soil. The Soil Framework Directive of the European Union (Encyclopedia Britannica, 2016) identifies seven important soil functions and services. These are:

- biomass production, including agriculture and forestry;
- storing, filtering and transforming nutrients, substances and water;
- biodiversity pool, such as habitats, species and genes;
- physical and cultural environment for humans and human activities;
- source of raw materials;
- acting as a carbon pool; and
- archive of geological and archaeological heritage.

This chapter reviews literature on soil erosion with special focus on soil erodibility and rainfall erosivity. Following this introduction is a general overview of soil erosion. The next section reviews the challenge of soil erosion on the environment. The next section will focus on soil erosion in mountainous areas so that the special circumstances of the study area will be highlighted. That will be followed by a review

of literature on the concept of wind driven rain. The disclosure of the knowledge gap that this research seeks to plug is presented before closing with a chapter summary.

2.2 Soil Erosion – a General Overview

Soil erosion is a cross cutting challenge researched by different sciences and from different perspectives. Therefore, no single literature review document can claim to cover nearly enough about soil erosion. As such this review focuses on what is relevant to this research.

Soil erosion is categorised under water, wind and tillage (FAO, 2019). Poesen (2018) adds land levelling and soil quarrying, by crop harvesting, and by explosion cratering and trench digging as other sources of erosion. In addition, soil erosion by mass wasting - through slumping, debris flows and other means - is of major importance in particular landscapes.

Whatever the type of erosion considered, the factors that drive soil erosion are the same. Soil loss is determined by the ability of the soil to resist erosion and the energy that drives soil particle movement. The ability to resist movement is termed soil erodibility. The energy that drives soil particle movement is termed erosivity and comes from either rainfall (water), wind or ice. For the purposes of this research, the focus is limited to rainfall energy only. This is because wind is considered under WDR while ice does not occur in the Soutpansberg range and, indeed, the rest of South Africa. The factors that influence erodibility in particular and erosion in general are summarised by Avwunudiogba and Hudson (2014) as illustrated in Figure 2.1. The factors include land use and land cover, lithology (geology) topography (slope position), cropping or land cover determined by vegetation and conservation practice. Each factor is reviewed in turn to indicate its importance in soil erosion.

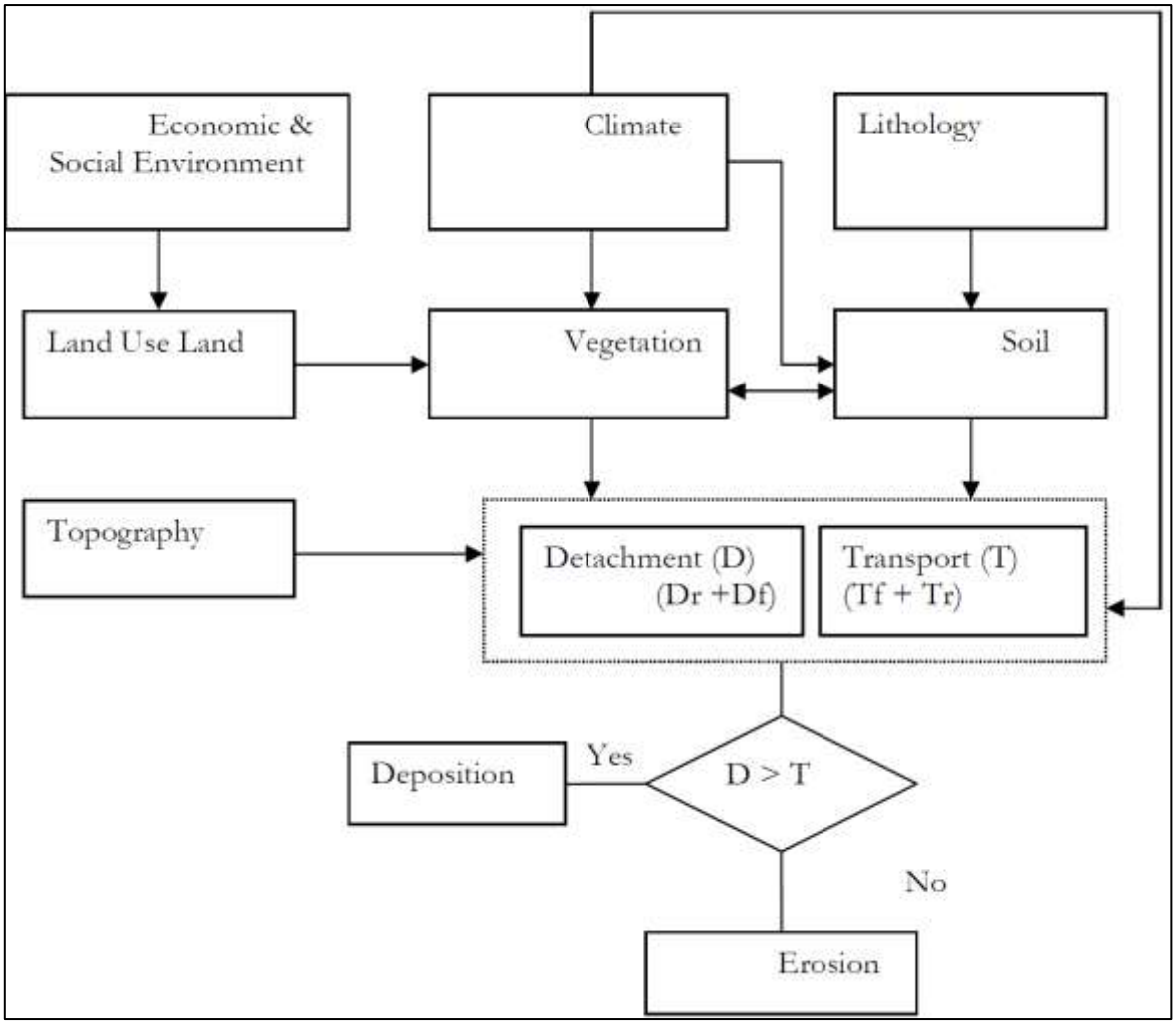

Figure 0.1: Factors Affecting Soil Erodibility (Source: Avwunudiogba and Hudson, 2014)

2.2.1 Intrinsic Soil Erodibility

Soil erodibility is a measure of the susceptibility of a soil to detachment by erosion agents (Kinnell, 2010; Kusumandari, 2014; FAO, 2019). It is an important secondary control on water erosion (FAO and ITPS, 2015). Knowledge of soil erodibility (and rainfall erosivity) is an essential requirement for erosion prediction, conservation planning, and the assessment of sediment related environmental effects of watershed agricultural practices (Wang *et al.*, 2013). That is why erodibility is the only other parameter with units (the other is erosivity) in soil erosion modelling (Renard *et al.*, 1997; Kinnell, 2010; Zeng *et al.*, 2017). Ultimately, soil erosion units are a fusion of soil erodibility and rainfall erosivity units. The erodibility of a landscape is determined by topographical parameters (such as slope gradient and

curvature), field characteristics (size and shape), and the physical properties of the soil (FAO, 2019). Important to this section are the physical (intrinsic) properties that determine soil erodibility.

The intrinsic factors that determine soil erodibility are controlled by soil texture and organic matter content (Bryan, 2000). Soil texture is determined by particle size distribution, soil structure, organic matter content and permeability (Wischmeier and Smith, 1958; Stocking *et al.*, 1988; Breetzke, 2004; O'geen, 2006; Kusumandari, 2014). Soil structure determines the amount and type of organic and inorganic bonding agents. The interaction of these properties determines intrinsic soil erodibility. However, the characterisation adopted for this research considers both intrinsic and extrinsic factors. The extrinsic factors are covered under section 2.2.1.2.

The intrinsic soil characteristics also determine whether water infiltrates or flows over the surface. As a rule, course grained soils have more infiltration capacity than fine grained ones (FAO, 2019). Deep soil layers can accommodate more water than shallow ones. Soils with higher organic matter content can absorb more water. The infiltration capacity determines the amount of water available on the soil surface for erosional purposes.

Soils are classified into four infiltration capacity categories. The first category is of deep sands and silt loams that are well-aggregated (FAO, 2019). Sands have at least 55% sand (O'geen, 2006). Silt loams have at least 70% silt, 60% sand and less than 30% clay. This category has the highest infiltration capacity. This is because sands are highly permeable due to their lack of aggregation properties. Hence the soil's erodibility is low.

The second highest infiltration capacity is found in silty loams and sandy loams (FAO, 2019). Sandy loams have at least 80% silt and 50% sand. The clay content is between 15 and 20%. This texture composition allows infiltration of up to 8mm/hr (FAO, 2019). The infiltration capacity is limited by the soil depth that is shallow.

The second least infiltration capacity is found in clay loams, shallow sandy loams, soils low in organic matter and soils high in clay (FAO, 2019). Clay loams have 60-70% silt, 30-40% clay and 30-65% sand. The high volume of clay clogs the pore spaces between soil particle, hence low infiltration capacity. Clays have the tendency

of expanding and forming a cementing effect when water is added. That makes water accumulate on the surface and exposes the soil to erosion.

The least infiltration capacity is found in soils of high swelling potential such as heavy clays (FAO, 2019). Clays contain 40-60% silt, 40-64% sand and above 40% clay (O'geen, 2006). The tendency of clay to expand on contact with water makes it absorb rather than allow water to pass through. The expansion closes pore spaces that could be used for infiltration by water. The existence of pore spaces in a soil is a function of particle size distribution.

Particle size distribution is aptly captured by the soil texture triangle (Figure 2.2). The soil texture triangle is a representation of the clay, silt and sand percentage by weight in a soil (O'geen, 2006). Soil particle size determines whether the soil is sand, silt or clay. Sand particles have a diameter of 0.05 to 2mm. Silt particles range from 0.002 to 0.05mm. Clay particles are less than 0.002 mm in diameter.

Texture is a permanent intrinsic soil characteristic that influences the water holding capacity of the soil as well as infiltration and through flow rates (Kusumandari, 2014). That determines soil structure. Soil structure refers to the arrangement and cohesion of soil particles into large aggregates of identifiable shape (O'geen, 2006). Good aggregation holds soil particles together and increase resistance to detachment (Stanchi *et al.*, 2013). A sandy soil has low erodibility because of the loose arrangement and cohesion of the particles that allows infiltration. In addition, sand particles are particularly heavy to detach and transport. However, that is also determined by the soil organic matter content.

Soil organic matter is the component of soil derived from all living or non-living biological sources. It is an indicator of soil health because of its effect on a variety of soil functions and properties (Arsyad, 2010), including erodibility. How the organic matter affects soil erodibility depends on whether it is decomposed or raw. Raw organic matter covering the soil surface protects the soil against raindrop impact, reducing soil detachment. Highly decomposed organic material in the soil, termed humus, binds soil mineral particles together into aggregates (O'geen, 2006; Kusumandari, 2014).

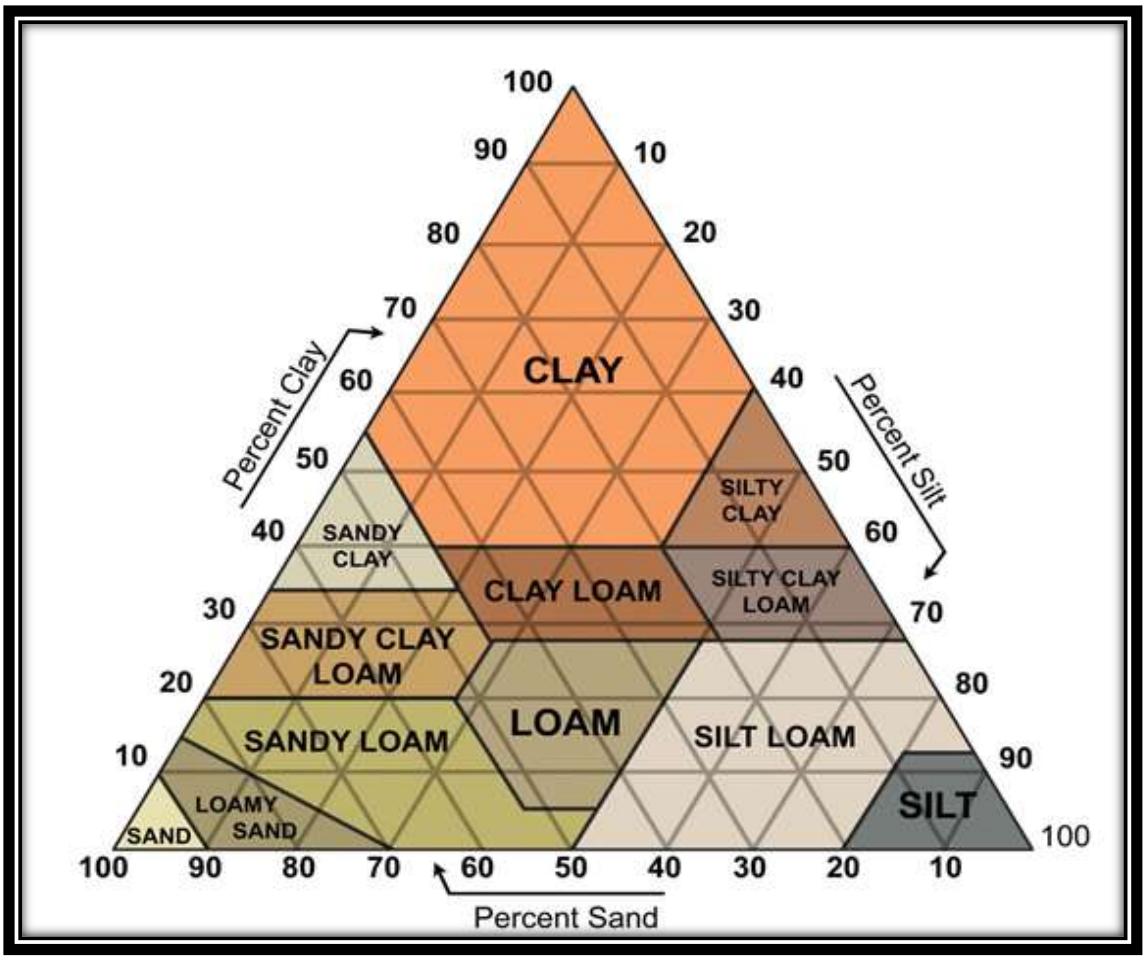

Figure 0.2: Soil Texture Triangle (Source: Food and Agriculture Organisation, 2019)

Therefore, soils with higher soil organic matter have higher well-structured soils develop a network of pores and cracks that allow water resistance to erosion (O'geen, 2006; Doran et al., 2020). The soil organic matter functions as a binding agent that improves soil aggregate stability. In addition, organic matter also functions as a sponge that absorbs water. Therefore, soils with high soil organic matter generally have low erodibility. That completes the intrinsic soil erodibility. The following section focuses on extrinsic soil erodibility.

2.2.2 Extrinsic Soil Erodibility

Different factors interact with soil particles or water before erosion happens. The interactions happen at different stages of the erosion process. Some factors influence how the raindrop hits the ground. Others influence how the soil handles or interacts with the water. Therefore, many factors exist. However, the extrinsic factors

that comprehensively influence soil erodibility and are considered in this research include (lithology) geology, slope, land-use-land-cover and hydrography (Stocking, 1980; Chakela and Stocking, 1988; Stocking *et al.*, 1988; Renard *et al.*, 1997; FAO and ITPS, 2015). These represent the geological setting, slope position, exposure to raindrops (erosion exposure) and landform position, respectively, in this research.

The geological setting or parent material is important in terms of soil hydraulic conductivity as well as soil formation rate (Wischmeier and Smith, 1978; Li *et al.*, 2009). The parent material also influences soil permeability. Soil characteristics such as texture are directly affected by the geological setting because soil is formed from rocks. Therefore, soil erodibility is aligned with geology (Laker, 2004) and hence, locally influences soil erosion. In addition, surface runoff, infiltration and percolation are influenced by the geological characteristics. Surfaces with hard outcrops generate more surface runoff that erode soils downslope.

Slope position is a representation of topography (Wischmeier *et al.*, 1958; Stocking, 1980). Topography has a direct effect on the spatial occurrence of surface erosion. As a simple rule, as slope increases, so does erosion (FAO, 2019). The higher the slope angle, the higher the probability of surface runoff. This is how the slope is represented in this research. Steep slopes such as cliffs are more prone to soil detachment than low lying areas such as open valleys. Therefore, cliffs, scree slopes, transportation mid-slopes, foot slopes and open valleys (Jenness, 2006; Melelli *et al.*, 2017) were considered to represent different slope positions. However, this is a representation according to gradient only. Water accumulation on slopes presents a different story.

Runoff accumulates down, and sometimes across, slopes. The accumulation of runoff discharge increases energy and, therefore, erosivity (Huggett, 2007; FAO, 2019). Therefore, as a rule of water accumulation, erosion increases downslope as shown in Figure 2.3. This is what is captured by the hydrography in the form of landform position.

Hydrography caters for the tendency of water to accumulate. This gives the position of landforms vis-à-vis water accumulation. Landform position classifies the landscape into steep sided ridges, flat topped plateaux, gentle plains, open slopes and river channels (Jenness, 2006) basing on water accumulation characteristics.

The landform potion is a function of different factors. The factors include the Topographic Wetness Index (TWI), drainage and point density, average river slope and shoreline development ratio (Jenness, 2006; Melelli *et al.*, 2017; Mattivi *et al.*, 2019; Zwoliński *et al.*, 2019; Kopecký *et al.*, 2021).

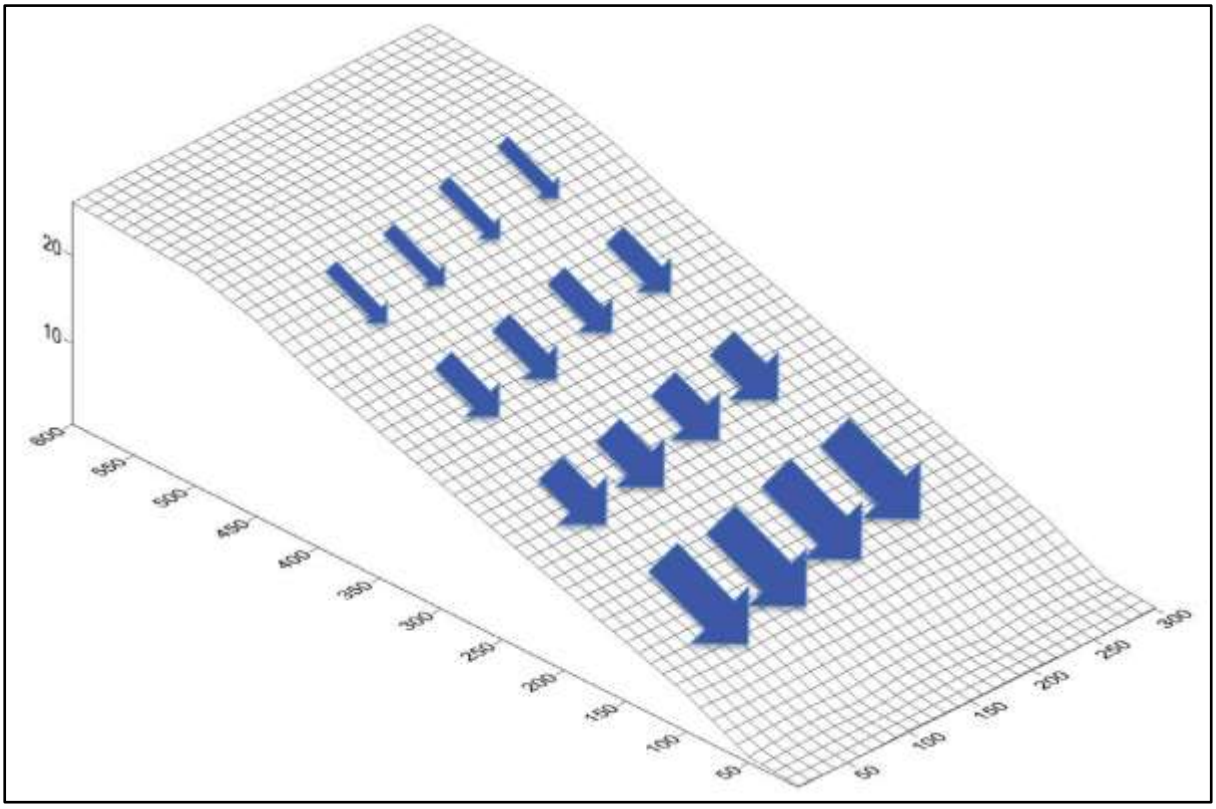

Figure 0.3: Increasing Depth and Velocity of Runoff Along a Slope: a Schematic Representation (Source: FAO, 2019).

The Topographic Wetness Index (TWI) is an important indicator of water behaviour in hydrogeomorphology. It is a model that estimates where water would accumulate in an area with variable elevation (Mattivi *et al.*, 2019; Kopecký *et al.*, 2021). The index is highly correlated with soil attributes such as horizon depth, silt percentage and organic matter content (Moore *et al.*, 1993). Therefore, the areas that would be indicated as high water accumulation areas due to slope are considered.

Another hydrography element is drainage and point density. Point density computes the sphere of influence of point hydrographical elements such as springs and waterfalls (Najwer and Zwoliński, 2014; Zwoliński *et al.*, 2019). This represents the effect of the presence of such a hydrological feature on soil erodibility. Antecedent moisture has an effect on soil loss from runoff (Wei *et al.*, 2007).

Land cover is also important as a factor that influences soil erodibility. The type of vegetation cover can be effective to the extent of doubling the surface area that has to be wetted before the raindrops reach the ground (FAO, 2019). Vegetation protects the soil from direct raindrop impact (FAO, 2019). That is why land use and cover is termed raindrop exposure in this research. Overall, moving from cropland to grassland to forest, with increasing vegetation density, there is an increase in soil protection from raindrop exposure and erosion (Torri and Poesen, 2014). Generally, soil detachment is reduced by 50% at about 20% vegetation covers, by 75% at 30 to 35% covers and by 90% at 60% covers (FAO, 2019).

2.2.4 Rainfall Erosivity – the Energy Behind Soil Erosion

Water erosion is a common phenomenon under all climatic conditions (Borrelli *et al.*, 2017). Rainfall erosivity is the potential ability of rainfall to cause soil detachment and transport (Zeng *et al.*, 2017; FAO, 2019). Rainfall erosivity is a function of the direct raindrop impact, storm duration and the runoff that rainfall generates (Lal, 1994; Zeng *et al.*, 2017). It is assumed that when factors other than rainfall are held constant, soil losses from cultivated fields are directly proportional to the total storm energy (E) times the maximum 30-min intensity (I_{30}) (Renard *et al.*, 1997; Kinnell, 2010). The two rainfall attributes commonly used to measure erosivity are rainfall amount and rainfall intensity (FAO, 2019). Potentially erosive rainfall is any amount that is above 12,5mm (Renard *et al.*, 1997). Rainfall intensity is the amount of rain falling in a place over a given period.

Rainfall energy can be influenced by raindrop characteristics (FAO, 2019). However, the commonly used erosivity computation considers the product of total kinetic energy of a storm multiplied by the maximum 30-minute intensity as developed by Wischmeier and Smith (1958). However, this has been criticised for lack of consideration of other important erosivity aspects. Kinnell (2010) criticises it for not considering runoff. Erpul (2013) and Marzen (2017) criticise this approach for leaving out the effect of wind on raindrops. This is the gap that this research wishes to address.

Borrelli *et al.* (2017) did a RUSLE-based modelling to estimate the potential rates of soil erosion by water for the land surface of 202 countries. Their results reveal 2.5%

increase in soil erosion between 2001 and 2012 worldwide. Of particular importance is the finding that sub–Saharan African countries' rate of erosion increased at three times higher than the developed economies because of poor land use practices in the developing world. However, of paramount importance to this literature review is how erosivity is computed.

2.2.4.1 Erosivity Factor (R) Calculation

The energy of a rainstorm is a function of the amount of rain and of all the storm's component intensities. The energy of a given mass in motion is proportional to velocity squared. Therefore, rainfall energy is directly related to rainfall intensity, which is the amount of rain received per time. The numerical value used for R in the USLE and in RUSLE must quantify the effect of raindrop impact and must also reflect the amount and rate of runoff likely to be associated with the rain (Renard *et al.*, 1997). Erosivity is a function of total storm energy (E) and maximum 30-min intensity (I_{30}). This should not be considered as an energy only parameter because raindrop erosion increases with intensity (Wischmeier and Smith, 1978). Hence R is a product of rainfall intensity and storm energy. The energy is a function of the impact frequency, size, shape, and terminal velocity that determine the kinetic energy (KE) of rain drops (Torres *et al.*, 1992; Kinnel, 2016). In short, energy is a function of raindrop characteristics which is embodied by kinetic energy as indicated in equation 2.1.

$$R = EI \qquad \textbf{(0.1)}$$

Where:

R = rain erosivity (MJ mm ha^{-1} hr^{-1})

E = energy (MJ/mm)

= 11.87+8.73log10*i* where *i* is rain intensity

I = Intensity (I_{3600}) (mm/s)

The EI (MJ/mm^{-1}/s) is an abbreviation for energy times intensity, and the term should not be considered simply an energy parameter. The Kinetic Energy is estimated using rainfall intensity. Storms with higher intensities and longer durations have higher erosion potential (Stone and Hibron, 2012). However, different authors found

different relationships between rainfall intensity and kinetic energy depending on the climatic conditions (Wischmeier and Smith; Salles *et al.*, 2002; Van Dijk *et al.*, 2002; Breetzke, 2004; Lobo and Bonilla, 2015). In addition, the R factor as represented in the USLE needs high temporal resolution rainfall data for over 20 years or more so that all rainfall variability is captured and bias eliminated (Vantas *et al.*, 2019). Such data are not readily available and are not readily available for Soutpansberg range. Therefore, researchers have developed R factors suitable for the data available and different geographical regions. Such R factor derivations include that used in the Soil Loss Estimation Model for Southern Africa (SLEMSA) (Stocking *et al.*, 1988), the African Rainfall Erosivity Sub-regional Empirical Downscaling (ARESED) (Diodato *et al.*, 2013) and the Daily Rainfall Erosivity Model (Yang and Yu, 2015). The models are comparable to the USLE and are elaborated below.

2.2.4.2 The Adapted R Factors

2.2.4.2.1 African Rainfall Erosivity Sub-Regional Empirical Downscaling (ARESED)

The African Rainfall Erosivity Sub-regional Empirical Downscaling (ARESED) is a reduced complexity model that can be applied to vulnerable African landscapes (Diodato *et al.*, 2013). It is developed with the full understanding of how the Inter-Tropical Convergence Zone (ITCZ) and the monsoon driven circulations control climate in central Africa and eastern Africa, respectively. In addition, other areas have unique ranges of latitude, relief and ecosystems that produce diverse patterns of convective and orographic- driven precipitation. ARESED is presented in equation 2.2.

$$R_{ARESED} = h * \left[\Phi(P(\boldsymbol{u})_{prc85})\right]^{K} \qquad \textbf{(0.2)}$$

Where:

R_{ARESED} = estimated mean rainfall erosivity (MJ/mm/ha^{-1}/hr^{-1}/y^{-1}) at a grid cell size of 10 km;

Φ (P(**u**)) = the regionalized variation component (dimensionless) determining the power of the rainfall-driven temporal pattern;

Φ = regional scaling operator (dimensionless). This is used to convert the hydro-climate data input [$P(\mathbf{u})_{prc85}$] from point data to continuous fields;

$P(\mathbf{u})_{prc85}$ = 85th percentile of the monthly precipitation (in mm) at location **u**, hereafter named the hydro- climate data input;

K = constant or a shape parameter (dimensionless) (value of 1.271);

h = weighted (dimensionless) geographical scalar factor deriving from the product of a 'horizontal' (H) and a 'vertical' (Z) component (η = H * Z). H is calculated using equation 2.3.

$$H = \alpha\text{*Lat} - \beta\text{*Long}^3 + \gamma \qquad \textbf{(0.3)}$$

Where:

Lat = latitude in decimal degrees;

Long = longitude of the area in decimal degrees;

α = scale parameter with the value of 0.01;

β = scale parameter with the value 0.00003;

γ = shift parameter with a value of 10

$$Z = 1 - \Delta * E \qquad \textbf{(0.4)}$$

Where:

Z = a parameter that arranges the local rainfall pattern;

E = elevation (in m) as obtained from the DEM;

Δ = elevation scale parameter with a value of 0.0001.

ARESED incorporates monthly precipitation percentiles and geographic data that capture climatic variability and rainfall erosivity over decadal time scales and across continental to other regional spatial scales. Daily precipitation data are readily

available, making ARESED usability quite easy. However, the Daily Rainfall Erosivity Model (Yang and Yu, 2015) brings in some robustness in erosivity computation.

2.2.4.2.2 The Daily Rainfall Erosivity Model

Though developed for Australia, the model is applicable to South Africa due to the climatological similarities between the two countries. In addition, Yang and Yu (2015) incorporate the latitude factor in the model as shown in equation 2.5.

$$\hat{E}j = \propto [1 + \eta\cos(2\pi fj - \omega)]\sum_{d=1}^{N} R_d^{\beta} \quad \textbf{(0.5)}$$

Where:

$\hat{E}j$ = rainfall erosivity for the month *j* (MJ mm ha-1 hr1);

R_d = daily rainfall amount (mm);

F*j* = sinusoidal function (dimensionless) with a fundamental frequency F = 1/12 is used to describe the seasonal (monthly) variation of the coefficient.

N = number of rain days in the month; and

α, β, h, and ω are model parameters (dimensionless).

$\alpha_0 = 1.05 * 10^{(2.05-1.58b)}$

β = 1:02 – 0.0209*L* where L = the latitude in decimal degrees,

h = rainfall seasonality factor (dimensionless).

ω = a parameter that implies that for a given amount of daily rainfall, the corresponding rainfall intensity is highest in January, when the temperature is highest. The parameter is set to $\pi/6$

2.3 The Environmental Challenge of Soil Erosion

Soil erosion remains a global challenge. This is because all life forms derive from the soil. It is intricately linked to poverty, food security and biodiversity. Therefore, severe soil erosion has the potential to upset the global ecological balance (FAO and ITPS, 2015; Marzen *et al.*, 2015; Global Soil Partnership, 2016; Marzen, 2017; Fu *et al.*, 2019). The Food and Agricultural Organisation (FAO) of the United Nations is a leading soil degradation research organ. Several soil degradation research initiatives have been carried out under it. An early initiative was the Global Assessment of Soil Degradation (GLASOD) project undertaken in the late 1980s to inventory soil degradation. GLASOD evaluated twelve types of soil degradation. These are:

- water erosion (topsoil loss and mass movement, including rill and gully formation),
- wind erosion (topsoil loss, terrain deformation – primarily dune activity),
- overblowing (surface burial from aeolian deposition),
- loss of nutrients,
- loss of organic matter,
- salinization,
- acidification,
- pollution,
- compaction
- physical degradation,
- waterlogging, and
- subsidence of organic soils.

It is notable that water erosion is the first listed type of soil degradation. Water is readily available in different areas in different forms and causes prolonged erosion. Prolonged erosion causes irreversible soil loss over time, reducing the ecological (e.g. biomass production) and hydrological functions (e.g. filtering, infiltration and water holding capacity) of soil (Le Roux and Smith, 2014; Zeng *et al.*, 2017). Soil erosion can disrupt ecological security patterns at both small and large scale.

The Soil Thematic Strategy of the European Union (2006) formalized the concept of threats to soil and its many functions. Five specific threats are identified under Article 6 of the draft Soil Framework Directive proposed in the Strategy. The threats are:

- erosion by wind and water;
- organic matter decline;
- compaction;
- salinization; and
- landslides of soil and rock material.

Again, erosion by water prominently features. This is because soil erosion has been with humanity since the beginning of permanent settlements. Borrelli *et al.* (2017) opine that accelerated soil erosion is a result of human activity and related land use change. This has considerable implications for nutrient and gas cycling, land productivity and in turn, worldwide socio-economic conditions, particularly food security (Le Roux, 2011; Borrelli *et al.*, 2017; Marzen, 2017). In addition, sediment pollution of water reservoirs increases costs of surface water storage and purification (Rickson, 2014; Poesen, 2018; Hill *et al.*, 2019). Hence, there is a recognition among both policy-makers and soil scientists that soil degradation is a major challenge to achieving food security in sub-Saharan Africa (FAO and ITPS, 2015). Managing the degradation process is one way of containing this challenge.

Therefore, this research does not focus on soil erosion or degradation in general. The focus is on soil erodibility and rainfall erosivity, the main factors that influence soil erosion (Renard *et al.*, 1997; Kinnell, 2010), especially in mountainous environments. Special focus is placed on establishing the spatial and temporal characteristics of soil erodibility and rainfall erosivity. Hence, the basis for this research is the two established soil erosion models – the Universal Soil Loss Equation (USLE) by Wischmeier and Smith (1958) and The Soil Loss Estimation Model for Southern Africa (SLEMSA) by Elwell (1978). As such, a logical next point for review is an overview of soil erosion processes.

2.4 Soil Erosion in South Africa

Soil erosion is a major environmental problem facing land and water resources in South Africa (Garland *et al.*, 1999; World Wildlife Fund (WWF)2010b; Ighodaro *et al.*,

2013; Le Roux and Smith, 2014; Parwada and Van Tol, 2016). Seutloali *et al.* (2017) posit that soil erosion induced land degradation is among the leading environmental problems in South Africa. A vast amount of productive South African land is affected by different types and intensities of soil erosion. Approximately 1 Mha of land experience soil losses greater than 150 t/ha^{-1} yr^{-1} (Baade *et al.*, 2012), ranking among the highest in the world (Parwada and Van Tol, 2016). However, this is in sharp contrast with De Villiers *et al.* (2003) and Le Roux and Smith (2014) who estimate soil loss at 2.5 t/ha^{-1} yr^{-1} and 12 t/ha^{-1} yr^{-1}, respectively. This is a further indicator of the disparities that exist in soil loss models. However, there is consensus regarding the existence of the soil erosion challenge in South Africa.

A gully erosion assessment done by Le Roux and Smith (2014) shows that the whole nation is affected by gully erosion. In terms of total eroded area, the Northern Cape and Eastern Cape are the most severely affected, followed by KwaZulu-Natal, the Free State, Limpopo, Western Cape, Mpumalanga, North West Province and Gauteng (Le Roux and Smith, 2014). However, proportionately, KwaZulu-Natal and the Eastern Cape are the worst affected. The least affected are Gauteng and Northwest as shown in Table 2.1. This paints a picture of a challenge that needs every one's input because loss of fertile topsoil and reduction of soil productivity affects all.

Another GIS based soil erosion study done in Transkei, Eastern Cape Province, by Seutloali *et al.* (2017) found that the place experiences different intensities of soil erosion ranging from none to very severe erosion. An important finding reported is the considerable decrease in density and eroded areas from 1984 to 2010. However, severe to very severely eroded areas slightly increased. The increase in the two categories was overshadowed by the significant increases in the none and slight erosion categories. Further analysis, however, shows that rill and gully erosion cause 70% of the soil loss.

The South African soil loss situation is made worse by the soil formation rate that is lower than the loss rate. The average predicted soil loss rate for South Africa is 12,6 tons/ha/year, while the average soil loss rate under annual cropland (grain crops) is

Table 0.1: South Africa Gully Erosion by Province (Erosion data from Le Roux and Smith, 2014)

Province	Area (ha)	Area Eroded (ha)	Percent Eroded
Eastern Cape	16896600	151759	0.90
Free State	12982500	64674	0.50
Gauteng	1817800	110	0.01
KwaZulu-Natal	9436100	87522	0.93
Limpopo	12575500	58669	0.47
Mpumalanga	7649500	17420	0.23
Northwest	10488200	10782	0.10
Northern Cape	37288900	160885	0.43
Western Cape	12946200	25403	0.20

13 tons/ha/year, which is much higher than the natural soil formation rate of less than 5 tons/ha/year (Le Roux and Smith, 2014). That makes a very significant proportion of South Africa potentially susceptible to degradation (Gibson, 2006). This places a large proportion of the national population at risk because their livelihoods are dependent on the natural resource.

The risk on the population emanates from the lost soil that causes off-site impacts related to sedimentation of rivers, resulting in siltation and pollution of water resources (Le Roux and Smith, 2014; Parwada and Van Tol, 2016; FAO, 2019). The Department of Water and Sanitation is concerned with sedimentation and siltation that is taking water reservoir capacities at an alarming rate. For example, the Welbedacht Dam near Dewetsdorp in the Free State lost 86% of its reservoir capacity within 20 years of completion due to siltation (Le Roux and Smith, 2014). This resulted in the Mangaung Municipality in Bloemfontein opting to expensively import water from the Katse Dam in Lesotho. Such a scenario affects even those whose livelihoods are not directly linked to soil use. This makes it important to critically analyse soil erosion and enhance its understanding in order to identify source areas and tame the challenge (Le Roux and Smith, 2014; FAO and ITPS, 2015; Poesen, 2018; Hill *et al.*, 2019).

Parwada and Van Tol (2016) reviewed soil erosion in Ntabelanga, Eastern Cape province and concluded that erosivity and erodibility factors influence soil erosion. This is one of the bases for analysing the erodibility and erosivity on the Soutpansberg range. The two factors have an important influence on soil erosion because South African soils are highly erodible because of scant vegetation cover (WWF, 2010b; Parwada and Van Tol, 2016). The lack of vegetation exposes the soil to erosive agents such as rainfall and wind.

In addition, South African soils are characterized by very low organic matter levels. Only 4% of the South African soils contains more than 2% organic carbon (Du Preez *et al.*, 2011). Soil organic carbon concentrations is a major indicator of soil quality. Concentrations of 2% (equivalent to 3.4% SOM) is an upper threshold, below which most soils become structurally weak and vulnerable to erosion (Parwada and Van Tol, 2016).

The vulnerable soil situation is exacerbated by human land use practices. Chief among the activities is poor farming practices and intensive agriculture (Le Roux and Smith, 2014; Parwada and Van Tol, 2016; FAO, 2019). Therefore, the spatial extent of the problem has to be established and monitored for effective prevention and remediation of soil erosion (Le Roux *et al.*, 2007). This service is offered by GIS and remote sensing. Hence several soil erosion related research have been done using the tools as summarised in Table 2.2.

Table 0.2: Summary of Selected Erosion Related Research in South Africa

Author	Title	Aim/Objective	Major Finding/Recommendation/Conclusion
Hill *et al.* (2019)	Assessing The Impact of Erosion and Sediment Yield from Farming and Forestry Systems and Selected Catchments of South Africa	1. Evaluate erosion and sediment dynamics with particular attention to: a) Sediment sources, sinks, pathways and associated mechanisms; b) Sediment associated NPS impacts with particular emphasis on phosphates; c) Erosion and sediment delivery rates. 2. To determine controlling factors of sediment dynamics for different land uses with consideration of: a) Climate/weather patterns and variability; b) Combination of landscape elements on fluxes of sediments; c) Land use and management practices.	1. The key driver of soil erosion is rainfall intensity. 2. Splash erosion is important. 3. There is a correlation between landscape positions (slope gradient) and both unit-area runoff and soil losses. 4. Tree cover and surface litter reduce soil surface exposure.

Le Roux (2012)	Water Erosion Risk Assessment in South Africa: Towards A Methodological Framework	Implement a multi-process and multi-scale approach to support establishment of a methodological framework for South African conditions. The approach includes assessment of: (i) sheet-rill erosion at a national scale based on the principles and components defined in the (Revised) Universal Soil Loss Equation, (ii) gully erosion in a large catchment located in the Eastern Cape Province by integrating eleven factors into a GIS, and (iii) sediment migration for a research catchment near Wartburg in KwaZulu-Natal by means of the Soil and Water Assessment Tool	1. Twenty per cent (26 million ha) of South African land is classified as having a moderate to severe actual erosion risk. 2. Severe gully erosion affects an area of approximately 5 273 ha in the large catchment (Tsitsa Valley) of the Eastern Cape Province and highlights gully factors likely to emerge as dominant between continuous gullies and discontinuous gullies. 3. Cabbage plot in the upper reaches of a research catchment near Wartburg is a significant sediment source but is counterbalanced by sinks (river channel and farm dams) downstream. 4. A combination of poor vegetation cover and susceptible parent material-soil associations are confirmed as the overriding factors in South Africa, and not topography and rainfall
Vetter (2013)	Soil Erosion in The Herschel District of South Africa: Changes Over Time, Physical Correlates and Land Users' Perceptions	Establish: 1. How the extent and severity of soil erosion have changed over time, 2. How soil erosion varies within the district and what variables correlate with elevated levels of soil erosion, and 3. How the perceptions of the local people reflect the realities of degradation.	1. The extent and severity of erosion increased since 1950, with the area affected by erosion doubling in some areas between 1950 and 1969. 2. Soils derived from alluvium and sedimentary rocks were more eroded than soils derived from basalt and dolerite. 3. Flat or gently sloping areas were the most severely affected by erosion. 4. The fact that most areas had been ploughed and since abandoned and used for grazing livestock supports people's perception that the abandonment of cultivated land was a major factor leading to increases in severe forms of soil erosion.
le Roux and van der Waal (2020)	Gully Erosion Susceptibility Modelling to Support Avoided Degradation Planning	Model areas that are susceptible to gully development in the Tsitsa River Catchment, as well as estimate the sediment yield potential from the susceptible areas if gully development occurs.	More than 30 000 ha (7%) of the catchment is intrinsically susceptible to further gully development, consisting of drainage paths with a large contributing area and erodible duplex soils.

Mararakanye and Sumner (2017)	Gully Erosion: A Comparison of Contributing Factors in Two Catchments in South Africa	Assess the influence of factors contributing to gully erosion using Geographic Information System (GIS) and Information Value (InfVal) statistics from two catchments coded X12 and W55 in the Mpumalanga Province of South Africa	1. The findings in catchment X12 support a commonly held assumption that gully formation is influenced by duplex soils underlain by colluvium and alluvial deposits on a lower slope position where overland flow converges and accumulates, resulting in high soil moisture. 2. Gullies were also influenced by soils developed over weathered granite, gneiss and ultramafic rocks. 3. The influence of a granite rock was further highlighted in catchment W55 where there is a variable thickness of very deep Hutton dominant soil form and shallow Lithosols with sandy texture, on an area of moderate to steep slopes where overland flow converges and accumulates, with high stream power in overgrazed grassland.
Makaya (2018)	Remote Sensing of Gully Erosion in The Communal Lands of Okhombe Valley, Drakensberg, South Africa.	Assess remote sensing applications for detecting and mapping the spatial distribution of gully erosion in the communal lands of Okhombe Valley, Drakensberg, South Africa.	The application of remote sensing for soil erosion studies has significantly increased by 45% since the 1960s.
Parwada and van Tol (2020)	Mapping Soil Erosion Sensitive Areas in Organic Matter Amended Soil Associations in The Ntabelanga Area, Eastern Cape Province, South Africa	Map areas sensitive to erosion by water and rainfall erosivity after addition of organic matter (OM) in highly unstable soils	Organic matter confers soil resistance to erosion up to a certain period before losing its effectiveness.
Sepuru (2018)	Assessing The Use of Multispectral Remote Sensing in Mapping the Spatio-Temporal Variations of Soil Erosion in Sekhukhune District, South Africa	Assess the use of multispectral remote sensing sensors in mapping and monitoring the spatio-temporal variations in levels of soil erosion in the former homelands of Sekhukhune District, South Africa	1. The dominant geology type, Lebowa granite experienced more erosional disturbances than other geological types. 2. Slopes between 2-5% (Nearly level) experienced more erosion and vice-versa. 3. The relationship between TWI and eroded areas showed that more erosion occurred between 3 and 6 TWI values in all the seasons for the two years.

Phinzi *et al.* (2021)	Soil Erosion Risk Assessment in The Umzintlava Catchment (T32E), Eastern Cape, South Africa, Using RUSLE and Random Forest Algorithm	Assess soil erosion risk in the Umzintlava catchment using two independent methods, i.e. RUSLE and Random Forest (RF), and explore the relationship between soil loss and erosion factors as represented by different RUSLE parameters.	1. A considerable portion (>90%) of the catchment area is of 'very low' to 'low' erosion risk, while the remainder suffers 'moderate' to 'extremely high' erosion risk. 2. The LS-factor (slope length and steepness) showed strong correlation with soil erosion. This suggests that areas with steep slopes are the most vulnerable to hillslope erosion, whereas gully erosion is prominent in areas with gentle to flat slopes.
Malibe (2015)	The Use of Remote Sensing and GIS in Assessing the Impact of Land Use Change on Soil Erosion of Mhlathuze Catchment, South Africa	Assess the impact of land use changes on erosion in the catchment	The most vulnerable areas are the ones under cultivation as the topsoil is loosened by the agricultural activities.
Nciizah and Wakindiki (2015)	Physical Indicators of Soil Erosion, Aggregate Stability and Erodibility	Review literature on trends, new perspectives, gaps and conflicts in soil erosion studies in the South African context.	Aggregate stability is a widely used physical indicator of soil inter-rill erodibility.
Le Roux (2011)	Monitoring Soil Erosion in South Africa at A Regional Scale	Review mechanisms leading to sheet, rill and gully development	1. Erosion is a major soil degradation problem in South Africa. 2. A water erosion prediction map of South Africa.
Makaya *et al.* (2019)	Geospatial Assessment of Soil Erosion Vulnerability in The Upper Umgeni Catchment in KwaZulu Natal, South Africa	Assess and map soil erosion vulnerability in the upper uMgeni catchment of South Africa.	Approximately 41% of the study area has a considerable risk of soil erosion.
Ebhuoma *et al.* (2022)	Soil Erosion Vulnerability Mapping in Selected Rural Communities of uThukela Catchment, South Africa, Using the Analytic Hierarchy Process.	Assess and model soil erosion vulnerability based on the Analytic Hierarchy Process (AHP) approach in Hofenthal and Kwa Maye communities within the uThukela Catchment, South Africa.	1. Slope, vegetation cover, and rainfall had the most considerable influence on soil erosion with factor weights of 29, 23, and 18%, respectively. 2. High-risk soil erosion areas occupy 21% of the total study area, while very high-risk areas are about 14%, and the east and central areas are most vulnerable to soil erosion.

2.5 Soil Erosion Models

Soil erosion models are valuable analysis tools that scientists and engineers use to examine observed data sets and predict the effects of possible future soil loss. Reducing soil erosion is necessary for the maintenance of the integrity, stability and sustainability of ecosystems (Avwunudiogba and Hudson, 2014; FAO and ITPS, 2015; Global Soil Partnership, 2016; Caon and Vargas, 2017; Fu *et al.*, 2019). A variety of modelling technologies are available in the area of water erosion, ranging from solely qualitative models, to merely quantitative equations (Erpul *et al.*, 2013). Models are necessary to improve the scientific understanding of erosion processes. There are still a number of processes imperfectly understood and some parameters are still difficult to assess (Stroosnijder, 2004).

Soil erosion models present an opportunity for the development of prognostic land use and management strategies. This is because combating soil erosion and its attendant geomorphic hazards especially in mountainous regions is difficult and expensive (Avwunudiogba and Hudson, 2014). Soil erosion models simulate and evaluate the effects of land use practices on erosion and inform the basis for identifying the impacts of land uses on the soil. That contributes to the development of appropriate soil loss intervention plans. However, finding a universally applicable soil erosion model has remained elusive. Therefore, there are many erosion models, some of which are summarised in Table 2.3. That makes reviewing all of them an enormous task. Therefore, in-depth review is limited to the two models that are used in this research.

2.5.1 The Universal Soil Loss Equation (USLE)

The Universal Soil Loss Equation (USLE) (Wischmeier and Smith, 1958) was originally applied to the prediction of soil losses from agriculture in the USA in order to preserve soil resources, but has been extended for use in numerous countries (Kinnell, 2010). The extended use in other countries resulted in the improvement of the model including the Revised Soil Loss Equation (RUSLE) 1 and 2. However, the basics and principles remain the same. Hence this review will not focus on the distinction of the USLE variants.

The USLE represents an erosion model developed for the prediction of soil losses in an average long-term sense (Vantas *et al.*, 2019). The USLE is based on the knowledge of the physical characteristics of the field area under study, along with the prevailing cropping and management system. The USLE has been widely tested in field conditions, and therefore its validity has been established. Important aims for the equation were that each factor:

- could be represented by a single number;
- could be predicted from meteorological, soil, or erosion research data for each location; and
- must be free from any geographically oriented base (Renard *et al.*, 1997). The USLE is expressed in equation 2.6

Table 0.3: Summary of Selected Soil Erosion Models

Model	Acronym	Author & Year	Remarks
(Revised) (Modified) Universal Soil Loss Equation	(R)(M) USLE	(Renard *et al.* (1997)) Wischmeier and Smith (1958)	A Lumped Parameter Model developed in the USA by the USDA Natural Resources Conservation Service. It measures annual soil loss (Mg ha^{-1} yr^{-1}) from erosion on slopes in agricultural fields. Has been extensively applied worldwide. Has been successfully applied in GIS.
Soil Loss Estimator Model for Southern Africa	SLEMSA	Stocking *et al.* (1988)	A Lumped Parameter Model developed in Zimbabwe for the southern African region. SLEMSA measure erosion hazard (in Erosion Hazard Units (EHU) on agricultural fields. Successfully work with GIS
Erosion Productivity Impact Calculator	EPIC	Williams (1989)	A Lumped Parameter Model developed in the USA USDA Agricultural Research Service. Primarily developed to determine the relationship between erosion and soil productivity. Continuously simulates the erosion processes.
Kentucky Erosion Model	KYERMO	Hirschi and Barfield (1988)	A Distributed Parameter event-based erosion model developed to isolate important sub-processes within the overall erosion process.
Water Erosion Prediction Project	WEPP	Nearing *et al.* (1989) Flanagan and Nearing (1995)	A Distributed Parameter process-based continuous simulation model developed for estimating soil erosion by water on hillslopes. Detachment, transport, and deposition processes were represented
2-D Rainfall Erosion Model	EROSION 2D/3D	Schmidt *et al.* (1999)	A Distributed Parameter process-based model that calculates rainfall induced soil erosion and deposition on single slopes (2D) and small watersheds (3D).
Guelph Model for Evaluating the Effects of Agricultural Management Systems on Soil Erosion and Sedimentation	GAMES	Rudra *et al.* (1986)	A Distributed Parameter model developed in Canada as a screening tool for watershed management. It simulates erosion and deposition at the field and watershed scales.
European Soil Erosion Model	EUROSEM	Morgan *et al.* (1998)	A Distributed Parameter model developed as dynamic distributed model, able to simulate sediment transport, erosion and deposition in single storms for both individual fields and small catchments.
Limburg Soil Erosion Model	LISEM	De Roo *et al.* (1996)	A Distributed Parameter process-based continuous simulation model developed for estimating soil erosion by water on hillslopes. Needs a large amount of data
The Areal Nonpoint Source Watershed Environment Response Simulation	ANSWERS	Beasley *et al.* (1980)	A Distributed Parameter process-based continuous simulation model developed for estimating soil erosion by water on hillslopes. Needs a large amount of data.

$$A = \mathbf{R \times K} \times LS \times C \times P \qquad \mathbf{(0.6)}$$

Where:

A = average (mean) annual soil loss (Mg ha^{-1} yr^{-1}) over the long term (e.g., 20 years),

R = the rainfall–runoff "erosivity" factor (MJ mm ha^{-1} h^{-1}),

K = the soil "erodibility" factor (Mg ha h ha^{-1} MJ^{-1} mm^{-1}),

L and S = the topographic factors that depends on slope length and gradient,

C = the crop and crop management factor, and

P = the soil conservation practice factor.

The USLE uses four dimensionless factors to calculate soil loss as described by dimensioned rainfall and soil factors (Renard *et al.*, 1997; Kinnell, 2010). The LS, C and P are dimensionless multipliers used to adjust the value of R and K to other conditions (Kinnell, 2010). Therefore, the model works mathematically in two steps as demonstrated below.

2.5.1.1 Mathematical Operation of the Model

The USLE is based on the unit plot concept of 22.1m long 5.14 degrees uniform slope. Only R and K have units, MJ mm ha^{-1} h^{-1} and Mg ha h ha^{-1} MJ^{-1} mm^{-1}, respectively. The rest of the factors are dimensionless. The L, S, C and P are reduced variables that are mathematically forced to take on values of 1.0 for the unit plot (Kinnell, 2010). This approach brings a challenge to the application of the model in a visual representation using Geographic Information Systems (GIS). The other factors, which is L, S, C and P, are not entirely inert. Their contribution may be less than others but need to be considered for analytical processes. That is why factor weighting is crucial in GIS overlay analysis. Factor weighting is applied in this research.

The USLE first predicts erosion for the unit plot condition (A_1) using R and K only using equation 2.7

$$A_1 = R\ K \qquad \textbf{(0.7)}$$

The result is then multiplied by appropriate values of L, S, C and P to account for the difference between the area of interest and the unit plot using equation 2.8 (Kinnell, 2010).

$$A = A_1\ L\ S\ C\ P \qquad \textbf{(0.8)}$$

In effect, R is the independent variable in a regression model where the product of K, L, S, C and P combine to give the value of the regression coefficient (Kinnell, 2010). Therefore, changing the erosivity factor from the EI_{30} index has implications on the value of the other factors in the model. The R factor is critical because rainfall is the driving force of erosion and has a direct impact on the detachment of soil particles, the breakdown of aggregates and the transport of eroded particles via runoff (Kinnell, 2010; Kusumandari, 2014; Food and Agriculture Organisation (FAO) 2019). Detachment may be caused by raindrops impacting the soil surface or by flow shear. Downslope transport may be associated with drop splash (splash erosion) or by the interaction between raindrop impact and flow (raindrop-induced saltation and rolling) (Kinnell, 2010). The rainfall erosion process is as shown in Figure 2.4 with the entry point of this research indicated by the red arrow.

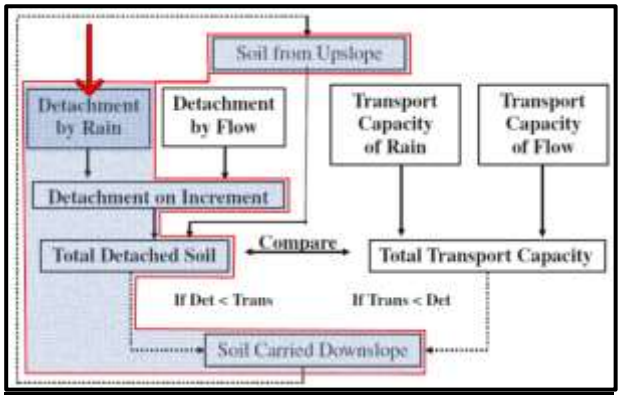

Figure 0.4: The Erosion Process (adapted from Renard *et al.*, 1997).

The way the raindrop impacts the surface and affects downslope transport is a function of the raindrop energy. Raindrop energy is determined by raindrop

characteristics. Raindrop characteristics are determined by different weather elements, including wind. Renard *et al.* (1997) admit that raindrop energy may substantially vary due to the wind component, especially up draughts and down draughts. Up draughts and down draughts are an important phenomenon in mountain regions' atmospheric circulation systems. In a nutshell, Table 2.4 shows the USLE, and the variables are explained below.

2.5.1.2 Variable Explanation

It has been indicated that erosivity (R) and erodibility (K) are the fundamental variables of the USLE. Erosivity explains about 80% of variations in average soil loss. Erodibility contribution, however, is not documented. However, both are considered important factors in explaining average annual soil loss.

2.5.1.2.1 Average (Mean) Annual Soil Loss

The potential long-term average annual soil loss (A) (Mg ha^{-1} yr^{-1}) is explained according to the "tolerable soil loss" limits. Soil-loss tolerance (T) is the maximum rate of soil erosion or soil loss that can occur in an area. It is the permissible soil loss or soil management sustainability value where soil loss does not considerably decrease soil fertility (Wischmeier and Smith, 1958; Li *et al.*, 2009; Morgan, 2009). It is the quantity of topsoil depth that can be lost without decreasing crop production over time. Wischmeier and Smith (1978) define soil tolerance as the maximum level of soil erosion that will permit a high level of crop productivity to be obtained economically and indefinitely. In short, soil tolerance is the maximum acceptable soil loss that still allows the long term maintenance of high level productivity.

Soil Tolerance ranges vary from very low to severe (Stone and Hibron, 2012). However, the values differ according to different circumstances that determine the impact of soil erosion (Li *et al.*, 2009). As such, some scientists (such as Larson, 1981; Skidmore, 1982) suggest the use of variable tolerance ranges that consider the effects

Table 0.4: The USLE in Brief

(# the basis for this is measurements of the velocities of water-drops of sizes ranging from one to six mm in diameter, falling in still air from heights of 0.5 meter to 20 meters (Laws and Parsons, 1943). ##used in the revised version of USLE (RUSLE*2*).)

Variable		Calculation formula	Unit of measurement	Scale range		Remarks and references
				Min	Max	
Erodibility (K)		$[2.1*10^{-4}*(12-OM)*M^{1.14}+3.25(s-2)+2.5(p-3)]/759$ OM = organic matter content (%) M = texture product [% silt*(% silt + % sand)] s = structure class p = permeability class. Length	Mg ha hr. ha^{-1} MJ^{-1} mm^{-1}	-	1.03	Highly dependent on the LS and R factors. If the nomograph is used the K-factor has a ceiling of 1.03 in very fine sand. This may differ if the formula is used.
Topography (slope) (LS)	Length Slope	$(x/22.13)^n$ *x* = slope length (m) 22.13 = slope length of the standard plot n = ratio of rill erosion to inter rill erosion (β/(1+β) $\beta=(\sin\theta/0.0896)/[3.0(\sin\theta)^{0.8}+0.56]$	m	22.13	-	The standard plot length given in the development of the model was 22.1 m. However, any slope length can be used.
	Slope	$3.0*(\sin\theta)^{0.8}+0.56$ Sin θ = the slope angle	Degree	-	180	The effect does not change significantly above 18^0
Vegetation / crop cover (C)		-	Dimensionless	-	-	This is generated using satellite images of land use land cover (Márquez *et al.*, 2019).
Conservation practice (P)		-	Dimensionless	-	-	Values for the support practice (P) factor are the most uncertain of all the factor values in the USLE (Renard *et al.*, 1997).
Rainfall erosivity (R)	Intensity (I_{30}) Energy (E)	Intensity (I_{30})	mm/time (hr/yr.)	13mm Or 6.5mm/15min	76.2 mm $hr.^{-1}$	Formula used when intensity is less than 76.2 mm/hr, if greater we use the max value (Renard *et al.*, 1997). Considered the only independent variable (Kinnell, 2010) in this model. The R unit is MJ mm ha^{-1} h^{-1} $yr.^{-1}$. Limit set because rain drop sizes do not continue to significantly increase beyond approximately 76.2 mm/hr (Nearing *et al.*, 2017).
	Energy (E)	$11.87+8.73\log_{10}i$# $0.29[1-0.72\exp(-0.082i)]$## i = rainfall intensity	MJ ha^{-1} mm^{-1}		0.283	
Annual soil loss (A)		R x K x LS x C x P	Mg ha^{-1} yr^{-1}	Very low (Tolerable)	Severe	

Table 0.5: Soil Tolerance Ranges (Stone and Hibron, 2012)

Soil Erosion Class	Potential Soil Loss (tons/hectare/year)
Very low (tolerable)	<6.7
Low	6.7 – 11.2
Moderate	11.2 – 22.4
High	22.4 – 33.6
Severe	>33.6

of floods, sediment deposition and eutrophication of waterbodies. Therefore, a dual tolerance, referred to as T_1 (lower limit) and T_2 (upper limit), is receiving prominence (Li *et al.*, 2009).

The lower limit of T value is the soil loss amount that permits soil productivity to reduce to a certain degree during the given period based on soil productivity, in accordance with soil formation rate in a thin soil or maintaining crop yields in a thick soil. The upper limit of T value is set in accordance with the environmental, social, economic and political demands, related to other erosion concerns that have reflected the social goals. The upper values' major factors include flood control, water pollution and acceptable sediment loads in rivers. Hence, soil tolerance levels vary, depending on various factors. Li *et al.* (2009) posit that soil tolerance is influenced by, among other factors, the

- rate of soil formation from parent material;
- rate of topsoil formation from subsoil;
- soil depth;
- the likelihood of rill and gully formation;
- sediment deposition within a field;
- sediment delivery from the erosion site;
- the availability of feasible, economic, culturally and socially acceptable, as well as sustainable soil conservation practices.

Generally, though, soils with deep, uniform, stone-free topsoil materials and/or not previously eroded have been assumed to have a higher tolerance limit than soils that are shallow or previously eroded.

2.5.1.2.2 Soil Erodibility (K) and Erosivity (R)

Soil erodibility (K) and erosivity (R) are the determinants of the unit of measurement for *A*. For example, if *K* is tons per hectare and *R* is for a year, units for *A* will be tons per hectare per year (t/ha/yr.). the two factors have been covered in detail in section 2.2.1.1 and 2.2.1.2, respectively. This section will, therefore, be brief.

Erosivity is rainfall-runoff erosivity factor, which is the rainfall erosion index. When factors other than rainfall are held constant, soil losses from cultivated fields are directly proportional to a rainstorm parameter EI - the total storm energy (E) times the maximum 30-min intensity (I_{30}) (Renard *et al.*, 1997; Kinnel, 2016). Rainfall factor used to estimate average annual soil loss (Mg ha^{-1} yr^{-1}) must include the cumulative effects of the many moderate-sized storms as well as the effects of the occasional severe ones (Renard *et al.*, 1997). The numerical value used for *R* must quantify the effect of raindrop impact and must also reflect the amount and rate of runoff likely to be associated with the rain.

Soil erodibility *K* (Mg ha hr. ha^{-1} MJ^{-1} mm^{-1}) is a measure of the susceptibility of soil particles to detachment and transport by rainfall and runoff (Renard *et al.*, 1997; Kinnell, 2010; Kusumandari, 2014). It is the soil-loss rate per erosion index unit for a specified soil as measured on a standard plot. The standard plot is 22.1m long 5.14 degrees uniform slope. The detachment of the soil particles is done by water, either as raindrops or overland flow.

2.5.1.2.3 Topography (LS), Vegetation Cover Management (C) and Land-use Support Practice

Topography is represented by slope length (L) and gradient (S). The slope length-gradient factor is given at a standard 22.1 m and 5.14 degrees, respectively. The steeper and longer the slope, the higher the erosion risk (FAO, 2019).

The vegetation cover-management factor (C) refers to specified cover and management to soil loss. The *C* factor is a ratio comparing the soil loss from land under a specific crop and management system to the corresponding loss from continuously fallow and tilled land (Wischmeier *et al.*, 1958; Renard *et al.*, 1997; Kinnell, 2010). The *C* Factor can be determined by selecting the crop type and tillage

method from prepared tables that corresponds to the field and then multiplying these factors together

The land use support practice factor (P) focuses on practices like contouring, strip cropping, or terracing. It reflects the effects of practices that will reduce the amount and rate of the water runoff and thus reduce the amount of erosion. The P factor represents the ratio of soil loss by a support practice to that of straight-row farming up and down the slope and is empirically determined.

Soil loss in the context of the USLE model is the mass of soil that passes across the downslope boundary of an area, divided by that area. However, detachment may occur within an area but not contribute to soil loss during an event if the transport processes are slow and hence do not cross the downslope boundary. This evokes the scale issue - temporal and spatial. Do we have to treat erosion from a hectare plot of land level or from a raindrop scale? At a raindrop scale, any soil particle displacement is erosion. At hectare level, the displacement must cross the plot boundary. Noteworthy, considering geomorphological time scales, any movement is important because effects are eventually noticed, albeit after a long period. Importantly, the effect, when noticeable, is a result of the cumulative small-scale displacements.

2.5.2 Soil Loss Estimation Model for Southern Africa (SLEMSA)

The SLEMSA is a technique to estimate and rank the potential of physical erosion over a specified area (Stocking *et al.*, 1988). It assumes that erosion is influenced by a combination of different factors, the dominant ones being climate, soil, relief and vegetation cover. Major control variables are selected for each system on the basis of dominance within its system and easy of measurement (Stocking, 1980). The control variables are subsequently combined into three sub-models - the bare soil sub-model, topographical sub-model, and the vegetation sub-model. The multiplication of the sub models then produces the main model as illustrated in Figure 2.5.

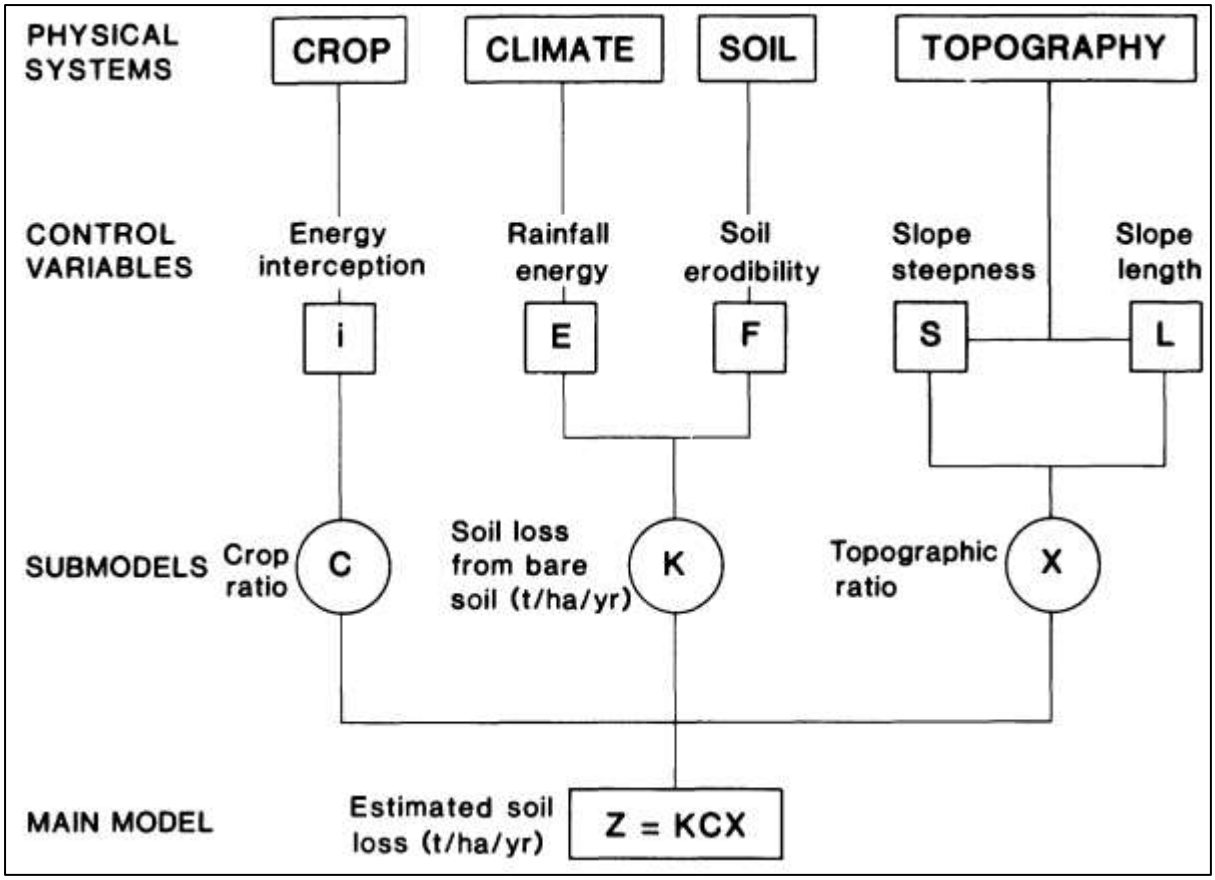

Figure 0.5: SLEMSA Model (Adapted from Stocking *et al.*, 1988)

Therefore, soil loss as depicted by SLEMSA is calculated as shown in equation 2.9.

$$Z = KCX \qquad \textbf{(0.9)}$$

Where:

Z = estimated soil loss or erosion hazard (Mg ha^{-1} yr^{-1})

K = soil loss as determined by rainfall erosivity plus soil erodibility (Mg ha hr ha^{-1} MJ^{-1} mm^{-1})

C = cover determined by vegetation (dimensionless); and

X = relief as determined by slope length (dimensionless) and steepness (dimensionless).

Of importance to this research is the rainfall energy (E) component of the K factor and the K factor itself. However, each component is elaborated on as it contributes to soil erodibility. This is because soil erodibility is a function of both intrinsic and extrinsic factors related to the soil (Renard *et al.*, 1997; FAO and ITPS, 2015). These

are the factors that guide the geomorphic classification in response to the first objective of this research. The following section focuses on each component. Soil erodibility has been covered previously under sections 2.2.1.1 and 2.5.1. Therefore, it will not be repeated here.

2.5.2.1 Vegetation Cover (C)

The vegetation cover factor (originally crop factor) (C) is the ratio of soil loss from a vegetated plot to that lost from bare fallow land (Stocking, 1980). Erosion is not a challenge in cultivated areas only, but in non-cultivated lands as well. This is especially true to fragile environments in the face of climate change. This research, therefore, replaces the crops factor in the original model with vegetation to represent all vegetation types, including crops.

The vegetation factor is derived from the energy interception factor, *i*, which provides an indication of the amount of rainfall that is intercepted by vegetation. It is determined by the vegetation type, yield and emergence date for crops, natural grasslands, dense pastures and mulches (Mughogho, 1998). It should be noted, however that it is difficult to allocate a constant C value because cover changes progressively through the seasons. Therefore, two *i* scenarios arise:

A. $$C = exp^{(-0.06i)}$$

when *i* = ≤50% or

B. $$C = \frac{2.3 - 0.01i}{30}$$

when *i* = > 50%.

It should be noted that different land uses may fall within the same geomorphic unit. To give the C factor value for such geomorphic unit, the percentage geomorphic unit area occupied by each specific land use is calculated. This gives the weighted C value for each land use whose total gives the C value for the geomorphic unit.

2.5.2.2 Relief (X)

Relief is a basic terrain factor that influences soil erosion. The relief factor, also called the slope or topography factor, consists of two elements – the slope gradient (S) and slope length (L). The relief factor considers the upslope contribution to run-off, the concavity and convexity of the topography and slope angle. The factors of

slope length and slope angle are combined in a single index (X) that expresses the ratio of soil loss under a given slope steepness and slope length.

Relief is an important factor as mountainous regions have well pronounced gradient and varied slope lengths. However due to the fact that slope length becomes increasingly less important as the variable increases (Stocking *et al.*, 1988) the maximum slope length considered is 100m (Stocking, 1980; Chakela and Stocking, 1988; Stocking *et al.*, 1988).

The slope-length factor grid (X) is created using equation 2.10

$$X = \sqrt{L} * \frac{(0.76 + 0.53 * S + 0.076S^2)}{25.65} \quad \textbf{(0.10)}$$

Where:

X = topographic ratio

L = slope length (m), and

S = slope gradient (%).

In a GIS approach, the slope length and slope steepness sub-factors are calculated from the filled DEM. The substitution of these factors into equation (2.9) will produce the relief (X) factor of the SLEMSA.

2.6 Soil Erosion in Mountainous Regions

Soil erosion by water is problematic in much of the hilly areas that are used as croplands on all continents (FAO and ITPS, 2015). Slope parameters are considered the most dominant factors influencing soil erosion in high altitude area. Therefore, elevation becomes a prominent feature of soil erosion models covering such areas. Knowledge of soil erodibility is an essential requirement for erosion prediction, conservation planning, and the assessment of sediment related environmental effects of watershed agricultural practices (Stanchi *et al.*, 2015).

Meghraoui *et al.* (2017) describe the Sabaa Chioukh Mountains in Algeria as dissected due to the irregular rains that characterize the Mediterranean semi-arid zones, the topography of the mountainous areas, the fragility of the soils, the absence of vegetation cover and the inappropriate cropping systems, as well as

frequent and violent floods. This is supported by Kulikov *et al.* (2020) who indicate that the erosion challenge in mountains is further exacerbated by mountain terrain and high precipitation values. Vegetation loss caused by overgrazing in mountainous rangelands worsens the soil erosion problem (Kulikov *et al.*, 2020). The Ourika watershed is characterized by higher than average flood flows, a rugged topography, a sparse vegetation cover and a friable substrate that makes it vulnerable to soil erosion.

One challenge with mountainous regions is data scarcity, especially rainfall data (Schönbrodt-Stitt *et al.*, 2013; Bagalwa *et al.*, 2021). This is apparent on the Soutpansberg range where most weather stations are concentrated on the southern slopes. This leaves analysis in the other areas to be based on interpolation. Schönbrodt-Stitt *et al.* (2013) estimated rainfall erosivity using regression analysis combined with elevation bands derived from a digital elevation model. This after data on rainfall were only obtainable in daily records for one climate station in the central part of the 3200km^2 Yangtze River (China) catchment and five stations in its surrounding area.

Rainfall erosivity is mainly controlled by rainfall amount and elevation (Schönbrodt-Stitt *et al.*, 2013; Bagalwa *et al.*, 2021). Rainfall amount is influenced by elevation. Higher elevation areas receive more rainfall due to the orographic effect (Berger *et al.*, 2003; Kabanda, 2004; Sobel, 2012; Kephe *et al.*, 2016). Hence, mountainous areas are more vulnerable to water erosion. For example, annual soil loss exceeds 20 t/ha^{-1} yr^{-1} in the Mountainous regions of northern Morocco and varies between 10 and 20 t/ha^{-1} yr^{-1} in the pre-Rif regions and 5 and 10 t/ha^{-1} yr^{-1} in Middle and High Atlas regions (El Jazouli *et al.*, 2017). This is on the high side compared to the average of 12 t/ha^{-1} yr^{-1} in South Africa. However, the mountain soil loss is in line with the global soil loss of 21.5 t/ha^{-1} yr^{-1} (FAO, 2015b). However, the inclusion of wind in the soil erosion estimation models may significantly impact this estimated amount.

2.7. The Wind Driven Rain Concept

In calm windless weather, raindrops fall vertically. This gives the usual assumption that water and wind erosion have little in common (Stroosnijder and Gabriels, 2004a). However, WDR is very complex and characterised by a high spatial and

temporal variability (Blocken and Carmeliet, 2010). As such, WDR is still an active research area, and much work remains to be done. There is growing evidence (see Stroosnijder and Gabriels, 2004a; Erpul *et al.*, 2013; Iserloh *et al.*, 2013; Marzen, 2017) of interaction between water and wind in erosion. Natural rain events often occur as rainstorms, adding a driving component to the falling raindrops (Ries *et al.*, 2010; Sobel, 2012; Iserloh *et al.*, 2013; Zorn and Komac, 2013). The wind makes the raindrop path oblique (Hens, 2010). The vertical component is precipitation, and the horizontal component is called wind-driven rain (WDR). Wind driven rain is a principle rooted in the building construction engineering field where WDR affects building facades.

Wind-driven rain refers to raindrops falling through the atmosphere under wind conditions. Wind affects the fall speed and inclination of individual raindrops. The wind causes the raindrops to move at an oblique angle to the vertical under the effects of both gravitational and drag forces (Erpul, 2013; Montero-Martínez and García-García, 2016). Figure 2.6 illustrates the effect of wind on raindrops.

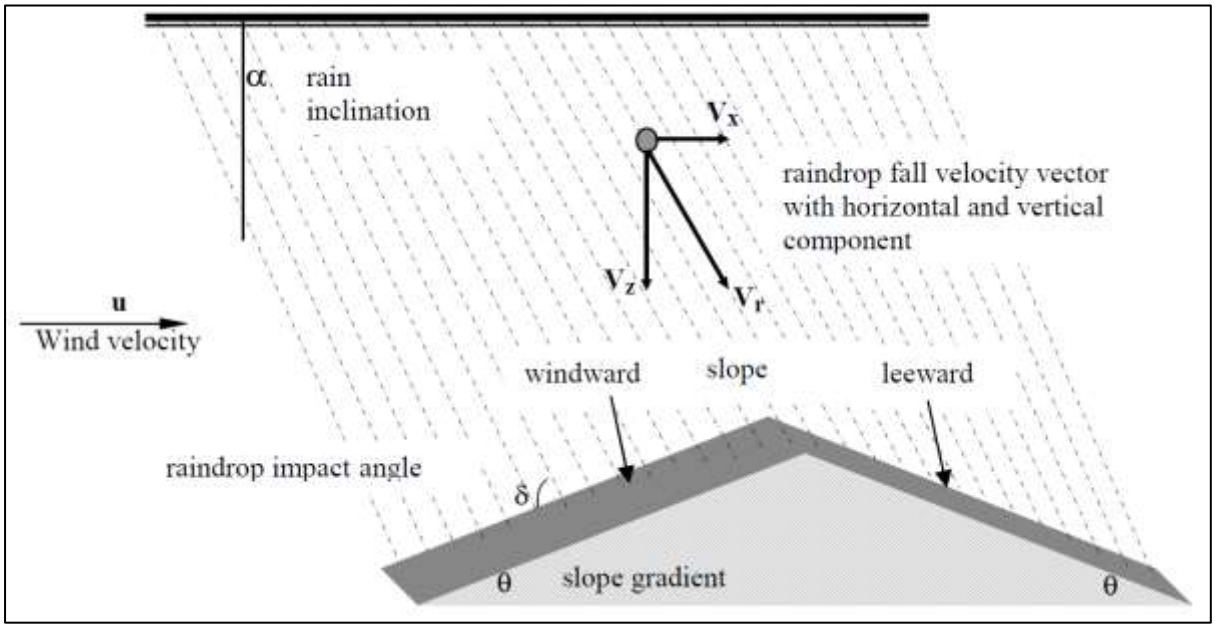

Figure 0.6: Schematic Representation of Wind Driven Rain (Erpul, 2013)

Models for estimating soil losses from the combined force of raindrop impact and wind transport have recently been developed. As such, significant studies of wind-driven rain (WDR) erosion processes have been conducted during the past few years (Erpul *et al.*, 2013). Work performed in a wind tunnel rainfall simulator at the

International Centre for Eremology (ICE), Ghent University, Belgium is one such example. The work focuses on the combined effects of wind and rain. The objective of the research is to understand WDR mechanisms and to develop a process-based erosion model.

Visser and Cornelis (2004) compiled papers on wind and rain interaction in erosion. Stroosnijder and Gabriels (2004a) highlighted the need for future work on wind and water interaction in erosion models. Both underscored the significant need for the development of a combined wind and water process-based erosion prediction model. This builds from the reality that most rain in tropical regions occurs as storms. The joint occurrence of wind and rain causes raindrops to travel through the atmosphere at an oblique angle as they approach the ground surface (Blocken and Carmeliet, 2004). Wind Driven Rain considers the raindrop, whose physical properties are easily and significantly affected by wind, as the main eroding agent (Marzen *et al.*, 2015). Wind affects the size distribution, energy, inclination and intensity of raindrops.

The amount of rain drops that eventually reaches the ground surface is a function of wind velocity and ground surface geometry, especially gradient and aspect (Erpul, 2013). The slope gradient can be positive or negative. A positive slope gradient indicates a windward slope while a negative gradient represents a leeward slope. A leeward slope implies a raindrop deficit with same values of slope gradient and raindrop inclination. This emphasizes the fact that the rate of WD raindrop impact on any surface is determined by the rate of raindrop inclination caused by horizontal wind velocity, slope gradient and slope aspect. For an understanding of dynamics of wind-driven raindrop, one needs to know the full spectrum of forces acting on the raindrops entering a wind field as elaborated below.

2.7.1 Raindrop Impact Frequency

The amount of rain drops that eventually reach the ground surface is a function of wind velocity and ground surface geometry, especially gradient and aspect as well as many other meteorological factors. Raindrop impact frequency is computed using formula 2.11

$$f = \frac{I_a}{I} = \cos(\alpha \mp \theta) \qquad (0.11)$$

Where:

f = impact frequency/efficiency

I = rainfall intensity in respect to a plane normal to the rain vector (mm/hr)

I_a = actual intensity (mm/hr)

α = raindrop inclination from vertical (degrees)

θ = slope gradient (degrees).

2.7.2 Angle of Rain Incidence

The mean angle of rain incidence between wind vector and the plane of the surface is calculated as a function of the rain inclination, slope gradient and aspect and given by the cosine law of spherical trigonometry (Erpul *et al.*, 2005).

$$\cos(\propto \mp\theta) = cos \propto cos\theta \pm sin \propto sin\theta \cos(z_{\propto} \mp z_{\theta}) \qquad (0.12)$$

Where

$z_{\propto}$ = direction from which rain is falling

z_{θ} = direction (aspect) towards which the plane of surface is inclined.

The vertical impact pressure of a WD raindrop differs from that of a vertically falling raindrop because of the horizontal and vertical velocities that incline the WD raindrop from the vertical. In general, if a raindrop falls at an angle of incidence (α ∓ θ), only the component of velocity vcos(α ∓ θ) normal to the surface gives rise to an impact pressure

2.7.3 Raindrop Impact Velocity

For an understanding of dynamics of wind-driven raindrop, one needs to know the full spectrum of forces acting on the raindrops entering a wind field. A two–dimensional analytical model to estimate raindrop trajectories, considering the forces

that act on a raindrop in both vertical directions (z) and horizontal along wind (x) is used as illustrated in formula 2.13 and 2.14.

$$m\frac{\partial^2 z}{\partial t^2} = mg - \rho_a g" - \frac{1}{2}c_d\rho_a(\frac{\partial_z}{\partial_t})^2 A \qquad \textbf{(0.13)}$$

$$m\frac{\partial^2 z}{\partial t^2} = -\frac{1}{2}c_d\rho_a(\frac{\partial_z}{\partial_t})^2 A \qquad \textbf{(0.14)}$$

If raindrops are considered spheres of diameter *d* (m) and density ρ_w (kg m^{-3}), then

m = mass of the raindrop = $(\rho_w /6)\pi d^3$ (kg);

A = projected frontal area = $\pi d^2/4$ (m^2) where *d* is raindrop diameter (m);

$\forall$ = raindrop volume = $\pi d^3/6$ (m^3)

g = gravitational acceleration (m s^{-2})

ρa = air density (kg m^{-3})

C_d = drag coefficient on the raindrop = function of Reynolds number (Re) = $\frac{\rho_a{}^{ud}}{\mu}$ where

u = free stream wind velocity (m s^{-1}) and μ = viscosity of air (N s m^{-2}).

An expression for the horizontal raindrop velocity with respect to the fall height, (∂x/∂t)/∂z, is derived using equations 2.13 and 2.14 to form equation 2.15

$$\frac{\partial x/\partial t}{\partial z} = \frac{3C_d\rho_a}{4_d\rho_w}\left[\left(\frac{\partial x}{\partial t}\right) - u\right] \qquad \textbf{(0.15)}$$

Where:

∂x = horizontal raindrop impact velocity

$$= u*t \qquad \textbf{(0.16)}$$

∂t = raindrop terminal velocity in the vertical direction (m/s)

$= 3.78D^{0.67}$ (Ulbrich, 1983)

Where:

D = raindrop diameter (m)

3.78 and 0.067 are constants

$-0.16603 + 4.91844d - 0.888016d^2 + 0.054888d^3$ (Dingle and Lee, 1972)

Equations 2.9 and 2.10 show that the forces acting on the raindrop are due to gravity, buoyancy, and drag. When raindrops impact a soil surface, the pressure builds up at the raindrop-soil interface. Pressure acting on the contact area leads to a force normal to the soil surface and forces the splash droplets to escape laterally, entraining soil particles. Rain splash detachment results from these splashes (Huang et al., 1982; Moss and Green, 1983).

Raindrop size can be expressed as a function of rainfall intensity (Straube, 2000). Iffa and Tariku (2016) used the following formula to calculate the predominant drop size, also called median drop size.

$$D_{50} = a \times c \qquad \textbf{(0.17)}$$

Where 0.69, a, p and n are constants. Their experimentally determined averages are:

$a = 1.3*I^{0.232}$

$c = 0.69^{\frac{1}{n}}$

n = 2.25 (Blocken et al, 2005)

I = intensity (mm/hr)

$= 0.2*v_w*I_{Prec}$ (Hugo, 2010; Straube and Burnett, 2000)

Where:

v_w = wind speed (m/s)

I_{Prec} = average precipitation intensity obtained by dividing precipitation amount by time (mm/hr).

Raindrop impact velocity should be calculated for all hours with at least 0.5 mm of liquid precipitation and 1.0 m/s or more wind speeds (Underwood and Meentemeyer, 1998). This provision ensures that trace amounts of precipitation are not included in WDR events. The literature does not discuss WDR in terms of trace rainfall, therefore only more-significant episodes are included (Underwood and Meentemeyer, 1998). However, for comparative purposes with the WFR models, the cut off was set at 12.5 mm/hr as set by USLE and SLEMSA

2.7.4 Rain Splash Detachment

Detachment of soil particles caused by rains plash is as an initiating process of soil erosion (Pedersen and Hasholt, 1995). If it is assumed that the effect of wind shear stress on the detachment is insignificant when compared to the effects of the impacting raindrops, the rain splash detachment rate (D) at which soil particles are supplied into the air is a linear function of the raindrop kinetic energy.

Erpul *et. al* (2002, 2003) proposed the KE model for WDR. Soil detachment by raindrop splash is a direct consequence of precipitation kinetic energy (Pedersen and Hasholt, 1995). The amount of soil particles detached positively correlates with rainfall energy and raindrop energy is an important index to evaluate the degree of soil erosion caused by rainfall (Fox, 2004; Fu *et al.*, 2019). Rainfall intensity, raindrop energy, and their variations in time and space have important effects on the prediction of rainfall erosion. However, the KE for WDR already incorporates intensity, area and exposure time. Therefore, the KE is the erosivity, as shown in equation 2.18.

$$KE = \frac{\rho_w}{2} ItAV^2 \qquad \textbf{(0.18)}$$

Where:

KE = kinetic energy (J);

ρw = raindrop density (kg m^{-3})

I = rain intensity (m s^{-1}).

t = exposure time (s)

A = projected frontal area. A = $\pi d^2/4$ (m^2) where d is raindrop diameter (m)

V = raindrop impact velocity (m s^{-1})

Alternatively, rain splash detachment can be given as in equation 2.16 as proposed by Erpul (2003).

$$D = K\left\{\frac{1}{2} m[V^2{}_r \cos^2(\propto \mp\theta)]\right\} 1$$

(0.19

Where:

K = soil detachment factor,

$$V^2_r = V^2_z + V^2_x$$

Where:

$$V_z = \partial z/\partial t$$

and

$$V_x = \partial x/\partial t$$

Since a given number of raindrops (Ξ) strike a soil surface under wind-driven rain, the total kinetic energy flux E_{rn} (W m^{-2}) is described by $E_m = I_a E_r = I E_r \cos(\alpha \mp \theta)$, equation 2.16 becomes:

$$D = KX\{\frac{1}{2}m[V^2{}_r \cos^3(\propto \mp\theta)]\} \qquad \textbf{(0.20)}$$

Where:

X = the number of raindrops and can be calculated from rain intensity and exposure time as

$$\mathbf{X} = \frac{\boldsymbol{ItA}}{\forall} \qquad \textbf{(0.21)}$$

The maximum soil detachment rate for the case of the rain splash transport occurs when there is no water running on the soil surface. Therefore, considering the effect of shallow overland flow depth on the detachment, the contribution of impacts of wind-driven raindrops in inter rill flow-driven sediment transport process can be given by equation 2.22.

$$D_{\mathrm{f}} = KX\{\frac{1}{2}m[V^2{}_r \cos^3(\propto \mp\theta)]\}\mathrm{f} \qquad \textbf{(0.22)}$$

Where:

$D\phi$ = the soil detachment term for overland flow-driven transport,

ϕ = the parameter introduced to distinguish the raindrop impact on a bare soil surface from the impact on a surface with a shallow water depth.

2.8 The Knowledge Gap

Soil erosion is among the most critical environmental hazards problem in South Africa (Le Roux, 2011). Large areas of land may be rendered unproductive, or at least economically unproductive, if erosion is not tamed (Lal and Elliot, 2017). Therefore, analysis of the factors influencing soil erosion is the foundation of erosion control (Yao *et al.*, 2016). Rainfall erosivity, land use or vegetation cover, soil erodibility, slope length and steepness or topography, and conservation practices influence soil erosion (Wischmeier and Smith, 1958; Stocking *et al.*, 1988; Renard *et al.*, 1997; Kinnell, 2010). However, rainfall erosivity and soil erodibility are the principal drivers of soil erosion (Renard *et al.*, 1997; Kinnell, 2010; Yao *et al.*, 2016). Hence the analysis of the two factors is essential for soil loss management.

Soil erodibility and rainfall erosivity analysis is important in policy terms because it indicates areas which have potential erosion risk. Knowledge about the extent of soil loss and the spatial distribution of soil erosion hot spots is essential to prevent water pollution by diffuse matter fluxes (Schönbrodt-Stitt *et al.*, 2013). This is because a few erosive events can contribute to a significant share of erosion (Vantas *et al.*, 2019).

However, soil erodibility is often inappropriately or inaccurately applied in describing soil loss caused by different soil erosion component processes and mechanisms (Wang *et al.*, 2013). Soil erodibility indicators are related to intrinsic soil properties and exogenic erosional forces. They are the topographical parameters (such as slope gradient and curvature), field characteristics (size and shape), and the physical properties of the soil (FAO, 2019). These have not received special focus but have been treated as components of whole models. This research provides that special focus.

In addition, rainfall erosivity research has mainly been inclined towards the spatial characteristics. This research adds the temporal aspect in terms of analysis of the occurrence of high erosion risk as well as the contribution of wind. Potentially erosive rainfall temporal distribution is crucial because some short duration events can significantly contribute to erosion (Vantas *et al.*, 2019). Therefore, the spatio-

temporal analysis of soil erodibility and rainfall erosivity is an essential step towards proposing appropriate erosion mitigation and soil management measures.

2.9 Chapter Summary

Soil is the basis of all livelihoods. However, erosion remains a serious threat to the existence of all life forms. There is no consensus on the extent and severity of soil erosion. Estimates vary from as low as 20 to as high as 200 Gt global soil loss per annum. However, there is convergence that the soil resource is under threat. The threat emanates from erosion, mainly by water.

Water is readily available in different areas in different forms and causes prolonged erosion. Prolonged erosion causes irreversible soil loss over time, reducing the ecological (e.g. biomass production) and hydrological functions (e.g. filtering, infiltration and water holding capacity) of soil. Such damage is detrimental to the global ecosystem because soil is the incubator of all primary production. As such, understanding soil erosion is important to manage the potential challenges.

Soil erosion is a natural complex process that is controlled by both intrinsic and extrinsic soil parameters. Mainly driven by rainfall energy, the way soils react to the energy to erode it is critical. The rainfall energy is called erosivity while the soil's resistance to erosion is erodibility. Intrinsic soil erodibility is determined by the soil texture and organic matter content(Bryan, 2000). Soil texture is determined by particle size distribution, soil structure, organic matter content and permeability. The extrinsic factors that influence soil erodibility include (lithology) geology, slope, land-use-land-cover and hydrography. These represent the geological setting, slope position, exposure to raindrops (erosion exposure) and landform position, respectively, in this research.

The soil erodibility and rainfall erosivity form the backbone of soil erosion models. The main models considered for this research are the Universal Soil Loss Equation (USLE) and the Soil Loss Estimation Model for Southern Africa (SLEMSA). The USLE was developed in the USA while SLEMSA was developed in Zimbabwe. Although technically the same. The two models treat erodibility and erosivity differently. The difference in the models is more apparent when considered under

mountainous conditions. However, both models treat erosivity from a wind free rain point of view.

Wind free rain assumes that wind does not play a role in influencing rainfall erosivity. However, the concept of Wind Driven Rain indicates that storms usually occur with wind. The wind has an influence on raindrop energy. Consequently, it is revealed that there is need for erodibility and erosivity analysis in a mountainous environment. The need emerges from the influence of mountains on soil erodibility characteristics, rainfall erosivity as well as wind distribution. How the research is carried out is elaborated in the methodology chapter that follows hereafter.

: RESEARCH METHODOLOGY

3.1 Introduction

The starting point for the research described here is the establishment of the erodibility characteristics of the Soutpansberg range. This addresses the first objective of the research. The second objective is addressed by revealing the distribution of rainfall erosive potential on the mountain range. This is followed by establishing the effect of topography on wind speed and rainfall erosivity on the mountain range which addresses the third objective. The research wraps up with comparing USLE and SLEMSA rainfall erosivity incorporating WDR erosivity to establish the influence of wind on soil erosion.

This research employs a variety of tools. The methods followed are strictly determined by the data type needed to achieve the specific objectives of the research. The research employs and follows the dictates of four main tools namely geomorphological mapping using ArcGIS, QGIS and SAGAGIS software, soil erodibility as well as rainfall erosivity assessment using the Soil Loss Estimation Model for Southern Africa (SLEMSA), the Universal Soil Loss Equation (USLE) and Wind Driven Rain (WDR). Comparison between different models were statistically assessed using multiple analysis of variance (MANOVA) (Pallant, 2016; Lund and Lund, 2018; Mathews, 2018). This chapter elaborates the methodology.

3.2 Research Design

This research was largely quantitative and is divided into three main stages. These are proposal development, data collection, data analysis and results presentation. Data for the research are predominantly secondary because of the diagnostic nature of the research. Primary data are, however, integrated into the research for validation of the diagnostic soil erosivity and erodibility computations done from secondary data.

Proposal development was the incarnation of the research idea. It is fed from literature search that focused on soil erosion models and the concept of Wind Driven Rain. The models of special focus are the USLE and SLEMSA. The special focus on the two models is premised on the worldwide use of USLE (Breetzke, 2004) and the

development of SLEMSA in southern Africa in response to USLE applicability in a different climatic environment. The Soutpansberg range is in South Africa.

Data collection is an important step in the execution of research. The diagnostic nature of the research demanded the use of predominantly secondary data. The variables of focus were determined by the specific objectives. The specific objectives also directed the analysis methods adopted to deliver the final outcomes of the research. The finer details of the research execution and outcomes are presented in the subsequent sections of this chapter. The research design is presented in Figure 3.1.

3.3 Data Needed and Data Sources

Soil, rain and wind speed are paramount in this research for the computation of soil erodibility as well as the rainfall – runoff erosivity, called the R factor. In wind free rain (WFR), erosivity is the rainfall erosion key. When factors other than rainfall in WFR are held constant, soil losses are directly proportional to rainfall erosivity (Renard *et al.*, 1997). However, in wind driven rain (WDR), wind plays an additional role in determining storm erosivity depending primarily on wind speed (Lyles and Allison, 1976; Erpul *et al.*, 2013; Marzen *et al.*, 2017). The WDR concept explains the energy derived from the movement of the raindrop through the atmosphere (Lyles and Allison, 1976; Guo *et al.*, 2013). Precipitation and wind speed data from 45 weather stations on the Soutpansberg range were obtained from the South African Weather Service for use in the computation of rainfall erosivity. The record used for this research ranges from January 2000 to November 2019.

The data were comprised of daily readings for all stations and hourly readings for 5 stations. The 5 stations' data were used for the computation of WDR storm erosivity. The daily data are used for the computation of daily erosivity using USLE and SLEMSA models. It is important to mention that the rainfall data used to compute USLE, SLEMSA and WDR R factor considered potentially erosive storms only, those that record at least 12.5 mm per hour (Renard *et al.*, 1997).

The 12.5 mm per hour cut off was considered for USLE, SLEMSA and WDR erosivity computation to allow comparability. The WDR cut off is 0.5 mm/hr and 1m/s

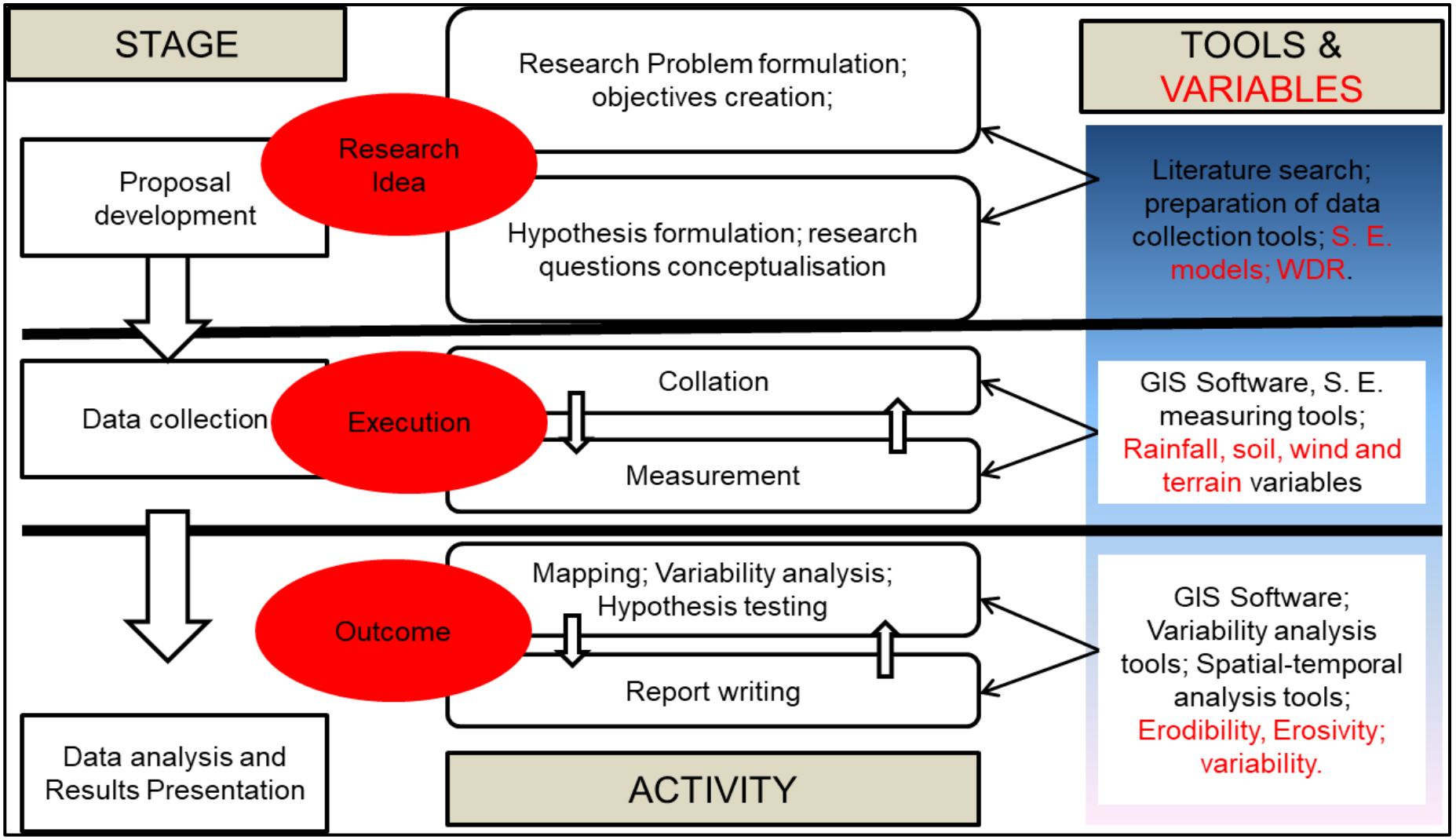

Figure 0.1The Research Design Flow

for rain and wind speed, respectively (Underwood and Meentemeyer, 1998). This would have resulted in more storms for WDR than the other models. Therefore, the same number of storms had to be considered for comparison using the USLE cut off. This resulted in 383 records across the five stations over the 20 year period.

Wind, eroded soil and rainfall data were collected during rainstorms. Wind and rainfall data were measured by the South African Weather Services weather stations while detached soil was collected by splash cups. The data needed for the characterisation of soil detachability on the Soutpansberg range consist of five factors. The first factor is the intrinsic erodibility (K factor) as guided by the USLE and SLEMSA. The K factor for USLE is a function of particle size distribution, soil structure, organic matter content and permeability (Wischmeier and Smith, 1958; Breetzke, 2004; O'geen, 2006; Kusumandari, 2014). For SLEMSA, they are soil type, texture and annual rainfall kinetic energy (Stocking, 1980; Stocking *et al.*, 1988; Morgan, 2009). Texture is an important intrinsic soil characteristic. It influences the water holding capacity of the soil as well as infiltration and through flow rates (Kusumandari, 2014). The Harmonized World Soil Database (HWSD v 1.21) layer was obtained from The International Institute for Applied Systems Analysis (IIASA) online database for all the soil data.

In addition to the online soil data, splash cups were set up at University of Venda experimental farm as well as at Tshivhase Tea Estate from November 2020 to March 2021. The splash cup design was adapted following Morgan (1981) and is elaborated in section 3.3.1. A further 1kg soil sample was collected for hydrometer analysis. The other four factors that affect soil erodibility are extrinsic. The extrinsic factors are topography (slope position), hydrography (landform position), geology as well as land-use-land-cover (rain exposure). The extrinsic actors are derived from the other factors considered for soil erosion in both USLE and SLEMSA as well as literature (see Mitasova *et al.*, 2013; Kusumandari, 2014; Li *et al.*, 2017; Ban *et al.*, 2020; Zhu *et al.*, 2021). There was strict restriction to factors that affect soil erodibility only. However, it is acknowledged that the same factors ultimately affect erosion.

Slope data were derived from the 30m pixel size Shuttle Radar Topography Mission (SRTM) Digital Elevation Model (DEM) obtained from National Geo-Spatial

Information (NGI). The derivations were done in SAGA GIS. Hydrographical systems indicate places where water has a tendency of accumulating. Water is the main driver of soil detachment in water erosion. Soil detachment is high where water is concentrated (Mitasova *et al.*, 2013; Li *et al.*, 2017). Therefore, hydrographical parameters indicated the landform position. Hydrography systems shape files were obtained from Department of Water Affairs, Forestry and Fisheries (DWAFF). However, for line density calculation, river systems were derived from the DEM. The fluvial channels were extracted through semi-automatic calculations in SAGA GIS and the Strahler's hierarchical classification of channels was applied at level seven (Araujo and Pereira, 2018). This was necessary to include waterways that are not captured in the DWAFF system.

The geology of an area determines soil erodibility by influencing slope stability (Shahabi *et al.*, 2016) and vertical water movement (Kheir *et al.*, 2008). Rock permeability and porosity influence percolation and runoff. Percolation has a direct effect on soil saturation and soil detachment by surface water as either raindrops or overland flow (see Kheir *et al.*, 2008). A rock that allows percolation promotes infiltration hence delays overland flow and soil detachment. Geological data were downloaded from South African Geosciences online database.

Land uses are human activities in fulfilling human requirements (Arsyad, 2010). Land management practices influence soil susceptibility to erosion (Stanchi *et al.*, 2013). Land uses affect land cover. Land-use-land-cover data were obtained from the South African National Land Cover 2018 dataset accessed online on the Department of Forestry, Fisheries and Environment website.

3.3.1 Splash Cup Design

The objective was to establish the influence of wind on rainfall erosivity. Therefore, empirical evidence of erosion had to be collected. This was achieved through the setting up of splash cups (also called the Morgan tray) at the University of Venda Experimental Farm and Tshivhase Tea Estate. The corresponding weather stations for the places are Thohoyandou and Tshivhase, respectively.

The splash cups were an adapted Morgan (1981) design. They were made from plastic bowls cut to the bounded instrument specifications. The bounded instrument specifications are such that only soil detached from a defined area can be collected in the splash cup (Fernández-Raga *et al.*, 2019). This would ensure easy of computations and extrapolation of rate of detachment. This is because the collected sediment would have come from a known surface area.

The centre of the bowl was cut to create an inner hollow cylinder of 10 cm diameter (Morgan, 1981). This gives 78.54 cm^2 from where soil detachment may occur. The outer part has a 30 cm diameter, creating a catching tray. The central hollow cylinder has a circumference guarded by a 2 cm high vertical lining that prevents collected soil from slipping back out. The same lining also prevents overland flow from interfering with collected sediments.

The catching tray has a 30 cm diameter. The edge of the catching tray is 5 cm high to prevent any splash form either leaving the tray or entering from outside. The base of the catching tray is perforated to create weep holes to drain water as shown in Figure 3.2.

The weep holes were plugged with a cotton cloth such that water would easily drain out leaving the soil. The splash cups were kept on the ground by at least three anchor pins. The pins were used in such a way that they do not interfere with the operations of the splash cup. Figures 3.3 and 3.4 illustrate the field settings of the splash cups. The data collected as alluded to in sections 3.3 and 3.3.1 were analysed as indicated in the following section.

Figure 0.2: Splash Cup Design (adapted from Morgan, 1981)

Figure 0.3: Splash Cup Set up Demonstration

Figure 0.4: Splash Cup Set-up in the Field

3.4 Data Analysis and Tools

Data analysis and the tools thereof was guided by the objectives of the research. Therefore, this section is divided into four sections. The first section addresses the first objective through geomorphic classification. The second section explains how the spatial-temporal characteristics of potentially erosive rain were revealed. The third section elaborates how the influence of topography on wind and rainfall was analysed. The fourth section deals with determining the influence of wind on soil erosion.

3.4.1 Geomorphic Classification

Geomorphic classification was done to illustrate the erodibility characteristics of the Soutpansberg range. This was to address the objective to classify geomorphic features of the Soutpansberg range. The classification was based on five factors. The factors are both intrinsic and extrinsic to the soil.

The intrinsic factor is the K factor. The K factor for USLE is a function of particle size distribution, soil structure, organic matter content and permeability (Wischmeier and Smith, 1958; Breetzke, 2004; O'geen, 2006; Kusumandari, 2014). For SLEMSA, they are soil type, texture and annual rainfall kinetic energy (Stocking, 1980; Stocking *et al.*, 1988; Morgan, 2009). The extrinsic factors are geology, slope, land-use-land-cover and hydrography (Stocking, 1980; Chakela and Stocking, 1988; Stocking *et*

al., 1988; Renard *et al.*, 1997; FAO and ITPS, 2015). These are analysed to produce maps that indicate the geological setting, slope position, exposure to raindrops (erosion exposure) and landform position, respectively.

Except for geology and land-use-land cover factors, data processing and analysis for geomorphic classification followed three stages of GIS analysis as guided by Najwer and Zwoliński (2014) and Zwoliński *et al.* (2019) as shown in Figure 3.4. Based on the five factors that influence soil erodibility indicated in section 3.3, the first stage was the geo-computation and extraction of factor indicator elements from the data source. The first stage included creating the various indicator element field on the attribute table of the various factor maps in QGIS.

A new field for the hydrology map where the shoreline development ratio (DL) and average slope was created. The ArcGIS Spatial Analyst computations for drainage density and point density as well as the SAGA GIS derivation of the Topographic Wetness Index create raster layers. All the raster layers were added together in the Raster Calculator to create on hydrography layer. The class field was added to the geology and land-use-land-cover vector maps attribute tables. The classification was done from expert knowledge (Zwoliński, 2004; Najwer and Zwoliński, 2014; Zwoliński *et al.*, 2019) of rock hardness and how raindrops are affected by land use and land cover. Two erodibility fields were added on the soils vector map attribute table. One is for the USLE, and the other one is for SLEMSA. The step by step computation of the different factor indicator elements is covered in section 3.4.1.1.

The second stage was the normalisation of each factor indicator element into five classes using Jenk's Natural Breaks (Jenks, 1967). Except for slopes that were derived from a DEM and produced as a raster layer, normalization started with rasterising the factor map using the factor indicator element as the rasterization field.

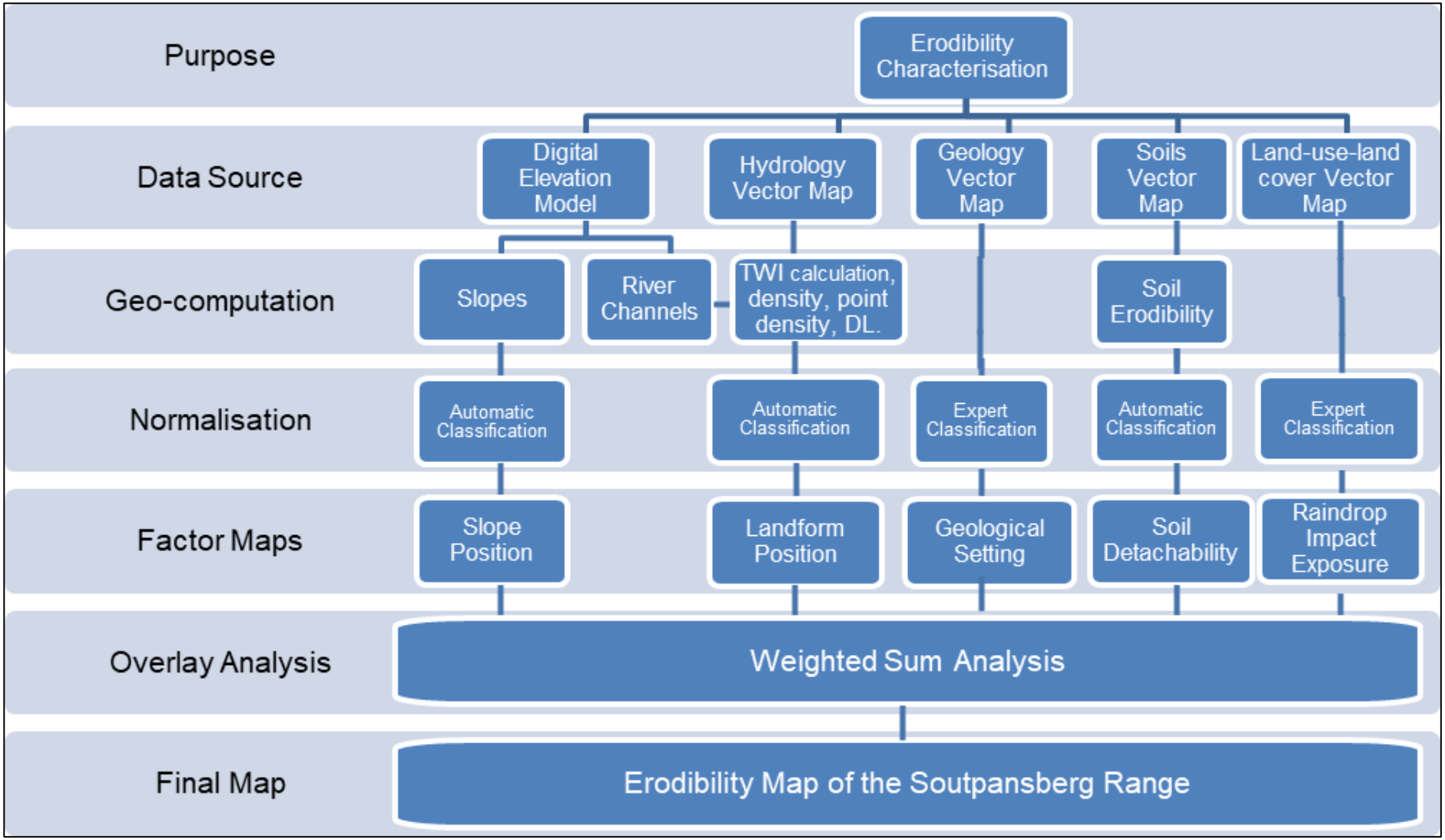

Figure 0.5: Soil Erodibility Characterisation Procedure (after Zwoliński *et al.*, 2019)

The normalisation was done either automatically or using expert classification. Automatic classification means that the indicator field was geo-computed. Expert classification means that the indicator field was created from the application of prior research findings or knowledge about the phenomenon in the classification. Rock hardness, following Moh's Hardness scale as well as porosity, were applied to geology. Hard rocks resist erosion while porous rocks reduce surface runoff through promotion of percolation. Both were classified as class five.

The normalisation produced the factor maps for slope position, landform position, geological setting, soil detachability and erosion exposure. The third stage was the weighting and overlaying of the factor maps to create a final soil erodibility map. The contribution of each factor to soil erosion is variable. Therefore, a representative map can only be produced if the final map is created in a manner that depicts the relative contribution of each factor. The relative contribution of each factor was determined by the Multi-Criteria Evaluation (MCE) using the Analytic Hierarchy Process (AHP). The MCE was done online using pairwise comparisons. The overlay was done using the raster calculator in ArcGIS.

3.4.1.1 Geo-computation and Normalisation

3.4.1.1.1. Soil Erodibility

Erodibility was classified using a five point Likert scale from very low to very high erodibility as illustrated in Table 3.1 adopted from Gilau (2015). However, Jenks natural breaks were employed in mapping. The Gilau (2015) classification gives the computed erodibility value that communicates the generic interpretation of erodibility. Jenks breaks are created in a way that groups similar values together and maximizes the visualisation of the differences between classes. In other words, Jenks breaks localise the classes, remove generalisations and make mapping possible.

Table 0.1: Soil Erodibility Classification (Gilau, 2015)

Soil Erodibility Class	Soil K Factor
Very High	> 0.70
High	0.50 - 0.70
Moderate	0.25 - 0.50
Low	0.13 - 0.25
Very Low	< 0.13

Soil erodibility (K factor) was computed based on the USLE and SLEMSA soil erosion models. The K factor produced based on the USLE was computed using equation 3.1 proposed by Wischmeier and Smith (1958). Soil USLE K factor was computed based on soil texture, organic matter, soil structure and soil permeability. The USLE K result from the calculations was added as another field in the attribute table of the soil shape file.

$$\frac{2.1*10^{-4}*(12-\mathrm{OM})*\mathrm{M}^{1.14}+3.25(\mathrm{s}-2)+2.5(\mathrm{p}-3)}{759} \qquad \textbf{(0.1)}$$

Where:

OM = soil organic matter content (%)

M = texture product [% silt*(% silt + % sand)]

s = structure class (dimensionless)

p = permeability class (dimensionless)

The K factor produced based on the SLEMSA was computed using equation 3.2 proposed by Stocking *et al.* (1988). Soil SLEMSA K factor was computed based on the rainfall energy (E) and soil erodibility (F) control variables. The USLE K result from the calculations was added as another field in the attribute table of the soil shape file.

$$ln\,K = b\,lnE + a \qquad \textbf{(3.2)}$$

Where

K = the soil erodibility factor (Mg ha hr ha^{-1} MJ^{-1} mm^{-1})

E = annual rainfall kinetic energy (J/m^2/year), and

a and *b* = functions of the soil erodibility factor (F) (Morgan, 1995). Where

$$a = 2.884 - 8.2109\,F \qquad \textbf{(3.3)}$$

and

$$b = 0.4681 + 0.7663\,F \qquad \textbf{(3.4)}$$

The derived soil erodibility values (F) were factored into equations 3.3 and 3.4 to determine variables *a* and *b*. The erodibility value is determined by a range of physical and chemical characteristics which influence the processes of the detachment and transport of soil particles (Stocking *et al.*, 1988). However the dominant factors are soil type and texture (Breetzke, 2004; Kusumandari, 2014). Therefore, the F factor was determined by soil type and texture values obtained from the indices summarised in Table 3.2. The F factor rating of 1 is for most erodible while 10 is the most resistant.

The soils collected from Univen Experimental Farm and Tshivhase Tea Estate were put through the hydrometer analysis. The hydrometer analysis will be explained in detail in section 3.4.3. The analysis gives the percentage content of silts and clays in a soil. The actual texture class, that also determines the F Index, was given by the soil texture triangle (Figure 2.2).

Table 3.2: Soil Erodibility Indices for SLEMSA (Elwell, 1978)

Soil Texture	Soil Type	*F* Value	Notes
Light	Sand	4	**Subtract the following from the F value:**
	Loamy sand		1 for light-textured soils consisting mainly of sands and silts
	Sandy loam		1 for restricted vertical permeability within one metre of the surface or for severe soil crusting
Medium	Sandy clay loam	5	1 for ridging up-and-down the slope
	Clay loam		1 for deterioration in soil structure due to excessive soil loss in the previous year (>20t/ha) or for poor management
Heavy	Sandy clay	6	0.5 for slight to moderate surface crusting or for soil losses of 10-20 t/ha in the previous year
	Clay		
	Heavy clay		
Add the following to the F value:			
2 for deep (>2) well-drained, light-textured soils			
1 for tillage techniques which encourage maximum retention of water on the surface, e.g. ridging on the contour			
1 for tillage techniques which encourage high surface infiltration and maximum water storage in the profile e.g. ripping			
1 for first season of no tillage			
2 for subsequent seasons of no tillage			

In addition, the SLEMSA rainfall energy (E factor) represents the kinetic energy of raindrops as they strike the ground (Stocking *et al.*, 1988; Morgan, 2009). The kinetic energy was calculated using equation 5. The equation was applied for both potentially erosive storms and daily rainfall.

$$E = 18.84 * P \qquad \textbf{(3.5)}$$

Where

E = kinetic energy (J/mm/s); and

P = precipitation (mm). The constant 18.84 was used in this research because the area experiences strong rains (Stocking *et al.*, 1988; Kabanda, 2003).

3.4.1.1.2. Landform Position

Landform position classifies the landscape into steep sided ridges, flat topped plateaux, gentle plains, open slopes and river channels (Jenness, 2006). This is informed by the river system development characteristics. Landform position was computed from hydrography data. Four factors are considered for the determination of landform position. The factors are shoreline development ratio, average river slope, point and drainage density, as well as Topographic Wetness Index (TWI).

Shoreline Development Ratio (DL)

The shoreline development ratio (or index) is a number that relates the measured shoreline length of a given lake, dam or pan to the shoreline length of a perfectly circular feature of equal area (Aronow, 1982). Equation 3.6 was employed for the computation of the DL for lakes, dams and pans found on the Soutpansberg range.

$$DL = \frac{L}{2\sqrt{\pi A}} \qquad \textbf{(3.6)}$$

Where

L = perimeter (m)

A = area (m)

Average River Slope

The average slope was computed for rivers and streams. The average slope was computed based on the average slope for 100 meter segments (Zwoliński *et al.*, 2019). Therefore, the first step was to split all rivers and streams into 100 metre segments. This was followed by the execution of the “Add Surface Information” function of in the 3D Analyst Functional Surface Tool of ArcGIS. Average slope is selected in the Add Surface Information tool. The result is saved as a new field in the attribute table of the rivers shape file. The layer is then rasterised using the Polyline to raster based on the average slope field.

Drainage and Point Density

Point density was necessary for the computation of springs and waterfalls sphere of influence on soil detachability. Drainage density depicts stream occurrence within the Soutpansberg range. Point density computation was done in ArcGIS using the Kernel Density function. Drainage density was generated using the Line Density Tool in ArcGIS.

Kernel Density calculates the density of point features around each output raster cell. Conceptually, a smoothly curved surface is fitted over each point. Springs and waterfalls were assessed based on density with the circle neighbourhood of 100

metre radius (Zwoliński *et al.*, 2019). The surface value is highest at the location of the point and diminishes with increasing distance from the point, reaching zero at the search radius distance from the point.

The drainage density is important because it is a function of erodibility and permeability. It assesses stream occurrence. Drainage density was derived from the rivers and streams falling within a given radius around each output raster cell, thus obtaining, as output, grid data (Melelli *et al.*, 2017). This was done at a radius of 300 metres in tandem with the 30 metres DEM resolution. The density was produced as a raster layer.

Topographic Wetness Index

The TWI quantifies topographic control of hydrological processes (Sörensen *et al.*, 2006). Therefore, it is important in hydrogeomorphology because it estimates where water would accumulate in an area with variable elevation (Mattivi *et al.*, 2019; Kopecký *et al.*, 2021). The index is highly correlated with soil attributes such as horizon depth, silt percentage and organic matter content (Moore *et al.*, 1993).

The TWI was calculated in SAGA GIS software, where it is called the SAGA Wetness Index. The SAGA Wetness Index is identical to the TWI. However, it is based on a modified catchment area calculation ('Modified Catchment Area'), which does not consider flow as a very thin film (Böhner *et al.*, 2006). Therefore, it predicts for cells situated in valley floors with a small vertical distance to a channel a more realistic, higher potential soil moisture compared to the standard TWI calculation.

3.4.1.1.3. Slope Position

The slope position factor classifies the landscape into cliffs, scree slopes, transportation mid-slopes, foot slopes and open valleys (Jenness, 2006; Melelli *et al.*, 2017). Slopes were obtained using the Topographic Position Index (TPI) in SAGA GIS. The TPI is the difference between a cell elevation value and the average elevation on a neighbouring area around the cell. The TPI was computed considering a 300m radius circle neighbourhood in tandem with the 30m resolution of the DEM.

3.4.1.1.4. Geological Setting and Land-use-land-cover

Geology and land-use-land-cover were assessed using expert classification. Houshold and Sharples (2008) suggested the inclusion of the interrelated character of assemblages in geodiversity assessment. In line with that, lithological diversity as well as hardness were considered in the production of the geology factor. The attributes (in the attribute table) of each polygon in the geology shape file indicate the presence of a dominant rock type plus the presence of up to four other rocks. Therefore, lithological diversity was assessed considering the number of lithologies each polygon had. One represented one rock type while five represented five rock types in the polygon.

Lithological diversity was merged with rock hardness classes. The rock hardness classes are shown in Table 3.3. The rock hardness classes were expertly classified from the main rock using Moh's hardness class, defined in the attribute table as litho1. Lithological diversity and rock hardness were combined using the raster calculator of ArcGIS to produce the geology factor.

Table 0.3: Geology Classes

Igneous	**Metamorphic**	**Sedimentary**
Granite (5)	*Gneiss (3)	Sandstone (4)
Norite (4)	Marble (3)	Arenite (4)
Dolerite (4)		Conglomerate (3)
Epidiorite (4)		Shale (3)
Basalt (4)		Siltstone (3)
Tuff (3)		Mudstone (2)
		Coal (2)
		Calcrete (1)

*Gneiss was classified as medium hardness because of the wide range of mineralogy.

Using South Africa's 2018 land use land cover map obtained from the Department of Forestry, Fisheries and Environment website, different land uses and cover were classified into five classes according to how they resist soil detachability and expose the soil to raindrops. Land uses and land covers that would promote soil compaction and resist detachment were classified as one. Those that would offer the least resistance were classified as five. Vegetation cover that gives highest interception

were classified as one while those that give the least interception were classified as five. Table 3.4 shows the classes.

Table 0.4: Land Use Land Cover (Rainfall Exposure) Classes

Land Use and Cover Type	Class	Land Use and Cover Type	Class
Contiguous (indigenous) forest	1	Fallow land & old fields (trees)	4
Contiguous low forest & thicket	1	Fallow land & old fields (bush)	4
Dense forest & woodland	1	Fallow land & old fields (grass)	4
Open woodland	1	Fallow land & old fields (bare)	4
Contiguous & dense plantation forest	1	Fallow land & old fields (low shrub)	4
Open & sparse plantation forest	1	Residential formal (tree)	2
Temporary unplanted (clear-felled) plantation forest	1	Residential formal (bush)	2
Low shrub land (other)	1	Residential formal (low veg / grass)	2
Sparsely wooded grassland	2	Residential formal (bare)	2
Natural grassland	2	Residential informal (tree)	2
Natural rock surfaces	1	Residential informal (bush)	2
Dry pans	3	Residential informal (low veg / grass)	2
Eroded lands	5	Residential informal (bare)	2
Bare riverbed material	5	Village scattered (bare & low veg/ grass combo)	3
Other bare	5	Village dense (bare & low veg / grass combo)	3
Cultivated commercial permanent orchards	2	Smallholdings (tree)	3
Commercial annual crops pivot irrigated	4	Smallholdings (bush)	3
Commercial annual crops non-pivot irrigated	4	Smallholdings (low veg / grass)	3
Commercial annual crops rain-fed / dryland	4	Smallholdings (bare)	3
Subsistence / small-scale annual crops	4	Urban recreational fields (tree)	2
Fallow land & old fields (wetlands)	4	Urban recreational fields (bush)	2
Land-fills	5	Urban recreational fields (grass)	2
Mine: tailings and resource dumps	5	Urban recreational fields (bare)	2
Mines: extraction pits, quarries	5	Commercial	1
Roads & rails (major linear)	1	Industrial	1

The factor indicators were used as the reference field for rasterization. Others were produced as raster layers from the computations. The raster layers would then be normalised into five classes using the Jenk's Natural breaks (Jenks, 1967) in ArcGIS. The normalisation used the reclassify tool of ArcGIS to create five classes for each factor. One is the lowest while five is the highest indicator class.

3.4.1.2 Overlay Analysis and Final Map Production

The final map was produced by weighted overlay of the factor layers. Factor weighting analysis was carried out before overlaying the layers to produce the overall soil erodibility map of the Soutpansberg Range. Factor weighting was done online using the Multi-Criteria Evaluation (MCE) using the Analytic Hierarchy Process (AHP).

Multi-Criteria Evaluation (MCE) using the Analytic Hierarchy Process (AHP) is critical to the objective computed weights for each factor map depending on their potential influence on the overall erodibility of the Soutpansberg Range. The calculation of weight was carried out by pairwise comparison following Saaty (2000). Consistency ratio (CR) should not be greater than 10%. The weights must add up to 100% (or 1).

The final erodibility map was produced by weighted overlaying. The Weighted Sum tool of ArcGIS was used. Each layer contributed the weight as indicated in Table 3.4. The output raster was reclassified using the Reclassify tool to create the five classes indicating soil erodibility on the Soutpansberg Range. One means very low while five means very high erodibility.

3.4.2 Potentially Erosive Rainfall Spatial-temporal Characterisation

Spatial temporal characterisation of potentially erosive rainfall addresses the second objective to reveal the distribution of erosion potential on the Soutpansberg range. This is important because properties that determine soil erodibility, such as soil aggregation and shear strength, are strongly affected by climatic factors such as rainfall distribution and frost action, and show systematic seasonal variation (Bryan, 2000). This section is divided into two parts. The first part deals with monthly and annual spatial temporal characterisation. The second part focuses on rainstorm

spatial-temporal characterisation. This distinction is important because only five weather stations could provide rainstorm event data. Therefore, event analyses are limited to the five stations while monthly and annual analyses cover the whole mountain range.

The monthly and annual spatial temporal characterisation was done using spatial interpolation and spatial autocorrelation. The potentially erosive storms spatial temporal characterisation was achieved using spatial autocorrelation only. Spatial interpolation was achieved through co-kriging. Spatial autocorrelation was determined by the coefficient of variation and the Moran's I as adopted from Zhang and Han (2017). Spatial interpolation and spatial autocorrelation are explained in sections 3.4.2.1 and 3.4.2.2, respectively.

3.4.2.1 Spatial Interpolation

Rainfall spatial temporal characterisation was done through spatial interpolation in ArcGIS using ordinary co-kriging. Spatial interpolation was necessary to exhibit the spatial distribution and temporal characteristics of potentially erosive rainfall over the mountain range. The interpolation was done using monthly average rainfall for the whole mountain range. The monthly layers were overlaid to produce quarterly layers. The quarterly layers were then overlaid to produce the annual distribution map.

Kriging is a geostatistical method for estimating unknown values by considering both the distance and the degree of variation between known data points (Burgess and Webster, 1980; Paramasivam and Venkatramanan, 2019). It generates an estimated surface from a scattered set of points (Gu *et al.*, 2019). The relationship between rainfall and the landscape is important to this research. Therefore, ordinary co-kriging was employed. Kriging is a two-stage analytical process, starting with the quantification of the spatial data structure. The second stage is the production of a prediction.

Quantification of the spatial data structure, known as variography, is the indicator of spatial autocorrelation or dependency (Burgess and Webster, 1980; Paramasivam and Venkatramanan, 2019). Kriging uses semi variance to the relationship between points on a surface. This is an indication of how data are similar or different over space. As points are compared to distant points, semi variance increases until a

point where there is no semi variance. That point is called the range and defines the maximum neighbourhood over which control points must be selected.

Therefore, the semi variogram depicts spatial autocorrelation of the measured points (Gu *et al.*, 2019). The semi variogram fitted model provides information on the spatial autocorrelation as well as the input parameters. The spatial autocorrelation is indicated by the range, sill and nugget of the semi variogram. The nugget is the variance at zero distance. The sill is the constant value on the vertical axis of the variogram when the variables do not influence each other. The range is the distance at which the value of one variable becomes spatially independent of another. See figure 3.6 for variogram.

The basic principle of spatial autocorrelation is that closer phenomena are more alike. Therefore, points closer together will have a smaller semi variance as compared to those far apart. In other words, autocorrelation is a function of distance

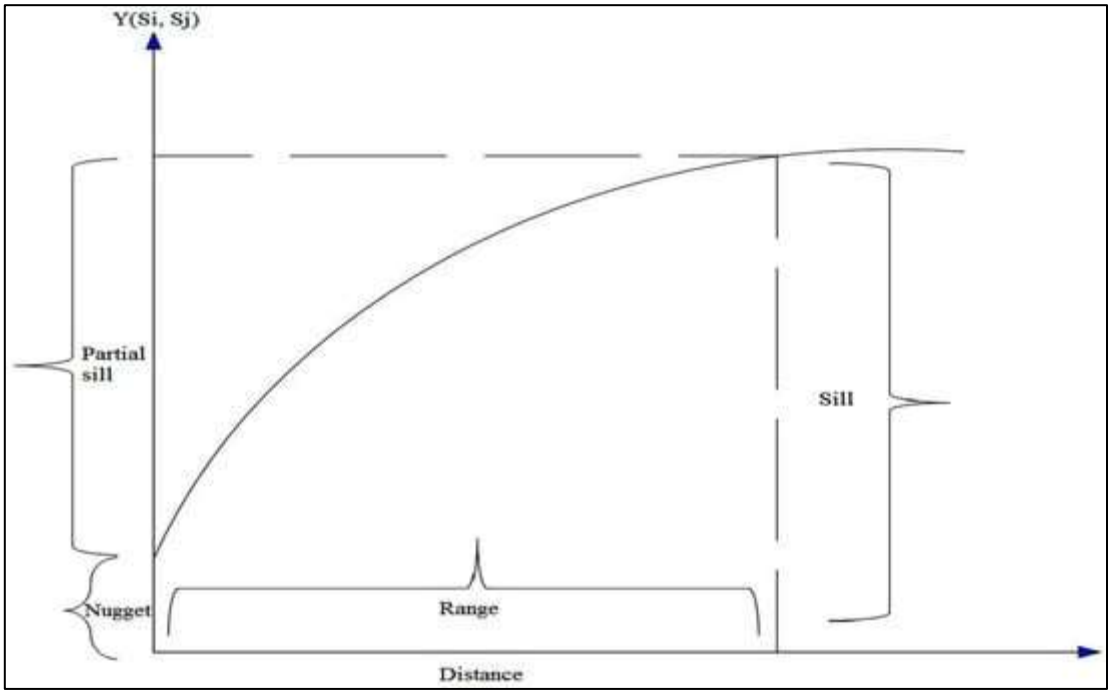

Figure 0.6: A Typical Viriogram

(Bijleveld *et al.*, 2012). Simply put, correlation decays with distance. Medium meso-meteorological network density standards of ~30 km radius (WMO, 2008) were applied. As such, some stations falling within ~30 km outside the physical boundary of the range were considered. Though they would be physically outside the mountain

range, they would still be meteorologically within range for scientific consideration in analyses.

The ratio of nugget to sill indicates the spatial dependency of variables (Al-Omran *et al.*, 2013). There are three classes used for model explanation (Tadayon and Rasekh, 2019). If the ratio is less than 25 %, it shows strong spatial dependence; if the ratio is between 25 and 75 %, it indicates moderate spatial dependence; and if the ratio is more than 75 %, it represents weak spatial dependence.

The point on the horizontal axis at which the model begins to flatten out is called the range. Points that are separated by a distance smaller than the range are spatially autocorrelated. The maximum range applied for this research is 30 km which is in line with the WMO (2008) meso-meteorological network density standards. Beyond the range, points become independent of each other (Bijleveld *et al.*, 2012).

The prediction stage of spatial interpolation encompasses the production of the unknown values. Bias and accuracy are important in the prediction of rainfall (Adhikary *et al.*, 2017). The cross-validation statistics become important. Bias was measured by the mean, while accuracy was determined by the root mean square standardised (RMSS) (Hengl *et al.*, 2004; Ikechukwu *et al.*, 2017). The closer to zero the mean is, the less the bias. The closer to one the RMSS is, the higher the accuracy. The acceptable model for this research was based on prior results and is one with a RMSS between 0.8 and 1.2, while the mean is between -0.2 and 0.2 (Hengl *et al.*, 2004; Ikechukwu *et al.*, 2017).

The following stages were followed in the production of Soutpansberg annual rainfall spatial distribution map through co-kriging in ArcGIS.

i. The co-kriging prediction. This is when the average monthly or annual rainfall figures from the 45 stations are spatially interpolated. This stage creates temporary spatial distribution layer. The temporary layers contain the prediction method summary.
ii. Creation of permanent layers. The temporary layers created in stage one are saved as raster layers to make them permanent.
iii. Classification. Using the Symbology function of the ArcGIS software, each layer was standardised into 5 classes representing:

1. Very low rainfall
2. Low rainfall
3. Moderate rainfall
4. High rainfall
5. Very high rainfall

The classification was based on Jenks Natural breaks and the rainfall range in each class was dependent on the rainfall figures considered. However, the rainfall threshold was 12.5 mmm, the cutting point for USLE and SLEMSA potentially erosive rain. The 5 classes are to remain consistent with the 5-class approach adopted for the geomorphic classification. Therefore, very high rainfall means very high erosive potential.

iv. Map Algebra Overlaying. Adding the monthly average rainfall layers together using the Raster Calculator in ArcGIS to produce one map. It is important to note that rainfall is spatially and temporally variable on the Soutpansberg range. Consequently, its contribution towards the final rainfall distribution and erosivity is also spatially and temporally variable. This dynamic was catered for through the Weighted Sum Overlay in the ArcGIS Raster Calculator. The relative contribution of each month and quarter was computed from its percentage contribution to the annual value. Monthly, quarterly and annual rainfall distribution maps are produced to reveal different spatio-temporal characteristics of rainfall on the Soutpansberg.

v. The final maps are reclassified into 5 classes using Jenks Natural breaks.

3.4.2.2 Spatial Variability Analysis

Spatial variability represents the relationship between neighbouring spatial phenomena, as seen on maps, where each unit is coded with a realization of a single variable (Getis, 2010). In this case the phenomenon is potentially erosive rainfall. This comes from the “Geographical Law” that everything is related to everything else. However, phenomena that are close are more related than distant ones. Spatial variability was analysed using the coefficient of variation (CV) and the Moran’s I.

The CV and Moran's I were especially applied on the 383 potentially erosive storms identified in the 20 years of rainfall data used here and based on the rainfall thresholds described above. However, monthly rainfall and days for the whole mountain range were also spatially analysed. Therefore, spatial variability assessment was done for monthly, quarterly, annual and event rainfall. It was also carried out for erosive days and wind. While the monthly, quarterly, annual rainfall and erosive days covered the whole mountain range, event analyses covered the five stations only as these were the only measurements with hourly data necessary for the analysis.

The CV (Equation 3.7) is a measure of relative variability of the standard deviation relative to the mean (Zhang and Han, 2017; Mestdagh *et al.*, 2018; Ospina and Marmolejo-Ramos, 2019). It gives variability within a rainfall record without considering rainfall spatial distribution. On the other hand, Moran's I (Equation 3.8) is a statistical tool to assess spatial autocorrelation between nearby locations in space (Griffith, 1987; Fortin and Dale, 2009; Getis, 2010; Zhang and Han, 2017) rather than values. Moran's I depicts the rainfall spatial autocorrelation based on both weather station locations and rainfall values, simultaneously.

$$CV = \frac{\sqrt{\sum_{i=1}^{n}(P_i - \overline{P})^2}}{\overline{P}} \qquad \textbf{(3.7)}$$

Where

CV = coefficient of variation

P_i = the rainfall value at the *i*th station, in mm.

P = the average rainfall of all stations, in mm.

n = the number of stations.

$$I = \frac{n}{\Sigma_{i=1}^{n}\Sigma_{j=1}^{n}W_{ij}} \frac{\Sigma_{i=1}^{n}\Sigma_{j=1}^{n}W_{ij}(P_i - \overline{P})(P_j - \overline{P})}{\Sigma_{i=1}^{n}\Sigma_{j}} (P_i - \overline{P})^2 \qquad \textbf{(3.8)}$$

Where

P_i = the rainfall value at the *i*th station, in mm

P_j = the rainfall at *j*th gauge, in mm.

W_{ij} = spatial weight obtained using equation 3.9.

$$W_{ij} = r_{ij}^{-b} \qquad \textbf{(3.9)}$$

Where

W_{ij} = spatial weight (defines spatial relationship between all weather stations within the Soutpansberg range).

point pairs within a specified area.

r_{ij} = the distance between *i*th station and *j*th station, in m.

b = a distance parameter. Distance parameter values are originally defined as 1 if *i*th and *j*th stations are adjacent, and 0 if otherwise. However, the 0 or 1 weighting is used for contiguous rather than discrete and geographic data (Zhang and Han, 2017). Therefore, the spatial weight parameter for this research was calculated by the inverse distance method where the distance parameter is 1.

The CV is expressed as a percentage or as a range from 0 to 1. It is presented in this research using the latter style. However, outliers sometimes produce a CV greater than 1. The higher the coefficient of variation, the greater the level of dispersion around the mean. Therefore, the higher the CV, the higher the rainfall variability (Zhang and Han, 2017). This gives an indication of the uniformity of rainfall distribution on the Soutpansberg Range. The levels of variability followed are guided by Morales *et al.* (2010) and Verdugo-Vásquez *et al.* (2016). The variability levels are <0.1 = very low, 0.1 – 0.2 = low, 0.2 – 0.3 = high, and >0.3 = very high variability.

Moran's I is expressed in a range of -1 to 1. It measures dispersion and clustering. The dispersion and clustering is described by the figures involved. Perfect clustering of dissimilar values, also called perfect dispersion is indicated by a -1. Perfect randomness, indicating no autocorrelation, is indicated by a 0. Perfect clustering of similar values is indicated by a 1. However, sometimes the value can exceed the

thresholds, as it does in this research. This arises due to the existence of extreme outliers.

The two measures, CV and Moran's I, consider variability from different perspectives. Therefore, spatial autocorrelation was determined by combining both measures following Zhang and Han (2017). This combination was found to be a reliable method to describe rainfall spatial variability (Zhang *et al.*, 2018). Zhang and Han (2017) adopted a matrix to combine the two statistical measures to describe spatial distribution. The matrix is adopted as depicted in Table 3.5.

Table 0.5: Rainfall Spatial Variability Matrix

(Zhang and Han, 2017).

		Coefficient of Variation	
		High (>0.3)	Low (=< 0.3)
Moran's I	High (>0)	Medium	Simple
	Low (=<0)	Complex	Medium

The matrix considers the variability caused by both rainfall magnitude and spatial distribution by fusing CV and Moran's I (Zhang and Han, 2017). The fusion expresses the variability manifested by the rainfall values (CV) and that manifested by the relative location of the rainfall stations (Moran's I). The matrix proposes a three-tier variability scale – simple, medium and complex. This comes from a scatter combination of high/low CV and Moran's I. A high CV (greater than 0.3) and low Moran's I (less than or equal to 0) depicts complex variability. A low CV (less than or equal to 0.3) and a high Moran's I (less than or equal to 0) indicates simple variability.

A simple variability is one where high rainfall values cluster, and they are close to the mean. This means that the rainfall variability is explainable by changes in space as calculated by Moran's I. A medium spatial variability is where high values cluster in space but are dispersed from the mean. Clustering of low values that are close to the mean is also medium spatial variability. Medium variability has a balance of space and non-space factors controlling rainfall distribution. Clustering of high rainfall values that are dispersed from the mean shows complex spatial variation. Complex

variation cannot be explained by space only. Other factors are at play in the rainfall distribution. This determination is important to consider for this research because of its focus on a mountain range.

Pursuant to the adoption of the spatial variability matrix, the CV and Moran's I scale had to be revised. The high values for CV are greater than 0.3. The high values for Moran's I are greater than 0. This readjustment allowed the use of the spatial variability matrix to determine areas with potential rainfall distribution similarities.

3.4.2.3 Potentially Erosive Rainfall Hotspot Analysis

A further spatial analysis was applied to the monthly rainfall. It is important to analyse the relationship between potentially erosive rainfall and the number of days over which it falls during the season. Using the total rainfall only may betray the rainfall erosive potential and its distribution. Erosive potential is derived from overland flow generated by the rain (Hui-Ming and Yang, 2009). Therefore, it was necessary to also analyse rain days vis-à-vis the amount of erosive rainfall received. This would indicate the temporal distribution of erosive potential and indicate some form of rainfall intensity. Knowledge about the extent of soil loss and the spatial distribution of soil erosion hot spots is essential to prevent water pollution by diffuse matter fluxes (Schönbrodt-Stitt *et al.*, 2013). A single intense rainfall event can cause a lot of erosion.

Hotspot analysis was adopted to characterise the number of rain days per weather station. This is important for identification of potential flash flood prone areas. Runoff generation depends on rainfall rate (Renard *et al.*, 1997). High rainfall rate can cause flash floods. Flash flood erosion is highly instrumental in gully formation (Mousazadeh and Salleh, 2014). A station that receives high potentially erosive rain in a few days has high potential to generate large volumes of surface runoff and, hence, flash flood erosion. Such information is critical for soil erosion planning and management.

Stations were ranked using the total number of potentially erosive rain days and rainfall. A station with more rainfall and few rain days was ranked first. The ranks were added onto the attribute table of the rainfall GIS layer. The rank field was used

in Symbology to create a hot spot map of the mountain range. Areas with more rainfall but few rain days are treated as hotspots. The risk levels were classified from very low to very high using Jenks Natural Breaks. Finally, the hotspot layer was overlaid on top of the interpolated rainfall distribution map.

3.4.3 The Influence of Topography on Wind Speed and Rainfall Erosivity

The aim of the research has been to analyse the spatial-temporal characteristics of soil erodibility and rainfall erosivity on the Soutpansberg range. This section seeks to establish the contribution of wind speed and topographical elevation to soil erosion. The contribution was established in the context of the USLE and SLEMSA erosion models. This section addresses the objective that seeks to assess the influence of topographical elevation on wind speed and rainfall erosivity. Two hypotheses were posited for the objective.

The first null hypothesis for this objective was that topographical elevation has no effect on rainfall erosivity. The second null hypothesis was that wind speed has no effect on rainfall erosivity. The alternative hypotheses were that topographical elevation and wind speed increase rainfall erosivity. Wind and rain are considered the two major drivers of erosivity (Erpul *et al.*, 2013; Marzen *et al.*, 2017). Both phenomena's behaviour is significantly influenced by topography. Therefore, it was imperative to analyse the influence of topography on wind speed and on erosivity.

While wind speed is a measured variable, erosivity is a computed variable. Therefore, erosivity figures are computed following SLEMSA and USLE formulae. The SLEMSA erodibility has already been explained in section 3.4.1.1.1 as given in equation 3.2. Therefore, no further attention will be given to it. The USLE and WDR erosivity computation are elaborated below. The WDR erosivity and wind speed were not regressed against elevation because the 383 rainfall events considered for this research were recorded from 5 stations only. Therefore, regression analysis would not be applicable.

However, the wind speeds for Wind Driven Rain and direction recorded are analysed using a five level Likert scale from calm, light, moderate, strong and very strong winds. The classes are developed from Montero-Martínez and García-García (2016), Scheper *et al.* (2021) and the Beaufort Scale (Huler, 2007). Calm winds travel at less

than 1.5 m/s^{-1}. Light winds have velocities are between 1.6 and 3.0 m/s^{-1}. Moderate winds travel at 3.1 and 4.5 m/s^{-1}. Strong winds range from 4.6 to 6 m/s^{-1} while very strong winds are above 6 m/s^{-1}. The percentage contribution of each wind speed level vis-à-vis the elevation of the station was used to determine the influence of elevation on wind speed.

3.4.3.1 USLE Erosivity Factor

Erosivity is a product of storm energy and intensity (Wischmeier and Smith, 1978). The storm energy is a function of the impact frequency, size, shape, and terminal velocity that determine the kinetic energy (KE) of rain drops (Torres *et al.*, 1992; Kinnel, 2016). Erosivity explains about 80% of variations in the average annual soil loss (Wischmeier and Smith, 1958). In short, energy is a function of raindrop characteristics which is embodied by kinetic energy and erosivity was computed following equation 3.10.

$$R = EI \qquad \textbf{(3.10)}$$

Where

R = rain erosivity (MJ mm ha^{-1} hr^{1})

E (MJ/mm^{-1}) = energy

= 11.87+8.73log10*i* where *i* is rain intensity

I (mm/s) = Intensity (I_{3600})

3.4.3.2 Wind Driven Rain (WDR) Erosivity

Wind Driven Rain (WDR) as proposed by Erpul *et al.* (2002) was used in this research. Wind Driven Rain explains energy from a physical point of view following the movement of the raindrop through the atmosphere. If a raindrop is regarded as a particle, individual raindrop's energy can be calculated according to physical basic laws if its quantity and velocity are known (Guo *et al.*, 2013). Wind acts upon the raindrop as it travels through the wind field. The gravitational and drag forces result in the raindrop travelling at an angle from the vertical (Erpul *et al.*, 2003). The

raindrop gains some horizontal velocity and strikes the ground at an angle deviated from the vertical. The significance of the changes in the raindrop trajectory is its effects on rain splash detachment process (Erpul *et al.*, 2003). The rain-plash detachment is the initiation of soil erosion (Lyles, 1977; Pedersen and Hasholt, 1995; Blocken and Carmeliet, 2004; Kinnell, 2005; Marzen *et al.*, 2015; Panagos *et al.*, 2015). The magnitude of the rain splash detachment is determined by a combination of impact velocity, impact angle or angle of incidence, and impact frequency of raindrops. All of these result in the detachment of soil particles.

Detachment of soil particles caused by rain-plash is an initiating process of soil erosion (Pedersen and Hasholt, 1995). If it is assumed that the effect of wind shear stress on the detachment is insignificant when compared to the effects of the impacting raindrops, the rain splash detachment rate at which soil particles are supplied into the air is a linear function of the raindrop kinetic energy.

Erpul *et al.* (2002) and Erpul *et al.* (2003) proposed the KE model for WDR erosivity. Soil detachment by raindrop splash is a direct consequence of precipitation kinetic energy (Pedersen and Hasholt, 1995). The amount of soil particles detached positively correlates with rainfall energy (Lyles, 1977; Choi, 2002; Erpul *et al.*, 2002; 2003; Gabet and Dunne, 2003; Brodowski, 2013; Marzen *et al.*, 2015; Lu *et al.*, 2016). Raindrop energy is an important index to evaluate the degree of soil erosion caused by rainfall (Fox, 2004; Fu *et al.*, 2019). Rainfall intensity, raindrop energy, and their variations in time and space have important effects on the prediction of rainfall erosion. Therefore, the WDR erosivity was computed using equation 3.11 from Erpul (2013).

$$KE = \frac{\rho_w}{2} ItAV^2 \qquad \textbf{(3.11)}$$

Where:

KE = kinetic energy (J).

ρw = raindrop density (kg m^{-3})

I = rain intensity (m s^{-1}).

t = exposure time (s)

A = projected frontal area. A = $\pi d^2/4$ (m^2) where d is raindrop diameter (m)

V = raindrop impact velocity (m s^{-1})

To that end, simple linear regression was done to establish the influence of altitude on wind speed. In addition, multiple analysis of variance (MANOVA) was run to compare the influence of rain and wind to erosivity computed using different methods. The 383 potentially erosive storms recorded during the period under review are considered for MANOVA. The MANOVA for each of the storms per station, as well as all for all of the storm data combined, were computed.

Interpretation of the outcomes of the two statistical tests is critical to establish whether to accept or reject the hypotheses. Hypotheses decisions are guided by important statistics from the computations. Regression produces three tables while MANOVA produces two tables. The interpretation of the statistical analyses is elaborated in the following section.

3.4.3.1 Regression Output Interpretation

The first two important statistics for regression are the multiple R and the R-squared. The multiple R is the correlation coefficient that tells the strength of the linear relationship. That is, how closely the variables move in tandem with one another (Mathews, 2018). A one means a perfect linear relationship while a zero means no relationship at all.

The R-squared (r^2) tells the number of values that are explained by the independent variable. The r^2 tells the percentage of erosivity values that are explained by elevation. This is usually converted to a percent for easy interpretation. This regression focused on explaining the relationship between variables. The purpose was to measure goodness of fit. Therefore, r^2 value was not important (Frost, 2018; Dušan, 2019). Significance F and p-value determine the decision to be made on the hypothesis and were important in this research.

Significance F determines the goodness of the regression model. This is where hypothesis testing begins. It gives the probability that the null hypothesis in the regression model cannot be rejected. A significance F ≤0.05 indicates that the null hypothesis should be rejected.

The significance F works together with the p-value. The p-value indicates the reliability or significance of the coefficient. In other words, the p-value indicates the "probability of an error" (Mathews, 2018). It is the probability that the coefficient of the independent variable of the regression is not reliable. A Cronbach's Alpha of ≤0.05 is generally acceptable, therefore adopted for this research, as an indicator of goodness of fit as well as p-value and for rejecting the null hypothesis (Frost, 2018; Mathews, 2018). A p-value ≤0.05 indicates that the null hypothesis should be rejected.

Another important regression statistic is the coefficient. The regression coefficient gives specific information about each component in the regression analysis. This gives the regression model. The coefficient indicates how much erosivity (wind speed) is explained by elevation (rainfall amount). The coefficient tells the change that would happen to erosivity (wind speed) if elevation (rainfall amount) changes by a unit. The sign accompanying the coefficient indicates the type of relationship. A negative sign indicates an inverse relationship. This is when an increase in elevation (rainfall amount) results in the decrease in erosivity (wind speed) by the magnitude of the coefficient. The significance of this relationship is determined by the p-value. A p-value ≤ 0.05 indicates a significant relationship and signals the rejection of the null hypothesis.

3.4.3.2 MANOVA Output Interpretation

The F statistic measures if the means of different samples are significantly different. It indicates the dispersal of data points around the mean. Higher F values indicate that individual data points fall farther from the mean. The F-statistic was compared with the F-critical value for deciding on the hypothesis. If the F value is larger than the F-critical, then the null hypothesis is rejected. In that case, it would indicate that wind speed has an influence on erosivity. It means that at least one mean of the three erosivity values would be different. A p-value less than or equal to 0.05 means

the difference is statistically significant and supports the rejection of the null hypothesis.

The purpose of the MANOVA was to test the hypotheses (Pallant, 2016; Lund and Lund, 2018). The null hypotheses were that topographical elevation and wind speed have no effect on rainfall erosivity. The MANOVA, therefore, indicates whether WDR erosivity is different from WFR erosivity through two tests. The first was the use of the multivariate test to establish the statistical significance of the variance. The second was the tests between subjects' effects.

The MANOVA analysis begins with establishing statistical significance of the MANOVA. Statistical significance was given by the Wilks' Lambda (Lund and Lund, 2018). This was done through multivariate tests. The value, significance and effect size are the important Wilk's Lambda statistics.

The Wilk's Lambda value gives the proportion of variance in the erosivity that is not accounted for by the intergroup variations. It tests the presence of differences between group means (Glen, 2015) for SLEMSA, USLE and WDR erosivity. Lambda measures the percent variance in erosivity not explained by differences in wind speed and rainfall amount. This is called the interaction effect (Pallant, 2016). A value closer to zero is ideal because it indicates the erosivity variance that is not explained by wind speed or rainfall amount (Lund and Lund, 2018; Mathews, 2018).

Significance of ≤0.05 indicates a statistically significant difference in erosivity based on wind speed or rainfall amount. This is represented by the p-value. The effect size indicates the degree to which erosivity is associated with wind or rainfall amount. Effect size is indicated by eta squared and is an indication of the strength of association (Pallant, 2016). Eta squared is important for this research as it indicates the strength of association between wind speed or rainfall to erosivity. The strength of association guides in decision making about the importance, or lack of it thereof, of including wind speed in soil erosion modelling. The effect size is either small (0.01), medium (0.06) or large (0.138) (Pallant, 2016). A statistically significant Wilk's Lambda rejects the null hypothesis (Glen, 2015; Lund and Lund, 2018). However, indications of individual differences are done on test between subject effects.

The test between subject effects gives the relationship between individual erosivity values and wind speed or rain. Therefore, this MANOVA was used to indicate individual variances against each independent variable (Lund and Lund, 2018). The significance is the important statistic. However, MANOVA does not indicate pairwise differences. Therefore, a post hoc test was needed to test each pair of means. A Bonferroni adjustment, commonly called a t-test is a scientifically accepted post hoc test (Mathews, 2018). A t-test is a pairwise comparison that modifies the p-value for each test. The pairwise comparison produced for this research were: WDR – USLE; WDR – SLEMSA; USLE -SLEMSA.

The new pairwise p-value (P (T<=t two tail)) indicates the probability of the groups to belong to the same population. A pairwise p-value ≤0.05 indicates that the pair is different. The aim of this section has been to find out if the inclusion of wind in erosivity computation brings a difference. Put in other words, does the WFR erosivity embed wind speed? The t-test was the tool to reveal that. The t-tests were for individual storms for the 2000 to 2019 period as well as for the data collected between November 2020 and March 2021.

3.4.4 The Influence of Wind on Rainfall Erosivity

The objective of this section has been to establish the influence of wind on rainfall erosivity on the Soutpansberg range. Therefore, there are two parts to this aspect – the wind free rain (WFR) and wind driven rain (WDR) rain erosion. Central to this objective is erosivity. Wind changes rainfall erosivity (Erpul *et al.*, 2013; Marzen *et al.*, 2017). Therefore, following rainfall erosivity was computations using the USLE (Wischmeier and Smith, 1958) and SLEMSA (Stocking *et al.*, 1988) models, there was need to link the WFR and the WDR for fair comparison.

The WDR KE energy had to be normalised to erosivity. The WDR KE value was multiplied by rainfall intensity to produce an USLE type of WDR erosivity. The SLEMSA approach went further by multiplying the WDR KE with rainfall amount. The product of the multiplication of WDR KE and rainfall intensity replaced the 18.84 rainfall energy constant of SLEMSA. The result was the WDR USLE and WDR SLEMSA erosivity, respectively.

The normalised WDR into the USLE or SLEMSA type of erosivity would replace the usual erosivity values in the empirical data calculations. The outcomes are compared with the total sediment collected from the splash cups set up at UNIVEN Experimental Farm and Tshivhase Tea Estate. Five storms from Thohoyandou (3) and Tshivhase Tea Estate (2) were used to establish the erosivity values that closely relate to reality. The following section elaborates the use of the soil loss models.

3.4.4.1 The Soil Loss Estimation Model for Southern Africa (SLEMSA)

The SLEMSA is a technique to estimate and rank the potential of physical erosion over a specified area (Stocking *et al.*, 1988). It assumes that erosion is influenced by a combination of different factors, the dominant ones being climate, soil physical characteristics, relief and vegetation cover. Major control variables are selected for each system on the basis of dominance within its system and easy of measurement (Stocking, 1980). The control variables are subsequently combined into three sub-models - the bare soil sub-model, topographical sub-model, and the vegetation sub-model. The multiplication of the sub models then produces the main model. The components are presentment in equation 12.

$$Z = KVX \qquad \textbf{(3.12)}$$

Where:

Z = estimated soil loss or erosion hazard (Mg ha^{-1} yr^{-1})

K = soil loss as determined by rainfall erosivity plus soil erodibility (Mg ha hr ha^{-1} MJ^{-1} mm^{-1})

V = cover determined by vegetation (dimensionless); and

X = relief as determined by slope length and steepness (dimensionless) (Stocking, 1980).

The soil loss as determined by rainfall erosivity plus soil erodibility (K) was covered in section 3.4.1. That is where the rainfall energy (E) component was tackled. Therefore, no further attention is paid to the erodibility component in this section. Hence the detailed explanation below focuses only on the cover determined by

vegetation (V) and relief as determined by slope length and steepness components of the model as applied in this research.

3.4.4.1.1 Vegetation Cover (C)

The vegetation factor (V) (originally crop factor (C)) is the ratio of soil loss from a vegetated plot to that lost from bare fallow land (Stocking, 1980). Erosion is not a challenge in cultivated areas only, but in non-cultivated lands as well. This is especially true to fragile environments in the face of climate change. This research, therefore, replaces the C for crops in the original model with a V for vegetation to represent all vegetation types, including crops.

The vegetation factor was derived from the energy interception factor, *i*, which provides an indication of the amount of rainfall that is intercepted by vegetation. It is determined by the vegetation type, yield and emergence date for crops, natural grasslands, dense pastures and mulches (Mughogho, 1998). It should be noted, however that it is difficult to allocate a constant V value because cover changes progressively through the seasons. Therefore, two *i* scenarios arise:

$$\text{C.} \qquad V = exp^{(-0.06i)} \qquad \textbf{(3.13)}$$

when i = ≤50% or

$$\text{D.} \qquad V = \frac{2.3 - 0.01i}{30} \qquad \textbf{(3.14)}$$

when i = > 50%.

It should be noted that different land uses may fall within the same geomorphic unit. To give the V factor value for such scenarios, the percentage geomorphic unit area occupied by each specific land use is normally calculated. This gives the weighted V value for each land use whose total gives the V value for the geomorphic unit. However, soil for this research was collected by a splash cup in a cleared area. Therefore, equation 3.13 was used indicating no vegetation cover. The V value becomes 1.

3.4.4.1.2 Relief (X)

The factors of slope length, L, and slope angle, S, were combined in a single index (X) which expresses the ratio of soil loss under a given slope steepness and slope length. Due to the fact that slope length becomes increasingly less important as the variable increases (Stocking *et al.*, 1988) the maximum slope length can be set at 100m (Chakela and Stocking, 1988; Stocking *et al.*, 1988). However, the inner hollow centre of the splash cup has a diameter of 10cm (0.1 m). That is the slope length employed in this research. The slope-length factor grid (X) was created using equation 3.15.

$$X = \sqrt{L} * \frac{(0.76 + 0.53 * S + 0.076S^2)}{25.65} \quad \textbf{(3.15)}$$

Where:

X = topographic ratio

L = slope length (m), and

S = slope gradient (%).

The slope length and slope steepness sub-factors were calculated from the filled DEM for the UNIVEN and Tshivhase points. The slope gradient is 2.720 and 10.555 for Thohoyandou and Tshivhase, respectively. The substitution of these factors into equation (3.15) produced the relief (X) factor of the SLEMSA. The overall SLEMSA model is depicted in Figure 3.5.

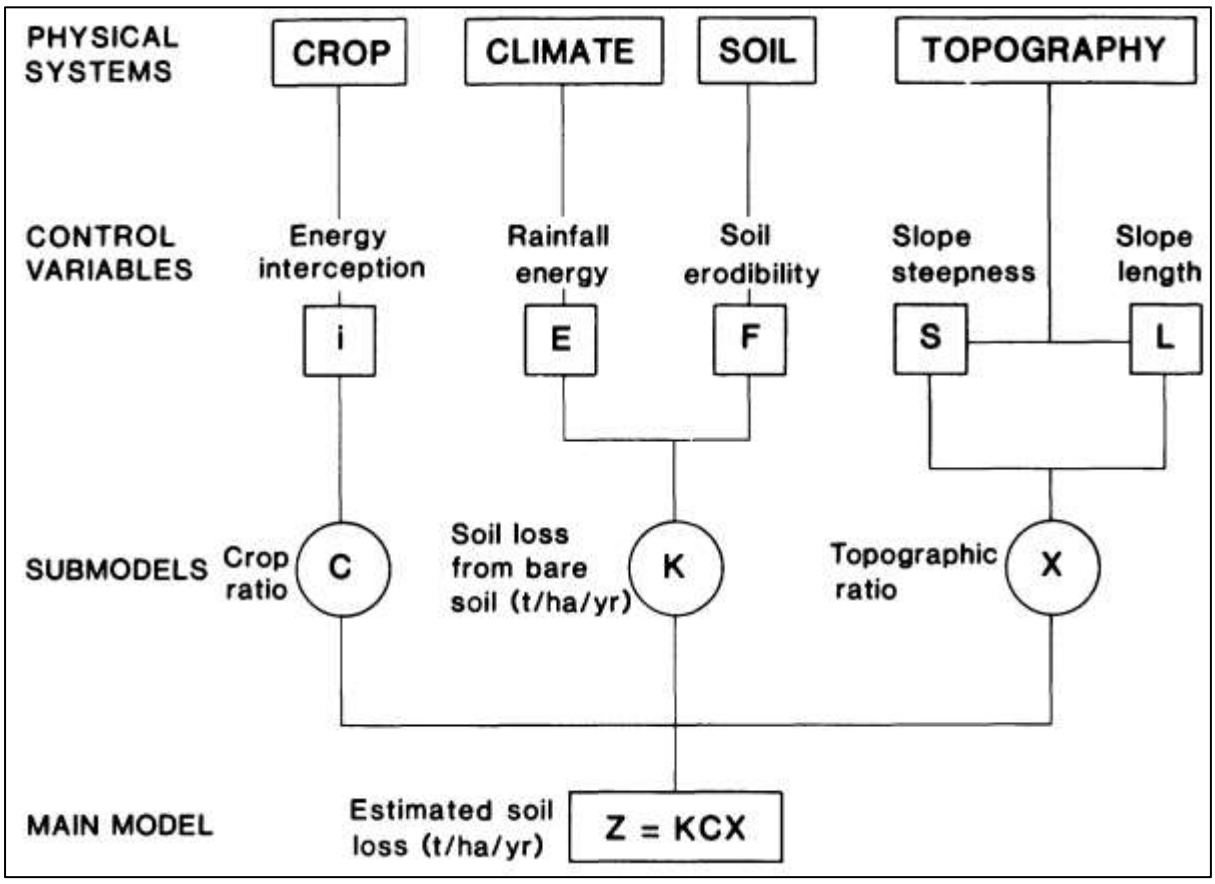

Figure 0.7: SLEMSA Model (Source: Stocking *et al.*, 1988)

3.4.4.2 The Universal Soil Loss Equation (USLE)

The USLE represents an erosion model developed for the prediction of soil losses in an average long-term sense (Vantas *et al.*, 2019). It is based on the knowledge of the physical characteristics of the area under study, along with the prevailing cropping and management system. It uses four dimensionless factors to calculate soil loss as described by dimensioned rainfall and soil factors (Renard *et al.*, 1997; Kinnell, 2010) as shown in equation 3.16.

$$A = R \times K \times LS \times C \times P \qquad \textbf{(3.16)}$$

Where

A = average (mean) annual soil loss (Mg ha^{-1} yr^{-1}) over the long term (e.g., 20 years),

R = the rainfall–runoff erosivity factor (MJ mm ha^{-1} hr^{1}),

K = the soil erodibility factor (Mg ha hr ha^{-1} MJ^{-1} mm^{-1}),

L and S = the topographic factors that depends on slope length and gradient,

C = the crop and crop management factor, and

P = the soil conservation practice factor.

Slope length and gradient, the crop and crop management factor and the soil conservation practice factor are dimensionless multipliers. They are used to adjust the value of the rainfall–runoff erosivity and the soil erodibility factors to other conditions (Kinnell, 2010). Therefore, only erosivity and erodibility have units. The other factors are reduced variables that are mathematically forced to take on values of 1.0 for the unit plot (Kinnell, 2010). The following is a detailed explanation of the variables and how they were computed. Note that erodibility and erosivity have been elaborated on under section 3.4.1.1 and 3.4.3.1. They will not be repeated here.

3.4.4.2.1 Topography Factor (LS)

Slope length (L) is the horizontal distance from the beginning of overland flow to the point of deposition (Renard *et al.*, 1997). The slope steepness factor (S) is the effect of the slope gradient on soil erosion in relation to the standard plot steepness of 9%. The slope length-gradient factor is given at a standard 22.1 m and 5.14 degrees, respectively. However, any slope length is usable (Kinnell, 2010). Therefore 10 cm (0.1 m) derived from the central hollow part of the splash cup was used for this research. The two aspects were computed separately before multiplication into a single topography factor figure. Equation 3.17 and 3.18 are used for slope length and angle computation, respectively. The figures for the slope length and angle were derived from the DEM using a slope length function available in ArcGIS software.

$$L = (\frac{x}{22.13})^n \quad \textbf{(3.17)}$$

x = slope length (m) along the horizontal projection rather along the sloping surface.

22.13 = slope length of the standard plot,

n = ratio of rill erosion to inter rill erosion

$$n = \frac{\beta}{1+\beta} \qquad \textbf{(3.17.1)}$$

$$\beta = \frac{sin\theta/0.0896}{[3.0*(sin\theta)^{0.8}+0.56]} \qquad \textbf{(3.17.2)}$$

Sin θ = the slope angle

$$S = 3.0 * (sin\theta)^{0.8} + 0.56 \qquad \textbf{(3.18)}$$

3.4.4.2.2 Vegetation or Crop Cover Factor (C)

The vegetation cover-management factor is specified cover and management to soil loss. The C factor is a ratio comparing the soil loss from land under a specific crop and management system to the corresponding loss from continuously fallow and tilled land. The main factors that control the cover and management factor are canopy cover, surface vegetation, prior land use, mulch cover, surface roughness and soil moisture (Lorentz and Schulze, 1995). The factor range is wide and considerably variable during the year (Mhangara *et al.*, 2012). That makes it generally difficult and costly to estimate when covering a large area.

Satellite imagery provides a basis for a good estimation of the cover factor that focuses on vegetation cover only (Mhangara *et al.*, 2012; Márquez *et al.*, 2019) over large areas. The C factor for this research was needed for the two stations where the splash cups were set up. Therefore, it was easy to scout the area and empirically determine the values. Following Wischmeier and Smith (1978) C factor guide for permanent pasture, veld and woodland, 0.45 was the appropriate value to use. This

is because the inner hollow cylinder of the splash cup was not covered by vegetation in all circumstances (see figures 3.2 and 3.3).

Suffice to say, Univen Experimental farm is an open cultivated space. Therefore, there was no canopy cover. However, there was about 80% surface cover by grass and /or grass like plants. On the other hand, Tshivhase Tea Estate has short tea bush with average drop fall height of half a metre. The tea bush covers at least 95% of the surface. However, the soil used in this research was collected from the central hollow cylinder of the splash cup.

3.4.4.2.3 Conservation Practice Factor (P)

The conservation practice factor focuses on practices like contouring, strip cropping, or terracing. It reflects the effects of practices that will reduce the amount and rate of the water runoff and thus reduce the amount of erosion. The P factor represents the ratio of soil loss by a support practice to that of straight-row farming up and down the slope. Support practice basically impacts soil erosion by altering the flow pattern, gradients, or direction of surface runoff and by reducing the amount and rate of runoff (Mhangara *et al.*, 2012). The conservation rating ranges from 0.001 to 1 (Wischmeier and Smith, 1978). A lower P value indicates the adoption of highly effective conservation practices to control soil erosion. Both places practice highly effective conservation practices. Tshivhase Tea Estate is highly vegetated and contoured. Tea is a permanent crop. The Univen Experimental farm is contoured for control of surface runoff. However, soil collected from splash was from the cleared inner hollow part of the splash cup. Therefore, both sites were granted a P factor value of 0.75 (Pennock *et al.*, 1987).

3.5 Chapter Summary

The aim of this research has been to analyse the spatial-temporal characteristics of soil erodibility and rainfall erosivity on the Soutpansberg range. However, soil erosion is a complex process that involves a variety of factors. Though erosivity is the main driver of erosion, its magnitude is affected by rainfall characteristics as well as by both intrinsic soil characteristics and other extrinsic factors. Therefore, the aim

of this research has been to analyse both the soil and rainfall components of soil erosion.

The first specific objective was to classify geomorphic features of the Soutpansberg range to show the erodibility characteristics of the mountain. The second was to characterise the spatial-temporal aspects of potentially erosive rainfall to reveal the distribution of rainfall erosive potential on the mountain range. The third specific objective was to assess the influence of topography on wind speed and rainfall erosivity on the mountain range to establish the effect of topography on wind speed and erosivity. The last objective was to compare USLE and SLEMSA rainfall erosivity incorporating WDR erosivity to establish the influence of wind on soil erosion. The specific objectives dictated the data needed as well as the analysis methods.

The classification of geomorphic features needed five sets of data. The sets are soil, hydrology, slope, geology and land-use-land-cover data. Soil data were obtained from the Harmonised World Soil Database (HWSD v 1.21) layer downloaded from The International Institute for Applied Systems Analysis (IIASA) online database. Additional soil data were obtained from field samples and splash cups. Hydrological data were downloaded from Department of Water Affairs, Forestry and Fisheries (DWAFF). However, for line density calculation, river systems derived from the DEM are used. Slope data were derived from the 30m pixel size SRTM DEM obtained from National Geo-Spatial Information (NGI). The derivations were done in SAGA GIS. Geological data were downloaded from South African Geosciences online database. Land-use-land-cover were extracted from the South African National Land Cover 2018 dataset accessed online on the Department of Forestry, Fisheries and Environment website.

Rainfall and wind speed data are the most essential for erosivity computation. These data were obtained from the South African Weather Service. The data record begins in 2000 to 2019. The data are in daily totals and hourly totals. Only five stations had hourly records constituting a combined 383 storms from 2000 to 2019. The five stations are the focus of the analysis since WDR, USLE and SLEMSA are storm based computations.

Erodibility was assessed using GIS tools to combine the five factors. Rainfall erosivity was computed from USLE, SLEMSA and WDR tools. The outputs of the different computations were tested for differences using MANOVA. Regression analysis was employed to determine the contribution of wind, elevation and rain to erosivity. In `summary, this research will be as presented in Table 3.6.

Table 0.2: Research Matrix

Objective	Research Questions	Key Variables	Data Sources	Analytical Tool(s)	Key Deliverables
1. Classify geomorphic features of the Soutpansberg range to show the erodibility characteristics of the mountain	a) What geomorphic factors define soil erodibility on Soutpansberg?	Soil erodibility; hydrography; geology; land-use-land-cover; terrain.	Online databases; DEMs	Geomorphic classification; GIS map agebra.	Soil erodibility map
	b) How do the geomorphic factors relate?				
	c) What erodibility representation is produced by the relationship between the factors?				
2. Characterise the spatial-temporal aspects of potentially erosive rainfall to reveal the distribution of rainfall erosive potential on the mountain range	a) How is erosive rainfall spatially distributed over the Soutpansberg?	Rainfall and rainfall erosivity spatial autocorrelation; rainfall erosivity and rainfall temporal correlation	SAWS Weather stations	Moran's I; Coefficient of Variation	Rainfall distribution map; rainfall erosivity distribution map; spatial autocorrelation values.
	b) How is the rainfall erosivity spatially distributed over the mountain range?				
	c) How is the rainfall temporally distributed over the mountain range?				
	d) How is the rainfall erosivity temporally distributed over the mountain range?				
3. Assess the influence of topography on wind speed and rainfall erosivity on the mountain range to establish the effect of topography on wind speed and erosivity	a) How does rainfall influence erosivity?	Wind speed; elevation erosivity.	SAWS Weather stations; Erosivity computaions	MANOVA; regression analysis; t-test	Decision on hypothesis.
	b) How does wind speed influence rainfall erosivity?				
4. Compare USLE and SLEMSA rainfall erosivity incorporating WDR erosivity to establish the influence of wind on soil erosion	a) How do the three rainfall erosivity values differ?	R values for USLE, SLEMSA and WDR	Formulae; field data	MANOVA and t-test	Decision on hypothesis.
	b) To what extent does wind contribute to the difference?				
	c) Which of the values represents reality better?				

: SOIL ERODIBILITY OF THE SOUTPANSBERG

4.1 Introduction

Soil erosion research has been growing in scope, depth and scientific rigor since the mid-20th Century. However, it is not in dispute that as a natural process, soil erosion is complex. Evaluation, comprehension and simplification of the components and factors controlling soil erodibility is the foundation of erosion control. The evaluation, comprehension and simplification is achievable through classification of the geomorphic features of the Soutpansberg range to illustrate the erodibility characteristics of the mountain. This addresses the first objective of this research. The logic behind this objective was to illuminate the base on which soil erosion occurs. This should illustrate the erosion risk associated with the mountain range from a soil perspective. Therefore, the reasonable starting point would be a view of the factors that control erosion in general before zeroing into erodibility. This will be followed by a presentation of the soils found on the Soutpansberg range before the geomorphic classification results.

4.2 Soil Erosion Control Factors

The factors that play a controlling role in soil erosion include rainfall erosivity (R), vegetation cover management factor (C), soil erodibility (K), slope length and steepness (LS), and conservation practices (P) (Wischmeier and Smith, 1958; Stocking, 1980; Renard *et al.*, 1997; O'geen, 2006; Irvem *et al.*, 2007). The erosivity factor (R) is the rainfall erosion index representing rainfall energy. This will be dealt with in more detail in Chapters 5, 6 and 7.

The vegetation cover-management factor (C) is a ratio comparing the soil loss from land under a specific crop and management system to the corresponding loss from continuously fallow and tilled land. Soil loss rate per erosion index unit for a specified soil as measured on a standard plot is the soil erodibility factor (K). The angle and length (LS) of slope that influence soil erosion was also considered. The effects of practices that reduce the amount and rate of water runoff and thus reduce the erosion rate is reflected by the land use support practice (P) factor. The P factor represents the ratio of soil loss by a support practice to that of straight-row farming up and down the slope.

It is important to highlight that the variables of importance for this research are erodibility (K) and erosivity (R). This is because soil erosion is principally determined by erosivity (R) and erodibility (K) (Renard *et al.*, 1997; Kinnell, 2010). They are the only dimensioned factors in soil erosion modelling (Renard *et al.*, 1997; Kinnell, 2010), whereas the rest of the factors involved are empirically determined constants or scaling factors. Erosivity explains about 80% of variations in erosion (Wischmeier and Smith, 1958). Yao *et al.* (2016) agree by indicating that erosivity is the primary driver of erosion, with considerable influence from erodibility.

Soil erodibility plays a significant role in determining soil particle detachability, and hence sediment movement (O'geen, 2006; Kusumandari, 2014; Uzun *et al.*, 2017). The extent of erosion on a given soil type, and hence the tolerance level, varies, depending on the soil characteristics and properties (Renard *et al.*, 1997; Stone and Hibron, 2012). The soil characteristics and properties, in a nutshell, is the soil erodibility. Soil erodibility represents the effect of soil characteristics and properties on soil erosion (Renard *et al.*, 1997).

In natural settings, erodibility is a soil's response to the erosive energy of rainstorms (Renard *et al.*, 1997). Simply put, erodibility represents a soil's reaction to erosion and hydrologic processes. How a soil reacts depends on its intrinsic characteristics as well as extrinsic factors. This takes into cognisance that erosional processes begin at soil detachment and transport by raindrop impact and surface flow, followed by deposition due to topography and land-use-land cover characteristics, and rainwater infiltration into the soil profile (Choi, 2002; Kinnell, 2005; Ritter, 2012). That is why the illustration of soil erodibility on the Soutpansberg range covers both intrinsic soil characteristics as well as extrinsic factors.

Although resistance to erosion is an innate characteristic of a soil, it is affected by other environmental characteristics. For example, the raindrop impact velocity and angle are influenced by land cover characteristics. For instance, urban development reduces green open space area thereby affecting soil erodibility (Kusumandari, 2014). Erodibility may increase if the surface is not compacted, while compaction reduces it. Overland flow depends on gradient, land surface characteristics, such as compaction, as well as water channelization. Infiltration and percolation depend on surface characteristics as well as geology.

Therefore, the geomorphological classification considers soil erodibility from an intrinsic perspective in conjunction with extrinsic factors. The extrinsic factors are derived from the adaptation of the Universal Soil Loss Equation (USLE) and the Soil Loss Estimation Model for Southern Africa (SLEMSA). Consequently, the slope (from LS), land use land cover (from the P and C factors), the hydrography (from the R factor) as well as the geology factors were incorporated in the geomorphological classification. The land use land cover factor combines the P and C factors because soil vegetation cover is determined by land use practices. The hydrography factor considers the runoff aspect of erosivity. It depicts the exposure of soil to detachment by flowing water. The geology factor flows from the soil and slope factors. Soil is formed from rocks while rock characteristics influence slope angle and length. The following are the results of the geomorphological classification that illustrates the erodibility characteristics of the Soutpansberg range.

4.3 Soutpansberg Soil Types

The mountain range has fourteen soil types belonging to five texture classes. Leptosols, Acrisols, Lixisols and Luvisols are the common soil types of the Soutpansberg range. Leptosols are the most dominant and occupy 54% of the range. They are found in the high elevation areas, above 1200 m.a.s.l. Acrisols occupy 12 % while Lixisols cover 10%. Luvisols cover just over 7%. Acrisols are found in areas between 800 and 1200 m.a.s.l. Lixisols and Luvisols occupy areas falling below 600 m.a.s.l.

The common soil texture is clay loam. The other granulometric groups found on the mountain range are sand, clay, sandy clay loam and sandy loam. Clay loam occupies 56% while sandy clay loam occupies 27%. Sandy Loam is found in 10% while clay occupies 5%. Sand is found in only 2% of the range. This is pertinent in informing erodibility because the granulometric characteristics of a soil have a significant influence on soil particle detachment (Renard *et al.*, 1997; Kusumandari, 2014; Uzun *et al.*, 2017). A detailed report on the soils will make this position clearer. The focus here, however, will be on clay loam, sandy clay and sandy loam because they occupy significant portions of the Soutpansberg range. Sand and clay occupy very negligible portions.

4.3.1 Clay Loam Soils

Eutric Leptosols, Lithic Leptosols, Chromic Cambisols and Eutric Cambisols are clay loam and occupy over half of the Soutpansberg range. Lithic Leptosols are the most dominant, occupying 32 % of the mountain range. Eutric Leptosols occupy 22% while Chromic Cambisols occupy 2%. Eutric Cambisols take only 1% of the mountain range. Clay loam contains 55-80 %, 20-45% and 15-50%, clay, sand and silt, respectively. Therefore, in general terms, clay loam is easily detachable because clay and silt particles are light (Food and Agriculture Organization for the United Nations, 1998). However, the level of detachability is determined by the exact amount of clay, loam, sand and organic matter (Kusumandari, 2014). Further details will dwell more on the two Leptosol units only because of their dominance of the Soutpansberg range. Figure 4.1 shows the distribution of the different soils while Table 4.1 shows the soil types and granulometric classes.

Leptosols are very shallow soils, less than 25 cm deep, overlaying hard rock or highly calcareous material (International Union of Soil Sciences Working Group, 2006; Encyclopedia Britannica, 2016). However, they can also be deep but with extremely high gravel and or stone content (International Union of Soil Sciences Working Group, 2006). Their dominance in this region is consistent with the location as they are common in medium to high altitude regions with strong dissection (International Union of Soil Sciences Working Group, 2006), like the Soutpansberg range. They are found in areas where erosion and soil formation are occurring at the same pace or has removed the top of the soil profile.

The Lithic Leptosol unit is one with a peat layer that is less than 10 cm thick. They usually have a continuous rock starting within 10 cm of the soil surface. Lithic Leptosols are found on the central crest of the Soutpansberg range. The unit is narrow on the western region of the mountain but widens from Dzanani to the eastern edge of the range. A large part of the soil belt is on the northern wing of the mountain. An ‘island’ of Haplic Lixisols stretching from south-eastern Tshixwadza to south-eastern Thengwe prevents Lithic Leptosols from covering the whole eastern region of the Soutpansberg crest. The soil unit forms most of the watershed of the Soutpansberg range.

The Eutric Leptosol unit is one where the layer containing the essential plant nutrient elements is directly above the continuous rock. This soil forms a narrow belt on the northern edge of the Lithic Leptosol. It occupies scree, transportational and foot slopes. Many Stage 1 streams flow on this soil.

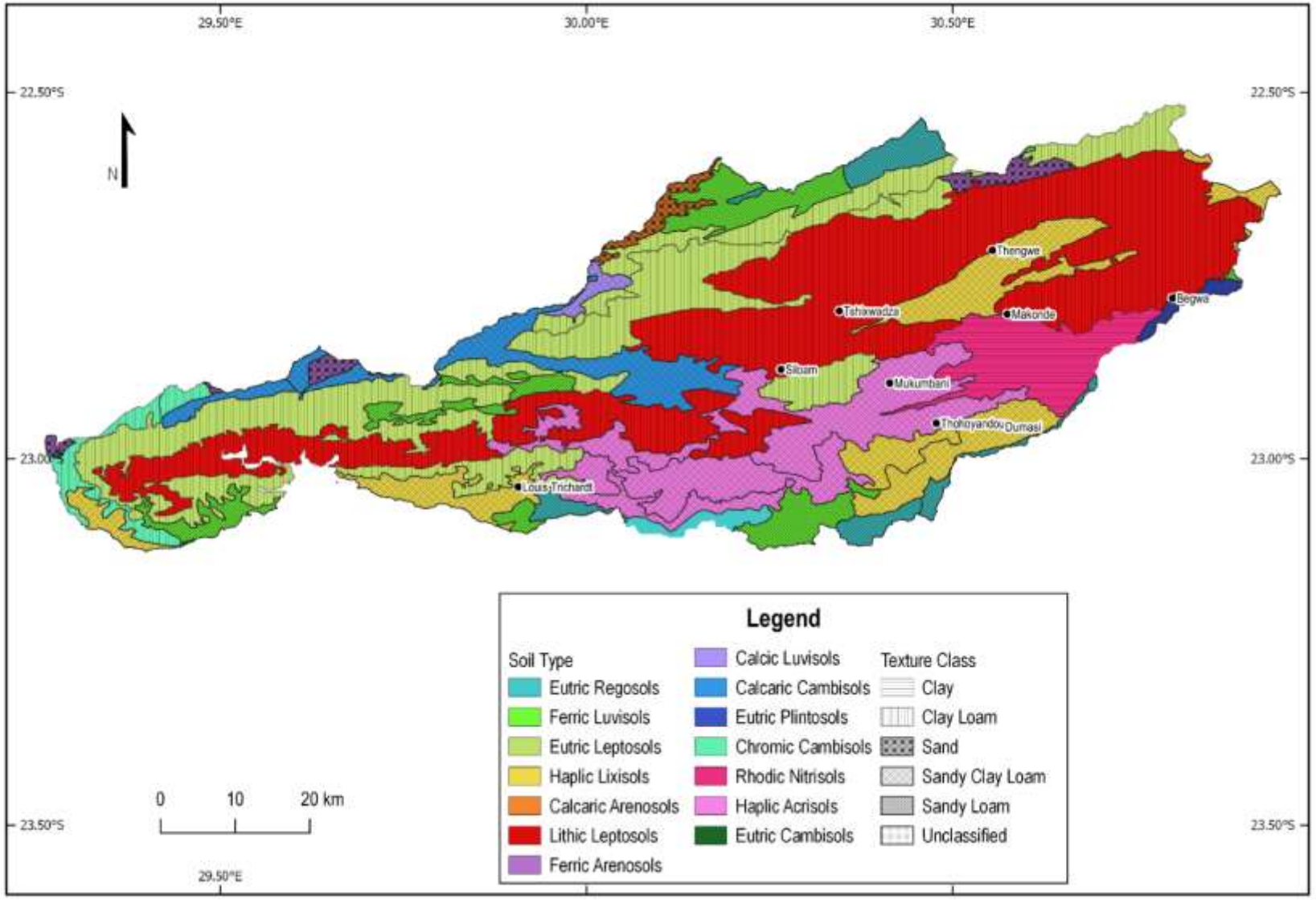

Figure 0.1: Soutpansberg Soil Types Distribution

Table 0.1: Soutpansberg Soils

Soil Type	Symbol	Granulometric Group	Soil Type	Symbol	Granulometric Group
Eutric Regosols	RGe	Sandy Loam	Calcic Luvisols	LVk	Sandy Clay Loam
Ferric Luvisols	LVf	Sandy Loam	Calcaric Cambisols	CMc	Sandy Clay Loam
Eutric Leptosols	LPe	Clay Loam	Eutric Plinthosols	PTe	Sandy Loam
Haplic Lixisols	LXh	Sandy Clay Loam	Chromic Cambisols	CMx	Clay Loam
Calcaric Arenosols	ARc	Sand	Rhodic Nitisols	NTr	Clay
Lithic Leptosols	LPq	Clay Loam	Haplic Acrisols	ACh	Sandy Clay Loam
Ferralic Arenosols	ARo	Sand	Eutric Cambisols	CMe	Clay Loam

4.3.2 Sandy Clay Loam Soils

The sandy clay loam texture class is composed of Haplic Lixisols, Calcaric Cambisols, Calcic Luvisols and Haplic Acrisols. Lithic Leptosols. Sandy clay loam contains 30-55%, 45-80% and up to 28% clay, sand and silt, respectively. Therefore, in general terms, sandy clay loam is moderately detachable because clay and loam particles are light while sand offers some resistance (Food and Agriculture Organization for the United Nations, 1998). However, organic matter content may change this status. Hence computations will give a substantive erodibility status of the soil group.

The dominant sandy clay loam is the Haplic Acrisol that occupies 12% of the mountain range. Haplic Lixisols occupies 10% while Calcaric Cambisols take 4%. Calcic Luvisols occupy a

very negligible 0.5% of the mountain range. Further details will focus on Haplic Acrisols and Haplic Lixisols because they occupy a significant part of the mountain range.

Acrisols are soils that have a higher clay content in the subsoil than in the topsoil (International Union of Soil Sciences Working Group, 2006). Acrisols are characterized by movement and accumulation of low-activity clays occurring on old hilly land surfaces where the relief is variable but often steeply sloping (Development Studies Associates (DSA) and Shawel Consult International (SCI), 2006; International Union of Soil Sciences Working Group, 2006; WMO, 2021). Haplic Acrisol units have a higher clay content in the subsoil than in the topsoil. This results from pedogenetic processes, such as clay illuviation, that form an argic subsoil horizon (International Union of Soil Sciences Working Group, 2006). The argic horizon is a subsurface soil layer that has a distinctly higher clay content than the overlying layer.

Haplic Acrisols occupy the prominent high elevation southern wing of the mountain range. The soil belt stretches from Louis Trichardt in the west to Mukumbani in the east. This is the belt where the Tea Estates are established and where splash cups were set. The soil occupies the flat-topped plateaux found in this part of the mountain range.

Lixisols are characterized by the subsurface movement and accumulation of low-activity clays and a high base saturation (Encyclopedia Britannica, 2019; WMO, 2021). They have a thin, brown, ochric surface horizon over a brown or reddish brown argic horizon. Lixisols are strongly weathered such that clay is washed out of the top, down to a lower horizon (Ebelhar *et al.*, 2008), forming the argic horizon (Spaargaren and Decker, 1995). Haplic Lixisols are uncategorised Lixisols that form over weathered voltaian sandstone on middle-slope and gentle sloping topography (Fosu-Mensah and Mensah, 2016). They have high sand content, are naturally acidic and generally have low nitrogen and organic carbon. Haplic Lixisols have no specific characteristics (Food and Agriculture Organization for the United Nations, 1998). Neither do they have a diagnostic horizon except an anthropopedogenic horizon. An anthropopedogenic horizon exhibits the long existence of cultivation the Soutpansberg range. The soils occupy a thin strip of the southern edge of the range where haplic Acrisol ends. It forms part of the Levubu valley as it occupies the open valleys along Luvuvhu river and fool slopes on the cliffs of the south facing slopes.

Luvisols have a distinct characteristic of distinct textural differentiation within the soil profile. They form on flat to gently sloping topography from unconsolidated materials including glacial till, and aeolian, alluvial and colluvial deposits. A subsurface layer called an argic horizon accumulates clay that is depleted from the surface horizon (International Union of Soil Sciences Working Group, 2006; WMO, 2021). Therefore, Luvisols have a higher clay content in the subsoil than in the topsoil due to argilluviation leading to an argic subsoil horizon. The surface horizon is typically brown to dark brown overlying a greyish brown or red argic subsurface horizon. Luvisols generally have mixed mineralogy, high nutrient content, and good drainage typically on gently sloping terrain (Encyclopedia Britannica, 2019). Calcic Luvisols are calcareous in the region between 20 to 30 cm from the surface (Batjes *et al.*, 2020). Calcic Luvisols occupy a very negligible portion of the gentle plains and open valley on a small portion of Mutamba River.

Cambisols are characterized by weak or the absence of distinct horizons of accumulated clay, humus, soluble salts, or iron and aluminium oxides (International Union of Soil Sciences Working Group, 2006; Food and Agiculture Organisation, 2015; Encyclopedia Britannica, 2016). They are young soils in the beginning of formation and occur in level to mountainous terrain. They differ from non-weathered parent material in their aggregate structure, colour, clay content, carbonate content, or other properties (International Union of Soil Sciences Working Group, 2006; Encyclopedia Britannica, 2016). Calcaric Cambisols are calcareous at least between 20 and 50 cm from the soil surface. They usually lack micronutrients, especially zinc and iron (Food and Agriculture Organization for the United Nations, 1998). Chromic Cambisols are reddish in colour and are found around Dzanani. There is a narrow belt of the soils from Dzanani going north to Mutamba river where another portion of the soil is found.

4.3.3 Sandy Loam Soils

The sandy loam granulometric group is composed of Eutric Regosols, Ferric Luvisols and Eutric Plinthosols. Ferric Luvisols occupy 7% while Eutric Regosols take 1%. Eutric Plinthosols are found in just 0.5% of the mountain range. Sandy loam has 50-70%, 15-20% and up to 50% sand, clay and silt, respectively. This means that sandy loam particles are not generally easily detachable due to the resistance offered by sand particles. However, the actual erodibility status can only be determined by computation.

The general characteristics of Luvisols were covered under 4.3.2. therefore, this section will focus on Ferric Luvisols only. The high sand content in the soil makes it well aerated, and therefore, iron oxidization to ferric state easy. The ferric oxides are highly insoluble and form a horizon in the soil profile. The ferric horizon starts within 100 cm of the soil surface. Ferric Luvisols are found in isolated pockets in all sections of the range. Notable, though, is that they are found along rivers.

Plinthosols are identifiable by the presence of plinthic, petroplinthic or pisoplinthic horizons (Food and Agiculture Organisation, 2015). A plinthic horizon is an iron-rich soil horizon more than 15 cm thick and containing more than 25% plinthite. Plinthe is an iron-rich, humus-poor mixture of clay with quartz and other highly weathered minerals. Eutric Plinthosols the uncategorised Plinthosols that form from weathering products with a high amount of iron on level to gently sloping topography (Food and Agiculture Organisation, 2015). The soils are found in a small portion in Begwa along Luvuvhu River in the southeast.

Regosols form a taxonomic remnant group containing all soils that could not be accommodated in any other group (International Union of Soil Sciences Working Group, 2006). Regosols are weakly developed, deep, well drained, medium textured non-differentiated mineral soils in unconsolidated materials on inert or slowly soluble parent material, recent deposits, or excavation spoils (International Union of Soil Sciences Working Group, 2006; WMO, 2021). They are the youngest soils with no pedogenic horizons and no evidence of soil forming processes (WMO, 2021). No diagnostic horizon exists. Neither do they have a mollic nor umbric horizon (International Union of Soil Sciences Working Group, 2006). Eutric Regosols are uncategorised Regosols formed on slopes and are defined as other Regosols (Food and Agriculture Organization for the United Nations, 1998). They have poor horizon development due to their young age (International Union of Soil Sciences Working Group, 2006). Eutric Regosols are found is some portions along the upper reaches of Luvuvhu river in the south and a small portion of Nwanedi River as the river exits the range on the northeast.

4.3.4 Sand and Clay Soils

Sand and clay soils occupy a combined 7 % of the mountain rage. Sand occupies 2% of the mountain range. Sand contains over 90% sand and less than 10% clay and silt. Occupying 5% of the mountain range, clay contains less than 45%, over 55% and up to 60% sand, clay and silt, respectively. Sand is composed of Arenosols while clay is made up of Nitisols. In general terms, clay is easily detachable because the particles are small and light. However, clays are cohesive with good soil structure, and it is difficult to dislodge soil particles when there is enough water. On the other hand, sand is highly resistant because it has heavy particles and high porosity.

Arenosols are sandy soils developed from the weathering of quartz-rich sediments or rock (International Union of Soil Sciences Working Group, 2006). The sediments are course textured and unconsolidated (Development Studies Associates (DSA) and Shawel Consult International (SCI), 2006). Ferralic and Calcaric Arenosols are the subunits found on the Soutpansberg.

Ferralic Arenosols are have a sandy loam or finer particle size subsurface concretion horizon resulting from long and intense weathering (Food and Agriculture Organization for the United Nations, 1998). They are very deep reddish brown to bright reddish brown sandy soils. Ferric Arenosols are found on flat to undulating to rolling topography. They are found on three small portions on the northern boundary of the range.

Calcaric Arenosols contains more than 2% calcium carbonate equivalent. The soils are found in a small portion of the mountain range along Mutamba and Nzhelele Rivers. They extend from just before the rivers confluence and continue for a short distance after the confluence. The soil occurs in the open valley.

Nitisols are deep (more than 150 cm) well drained dusky red or dark red soils with a subsurface horizon with more than 30% clay (International Union of Soil Sciences Working Group, 2006). They are well drained with deep horizons (Food and Agiculture Organisation, 2015). That subsurface horizon is the nitic layer from which the soil group derives its name. They are characterized by the strong development of structure. They originate from basic and

intermediate rocks or sediments derived under relatively intense weathering conditions. Rhodic Nitisols are found on the small portion of the range in the southeast. The portion stretches from Makonde in the east to close to Mukumbani in the west and reaches Luvuvhu river in the south.

4.4 Soutpansberg Soil Erodibility Mapping

Soil erodibility is a measure of the susceptibility of soil particles to detachment and transport by natural agents such as wind, rain drops and water runoff. The interrelation and interaction of the natural agents bring into play the role played by other external factors to influence soil erodibility. Therefore, besides intrinsic soil erodibility, Soutpansberg erodibility is illustrated through the interplay of four other factors. The factors are rain exposure, geological setting, landform and slope position. Rain exposure is derived from land-use-land-cover data, geological setting is derived from geological data, landform position is derived from hydrological data and slope position is derived from slope data. The results are presented in factor maps.

4.4.1 Intrinsic Erodibility

Two intrinsic erodibility computations are done following the USLE and SLEMSA approaches. This is done for each soil polygon. The erodibility classification was performed using the erodibility classes as given by Gilau (2015) and also using Jenks Natural Breaks (Jenks, 1967) for mapping purposes. The Gilau (2015) classification gives the computed erodibility value that communicates the generic interpretation of erodibility. Jenks breaks are created in a way that groups similar values together and maximizes the visualisation of the differences between classes. Therefore, Jenks breaks localise the classes, remove generalisations and make mapping possible.

Gilau (2015) erodibility classification results show very low erodibility status for all USLE method computed erodibility. Although the general outlook is the same for the SLEMSA computed erodibility, there are several cases where USLE indicates very low while SLEMSA indicates moderate erodibility. It is only in four polygons where USLE records very low while SLEMSA reports high or very high erodibility. Table 4.2 shows the erodibility results.

It is not readily possible to establish why such differences exist. However, a reasonable explanation is the inclusion of rainfall in the USLE formula. Nonetheless, it is not possible to establish that from the table of results presented here. This can only be established when

Table 0.2: Soutpansberg Soil Erodibility Classification

Polygon Number	Soil Type	USLE_K	SLEMSA_K	Erodibility Class	Polygon Number	Soil Type	USLE_K	SLEMSA_K	Erodibility Class
ZA13	Eutric Regosols	0.05	0.21	VL/M	ZA81	Ferralic Arenosols	0.04	0.04	VL
ZA28	Ferric Luvisols	0.05	0.29	VL/M	ZA93	Eutric Regosols	0.05	0.80	VL/VH
ZA31	Eutric Leptosols	0.05	0.05	VL	ZA91	Haplic Acrisols	0.05	0.27	VL/M
ZA37	Eutric Leptosols	0.05	0.02	VL	ZA94	Eutric Leptosols	0.05	0.31	VL/M
ZA41	Haplic Lixisols	0.05	0.04	VL	ZA90	Eutric Leptosols	0.05	0.02	VL
ZA38	Ferric Luvisols	0.05	0.29	VL/M	ZA89	Calcaric Cambisols	0.04	0.00	VL
ZA46	Calcaric Arenosols	0.04	0.24	VL/M	ZA96	Ferric Luvisols	0.05	0.24	VL/M
ZA50	Lithic Leptosols	0.04	0.09	VL	ZA95	Eutric Leptosols	0.05	0.01	VL
ZA49	Ferralic Arenosols	0.04	0.35	VL/M	ZA100	Lithic Leptosols	0.04	0.06	VL
ZA48	Eutric Leptosols	0.05	0.06	VL	ZA104	Haplic Lixisols	0.05	0.16	VL/L
ZA54	Eutric Leptosols	0.05	0.06	VL	ZA103	Lithic Leptosols	0.04	0.31	VL/M
ZA51	Ferralic Arenosols	0.04	0.09	VL	ZA108	Haplic Lixisols	0.05	0.23	VL/M
ZA60	Haplic Lixisols	0.05	0.16	VL/L	ZA102	Lithic Leptosols	0.04	0.01	VL
ZA65	Ferric Luvisols	0.05	0.06	VL	ZA109	Haplic Acrisols	0.04	0.05	VL
ZA61	Eutric Leptosols	0.05	0.06	VL	ZA107	Eutric Cambisols	0.05	0.01	VL
ZA66	Calcic Luvisols	0.05	0.04	VL	ZA110	Eutric Leptosols	0.05	0.05	VL
ZA70	Calcaric Cambisols	0.04	0.08	VL	ZA112	Haplic Lixisols	0.04	0.19	VL/L
ZA78	Eutric Plinthosols	0.05	0.42	VL/M	ZA119	Haplic Acrisols	0.02	0.03	VL
ZA72	Chromic Cambisols	0.03	0.02	VL	ZA122	Ferric Luvisols	0.05	1.06	VL/VH
ZA74	Eutric Leptosols	0.05	0.03	VL	ZA118	Ferric Luvisols	0.05	0.09	VL
ZA73	Calcaric Cambisols	0.04	0.01	VL	ZA121	Eutric Regosols	0.05	0.08	VL
ZA84	Rhodic Nitisols	0.02	0.04	VL	ZA112	Haplic Lixisols	0.05	0.05	VL
ZA75	Ferralic Arenosols	0.04	0.05	VL	ZA126	Eutric Regosols	0.05	0.69	VL/H
ZA35	Chromic Cambisols	0.04	0.05	VL	ZA120	Ferric Luvisols	0.05	0.35	VL/M
ZA77	Chromic Cambisols	0.03	0.01	VL	ZA127	Eutric Regosols	0.05	1.06	VL/VH
ZA79	Chromic Cambisols	0.03	0.00	VL	**Key: VL = Very Low; L = Low; M = Moderate; H = High; VH = Very High.**				

erodibility results are spatially represented so that they can be juxtaposed with rainfall distribution. That is why erodibility had to be mapped. Mapping gives the visual impression of the spatial characteristics of erodibility.

Although the classification used for mapping is different from the one used in the table, the representation remains the same. Erodibility ranking is not altered. Jenks natural breaks make a clearer distinction of the classes. This is where the differences in erodibility are exposed. While the Gilau (2015) classification picks a few differences, natural breaks show significant differences. The inclusion of rainfall in SLEMSA formula becomes apparent. SLEMSA classified the whole western wing of the range as very low erodibility while USLE only has negligible portions of the same class on the whole range. The western regions of the range are generally very low rainfall areas (further details in Chapter 5). The erodibility is illustrated in Figures 4.2 and 4.3.

Both models show the dominance of low and medium erodibility. Both have above 40% of the area under low erodibility. However, the SLEMSA model has more very low erodibility (18.8%) than the USLE (3.34%). Conversely, USLE (11.44%) records more areas with very high erodibility than SLEMSA (8.7%).

A further look at the two maps, however, indicates that there is no major difference between the SLEMSA and the USLE erodibility classes. Discounting the western wing, the major belt in the eastern wing occupied by Lithic Leptosols is classified as low erodibility in both methods. However, the Gilau (2015) method classifies them as very low erodibility. This should be explained by the Jenks adjustment.

The area in Levubu, Tshakhuma and Tshivhase are classified as high erodibility areas by both methods. The polygon based erodibility computation and Gilau (2015) classifies the soils as very low erodibility for Rhodic Nitisol and Calcaric Cambisols. Haplic Acrisols are classified as very low to medium erodibility. However, the Jenks natural breaks classify the areas as high to very highly erodible. The difference is brought out by the fact that the natural breaks approach is flexible and adaptable while the Gilau (2015) approach is rigid. Therefore, in general terms the places have low erodibility. However, in terms of natural breaks, they are highly erodible.

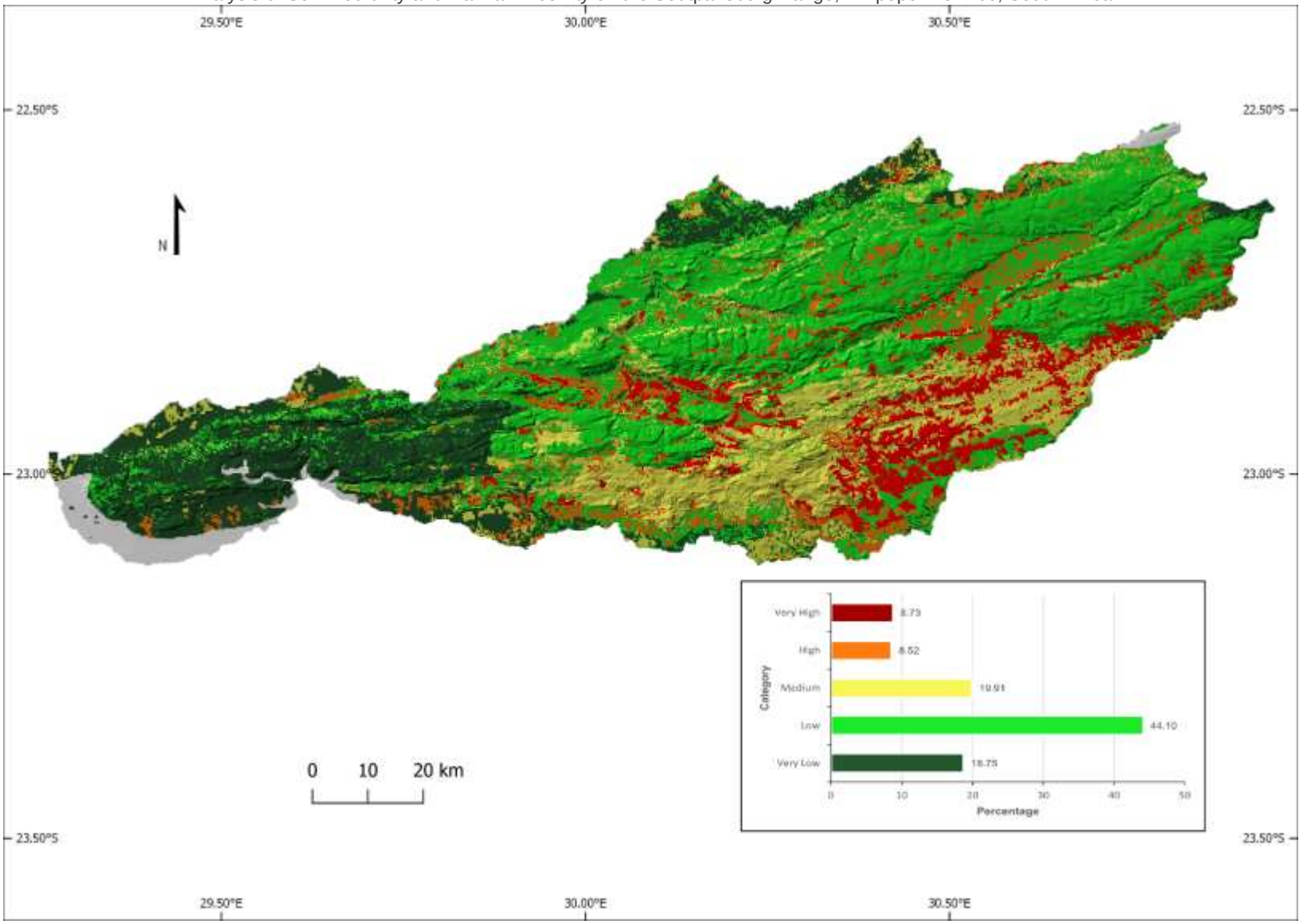

Figure 0.2: Intrinsic SLEMSA K-Erodibility

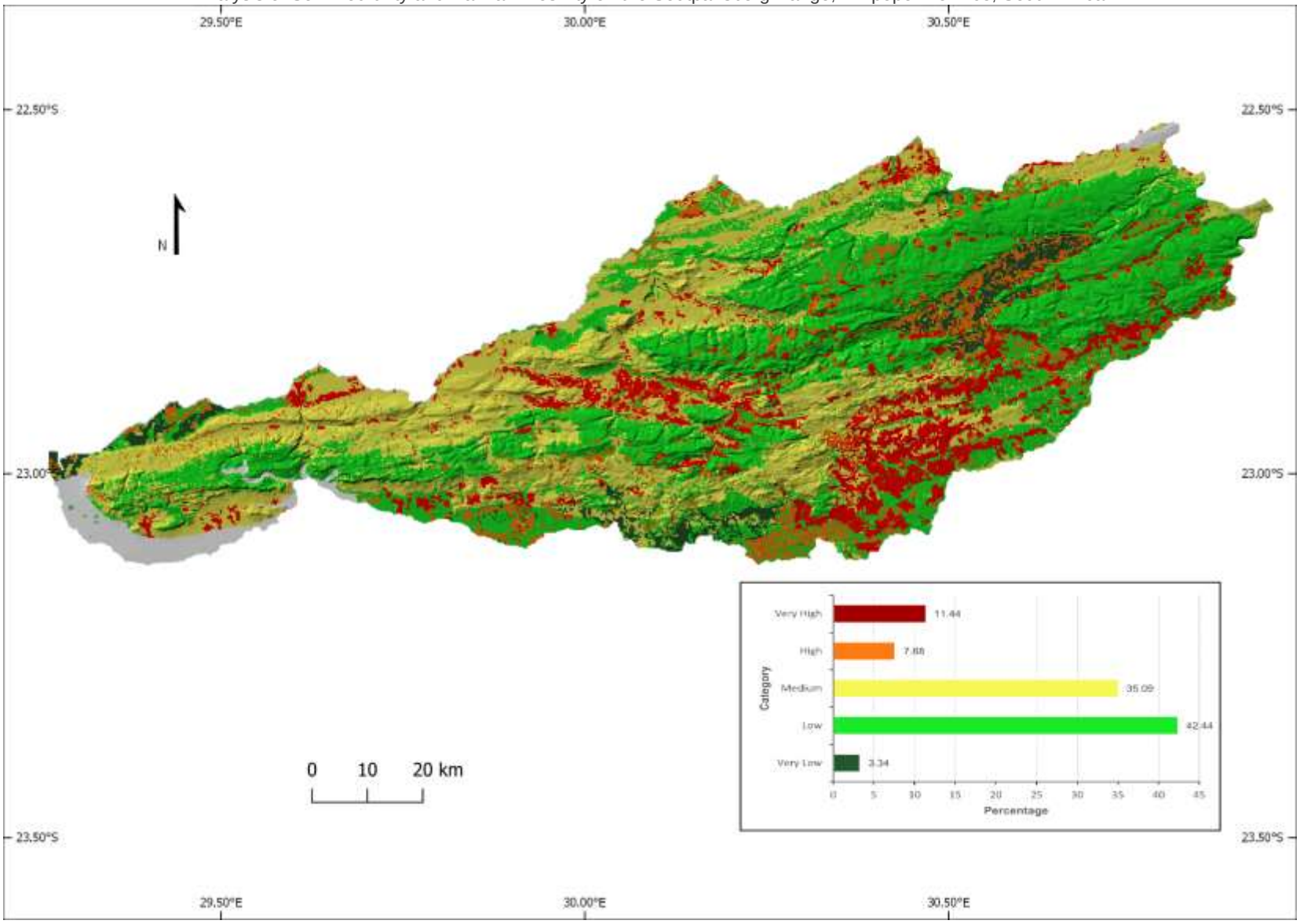

Figure 0.3: Intrinsic USLE K-Erodibility

Major differences emerge on the low and moderate erodibility classes. While USLE classifies most north facing slopes as mostly moderate, SLEMSA codes them as mostly low erodibility areas. Although just a single unit apart, the influence of the inclusion of rainfall in the SLEMSA model is apparent. The north facing slopes are generally dry and, therefore, have low SLEMSA erodibility potential. This justifies the inclusion of extrinsic factors in erodibility characterisation.

4.4.2 Extrinsic Factors to Erodibility

The extrinsic factors are land-use-land-cover, geology, hydrography, and slope. The extrinsic factors have a bearing on soil susceptibility, thereby affecting the detachability of soil particles. Land-use-land-cover factor focuses on establishing how rain drops and surface runoff end up interacting with the soil. A well vegetated area has a covering effect on the rain drop as it travels towards the ground. In addition, vegetation affects overland flow by reducing its speed, hence erosivity. In addition, some land uses promote compaction while others loosen the soil. This gives the exposure risk of the surface.

Geology determines the continued downward movement of the soil beyond the soil zone. Geology that allows water to pass through reduces the chances of water accumulating on the surface. Surface water accumulation creates the Hortonian overland flow that may erode soil. Therefore, the geological setting has a bearing on the susceptibility of soil to erosion.

The hydrography shows the places where water tends to accumulate. Places where water get concentrated have a higher risk of erosion. Therefore, the range is classified into landform position using the hydrographic information. This gives steep sided ridges as the areas farthest from places of water accumulation. River channels indicate areas where water accumulates and, sometimes, flow. The two landform positions give the very low and very high erodibility, respectively.

Slopes classify the landscape into categories from cliffs to open valleys using gradient. Slope is the angle of the Earth’s surface from the horizontal. The slope length and gradient greatly influence soil detachment through its control of surface water runoff and gravity. Hence, slope gradient is directly proportional to overland flow energy. Cliffs are the steepest while the open

valleys are the gentlest. Laws of gravity dictate that higher gradient generates more energy. Therefore, cliffs are the high erodibility while open valleys are the low erodibility. A detailed presentation of the results follows below.

4.4.2.1 Erosion Exposure

Applying expert classification, land-use and land-cover was classified into a five-spectrum scale from very high to very low exposure. Very high exposure (0.4%) represents areas where the land use and or land cover does not impede raindrops as they travel through the atmosphere. Neither does it inhibit soil particle detachment or overland flow. This includes land uses that loosen soil particles leading to easy detachment and or transportation. Thus, the soil would be highly exposed to rain.

Results show that a very large part of the mountain range falls under low and very low exposure (16 and 73%, respectively). This is because large segments of the mountain range are used for agroforestry and, as such, vast tracts of the range are under forests, thickets, woodland and grassland. A significant part is also under residential land use. Vegetation obstructs both raindrops and overland flow, thereby reducing the ground exposure to erosion. Residential areas tend to have compacted surfaces that make it difficult for detachment of soil particles.

Figure 4.4 shows the erosion exposure of the Soutpansberg range. It is clear from this figure that the Soutpansberg range is host to several farms practicing large scale agroforestry. The Tshivhase and The Mukumbani Tea Estates as well as Entabeni, Roodewal and Shefeera, among others, are large scale agroforestry projects on the range. The Levubu valley adds the banana, macadamia and other fruits plantations to the land use map. All these have the effect of shielding the soil from direct raindrop impact and reduce overland flow. The ultimate result is reduced soil detachment.

In addition, the range has several settlements. There is Thohoyandou, Louis Trichardt, Dzanani, Makhado and Siloam among the major settlements. The land compaction related to settlement has the effect of reducing soil particle detachability (Kusumandari, 2014). This is

actualised by several activities such as paving residential spaces and tarring roads. The dwelling structures also shield the soil.

4.2.2.2 Geological Setting

Expert knowledge was used to classify rocks according to their hardness. The hardness is associated with the rock's porosity. Granite is the most impermeable of the rocks. It covers transportational and foots slopes of the southern slopes. It also covers the same slope positions along the Nzhelele river valley form Dzanani/Siloam to Nzhelele Dam.

A large portion (84.2%) of the mountain crest is covered by Norite, Dolerite, Epidiorite, Basalt and Arenite. All these rocks are considerably hard and impermeable. They cover much of the high elevation areas in all directions. The soft and very soft rocks cover a negligible space of the range which indicates a high to very high probability of lack of vertical water movement beyond the soil zone. Such a scenario results in water accumulating of the surface and promoting Hortonian overland low. Therefore, the geological setting in the Soutpansberg range promote high erodibility. The geological setting is illustrated in Figure 4.5.

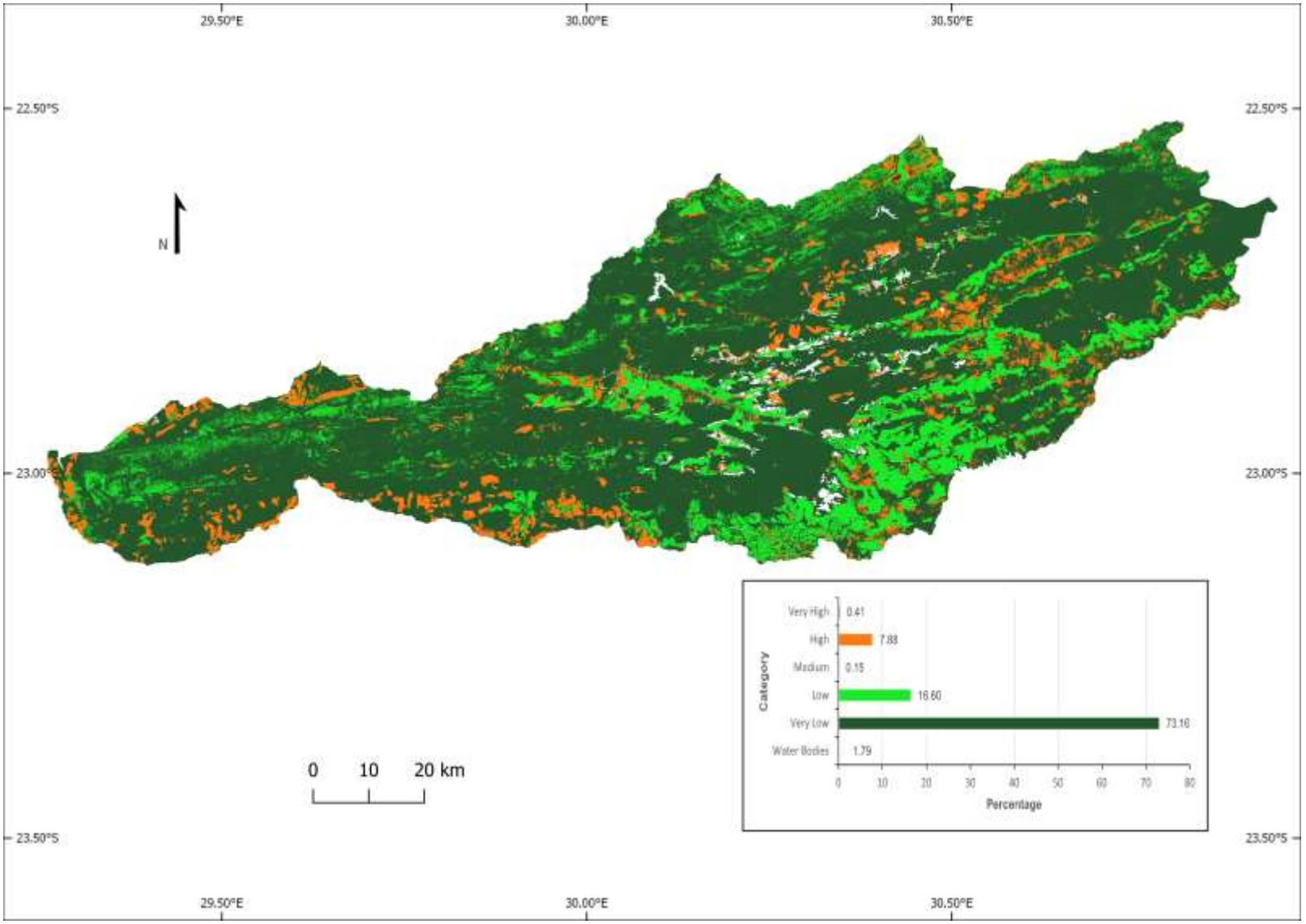

Figure 0.4: Erosion Exposure

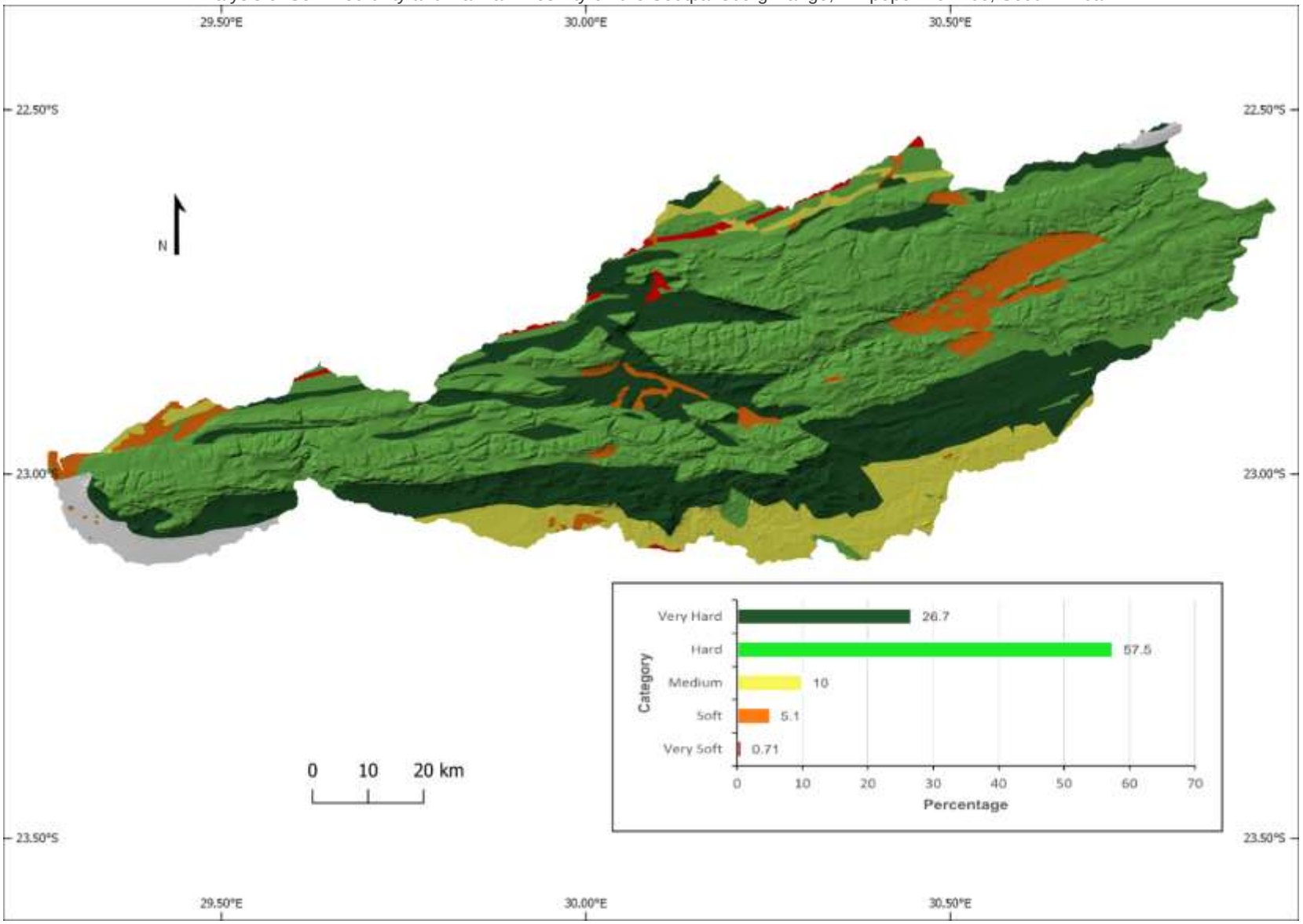

Figure 0.5: Geological Setting

4.2.2.3 Landform Position

Landform position is determined by the hydrological systems on the range. Landform position classifies the landscape into steep sided ridges, flat topped plateaux, gentle plains, open slopes and river channels (Jenness, 2006). It illustrates places where water would concentrate or otherwise to indicate the potential to promote soil erosion. Therefore, four hydrography related factors were considered. They are shoreline development ratio for large water bodies, river gradient, drainage density and Topographic Wetness Index.

Results show that areas between 800 and 1000 m.a.s.l. are flat topped plateaux that occupy 37.5% of the mountain range. Steep sided ridges (13.9%) form the crest of the mountain at more than 1000 m.a.s.l. Open slopes and river channels dissect the mountain range everywhere but occupy less than 13% of the range. There is no pattern that can be discerned. However, links with geology and soils can be established.

The steep sided ridges and flat topped plateaux coincide with hard and very hard rock areas. They also coincide with low erodibility soils, except the western wing for SLEMSA. That part has very low erodibility. Thus, it is reasonable to put it that landform position is influenced by geology and soil. Water follows a route with the least resistance.

The heavy dissection demonstrates the importance of the mountain range as a major catchment for four major rivers in Vhembe District. The Soutpansberg is the source for Luvuvhu, Mutale, Nzhelele and Sand rivers. All of them are Limpopo River tributaries. Figure 4.6 illustrates landform positions on the Soutpansberg range.

4.2.2.4 Slope Position

The slope position factor tells a story of the dominance of open valleys and foot slopes (44.5 and 26.6%, respectively). Cliffs and scree slopes (2.8 and 9.4%, respectively) occupy a very small portion of the mountain range. However, they are very prominent at higher elevations, especially above 1200 m.a.s.l. This is an interesting geomorphological set-up considering that the study area is a mountain range. A logical scenario would have been one of the dominance of scree slopes and cliffs.

However, the age and formation of the mountain range provide insights into the scenario. The mountain range was formed approximately 1800 million years ago by an east-west trending asymmetrical rift or half-graben along the Palala Shear Belt (Berger *et al.*, 2003). There is no recent history of any tectonic disturbances in the region. Therefore, it can be argued that erosive agents have had a long time to carve valleys and eat away any cliffs and steep slopes to establish rivers systems. As such, the Soutpansberg range is a major watershed in Vhembe District. Figure 4.7 shows the slope position characteristics of the Soutpansberg range.

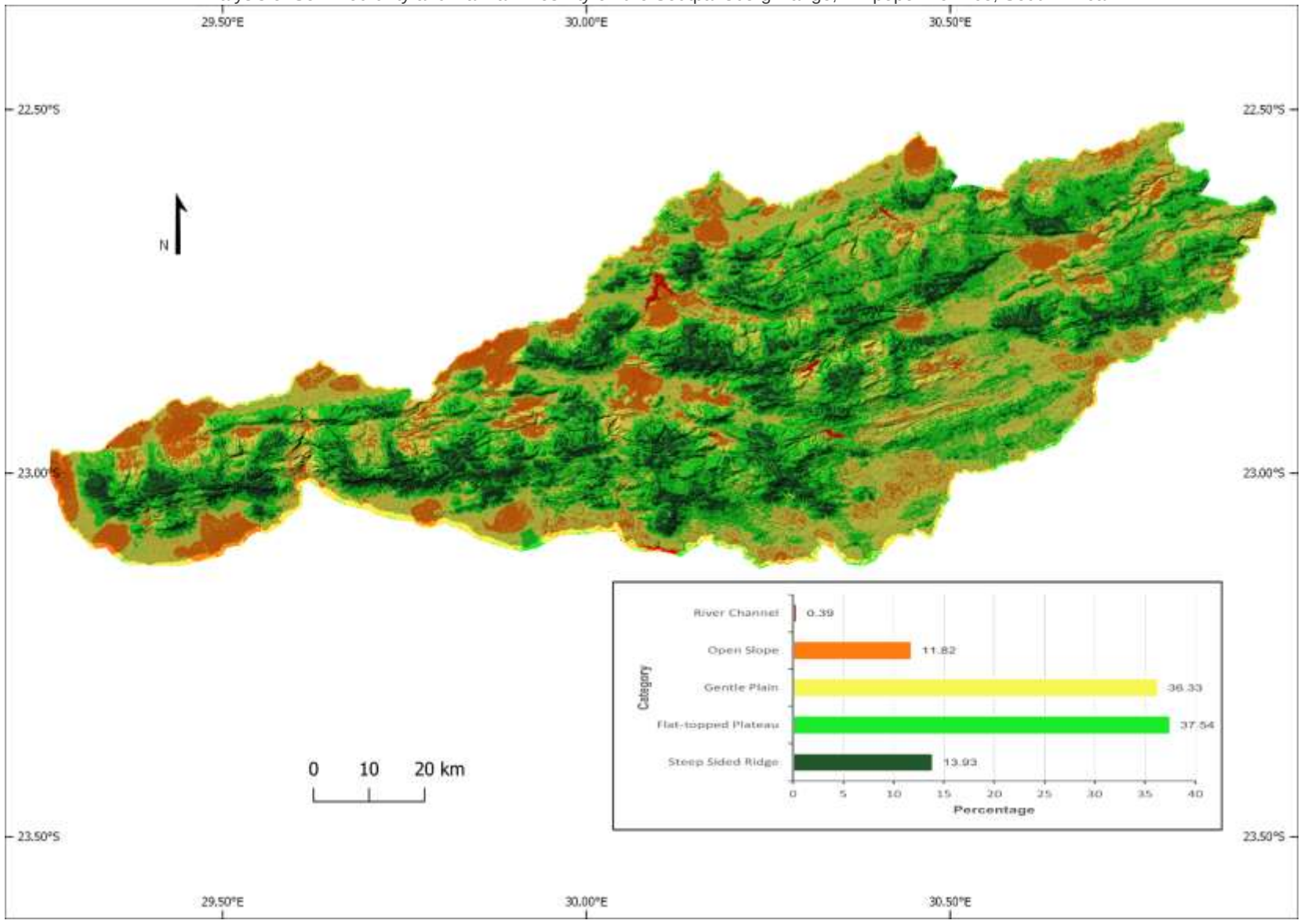

Figure 0.6: Landform Position

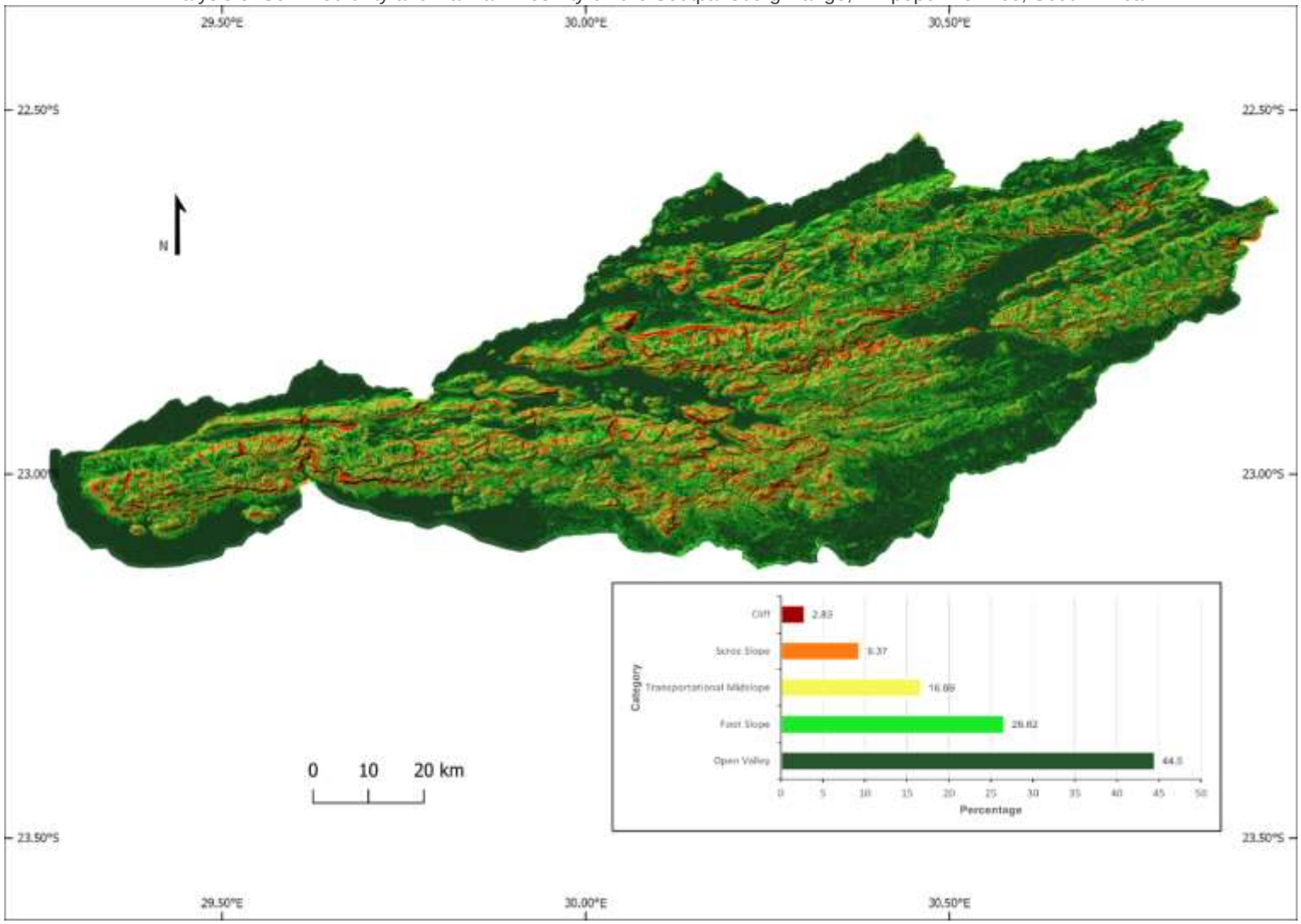

Figure 0.7: Slope Position

4.3 The Final Erodibility Maps

The two final erodibility maps are produced from overlaying all the five factors. One set considers the USLE while the other considers the SLEMSA erodibility. This presents the geomorphological setting of soil erodibility on the mountain range from the two different perspectives. However, before overlaying the five factors to produce the overall soil detachability map of the range, an online factor ranking by Multi-Criteria Evaluation (MCE) using the Analytic Hierarchy Process (AHP) was done.

The factor weighting reveals the dominance of intrinsic soil erodibility and rain exposure in determining soil erodibility. Conversely, landform position and geology carry the least weight, respectively. However, that does not mean that the influence of the other factors is negligible. As will be seen in the final maps, there are portions of the range where the influence of factors other than rain exposure and erodibility is evident. Table 4.3 presents the factor weighting results.

Table 0.3: Factor Weighting (Consistency Ratio = 7%)

Category	Weight	Rank	(+)	(-)
Intrinsic Soil Erodibility	36.1%	1	24.6%	24.6%
Geology	11.6%	4	11.4%	11.4%
Slope Position	12.8%	3	5.7%	5.7%
Rain Exposure	36.1%	1	1.9%	1.9%
Landform Position	3.3%	5	1.7%	1.7%

Nonetheless, the ranking is sensible because soil erodibility represents the intrinsic detachability resistance of a soil. Erodibility is determined by soil texture, structure, permeability and soil organic matter content. Land use and cover affects how water moves as well as soil structure. Land cover determines how raindrops travel through the atmosphere. Vegetated areas have high interception rates as opposed to bare ground. Land uses influence soil structure and characteristics. Tillage loosens soil particles and make them easily detachable. Hence, the two factors are weighted higher than the others.

It is also interesting to note that landform position is ranked lowest despite its derivation from hydrological parameters. Although hydrographical features indicate areas with the potential for erosion, it does not necessarily mean that the water would be moving and, hence, eroding. However, the hydrological channels are where the highest water erosion would mostly occur. This stems from the simple logic that more water has more energy. More water is found in the hydrological channels. However, not all water will always reach the waterways. The explanation, however, is different for slope position and geology.

When a rain drop eventually reaches the soil surface, its effect on erosion depends on the soil and slope characteristics. The soil is the primary receiver of the raindrop, hence a higher ranking on the weighting. The next level would be determined by the slope gradient. Water will only interact with geology if the soil allows infiltration, and the ground surface slope promotes it, rather than overland flow. That is why slope position is ranked higher than geology. However, some places have surface outcrops. Hence the ranking is not significantly different. A look at the final erodibility maps sheds more light to the factor weighting.

The two final soil detachability maps reveal the variable influence of the different factors in different places. The USLE generated final map shows minute areas on very low erodibility. The SLEMSA generated final map has a large part of the region west of Sand River classified as very low erodibility.

However, other factors are not silent. Both maps show high to very high detachability in the south facing slopes in areas including Thohoyandou, Tshakhuma, Tshivhase and Phiphidi areas. The belt stretches eastwards to Makonde and Begwa. Another belt of high to very high erodibility is found along Nzhelele River from Siloam westwards to a pass just after Dzanani. From the pass, the belt stretches westwards. The places have clay (Rhodic Nitisols) and sand clay loam (Haplic Acrisols and Calcaric Cambisols).

In general terms, sand clay loam is moderately erodible while clay is highly erodible. The same portions have a mixture of low and high rainfall exposure and very hard rocks. The landforms are gentle plains and open slopes while they are in open valleys and foot slopes. This shows the dominance of intrinsic soil erodibility, rainfall exposure and geology in the parts indicating high to very high erodibility in the final map.

Intrinsic soil erodibility, landform position, rainfall exposure and geology also reveal their strong influence on the low and very low erodibility on the SLEMSA generated map. The western wing of the range from Mutamba river is classified as low and very low erodibility. This section is dominated by clay loam. Clay loam is generally easily eroded. However, the region receives very low rainfall. Hence, there is no energy, according to the SLEMSA erodibility computation, to erode the soil. Therefore, the SLEMSA intrinsic erodibility emphasises very low erodibility.

The rainfall exposure factor indicates low to very low exposure on the western wing. So does the geology and landform position factors. The geology in the western wing is mainly hard rocks. The region has some of the largest rock outcrops on the mountain range. The rock outcrops create steep sided ridges and flat topped plateaux. The highest point of the range at Lajuma is in this region. The land uses and land cover are mainly forests and, hence, low erodibility.

Slope reveals its strongest influence on the edges of the south facing side of the range. This region is dominated by cliffs. Land use-land cover exercises its dominance together with soil erodibility along the crest of the range. The region has high elevations and clay loam soils. Clay loam soils promote agroforestry and therefore, the areas are occupied by forests. That is where rainfall exposure as represented by land-use-land-cover imposes its influence on the final erodibility picture of the Soutpansberg range.

Another major difference in the final erodibility maps is on the north facing slopes. The SLEMSA map classifies low erodibility in many places, whereas the USLE low erodibility is more pronounced in elevations above 1000 m.a.s.l. This indicates the strong influence of the intrinsic erodibility in the two models. The differences embedded in the intrinsic erodibility manifest in the final erodibility maps shown in figures 4.8 and 4.9.

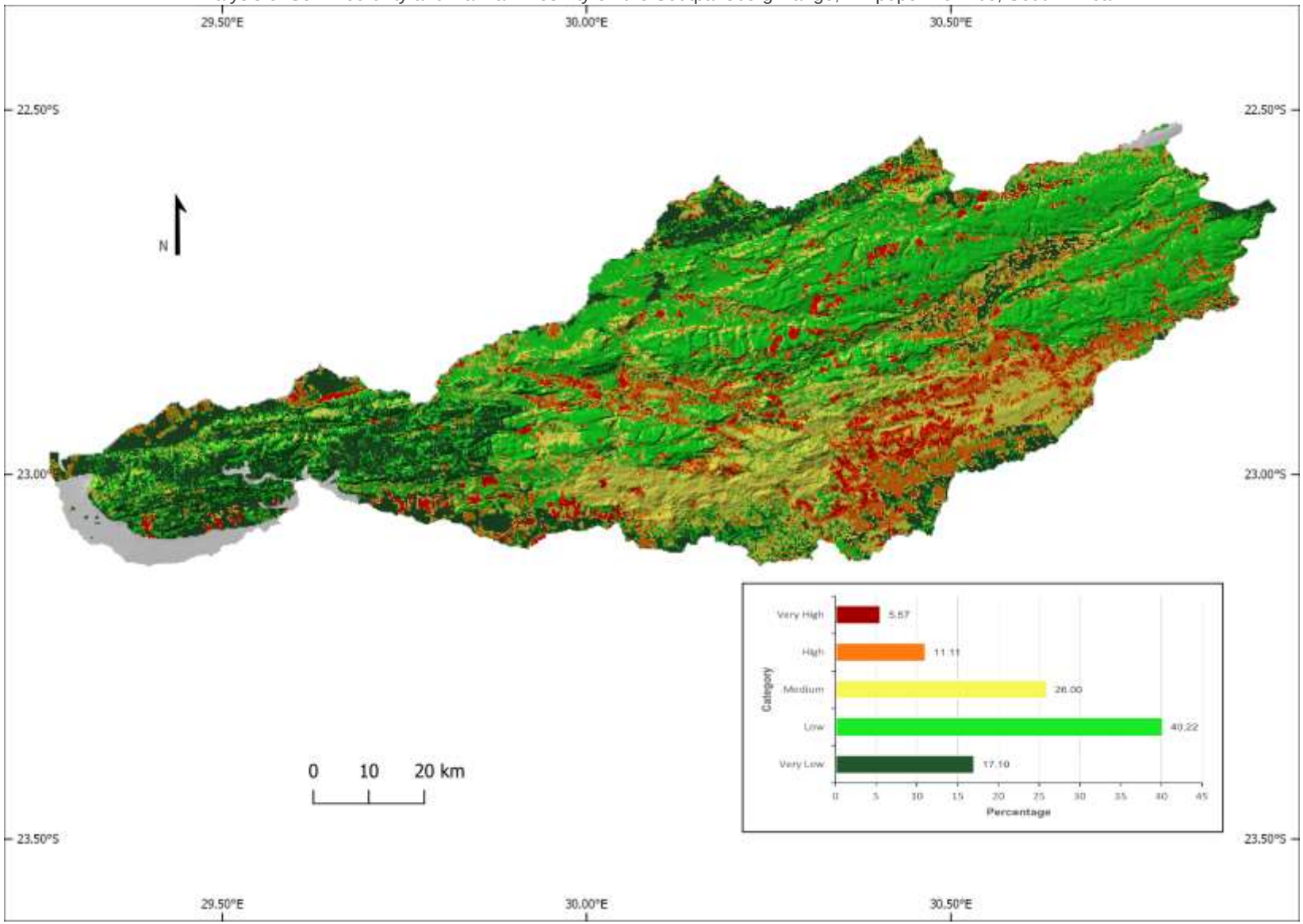

Figure 0.8: SLEMSA Based Total Erodibility

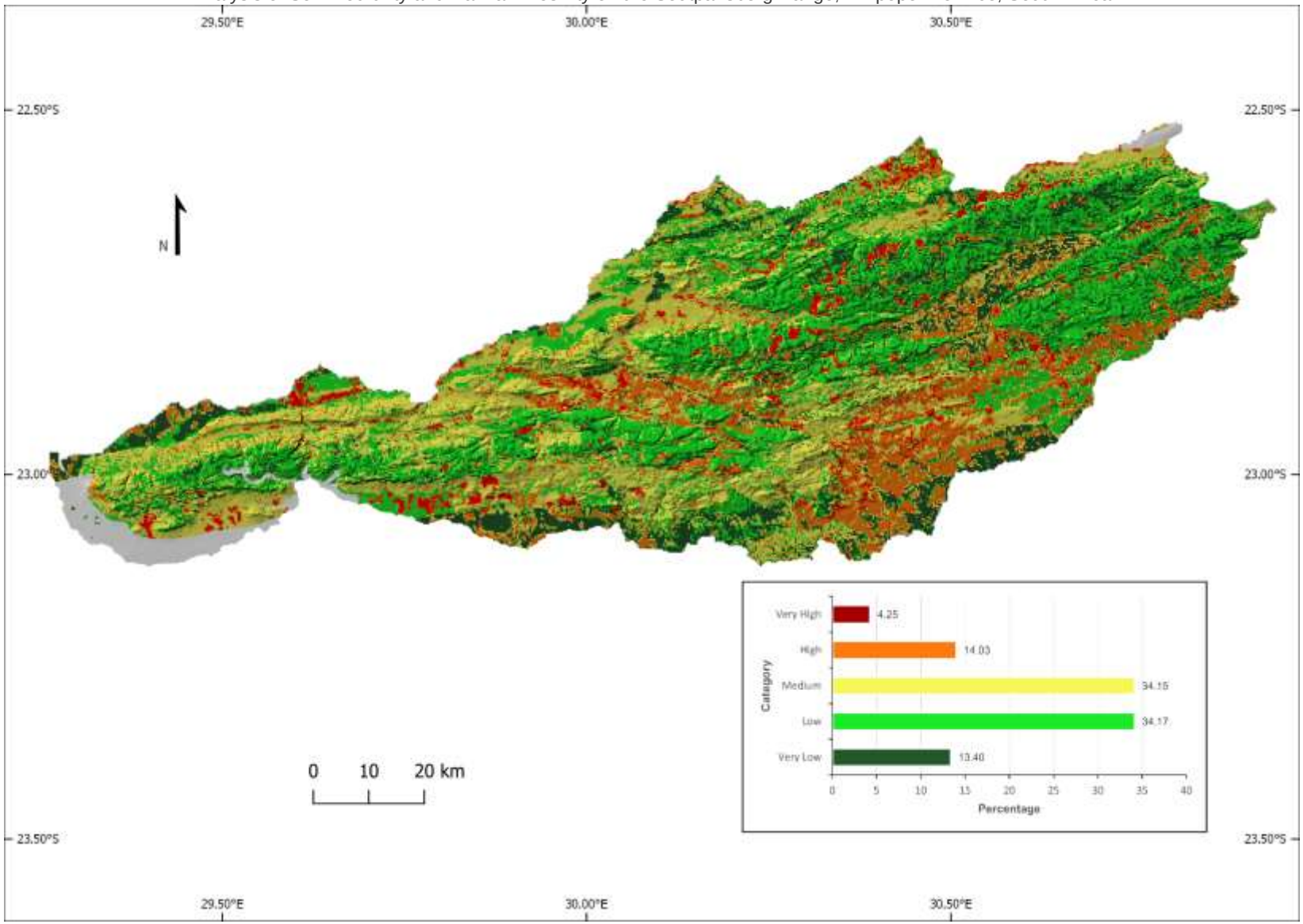

Figure 0.9: USLE Based Total Erodibility

4.4 Chapter Summary

The aim of this chapter was to illustrate the characteristics of soil erodibility of the Soutpansberg range. This was achieved through the classification of geomorphic features of the mountain range and addressed the objective to classify geomorphic features of the Soutpansberg range. The classification is based on the erosion control factors as presented by the USLE and SLEMSA. The factors include intrinsic erodibility, landform position, slope position, geological setting as well as rain exposure and operate on fourteen soil types found on the Soutpansberg range that fall into five granulometric groups.

The mountain range is dominated by clay loam soils composed of Eutric Leptosols, Lithic Leptosols, Chromic Cambisols and Eutric Cambisols. Lithic and Eutric Leptosols are the most dominant, occupying a combined 54% of the Soutpansberg range. Lithic Leptosols occupy 32% of the range. Generally, clay loam is easily erodible because clay and loam particles are light and easily displaced. The other granulometric classes are sandy clay loam, sandy loam, sand and clay. Clay occupies just 5% of the mountain range. Sand occupies 2% while sandy clay loam occupies 26% and sandy loam takes 9%. Though very important, the granulometric characteristics are also affected by other factors to influence erodibility.

The other extrinsic factors that influence soil erodibility showed different strength in different areas of the mountain. Rain exposure is largely low to very low due to the extensive agroforestry and residential land use. Forests protect the soil from detachment. Residential areas also tend to compact the soil or pave surfaces resulting in reduced soil detachability. In the same breath, the geological setting is dominated by hard and very hard rock. This promotes high erodibility due to its percolation suppression properties. Landform position reveals the dominance of steep sided ridges, flat topped plateaux and open valleys. The former two landforms discourage water accumulation while the later promotes it. Slope position is dominated by open valleys and foot slopes. Both slope positions have low gradient, hence create less gravitational energy.

The final erodibility maps are the result of a weighted sum overlay of all the erodibility factors. Intrinsic erodibility and rain exposure have the highest factor

weighting. Landform position has the least weighting. The final soil erodibility maps show high to very high erodibility on the south facing slopes of the mountain range. The USLE generated erodibility has minute portions of very low erodibility. However, a large part of the range west of Mutamba river is classified as very low erodibility in the SLEMSA method.

Soil erodibility reveals places that have soils that are at different risks of erosion. However, the erosion is driven by rain. The power of rainfall to erode is termed erosivity. The following chapter reveals the distribution of rainfall erosive potential on the mountain range.

: SOUTPANSBERG POTENTIALLY EROSIVE RAIN SPATIAL-TEMPORAL CHARACTERISTICS

5.1. Introduction

The aim of this research has been to analyse the spatial-temporal characteristics of soil erodibility and rainfall erosivity on the Soutpansberg range. The second specific objective of the overarching research was to characterise the spatio-temporal aspects of potentially erosive rainfall to reveal the distribution of rainfall erosion risk of the Soutpansberg mountain range. Data from forty-five meteorological stations were used for this research. Some stations fall ~30 km out of the mountain range physical boundary but are nevertheless considered due to their meteorological influence within that range (WMO, 2008). Five stations, namely Mara, Levubu, Thohoyandou, Tshivhase and Punda Maria, are fully automatic weather stations and can record wind as well. They have hourly data and are therefore, used for the storm erosivity computations.

Rainfall data were considered at monthly and annual timescales as well as at storm timescales. The first part of this chapter deals with monthly and annual spatial characteristics. The second part focuses on potentially erosive rainstorm spatial-temporal characteristics. This distinction was necessary because only five weather stations could provide rainstorm event data on the short timescales necessary to assess this. Therefore, event analyses are limited to the five stations while monthly and annual analyses cover the whole mountain range. As such, the analyses blended the spatial and temporal aspects of rainfall erosion risk.

Kriging was used for the spatial interpolation of the monthly rainfall to cater for the spatial-temporal distribution of potentially erosive rainfall on the mountain range. Temporal distribution is depicted by the monthly and annual averages derived from monthly and annual totals over the 20-year period. This distribution is represented on maps indicating the places where specific rainfall erosion risk characteristics can be located.

The Global Moran's I and Coefficient of Variation characterize the spatial variability (Zhang and Han, 2017) of 383 potentially erosive storms identified in the hourly data from the five rainfall stations mentioned earlier. The spatial variability is described as either simple, medium or complex. Simple spatial variability indicates a cluster of high values that are close

to the mean. Such variability is explainable by changes in space as depicted by Moran's I. Medium spatial variability depicts the clustering of both low and high values. However, the high values would be dispersed from, while the low values would be close to, the mean. Medium variability has a balance of space and non-spatial factors controlling rainfall distribution. Complex spatial variability represents clustering of high values that are dispersed from the mean. Complex variation cannot be explained by space only. Other factors, especially the presence of the Inter-tropical Convergence Zone (ITCZ) in the region that can bring tropical-temperate troughs, tropical lows, cut-off lows and tropical cyclones during summer (Kundu *et al.*, 2015; Dedekind *et al.*, 2016), influence the rainfall distribution, overriding the local factors such as elevation and aspect.

Before presenting rainfall erosion risk results, it is logical to begin with general rainfall summary statistics for the period under review. The summary statistics give an overview of the rainfall spatial temporal variability over the Soutpansberg Range. The statistics of focus are coefficient of variation and standard deviation. This is covered in greater detail in the following section.

5.2 General Rainfall Characteristics

An overview of rainfall data shows that the lowest rains occur between May and October, with many areas such as Dzanani-Biaba, Alldays, Marken and Waterpoort recording no rainfall at all during this time period. The highest rainfall is recorded in January, with Matiwa, Entabeni and Phiphidi recording highs above 300mm per month. Folonhondwe, Biaba and Alldays receive less than 350 mm per annum whereas New Agatha Bos, Entabeni Bos and Matiwa record above 1390mm per year. Matiwa receives the highest rainfall, above 1600mm, per year. This trend agrees with previous findings such as by Kabanda (2004), Kephe *et al.* (2016), and Kabanda and Munyati (2010).

On a general scale, the rainfall on the Soutpansberg Range fluctuated by 84% during the period under review as indicated by the CV and is thus highly variable. The SD deviation suggests that the fluctuation is at least four-fold (53 mm) of the minimum potentially erosive rainfall threshold and is closer to the upper ceiling of potentially erosive rainfall of 76.2 mm. The mean rainfall calculated for the period is 61.45 mm. Considering the 53 mm SD, rainfall in

the Soutpansberg Range, therefore, statistically falls between 8 mm (mean (61 mm) minus SD (53 mm)) and 114 mm (mean (61 mm) plus SD (53 mm)) of rainfall. However, this is based on figures incorporating all 45 stations. Therefore, a look at some individual stations can give a better nuance of the rainfall characteristics.

The lowest SD of 23 mm is recorded from Dzanani-Biaba and Pontdrift stations suggesting higher predictability of rainfall in the areas. The minimum rainfall for Dzanani-Biaba is 9 mm while Pontdrift recorded 7 mm. The maximum for Dzanani-Biaba is 84 mmm while Pontdrift is 76 mm. The CV for Dzanani-Biaba is 51% while for Pontdrift it is 73% suggesting more rainfall variability at Pontdrift than Dzanani-Biaba, although variability at both stations is very high (>30%).

The 22 point CV difference can be attributable to topographic forcing on rainfall. Pontdrift is located on the western periphery, 139km west of Dzanani Biaba in the central areas of the Range, sandwiched between crests on both sides. The crests and valley topography can create a local scale circulation system (Dedekind *et al.*, 2016) such as the mountain winds, that can make rainfall less variable around Dzanani-Biaba. Pontdrift is in a uniform topographic relief area where many other factors may be at play. As such, this should be explored as part of further research. However, the effect of the wet and dry seasons is apparent. This effect is more manifest in the summary statistics of the high rainfall areas as shown in Table 5.1.

Entabeni Bos, Joubertstroom Plantation, Matiwa, Phiphidi and Tshivhase Tea Plantation fall in the high rainfall areas on the Soutpansberg Range. Joubertstroom Plantation recorded a high SD of 154 mm and a CV of 114%. This is extremely variable. The other stations also recorded SD of more than 100. In addition, the CV for all of these stations indicates very high rainfall variability. This suggests the existence of both extremes of rainfall events, that is, very low through very high rainfall rates. High rainfall extremes are of interest to erosion research because high rainfall carries more erosion potential and risk. Although seasonality is a major contributor, elevation and orographic position play significant roles. All the stations are above 1200 m.a.m.s.l. in the central parts of the south facing slope, and they are not far apart, as spatial characterisation will reveal.

Table 0.1: Total Rainfall Summary Statistics

Station Name	M/Mean	Min (mm)	Max (mm)	SD	CV
Alldays Haly ARS	27.42	0.50	81.40	27.19	99.13
Bandelierkop	34.56	2.08	75.42	26.22	75.88
Dendron	42.69	11.50	74.93	24.94	58.43
Dzanani Biaba Agric	46.09	8.64	83.59	23.33	50.62
Elim – Hosp	56.66	4.60	161.47	53.76	94.90
Entabeni Bos	123.83	19.36	337.62	110.47	89.21
Folonhondwe	37.03	1.68	74.87	26.44	71.42
Goedehoop	85.43	10.92	210.32	70.71	82.77
Hanhlip	63.13	3.94	176.16	57.40	90.93
Joubertstroom Plantation	106.44	7.26	559.69	153.46	144.17
Klein Australie	99.16	12.16	259.13	87.92	88.67
Kleinfomtein	67.14	12.86	162.93	53.68	79.96
Legkraal	41.71	5.83	101.49	30.73	73.67
Levubu	63.98	8.72	172.42	55.72	87.09
Louis Trichardt	62.89	5.36	159.16	52.41	83.35
Mara	35.16	2.11	78.50	29.62	84.24
Marken	32.22	0.65	68.65	25.88	80.30
Matiwa	136.09	22.84	323.24	109.87	80.73
Messina-Pol	36.36	2.84	83.69	28.37	78.03
Venda	80.45	8.53	223.47	74.41	92.49
Nooitgedacht	77.49	11.92	195.78	66.15	85.37
Palmaryville	73.97	7.03	200.30	66.08	89.33
Phiphidi	111.29	16.81	312.42	102.65	92.23
Platjan Grensbos	39.33	8.38	75.73	26.10	66.36
Pontdrift	32.72	7.35	76.15	23.97	73.25
Punda Maria	40.77	2.38	104.67	38.10	93.46
Rambuda	62.12	10.96	147.05	50.13	80.70
Roodewal Bos ARS	63.44	5.85	165.21	57.09	89.99
Saamboubrug - Pol	37.52	2.50	87.53	30.14	80.34
Shefeera	108.22	13.40	268.71	92.37	85.35
Shingwedzi Vlakteplaas	40.90	2.47	109.86	35.48	86.75
Teba Pafuri	33.46	1.23	84.54	32.70	97.74
Thohoyandou	61.34	7.39	191.39	59.08	96.32
Tolwe - Pol	34.09	3.00	67.45	24.57	72.07
Tshakhuma	81.69	15.75	244.16	72.95	89.29
Tshipise	34.59	5.00	80.45	28.15	81.38
Tshivhase	120.64	18.31	283.71	102.41	84.89
Tsianda	72.76	11.74	188.83	63.99	87.95
Una – Agr	35.83	1.80	86.27	28.02	78.18
Villa Nora-Pol	30.91	1.00	68.72	23.63	76.43
Vondo – Bos	104.40	18.64	254.72	87.75	84.05
Vreemdeling	67.86	7.40	162.10	51.83	76.38
Centre	46.07	5.70	148.62	43.36	94.10
Waterpoort	29.92	0.60	71.73	25.49	85.18
Zwartrandjes	45.29	5.35	105.76	36.85	81.36
Average	**61.45**	**7.65**	**161.11**	**53.15**	**84.32**

5.3 Potentially Erosive Rainfall Spatio-temporal Variability

The spatio-temporal variability analysis was done through spatial interpolation and spatial autocorrelation. Ordinary co-kriging spatial interpolation methods and hotspot analyses were used to analyse average monthly and annual rainfall from the 45 stations covering the Soutpansberg range. This gives the rainfall spatial temporal distribution. Spatial autocorrelation using Moran's I and CV were employed on both average monthly data as well as the 383 potentially erosive storms recorded at five stations over the period under review. This gives the rainfall spatial temporal variability. The results are presented in section 5.3.1 and 5.3.2, respectively.

5.3.1 Rainfall Spatial-temporal Distribution

The monthly spatial distribution layers were overlaid to produce quarterly distribution layers. The quarterly distribution layers were then overlaid to produce the annual distribution map. This gave a visual representation of the spatial distribution of rainfall erosion risk over the mountain range during specific periods of time. In addition to the rainfall spatial temporal distribution, hotspot analysis was necessary to indicate diurnal distribution of the potentially erosive rainfall. This is important as it indicates the potential for flash flooding caused by a high concentration of potentially erosive rain in a few days. Therefore, an area recording high potentially erosive rain, but only a few rain days, has a high potential for flash flood erosion even though it may produce low monthly or annual rainfall. Results are presented on a quarterly basis as well as an annual map.

5.3.1.1 Spatial Temporal Interpolation

The first step in spatial interpolation using co-kriging is the computation of spatial data structure, known as variography. The data structure is given by the range, sill and nugget. The range is the distance at which the value of one variable becomes spatially independent of another. That is, the range marks the end of spatial autocorrelation. It is read on the horizontal axis of the variogram (see Figure 3.6). The sill is the value on the vertical axis of the variogram when the variables do not influence each other. It is the value on the vertical

axis where the model begins to flatten. The nugget is the variance at zero distance, where the graph crosses the y-axis.

The important interpretation of the spatial structure is on the relationship between the nugget and sill. The ratio of nugget to sill indicates the spatial dependency of variables (Al-Omran *et al.*, 2013). This research follows three classes to explain spatial dependency (Tadayon and Rasekh, 2019). Spatial dependency can be strong, moderate or weak. Strong dependency is indicated by a ratio of less than 25% while a ratio of 25 to 75% indicates moderate spatial dependency. Weak spatial dependency is reported by a ratio above 75%.

Month by month spatial interpolation results show strong rainfall spatial dependency in July and November only, whereas January, April, May and September rainfall have weak spatial dependency. Overall, eight months of the year receive rainfall that is spatially dependent. This suggests the strong influence of topographical relief on rainfall distribution on the mountain range regardless of the rainfall producing systems at play at any time. This largely agrees with other research (Kabanda, 2003; 2004; Kephe *et al.*, 2016; Rapolaki *et al.*, 2019) that observed the influence of topography on rainfall distribution. Topographic forcing can produce localised rainfall distribution patterns (Kundu *et al.*, 2015; Dedekind *et al.*, 2016) that may explain the rainfall spatial dependency revealed on the Soutpansberg range.

An intriguing feature of the rainfall spatial analysis results is that the highest average rainfall in the region is recorded in January yet there is weak spatial dependency. This suggests that the highest rainfall recorded on the Soutpansberg Range is not generated from topography related processes. Rapolaki *et al.* (2019) indicate the presence of synoptic cyclonic conditions in the Limpopo River Basin during January to March. Rainfall in southern Africa is largely influenced by seasonality where the tropical temperate troughs (TTT), and the cut-off lows (COL) are the main rain bearing systems (Dedekind *et al.*, 2016; Rapolaki *et al.*, 2019). Table 5.2 shows the potentially erosive rainfall spatial data structure used in the interpolation. The interpolation and hotspot analysis results are presented as rainfall spatial temporal variability.

Table 0.2: Soutpansberg Potentially Erosive Rain Spatial Data Structure

Month		**Jan**	**Feb**	**Mar**	**Apr**	**May**	**Jun**	**Jul**	**Aug**	**Sep**	**Oct**	**Nov**	**Dec**
Kriging Type		Ordinary	Ordinary	Ordinary	Ordinary	Ordinary	Ordinary	Ordinary	Ordinary	Ordinary	Ordinary	Ordinary	Ordinary
Order of Trend Removal		Second	Second	Second	Second	Second	Second	Second	Second	Second	Second	Second	Second
Kernel Function		Exponential	Exponential	Exponential	Gaussian	Exponential	Exponential	Exponential	Exponential	Exponential	Exponential	Exponential	Gaussian
Semivariogram Model		Stable	Gaussian	J-Bessel	Stable	Stable	Gaussian	Exponential	Stable	Stable	Stable	Exponential	J-Bessel
Anistropy		No	No	No	No	No	No	No	No	No	No	No	Yes
Neighbourhood	Max	8	8	8	5	8	5	8	5	8	5	8	8
	Min	2	2	2	2	3	2	2	2	2	2	2	3
Sectors		8	4	8	4 with 45° offset	4	8	8	8	8	4 with 45° offset	Full	Full
Mean Error		-0.05	0.03	0.04	0.06	-0.01	0.04	-0.18	0.08	0.03	-0.02	0.07	0.14
Root Mean Square Standardised		0.90	0.96	0.80	1.10	0.96	0.93	0.88	0.96	0.98	0.91	0.86	0.82
Nugget		2762.64	680.04	570.70	1069.42	72.80	120.90	0.00	129.04	158.63	143.04	0.00	983.03
Partial Sill		35.23	1486.16	1000.98	0.66	2.66	133.45	200.78	55.83	0.04	143.04	700.61	802.87
Range (metres)		27463.42	13537.17	15561.25	122627.70	47402.08	13398.16	19566.78	95227.40	108902.36	15561.25	8912.05	31721.39
Spatial Dependency		98.74	31.39	36.31	99.94	96.47	47.53	0.00	69.80	99.98	50.00	0.00	55.04

5.3.1.2 Spatial-temporal Visualisation

Rainfall spatial temporal interpolation produces a data structure that is used by GIS software to produce a continuous surface from point data. The continuous surface is the visualisation of the rainfall distribution. The surfaces are raster layers indicating different potentially erosive rainfall characteristics. After interpolation, used to create temporary layers of spatial distribution, the following processes were done through co-kriging in ArcGIS.

i. Save the temporary layers created through interpolation as raster layers to make them permanent.
ii. Classify the raster layer using the Symbology function of the ArcGIS software into 5 classes representing:

    1. Very low rainfall
    2. Low rainfall
    3. Moderate rainfall
    4. High rainfall
    5. Very high rainfall

The classification is based on Jenks Natural breaks and the rainfall range in each class is dependent on the rainfall figures considered. However, the rainfall minimum threshold is 12.5 mm, the cutting point for USLE and SLEMSA potentially erosive rain. The 5 classes are to remain consistent with the 5-class approach adopted for the geomorphic classification. Therefore, very high rainfall means very high erosive potential.

iii. Add the monthly average rainfall layers together using the Raster Calculator in ArcGIS to produce one map. It is important to note that rainfall is spatially and temporally variable on the Soutpansberg range. Consequently, its contribution towards the final rainfall distribution and erosivity is also spatially and temporally variable. This dynamic was catered for through the Weighted Overlay in the ArcGIS Raster calculator. The relative contribution of each month and quarter was

computed from its percentage contribution to the annual value. Monthly, quarterly and annual rainfall distribution maps are produced to reveal different spatio-temporal characteristics of rainfall on the Soutpansberg.

iv. The final map are reclassified into 5 classes using Jenks Natural breaks.

The final maps tell the story of rainfall spatial distribution at a quarterly and annual spatial scale. The quarterly data presentation is also the norm in meteorological research. The following sections analyse the maps in greater detail.

5.3.1.2.1 JFM Rainfall Characteristics

The highest average total rainfall over the Soutpansberg mountain range was recorded during the January to March period, with the maximum received in January. The spatial data structure indicates a weak rainfall spatial dependency. This suggests the presence of synoptic weather systems that drive rainfall distribution on the Soutpansberg range in January. Rapolaki *et al.* (2019) and Dedekind *et al.* (2016) indicate the strong influence of the tropical temperate troughs and cut-off lows during this period, and it appears that such systems are the cause of these weak spatial dependencies.

The very high and high classes are concentrated in the high elevation areas in Matiwa, Tshivhase and Entabeni. The two zones cover about 38% of the mountain range, the same area that the low and very low rainfall erosive potential zones cover. This is an indication that there is a balance between the two extreme classes of rainfall erosive potential in terms of extend on the mountain range.

However, only one flash flood hotspot at Tshakhuma is in the very high rainfall region. The other two hotspot stations are Dzanani and Folonhondwe. Both stations fall in the zone of low rainfall erosive potential. These results indicate the highest flash flood risk and the associated erosion hazards lie in the low rainfall zone. This is because, while the potentially erosive rainfall may be low in these regions, it is concentrated in only a few days. While high rainfall areas are obvious areas of focus for intervention programmes, low rainfall areas with rainfall days' hotspots need attention too. Figure 5.1 shows the rainfall characteristics for the first quarter of the year. The blues indicate rain erosion risk while the dots show flash floods risk categories.

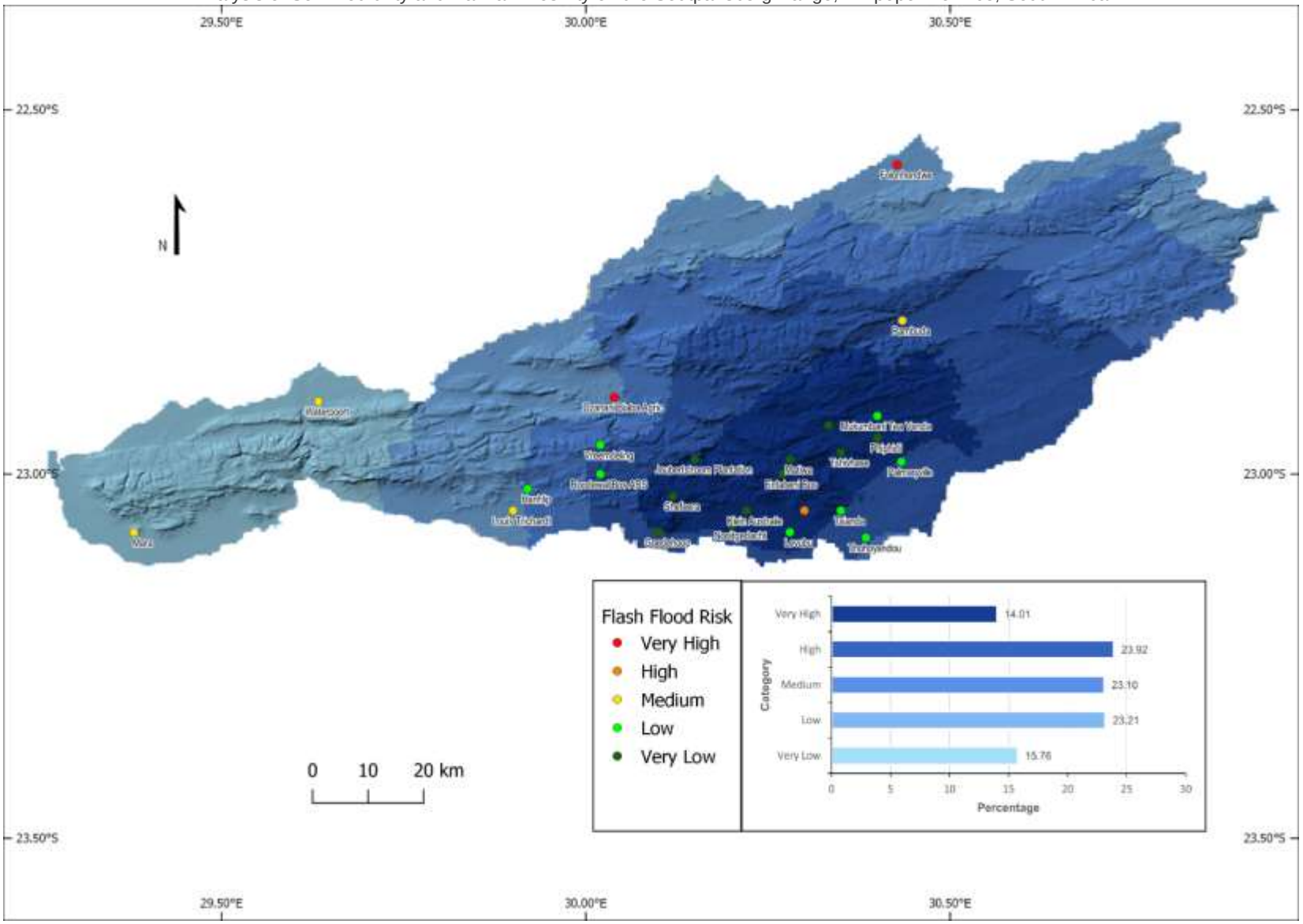

Figure 0.1: JFM Rainfall Erosion Risk and Flash Floods Hotspots

5.3.1.2.2 AMJ Rainfall Characteristics

The second quarter presents an interesting trend in rainfall spatial characterisation. The rainfall season would typically be receding, as rainfall usually ends in March or April (Kabanda, 2004; Kephe *et al.*, 2016; Rapolaki *et al.*, 2019). Rainfall in the Soutpansberg in both April and May indicate weak spatial dependency. April has the longest spatial range of 122 km. This once again points to the existence of a large scale weather system as May has a range of only 47 km. The existence of a large scale weather system has the tendency to bring large amounts of rainfall over a large area for a short period of time.

The spatial characterisation indicates a widespread shift and sometimes an expansion of all rainfall zones. Significant changes are seen on the high rainfall zone. It shifts north and east, but slightly shrinks in extent. The low rainfall zone significantly extends west. Waterpoort becomes the fourth flash flood potential area in addition to Dzanani, Folonondwe and Tshakhuma. The hotspots remain in the low and very low rainfall zones as illustrated in Figure 5.2.

5.3.1.2.3 JAS Rainfall Characteristics

The July to September quarter is in the middle of the dry season on the mountain range (Kabanda, 2004; Kephe *et al.*, 2016; Rapolaki *et al.*, 2019). Rainfall totals are, therefore, low during this period. Although the rainfall amounts are low, the temporal distribution is important for flash flood risk assessment. The absolute amounts of very high potentially erosive rainfall drastically fall to just above 160mm. However, the very high rainfall erosive potential region expands by about 8 percentage points to the northeast. Tshakhuma and Waterpoort cease to be flash flood hazard areas. Mara station becomes a new flash flood risk hotspot in the west.

It appears that the rainfall distribution is driven by local conditions. Although September has a weak spatial dependency, July has a strong spatial dependency while August has a moderate spatial dependency. The importance of this characteristic is that despite falling in the low potentially erosive rainfall category, the flash flood risk areas carry a high erosion risk tag during this period. The high erosion risk status is due to the fact that relatively high rainfall rates are received in a short period of time. However, the usual high rainfall zone spatially

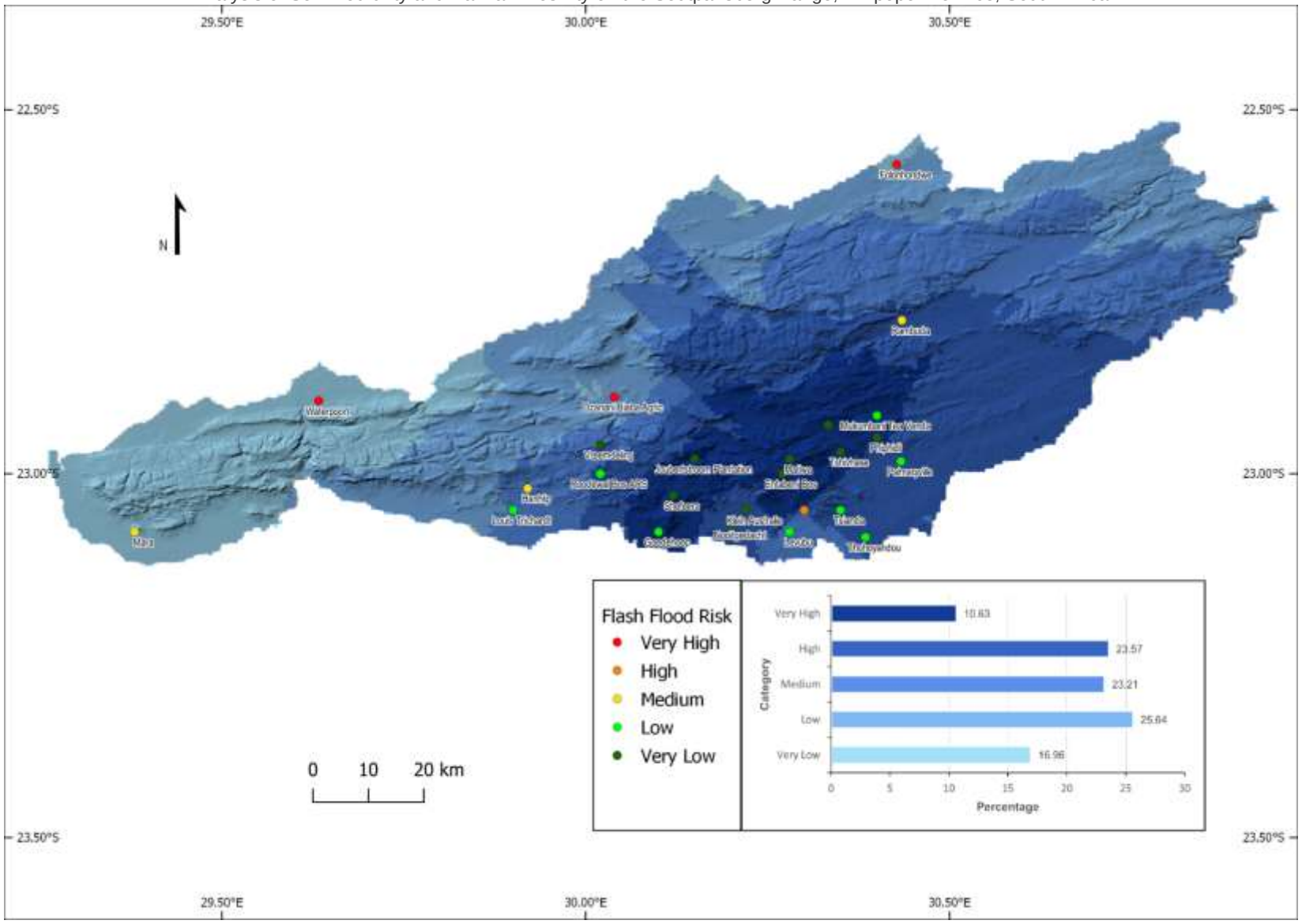

Figure 0.2: AMJ Rainfall Erosion Risk and Flash Floods Hotspots

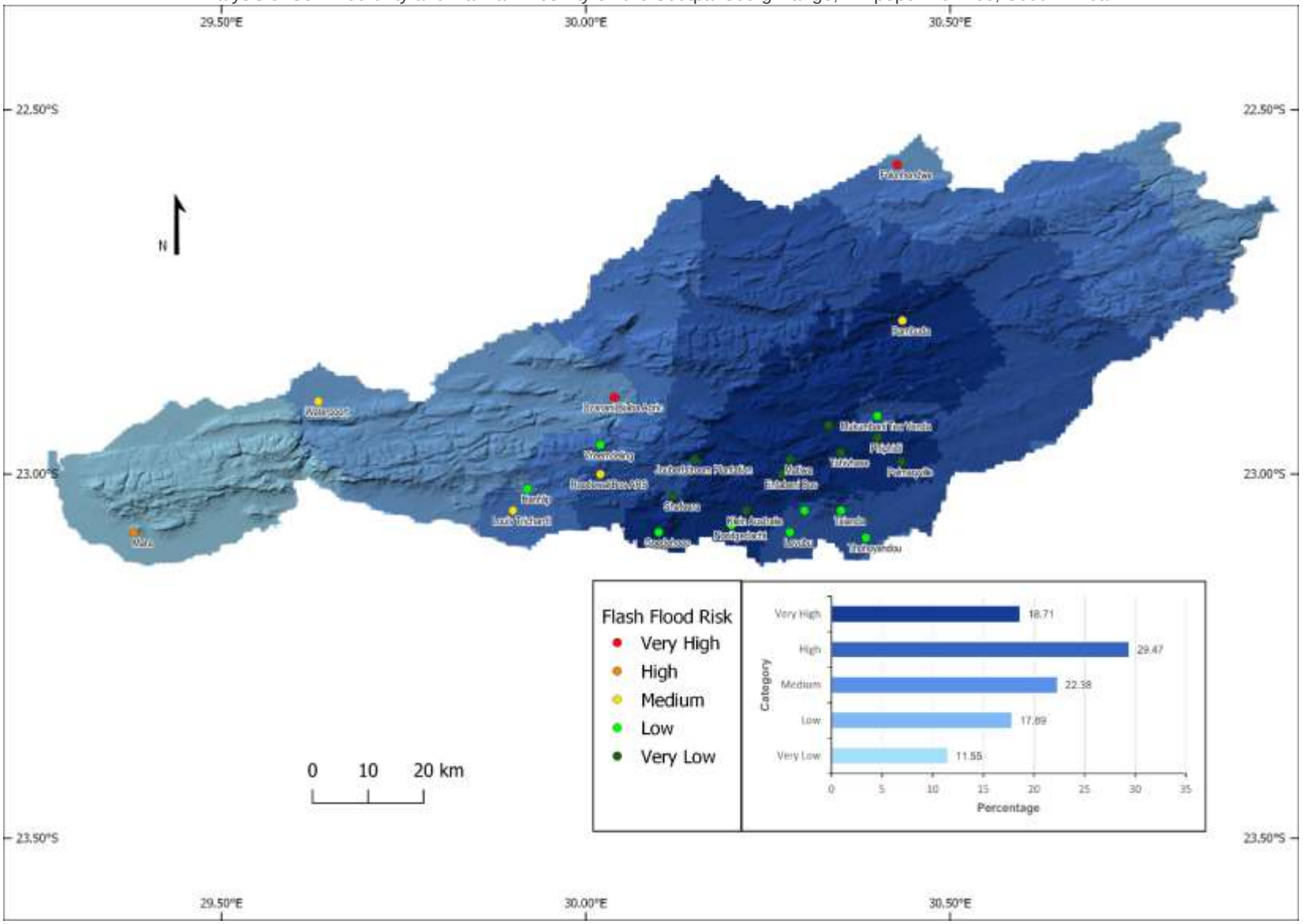

Figure 0.3: JAS Rainfall Erosion Risk and Flash Floods Hotspots

remains the in the middle of the south facing slopes of the mountain range as depicted in Figure 5.3.

5.3.1.2.4 OND Rainfall Characteristics

The last quarter of the year presents a mixture of the end of the dry season and the beginning of the rain season. Rainfall in the Soutpansberg may begin either in October or November (Kabanda, 2003; Rapolaki *et al.*, 2019). This presents a rainfall distribution curve ball because October months of some years would be dry while others would be wet. Therefore, the quarter presents an interesting spatial dependency.

November rainfall indicates strong special dependency. However, October and December present only moderate spatial dependency. Such a scenario can be explained through the September and January spatial dependency. The moderate October spatial dependency may be due to the remnants of the retreat of the synoptic air mass regime that brought the weak spatial dependency in September. On the other hand, the moderate spatial dependence depicted in December could be the precursor of the approach of the large scale weather systems that dominate the region from January (Dedekind *et al.*, 2016; Rapolaki *et al.*, 2019).

The spatial distribution sees the very high potentially erosive rain zone shrinking slightly from the JAS period, and the high zone decreases by 10 percentage points. The very low and low rainfall regions expand by 6 and 10 percentage points, respectively. This is illustrated in Figure 5.4.

5.3.1.2.5 Annual Rainfall Characteristics

The four quarterly rainfall distribution maps were overlaid using Weighted Overlay in ArcGIS Raster calculator. The weight of each quarter was computed following the relative contribution of each quarter to the annual rainfall total over the period under review. The average contributions are 49.5, 14, 8.1 and 28.4 percent for JFM, AMJ, JAS and OND, respectively. Weighting allows the comparative contribution of each quarter of the year towards erosion potential to be made evident. This produces a practical representation of the rainfall characteristics.

The final map indicates the dominance of the first quarter that contributes almost half of the rainfall on the mountain range. The very high potentially erosive rainfall zone core is anchored on the high elevation area covering about 11% of the mountain range, including Tshivhase, Matiwa and Entabeni. The high potentially erosive rainfall zone radiates to the east from the very high potentially erosive rainfall zone and covers about 25% of the Soutpansberg range. The low potentially erosive rainfall zone touches the periphery of the mountain from the eastern parts creating a ring on the northern edge. The northern low rainfall ring expands southward as it covers Dzanani in the central interior of the mountain range. It touches the southern edge south of Roodewal, near Louis Trichardt. It then extends westwards covering the whole range until a little distance before Waterpoort in the west. The low potentially erosive rainfall region occupies the largest part of the mountain range at 29%. This is followed by the very low potentially erosive rainfall range that covers 18% of the range. The rest of the western wing is a very low rainfall erosion area. This confirms that the Soutpansberg range is dominated by below moderate potentially erosive rainfall totals because the low and very low rainfall zones occupy a combined 47% of the mountain range. The high and very high rainfall zones occupy a combined 36% of the mountain range. Hence, it can be said that the mountain range has low rainfall erosion risk based on the rainfall spatial characteristics presented. However, flash flood risk is high to very high in the low and very low rainfall areas.

The 2000 to 2019 period recorded 383 potentially erosive storms on 5 stations. That gives an average of lowly 19 potentially erosive storms per year over the 20 year period. That indicates the general low rainfall erosion risk profile of the mountain range. However, Dzanani, Folonhondwe and Waterpoort fall in the low and very low rainfall erosive potential zones but are flash flood risk areas. Soil erosion management practices on the Soutpansberg Range need to take this into cognisance. Figure 5.5 shows the annual rainfall spatial characteristics of the Soutpansberg Range.

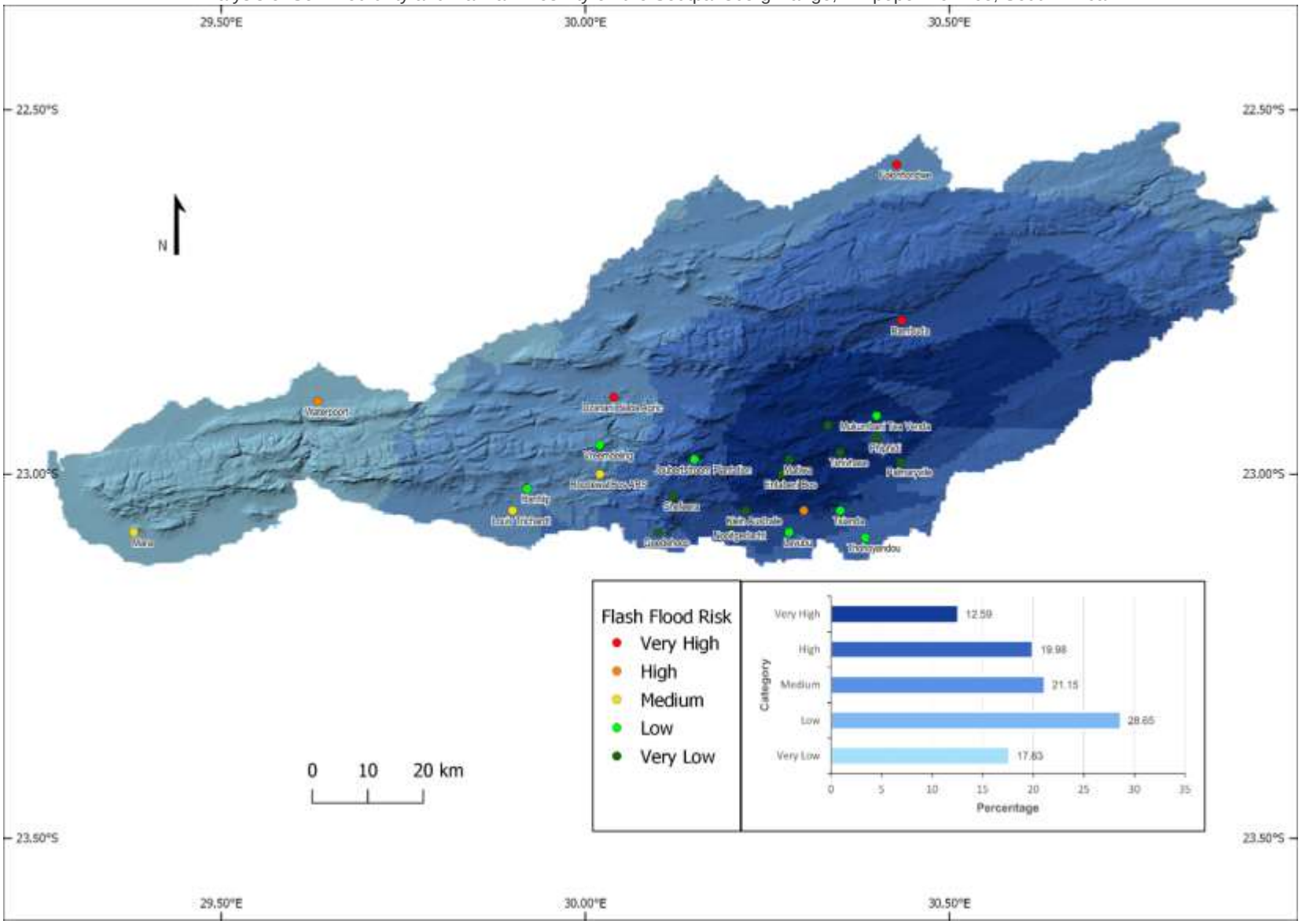

Figure 0.4: OND Rainfall Erosion Risk and Flash Floods Hotspots

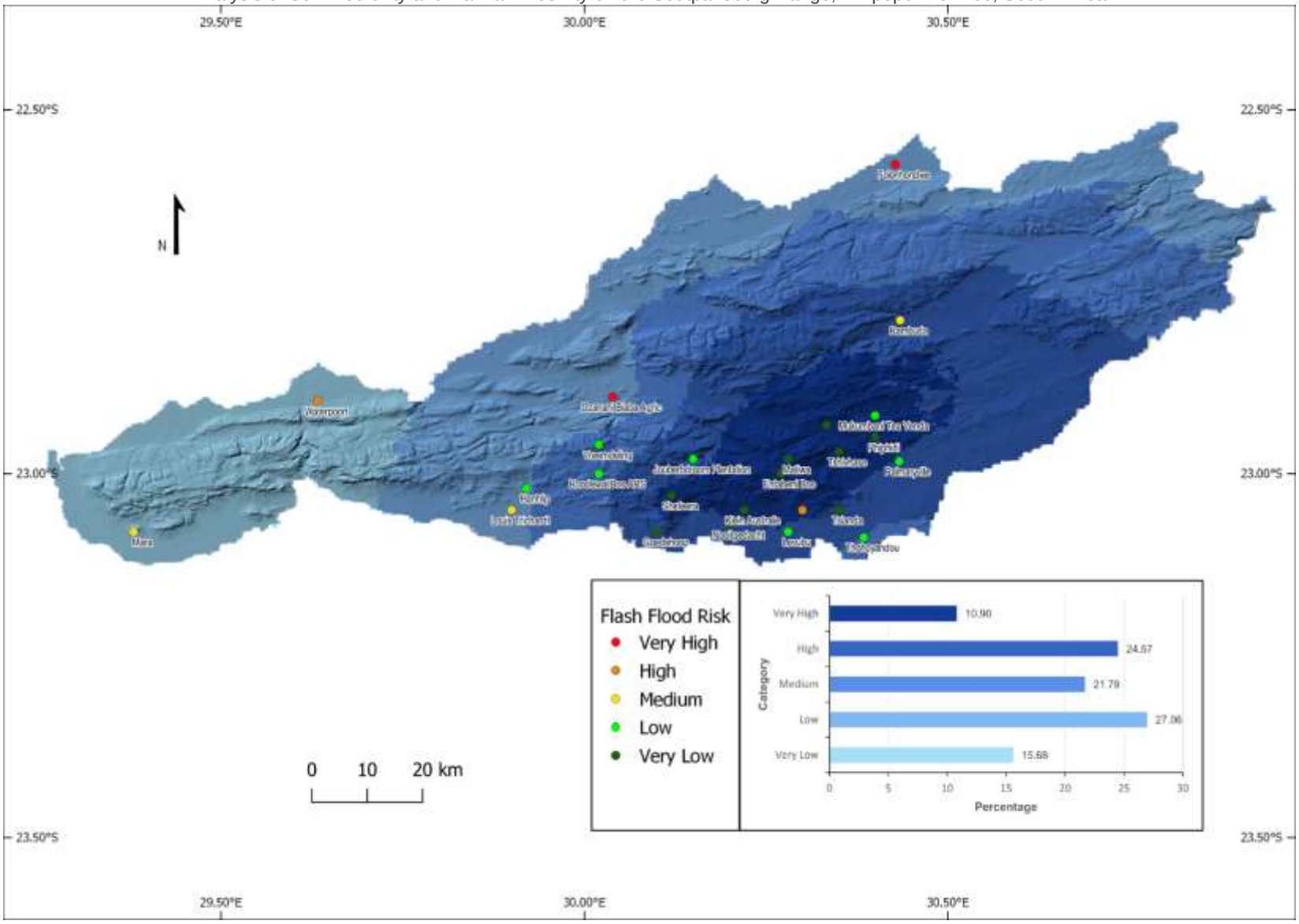

Figure 0.5: Annual Rainfall Erosion Risk and Flash Floods Hotspots

5.3.2 Rainfall Spatial-temporal Variability

Rainfall spatial temporal variability is demonstrated by the statistical characterisation of rainfall using Moran's I and coefficient of variation. The two statistics are used as proposed by Zhang and Han (2017) to produce the spatial variability matrix. This combination was found to be a reliable method to describe rainfall spatial variability (Zhang *et al.*, 2018). The spatial variability is presented for a period from 2000 to 2019, thereby also offering a temporal aspect to the analysis. The analysis is done for the 383 potentially erosive storms recorded from five stations as well as for the whole mountain range. The mountain range analyses cater for both potentially erosive rainfall and the number of days in which the rain was received.

5.3.2.1 Hourly Potentially Erosive Storms Spatial-temporal Variability

Storms were recordable from five automatic weather stations. The stations are Punda Maria, Mara, Thohoyandou, Tshivhase and Levubu. The lowest average rainfall, monthly and annually, is recorded at Punda Maria and Mara weather stations. The highest average rainfall is recorded at Thohoyandou and Tshivhase weather stations. At above 1300mm per annum, Tshivhase records way more than the other automatic stations. Mara records just above 430mm per annum.

Spatial variability shows that 53% of the storms over the period had simple spatial temporal variability. Spatially complex storms constituted 26% while the rest were moderately spatially variable storms. It was to be expected that most storms would demonstrate simple spatial variability as 3 of the 5 stations are on the central part of the windward slope of the mountain range and hence are subject to the orographic effect. However, some light should be shed on the complex storms.

The most complex storm of the period was recorded at Levubu station on 2016/02/26 at 16:00:00. Interestingly, that was the only complex storm recorded at Levubu station. Most of the complex storms were recorded at the Thohoyandou station with records on 2019/02/13 at 22:00:00 and 23:00:00. This persuades the observation that although the other stations experienced complex potentially erosive storms, Thohoyandou is exceptional and may need

further analysis. This is because the other stations' complexity is remarkably close to moderate and simple classes.

Thohoyandou's relative location and land uses and land cover may have played a role in rainfall generation in the area. Thohoyandou is in the 641-920 elevation zone, the second lowest topographical elevation of the region. That causes slight uplifting of the dominant moist SE winds that prevail in the area, initiating orographic rainfall formation processes. The area is generally built up, creating the urban heat island effect that aids in rainfall formation. There is also the effect of Nandoni Dam, to the east of Thohoyandou, on wind moisture content, hence increasing rainfall occurrence. These could be the reasons why Thohoyandou recorded more complex storms than any other station. Figure 5.6 shows the hourly storms spatial variability.

Although the hourly storm spatial variability gives a picture regarding where more focus may be necessary, the analyses are limited to five stations only. Therefore, a spatial temporal variability covering the whole mountain range becomes important. Hence, minimum potentially erosive monthly rainfall per weather station was considered for analysis. The number of days that the rain fell were also considered. The results of the analysis are presented in the following section.

5.3.2.2 Spatial-temporal Variability of the Monthly Potentially Erosive Rainfall and Rain Days

5.3.2.2.1 JFM Rainfall and Rain Days' Spatial Variability

The first quarter has a balance regarding rainfall spatial variability. Most stations experienced simple (38%) rainfall variability. Medium and complex variability were not far behind at 36% and 26%, respectively. However, rain days (the number of days in which potentially erosive rainfall was received) are dominated by medium variability at 42%. Simple and complex variability statistics are similar at 31% and 27%, respectively. This indicates that rainfall variability and rain days' variability during the first quarter do not necessarily correlate. However, a view of the extreme values that exceeded the Moran's I threshold can shed some interesting light.

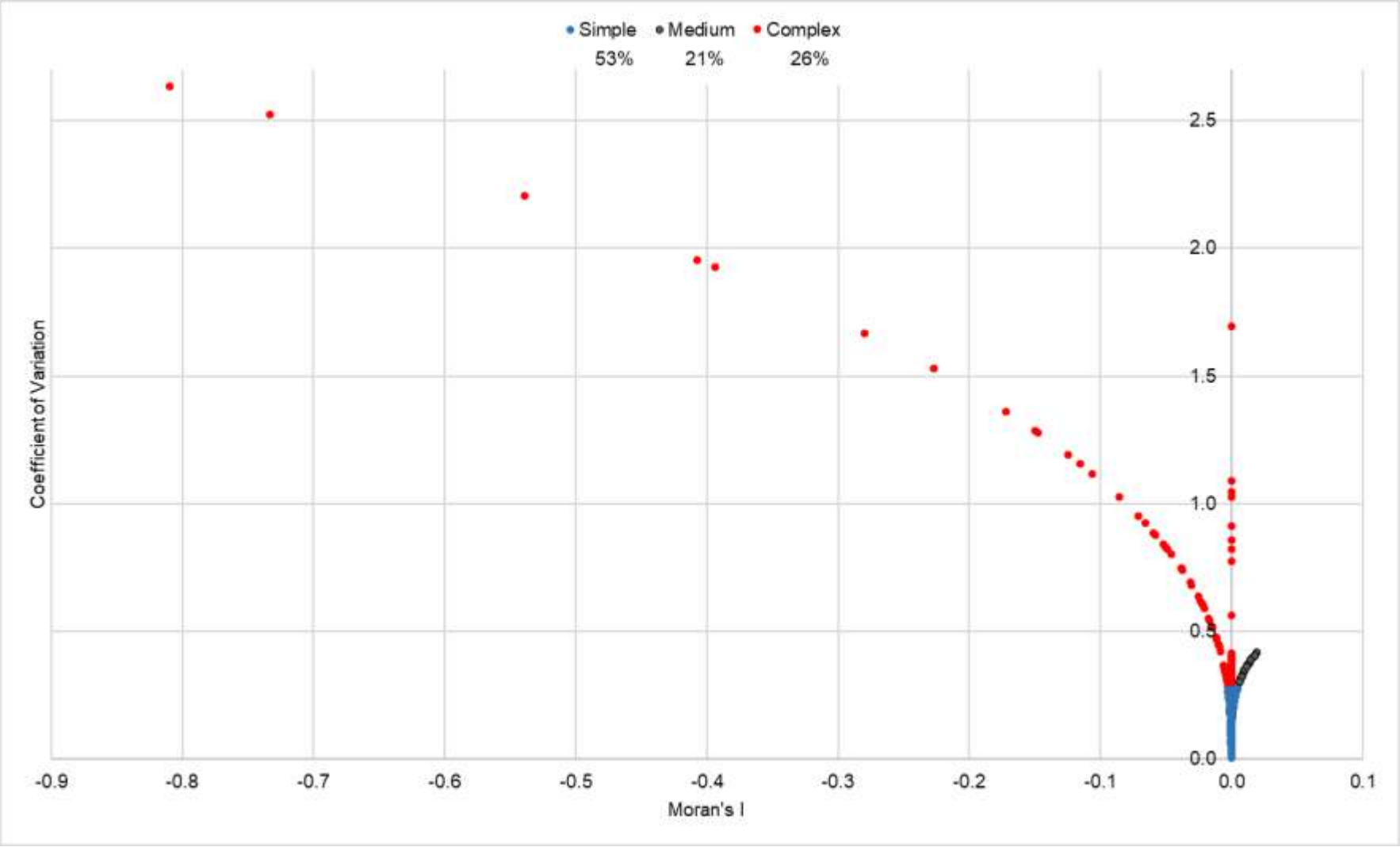

Figure 0.6: Potentially Erosive Storms Spatial Variation

Rainfall variability indicates that all but one station in the complex variability exceeded the -1 minimum limit. Complex variability represents clustering of high values that are dispersed from the mean, and this indicates weak spatial dependence. The stations falling in this category as shown in figure 5.7(a) are testimony to this result. Only Entabeni and Matiwa stations are within 30 km of each other. This reinforces the existence of a synoptic weather system on the range during the first quarter (Rapolaki *et al.*, 2019).

The rain days' variability analysis makes the results more interesting. The stations that experience extremely complex rainfall variability are almost the same as those that experience extremely complex rain days variability. While 9 stations experienced extremely complex rainfall variability, 8 experienced the same variability on rainy days. All 8 also recorded extremely complex rainfall variability and indicate a correlation between rainfall and rain days variability. This suggests that the same factor(s) control(s) rainfall amount and distribution, and the factors are not limited to topography.

5.3.2.2.2 AMJ Rainfall and Rain Days' Spatial Variability

The second quarter is characterised by wet April and dry May and June. Rainfall ends in April in the region (Kabanda, 2004; Kephe *et al.*, 2016; Rapolaki *et al.*, 2019). Therefore, April figures have a bearing on the overall variability. However, the dissipation of the mesoscale weather system is apparent. Simple variability constitutes 60% of the rainfall recorded during the period under review and suggests the strong influence of May and June rainfall patterns. This, however, does not agree with the spatial dependency statistics. The statistics indicate that April and May rainfall has weak spatial dependency. However, rain days' variability paints a different picture.

Rain days are moderately variable (50%) with a bias towards complexity (30%). This again brings into play the strong influence of the synoptic cyclonic systems that bring rain in April, while their dissipation makes May and June dry. Therefore, while more rain days are recorded in April, very few are recorded in May and June, striking a balance in the distribution of rain days. That the four stations that recorded extreme rain days' complexity fall just outside the physical boundary of the mountain range, as illustrated in Figure 5.8, is an indication of the influence of synoptic weather systems. This is because synoptic weather systems produce

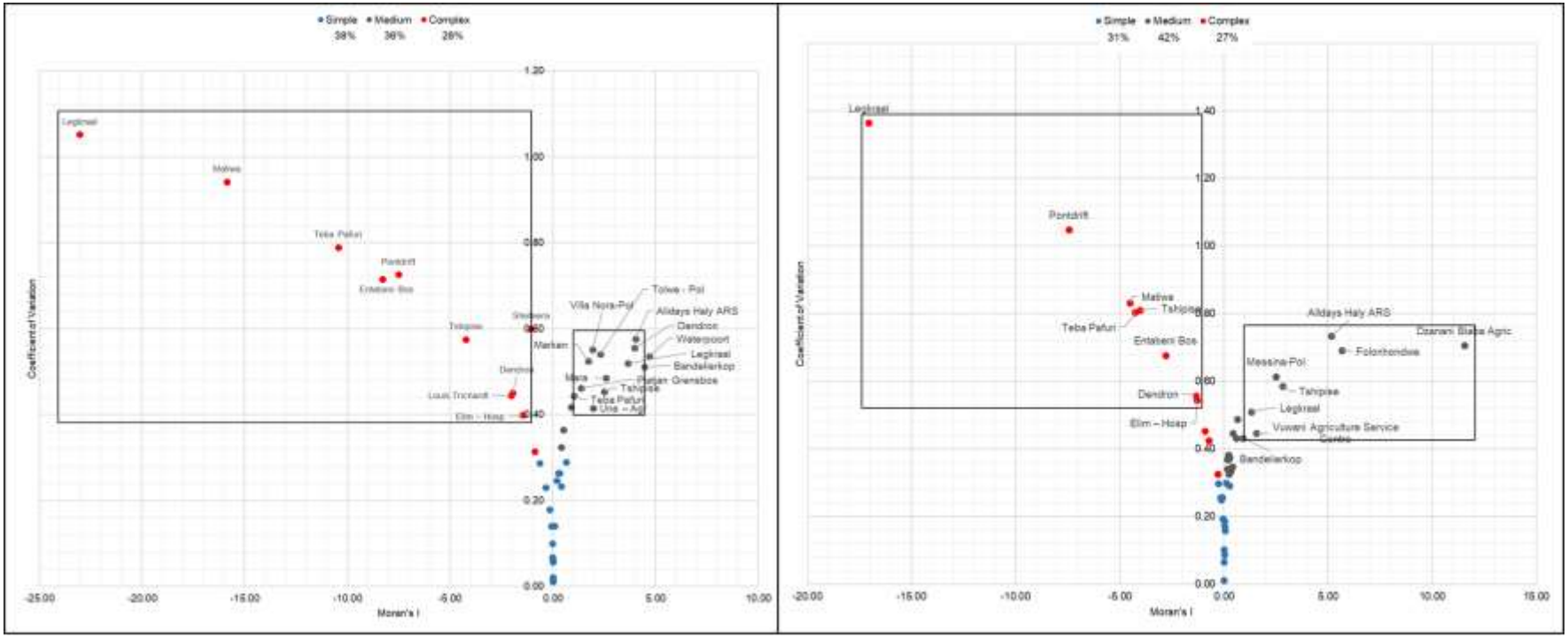

(a) JFM Rainfall Variability

(b) JFM Rain Days Variability

Figure 0.7: JFM Rainfall and Rain Days' Spatial Variability

large amounts of rain within a short period of time. Such large amounts that are not close to the mean make rainfall spatial variability analysis return a result indicating complex storms.

5.3.2.2.3 JAS Rainfall and Rain Days' Spatial Variability

The third quarter of the year is composed of generally dry months only in terms of rainfall seasonality. However, potentially erosive rainfall is still recorded, though in very low quantities. That is why 40% of the rainfall recorded during this time had simple variability. Complex and medium variability are not far apart in terms of their contribution at 31% and 29%, respectively. However, the influence of elevation is apparent in the rainfall spatial variability.

All stations that recorded extreme complexity beyond the -1 Moran's I are located above 1200 m.a.m.s.l. This can be explained by the orographic effect of the mountain range. This is supported by very strong and moderate spatial dependency ratios for July and August, respectively. However, rain days' variability does not indicate the influence of topography. Figure 5.9 illustrates that only 20% of the rain days had simple variability. Moderate variability had the majority at 50% while complex variability had 30%. This indicates a balance between local topography and other factors (such as mesoscale circulation and land use/land cover) in influencing rain days variability. The distribution is biased towards complexity.

5.3.2.2.4 OND Rainfall and Rain Days' Spatial Variability

The last quarter depicts interesting variability statistics. Both rain days and rainfall variability statistics indicate the dominance of simple variability. This is supported by spatial dependency statistics. November has very strong rainfall spatial dependency while October and December have only moderate values. Therefore, rainfall in the fourth quarter can be primarily explained by local topographical effects. Therefore, one can conclude that the absence of the mesoscale weather systems allows the mountain range to create the mountain winds during the fourth quarter of the year.

Figure 5.10 indicates that 51% and 29% of both rainfall and rain days' variability was simple and moderate, respectively. Complex variability constituted 20% only. A further view of the figure show that Legkraal and Teba Pafuri stations recorded the most extreme variability of

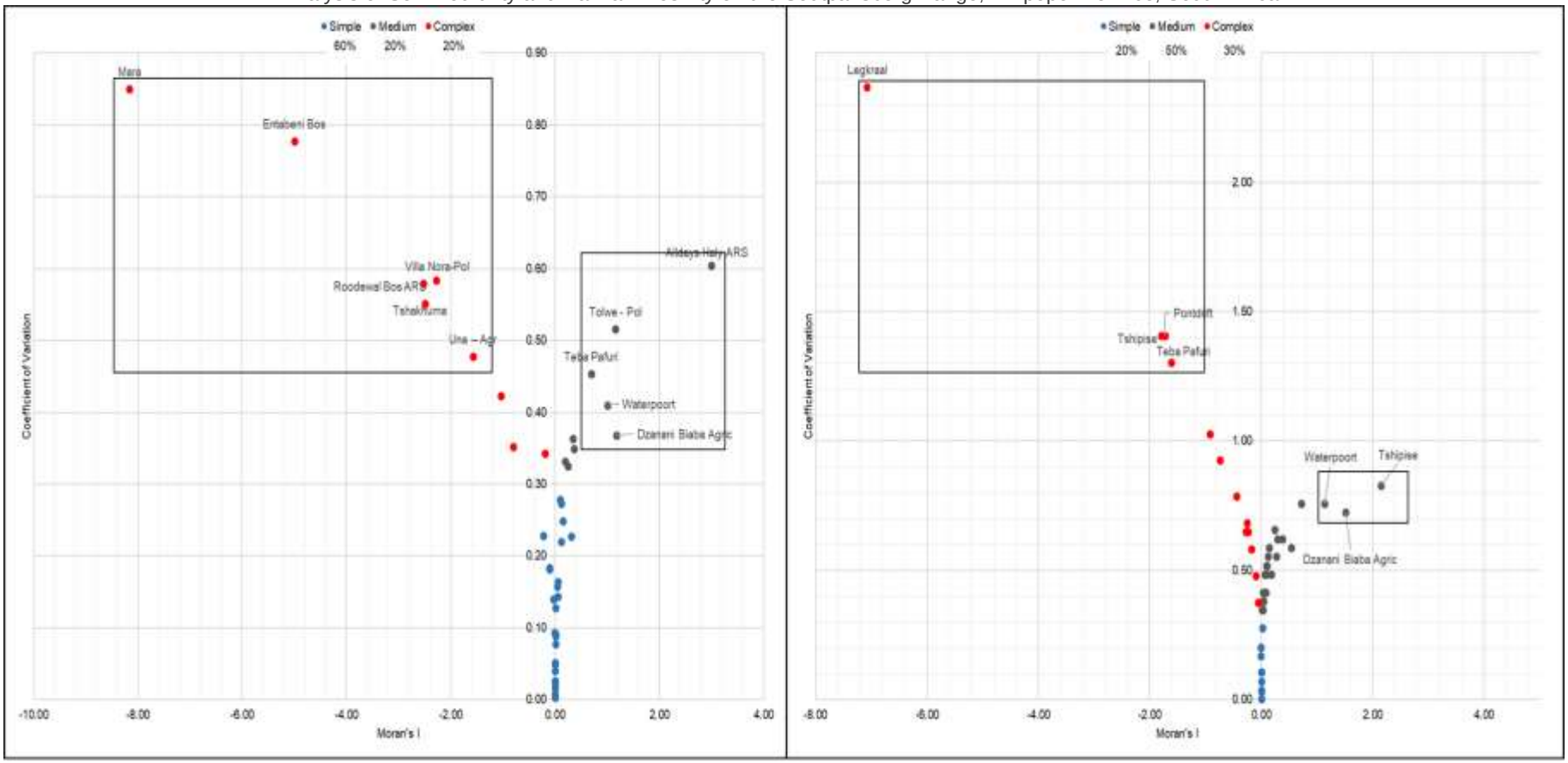

Figure 0.8: AMJ Rainfall and Rain Days Spatial Variability

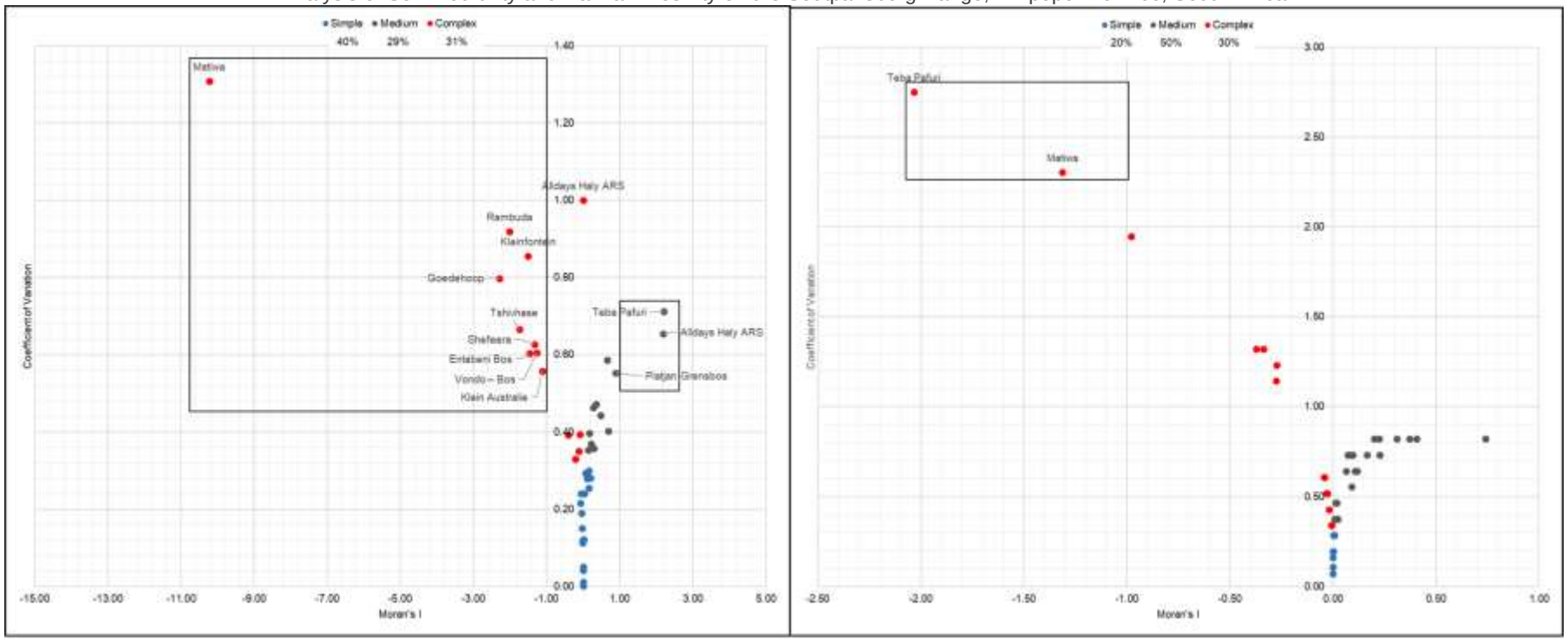

(a) JAS Rainfall Variability

(b) JAS Rain Days Variability

Figure 0.9: JAS Rainfall and Rain Days Spatial Variability

both rain days and potentially erosive rainfall totals. This may an indicator of the influence of additional factors such as land use and land cover on rainfall variability. Land use and land cover influence differential heating and cooling, which create the valley and mountain breezes on mountain slopes, hence complex rainfall variability.

5.3.2.2.5 Annual Rainfall and Rain Days' Spatial Variability

The annual spatial variability represents the general rainfall and rain days' picture of the mountain range. The two variables under review depict different variability characteristics. Total rainfall variability is dominantly simple while rain days' variability is split between moderate and complex variability. This reveals the interplay of local topography and synoptic scale weather systems.

The general rainfall variability on the mountain range is simple. Despite the first quarter dominance of a synoptic weather system and January indicating weak rainfall spatial dependency, the moderate and strong spatial dependency in the other months overshadowed this. Stations located in the high elevation areas record the highest rainfall on the mountain range. They also indicate extremely complex rainfall variability. This indicates that although topography influences rainfall distribution, other factors such a mesoscale weather systems as well land use and land cover also may also be playing a role in rainfall distribution on the Soutpansberg mountain range.

On the other hand, the low (11%) rain days' simple variability indicates the inferior contribution of topography to rainfall variability. No station that experienced extremely complex rainfall variability also experienced the same complexity on rainy days. This paints a lack of correlation between rainfall variability and rain days' variability which means that different factors influence rainfall amount and distribution over the mountain range. While all four stations with extremely complex rainfall variability are on high elevation, the ones found on rainy days include three from very low elevation areas as illustrated in Figure 5.11.

5.4 Chapter Summary

This chapter presented the spatio-temporal characteristics of potentially erosive rainfall on the Soutpansberg range. Spatio-temporal characterisation addressed the second objective of the

research. The aim has been to reveal areas that pose rainfall erosion risk and may need special focus in terms of erosion management. The results are presented in three parts. The first part focuses on the general rainfall characteristics. The second part presents the spatial-temporal distribution. The third part presents spatial-temporal variation.

The general total rainfall characteristics indicate that rainfall on the Soutpansberg Range is very highly variable. The variability is at least four-fold that of the minimum potentially erosive rainfall. The potentially erosive rainfall spatial distribution is statistically represented by variography where spatial dependence is computed. Results reveal that four months of the year (January, April, May and September) have weak spatial dependence. Two months, July and November, have strong spatial dependency. The rest have moderate spatial dependency. Therefore, overall, potentially erosive rainfall distribution is primarily spatially dependent on the mountain range. Hence, it is concluded that the mountain range influences rainfall spatial distribution.

The spatial dependence is revealed by a visual display of the rainfall distribution. Most rainfall within the Soutpansberg range is concentrated in the central areas of the south facing slope. The epicentre is located at elevations above 1200 m.a.m.s.l. The elevation forces the dominant southeast winds to rise and cause rainfall. The western wing of the range from just before Waterpoort is a dry region. Quarterly distribution maps show minor shifts in the quarterly rainfall and hotspots, respectively.

Rainfall spatial variability is analysed using the fusion of the coefficient of variation and Moran's I. While the CV gives the variation within the data set, Moran's I considers the influence of space in the data variation. The fusion produced a spatial variability matrix that describes variability as simple, medium or complex. Simple spatial variability indicates the influence of the landscape on rainfall variability. Moderate variability is a balance while complex variability indicates outside influences on the rainfall rates and variability.

Results of the spatial variability analysis indicate that rainfall variability is generally influenced by the landscape. Both potentially erosive storms and total rainfall are dominated by simple variability. However, rain days are dominated by medium spatial variability. Therefore, a logical conclusion is that rainfall distribution on the Soutpansberg range is influenced by

topographic relief, though not exclusively. High erosion potential areas are in the central parts of the south facing slopes above 1200 m.a.m.s.l. However, flash flood hotspots are in low to very low rainfall regions. Such a scenario leads to the conclusion that high erosion areas are not defined by total rainfall amounts only. The temporal distribution of the rainfall is also important. In addition, wind characteristics also matter. The influence of the mountain range on rainfall erosivity and wind speed is covered in Chapter 6.

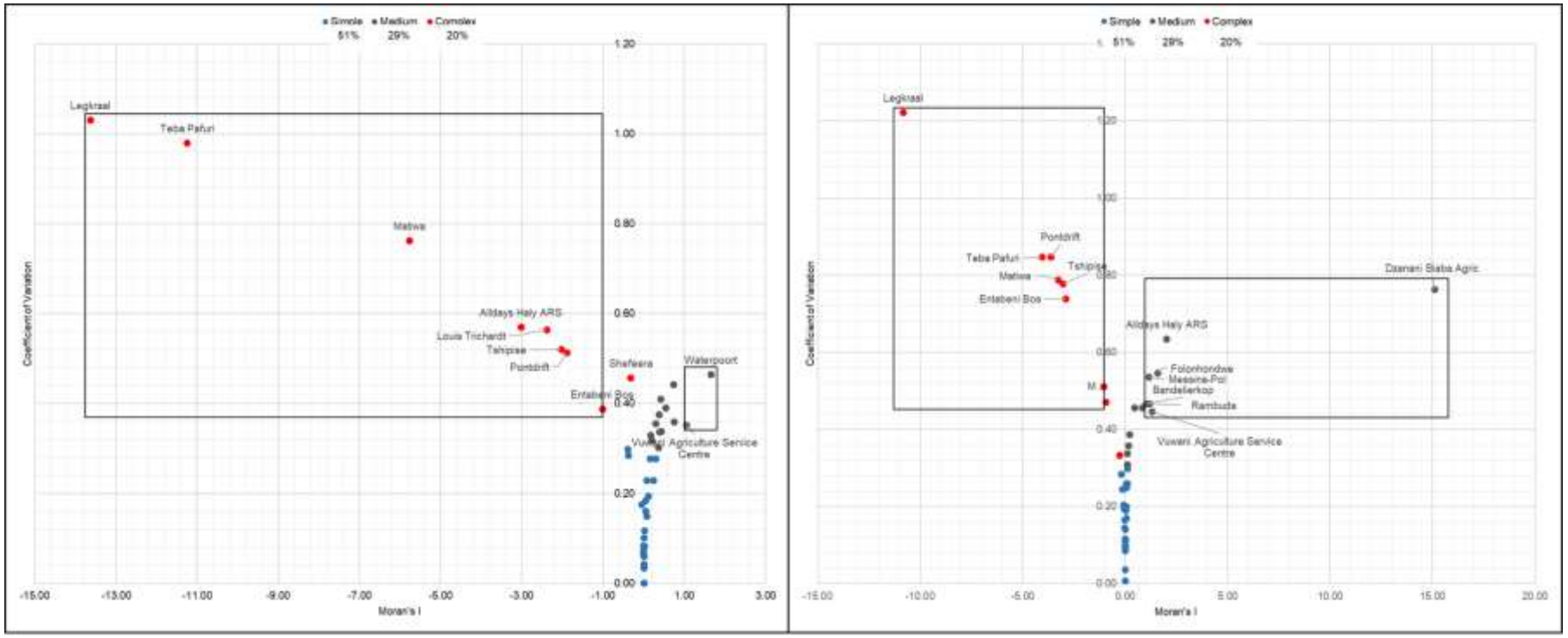

(a) OND Rainfall Variability

(b) OND Rain Days Variability

Figure 0.10: OND Rainfall and Rain Days Spatial Variability

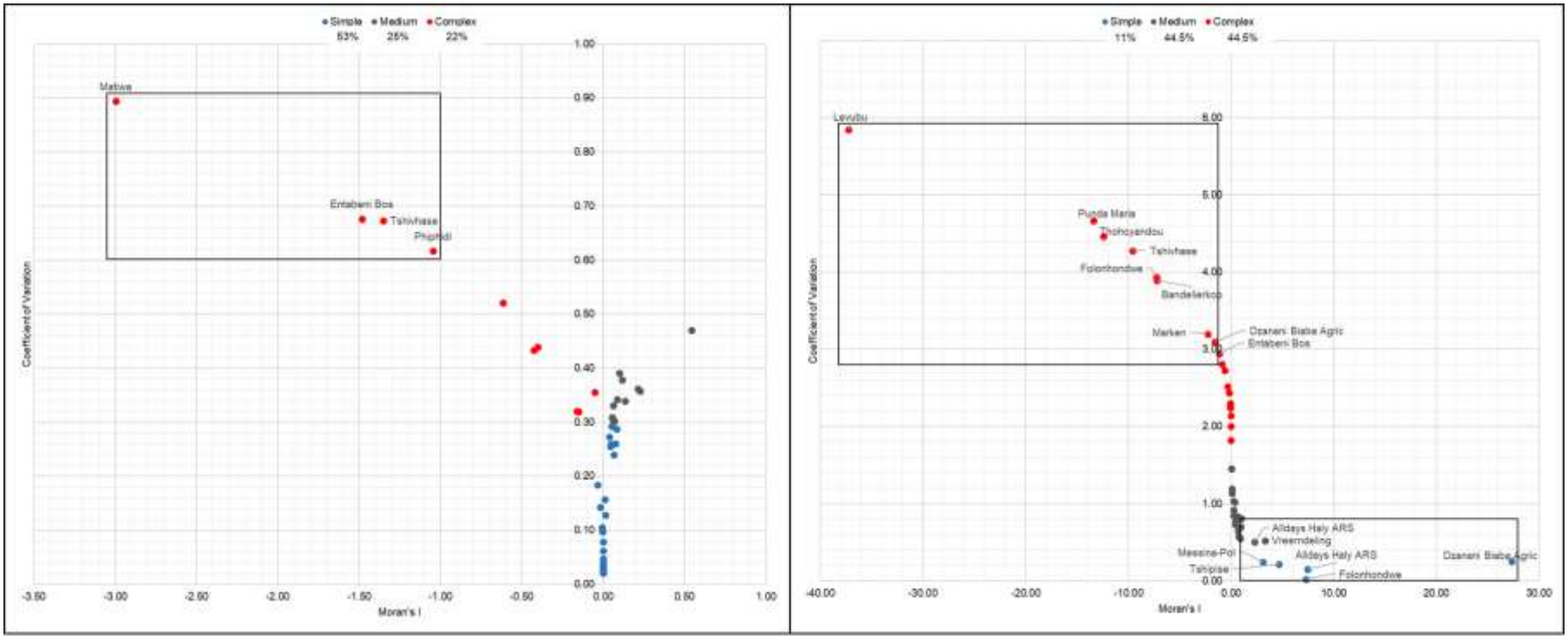

(a) Annual Rainfall Variability

(b) Annual Rain Days Variability

Figure 0.11: Annual Rainfall and Rain Days Spatial Variability

: THE INFLUENCE OF TOPOGRAPHY ON WIND SPEED AND RAINFALL EROSIVITY

6.1 Introduction

The aim of the research has been to analyse the spatial-temporal characteristics of soil erodibility and rainfall erosivity on the Soutpansberg range. Chapter 5 demonstrated the erosive potential of the rainfall received on the Soutpansberg range. This chapter addresses the third objective of this research that seeks to establish the influence of topography on wind speed and erosivity. Wind and rain are the considered major drivers of erosivity for this research (Erpul *et al.*, 2013; Marzen, 2017). The behaviour of both phenomena is greatly influenced by topography.

Wind speed and direction are directly measured while erosivity is derived from rainfall (and wind, for Wind Driven Rain (WDR)). Wind speed is crucial for Wind Driven Rain erosivity computation. However, the Soil Loss Estimation Model for Southern Africa (SLEMSA) and the Universal Soil Loss Equation (USLE) compute erosivity without considering wind. Therefore, it is important to demonstrate that the rainfall distribution patterns indicated in Chapter 5 give an insight into the spatial characteristics of rainfall erosivity.

The third objective presented in this chapter has two parts. The first part focuses on the influence of topographic elevation on wind speed. The second part focuses on the influence of topographic elevation on erosivity and address the null hypothesis that rainfall erosivity is not influenced by topographic elevation.

This section is followed by a representation of the wind characteristics as recorded at the five stations and the 383 potentially erosive storms considered for the period under review. This focuses on establishing the prevailing wind directions and the dominant wind speeds. This part of the chapter is followed by a statistical assessment of the relationship between rainfall erosivity and elevation. This is done by simple linear regression of annual and monthly erosivity figures. The chapter closes by presenting a position of how topography affects wind speed and erosivity.

6.2 Wind on the Soutpansberg

Wind recorded at the five stations over the period of interest indicates the prevalence of winds from the south-eastern direction over the Soutpansberg. Of importance, however, are the wind speed ranges. This is because wind speed has a direct link with rainfall kinetic energy, especially for Wind Driven Rain (WDR) (Van Boxel, 1998; Erpul, 2013; Overton, 2013; Marzen *et al.*, 2017). Rain drops in Wind Free Rain (WFR) are assumed to fall vertically (Erpul, 2013; Overton, 2013; Marzen *et al.*, 2017). However, horizontal wind increases the momentum, and hence kinetic energy of raindrops under certain circumstances, and these subsequently increase the raindrop erosivity (Van Boxel, 1998; Erpul, 2013; Marzen *et al.*, 2017).

Horizontal wind speed is critical to this research because its influence pertains to raindrop velocity, the deviation from the vertical course of fall and a modification of size and number of raindrops (Iserloh *et al.*, 2013) that significantly affect the raindrop erosivity. Research has shown that such effects are significant (Blocken and Carmeliet, 2010; Erpul, 2013; Iserloh *et al.*, 2013; Marzen *et al.*, 2015; Derome *et al.*, 2017). Critical to this point is that wind imposes a raindrop horizontal velocity component proportional to wind speed (Erpul, 2013; Overton, 2013; Marzen *et al.*, 2017) resulting in an increased raindrop kinetic energy of up to three times greater than in quiescent conditions (Lyles and Allison, 1976; Erpul, 2013; Marzen, 2017). Therefore, an observation of the horizontal wind speed characteristics at the five stations will give light to the potential erosion that each area is exposed to.

It is important to restate that wind was considered for the 383 storms recorded from five automated stations of interest. Therefore, the effect of elevation on wind speed is a view of the dominant wind speeds in relation to the weather stations. The wind speeds and direction recorded are analysed using a five level Likert scale ranging from calm, light, moderate, strong to very strong winds. The classes were developed from Montero-Martínez and García-García (2016), Scheper *et al.* (2021) and the Beaufort Scale (Huler, 2007). Calm winds travel at less than 1.5 m/s^{-1}. Light winds have velocities between 1.6 and 3.0 m/s^{-1}. Moderate winds travel between 3.1 and 4.5 m/s^{-1}. Strong winds range from 4.6 to 6 m/s^{-1} while very strong winds are above 6 m/s^{-1}.

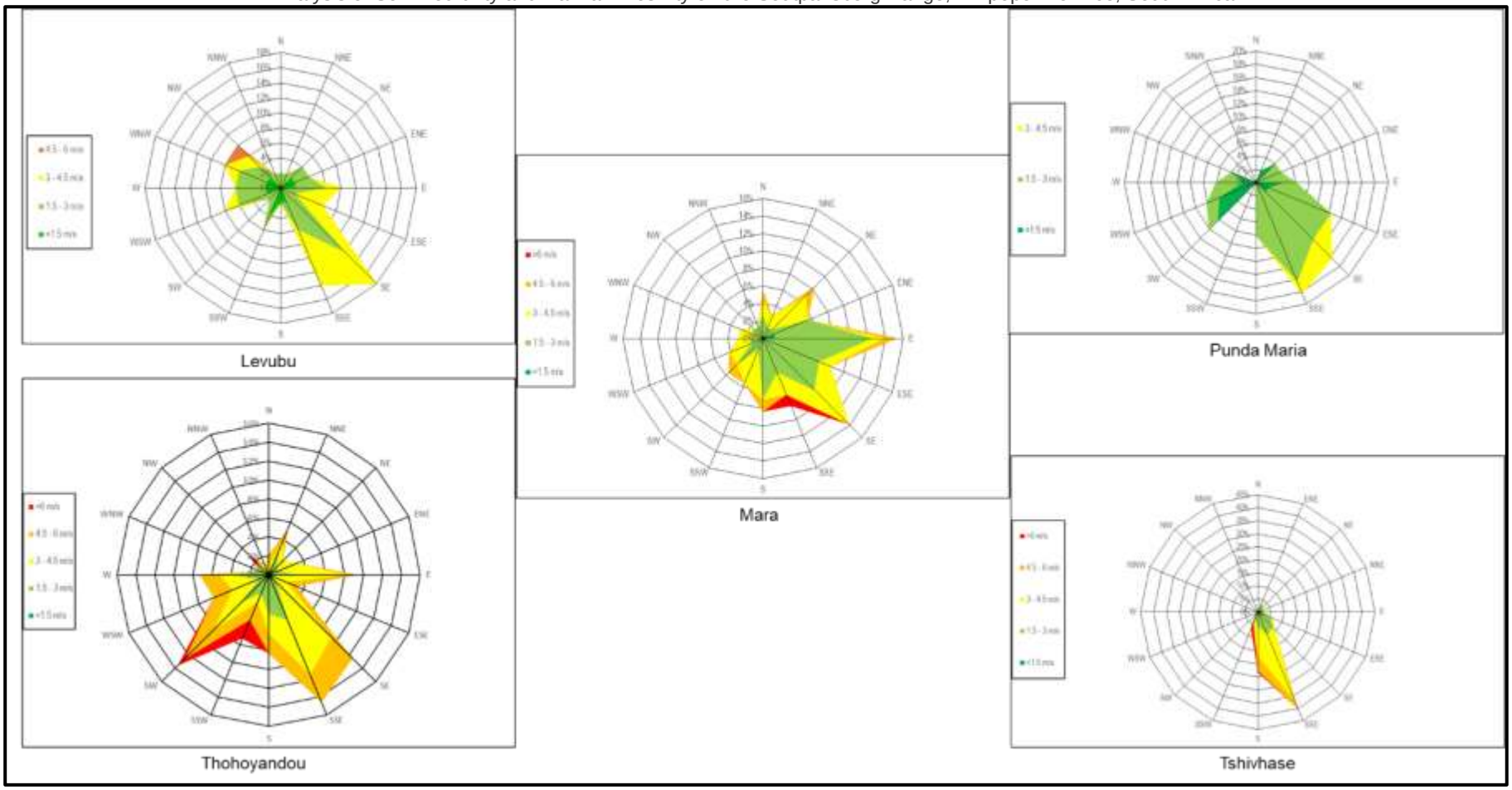

Figure 6.1: Potentially Erosive Storms Wind Roses

A general overview of the horizontal wind statistics indicates that most of the wind over the Soutpansberg blew from the eastern direction as indicated in figure 6.1. The East, East of Southeast, the Southeast and South of Southeast are the four dominant wind directions. The winds are predominantly light. Levubu and Punda Maria stations did not record any very strong wind during the period under review whereas Thohoyandou and Tshivhase recorded at least 10% strong winds.

Thohoyandou recoded 23% and 4% strong and very strong winds, respectively, at 614 m.a.m.s.l. However, the highest elevation of the five stations under consideration is 976 m.a.m.s.l at Tshivhase where strong and very strong winds were 10% and 3%, respectively. The highest wind speed of 8.0 m/s^{-1} was recorded at Thohoyandou weather station. Such statistics indicate that topographic elevation did not consistently result in an increase wind speed for the stations under review. Considering that only the five stations shown in Table 6.1 are studied, further research is necessary to assess whether these results are statistically significant. However, a detailed analysis of each station can shed more light to the winds that blow over the Soutpansberg mountain range. The stations are considered in alphabetical order.

Table 0.1: Soutpansberg Wind Speeds

Station	Elevation (m)	Wind Speed % (m/s^{-1})				
		<1.5	1.5 - 3	3 - 4.5	4.5 - 6	>6
		Calm	Light	Moderate	Strong	Very Strong
Levubu	706	22	50	26	2	0
Mara	914	7	56	29	7	1
Punda Maria	457	37	57	6	0	0
Thohoyandou	614	3	30	40	23	4
Tshivhase	976	12	31	44	10	3

Rainstorms recorded at Levubu weather station, at 706 m.a.m.s.l., indicate the dominance of wind from the Southeast (SE) and South of Southeast (SSE). The SE comprised 18% of the wind direction, while SSE constituted 14%. Some winds also blew from the East, NW, WNW as well as WSW, with each direction contributing 8% prevailing winds. Recording a maximum wind speed of 4.7m/s^{-1}, Levubu station experienced strong winds 2% of the time. The dominant winds were light (50%)

followed by the moderate (26%) and the calm (22%) categories. It is worth noting that the winds in the light category have the capacity to increase rain drops kinetic energy by between 3.2 to 3.5 times that of windless rain (Lyles and Allison, 1976; Helming, 1999). Therefore, the erosivity at Levubu potentially increased by at least 3.2 times due to wind in at least 78% of the storms during the period under review.

The Mara weather station is at the extreme western part of the Soutpansberg range at 914 m.a.m.s.l. The prevailing wind directions for the period under review were East and Southeast. The East contributed 15% while the Southeast contributed 14% of the wind recorded during the period under review. Also, important to note is that ESE, S and SSE directions all contributed 8% wind each.

The Mara station recorded mainly light winds, constituting 56% of the recorded wind speed during the period under review. Moderate winds constituted 29% while calm and strong winds constituted 7%. Following observations by Lyles and Allison (1976) and Helming (1999), erosivity at Mara potentially increases by at least 3.2 times due to the predominant wind speed in at least 93% of the storms during the period under review. Considering elevation in comparison with Levubu, one can reasonably argue that elevation may have played a part in influencing wind speed and erosivity.

The storm erodibility of ~78% of the storms recorded at low lying Levubu potentially increased, while ~93% were potentially affected in the same manner at Mara. The 208m elevation difference between the two stations could be the reason for the 15% point difference potential effects. The difference is also indicated by the maximum wind speeds recorded at the two stations. Levubu recorded the maximum wind speed of 4.7m/s^{-1} while Mara's was 7.1m/s^{-1}. This is also apparent in comparison with the other stations, particularly Punda Maria.

Punda Maria (457 m.a.s.l) station recorded winds mainly from SSE, SE, ESE and SW, respectively. The directions prevailed 18%, 16%, 12% and 10%, respectively. The dominant winds were light and contributed 57% of the prevailing winds. Calm winds constituted 37%, while moderate winds were 6% of the prevailing winds during the period under review. Neither strong nor very strong winds were recorded during the period under review. This reinforces the observation that increases in elevation

are associated with increases in horizontal wind speed. Low lying Punda Maria had 63% storms with the potential to increase erosivity by at least 3.2 times the Wind Free Rain erosivity. The maximum speed recorded was 3.6m/s^{-1}. However, Thohoyandou station presents a different picture.

Thohoyandou station is at 614 m.a.m.s.l. Wind blew predominantly from SSE, SE and SW during the period under review. The directions contributed 15%, 14% and 13% of the prevailing winds, respectively. Moderate winds were the most dominant at 40% while light winds constituted 30% of the recorded wind speeds. Strong winds constituted 23% while very strong winds were 4% to the recorded wind speeds. Calm winds were 3% of the recorded wind speeds. This means that 97% of the storms recorded during the period under review had the potential to increase their erosivity by at least 3.2 times. This is an interesting wind speed pattern as elaborated below.

Thohoyandou station falls in the very low elevation category in terms of local topographic elevation classes. Levubu station did not record any very strong wind, whereas Punda Maria station recorded both strong and very strong winds. Both stations (Punda Maria and Levubu) recorded significant calm storms. However, Thohoyandou recorded more very strong winds than calm storms. Despite Levubu being located at a higher elevation, there was no record of strong winds during the period under review. This puts into question the concept that elevation promotes wind speed. The highest wind speed of 8 m/s^{-1} during the period was recorded at Thohoyandou. The question about whether elevation increases horizontal wind speed is further exposed by a comparison between Thohoyandou and Tshivhase station.

Tshivhase Tea Estate station is at 976 m.a.m.s.l. This is moderate elevation within the Soutpansberg range. The station recorded SSE as the prevailing wind direction (40%) during the period under review. Southerly winds contributed 23% to the prevailing wind direction. The dominant wind speed (moderate) comprised 44% of the winds recorded at Tshivhase station during the period under review. Light winds constituted 31% while calm winds were 12%. Strong and very strong winds constituted 10% and 3%, respectively. Therefore, at least 88% of the storms

recorded during the period had the potential to increase erosivity by at least 3.2 times.

Despite occurring at a higher elevation than Thohoyandou, Tshivhase station recorded less strong and very strong winds. The highest speed recorded at Tshivhase was 6.9 m/s^{-1} while it was 8 m/s^{-1} at Thohoyandou. In addition, Thohoyandou recorded 13% and 1% more strong and very strong wind, respectively. While the difference for very strong wind is negligible and can be ignored, the difference for the strong winds is too wide to ignore. That Thohoyandou station has more strong and very strong winds than Tshivhase (27% to 13%) questions the concept that wind speed increases with elevation. However, a comparison between the other stations, excluding Thohoyandou, confirms that wind speed does appear to increase with elevation. Mara and Tshivhase stations recorded strong and very strong winds whereas Levubu had strong winds only 2% of the time. Punda Maria recorded neither strong nor very strong winds during the period 2000 to 2019. This is a strong indicator of the influence of elevation on wind speed. The results at Thohoyandou station need further investigation. More stations may provide additional data to shed light on the phenomenon at play.

6.3 The Influence of Topography on Rainfall Erosivity on the Soutpansberg

The rainfall erosivity considered for this section is that which was calculated following the SLEMSA and USLE formulae as presented in sections 3.4.1.1.1 and 3.4.3.1, respectively. This section addresses the hypothesis that topographic elevation increases rainfall erosivity. Monthly erosivity values for both models were computed into quarterly values that were eventually combined into annual values. Hence, the regression analysis was run for the quarters as well as the year erosivity figures for the 45 weather stations covering the Soutpansberg range.

Chapter 5 focused on rainfall spatial temporal distribution. The spatial aspect considered elevation. Spatial interpolation indicated the presence of weak rainfall spatial dependence. Both SLEMSA and USLE erosivity are direct derivations from rainfall. This section seeks to establish the relationship between erosivity and elevation. Considering that rainfall spatial dependency has already been established, some light should be shed on multiple r and r^2. This refocuses the results presented

in this chapter back to the aim to analyse the spatial characteristic of rainfall erosivity on the Soutpansberg range. Therefore, the proportion of erosivity explained by elevation in a WFR model hints at the closeness of the Wind Free Rain (WFR) models in representing the natural setting. However, model fit, and hypothesis testing are the ultimate goals of this chapter.

This section focuses on revealing whether the spatial distribution scenario revealed in Chapter 5 extends to erosivity. SLEMSA and USLE erosivity are direct derivatives from rainfall. Therefore, there is a constant implicit reference to the rainfall spatial dependency outcome reported in Chapter 5. The multiple r is graded at 0.2 intervals from very weak to very strong correlation. The r^2 used the same interval with descriptors from very low to very high. The results are also in quarters and annual time scales for easy comparison. The following section presents the results of the regression analysis.

6.3.1 JFM Erosivity

The SLEMSA erosivity regression results produced a multiple r that indicates a moderate correlation (0.411) between elevation and erosivity. However, only very low (17%) erosivity values are explained by the elevation (r^2 = 0.169). The two statistics corroborate with the weak rainfall spatial dependency reported in Chapter 5 for the same quarter. However, significance F is 0.005, indicating a good regression model. In addition, there is a significant positive coefficient between elevation and erosivity ($p \leq 0.05$). Therefore, despite the weak rainfall spatial dependency and moderate correlation, the regression model is good. Consequently, it is concluded that elevation influences erosivity. The null hypothesis is rejected.

The USLE erosivity regression results produced a multiple r that also indicates a moderate correlation (0.492) between elevation and erosivity. However, elevation explains the low 24% of the erosivity values (r^2 = 0.242). The two statistics corroborate with the weak rainfall spatial dependency reported in Chapter 5 for the same quarter. Significance F is 0.001, indicating a good regression model. In addition, there is a significant negative correlation between elevation and erosivity ($p \leq 0.05$). Therefore, despite the weak rainfall spatial dependency and correlation, the

regression model is good. Consequently, it is concluded that elevation influences erosivity. The null hypothesis is rejected.

Both SLEMSA and USLE erosivity have good regression models that are statistically significant. However, it is intriguing that SLEMSA has a positive while USLE has a negative coefficient. One reason could be the differences in the derivation algorithms of the models inherited from the model's development settings. The SLEMSA was developed in southern Africa while USLE was developed in the USA. However, this discrepancy would need to be investigated further in more detail.

6.3.2 AMJ Erosivity

Regression results for determining how topographic elevation influences the SLEMSA erosivity suggests a moderate correlation (multiple r = 0.569) where ~32% of the erosivity values are explained by topographic elevation (r^2 = 0.324). The two statistics do not fully corroborate the strong rainfall spatial dependency reported in Chapter 5 for the same quarter. The correlation is not far from the strong spatial dependency, however, the r^2 is low.

The significance F of 0.000 indicates a good regression model. This means that topographic elevation influences erosivity and the probability of accepting that the SLEMSA erosivity is a function of rainfall only is nil. In addition, there is a significant positive correlation between elevation and erosivity ($p \leq 0.05$). Therefore, the influence of elevation on erosivity is not by chance, despite the lack of full collaboration between rainfall spatial dependency and correlation. Consequently, it is concluded that elevation influences erosivity, at least for this quarter.

The multiple r for the USLE erosivity regression indicates a moderate correlation (0.558) between topographic elevation and erosivity. This is weakly supported by the low 31% of the erosivity values that are influenced by elevation (r^2 = 0.312). It is interesting to note that the two statistics are similar for both the SLEMSA and USLE and do not fully corroborate the strong rainfall spatial dependency reported in Chapter 5 for the AMJ quarter. The correlation is close to the strong spatial dependency, however, the r^2 is low.

The significance F is 0.000, indicating that the USLE erosivity is influenced by topographic elevation. In addition, there is a significant positive correlation between elevation and erosivity ($p \leq 0.05$). Therefore, despite the lack of full corroboration between rainfall spatial dependency and correlation, the regression model indicates that topographic elevation indeed influences the USLE erosivity. Accordingly, it is concluded that topographical elevation influences erosivity and the null hypothesis is rejected for this quarter.

6.3.3 JAS Erosivity

The SLEMSA erosivity regression results for the JAS quarter produced a multiple r that indicates a weak correlation (0.361) between elevation and erosivity. A very low percentage (13%) of the erosivity values are explained by elevation ($r^2 = 0.130$). The two statistics contradict the strong rainfall spatial dependency reported in Chapter 5 for the same quarter.

Significance F is 0.015, indicating a good regression model supported by a significant positive correlation between elevation and erosivity ($p \leq 0.05$). Therefore, despite the very low explanatory influence and weak correlation, the regression model is still good. This means that the weak topographic influence is still significant in influencing erosivity. Consequently, it is concluded that elevation influences erosivity. The statistics are similar for the USLE erosivity regression results. Therefore, the conclusion is the same.

6.3.4 OND Erosivity

The SLEMSA erosivity regression results have a multiple r that indicates a weak correlation (0.392) between elevation and erosivity. This is supported by the fact that a low percentage (15%) of the erosivity values are explained by elevation ($r^2 = 0.154$). The two statistics do, however, contradict the strong rainfall spatial dependency reported in Chapter 5 for the same quarter. The contradiction statistics, however, is not the basis for the final decision as model fit and regression coefficient determine the strength of the findings.

A significance F of 0.008 indicates a good regression model. This is supported by a significant positive correlation between elevation and erosivity ($p \leq 0.05$) indicating a

significant topographical influence on erosivity. As such, it is concluded that elevation influences SLEMSA erosivity, rejecting the null hypothesis for this quarter of the year.

The multiple r for the USLE erosivity regression indicates a weak correlation (0.254) between elevation and erosivity. This is supported by the fact that only 6% of the erosivity values are explained by elevation (r^2 = 0.064). The two statistics contradict the strong rainfall spatial dependency reported in Chapter 5 for the same quarter.

The significance F of 0.093 indicate the poor influence of topographic elevation on USLE erosivity. In addition, there is an insignificant positive correlation between elevation and erosivity ($p \geq 0.05$). Therefore, despite the strong rainfall spatial dependency as reported in Chapter 5, correlation between topographic elevation and USLE erosivity is weak and insignificant while the regression model is poor. Consequently, it is concluded that elevation does not influence erosivity within the context of the USLE for OND. The null hypothesis is, therefore, retained for this quarter.

The discrepancies in the regression models for JFM and OND are instructive. While the JFM difference was on the direction of relationship (the correlation coefficient is negative), the OND one was on the influence of elevation on erosivity. Both SLEMSA and USLE erosivity are directly derived from rainfall. Chapter 5 confirmed the spatial dependency of rainfall to be strong in OND. The rejection of that aspect by the erosivity regression model should be taken as a strong indicator of the inapplicability of USLE erosivity model in the Soutpansberg, and hence, southern Africa. The negative relationship outcome for the JFM quarter supports this view. However, an examination of annual figures determines whether they shed better light on this observation.

6.3.5 Annual Erosivity

The SLEMSA erosivity regression results produced a multiple r that indicates a moderate correlation (0.455) between elevation and erosivity. A low percentage (21%) of the erosivity values are explained by elevation (r^2 = 0.207). The two statistics contradict the strong rainfall spatial dependency reported in Chapter 5 for

annual rainfall. Significance F is 0.002 indicating a good regression model. In addition, there is a significant positive coefficient between elevation and erosivity ($p \leq 0.05$). Therefore, despite the low explanatory relationship and moderate correlation, the regression model is good. Consequently, it is concluded that elevation influences erosivity. The null hypothesis is rejected. The annual statistics are similar for the USLE and, therefore, the analytical outcome is the same.

The annual regression statistics for both SLEMSA and USLE erosivity are very similar. Both have moderate correlation. Both have very low erosivity values explained by elevation. Both have good regression models and statistically significant positive coefficients. Therefore, from a Wind Free Rain perspective, it is concluded that elevation has a statistically significant influence on erosivity. The null hypothesis is rejected.

6.4 Chapter Summary

The chapter addressed the third objective of the research. The objective has been to assess the influence of topography on wind speed and rainfall erosivity on the Soutpansberg range to establish the effect of topography on wind speed and erosivity. The chapter was presented in two parts. The first part focused on wind speed as recorded at five weather stations: The weather stations are Levubu, Mara, Punda Maria, Thohoyandou and Tshivhase. The second part focused on the effects of topography on rainfall erosivity. The period under review from 2000 to 2019 recorded 383 potentially erosive storms that were used in this research.

Results show that the dominant wind category was light (1.6 – 3 m/s^{-1}), comprising about 44% of the winds during the period under review. The strongest winds were recorded at Thohoyandou station, at 614 m.a.s.l. However, Tshivhase station is at the highest elevation of 976 m.a.m.s.l. While this indicates that wind speed was not influenced by elevation, at least for these cases, the other stations indicate an influence of elevation on wind speed.

Levubu and Punda Maria stations are located at a very low elevation. The Punda Maria station recorded neither strong nor very strong winds. Levubu station recorded just 2% strong winds and no very strong winds. On the other hand, Mara and

Tshivhase stations both recorded strong and very strong winds. The highest speeds at Levubu and Punda Maria were 4.7m/s^{-1} and 3.6m/s^{-1}, respectively. Tshivhase and Mara recorded highest wind speeds of 6.9m/s^{-1} and 7.1m/s^{-1}, respectively. This clearly indicates the influence of elevation on wind speed.

The influence of elevation on erosivity was examined through a simple linear regression analysis of 45 weather stations on the Soutpansberg range. The erosivity values were grouped into quarterly and annual computations for SLEMSA and USLE. Regression results indicate good regression models and significant positive relationships between elevation and erosivity. However, detailed analyses showed a negative relationship between the elevation and USLE erosivity during the JFM quarter. The null hypothesis was also retained for USLE erosivity in the OND quarter. Nonetheless, these were minor and, therefore, negligible because it only occurred to the USLE model in only two quarters. All the SLEMSA and two other USLE erosivity computations rejected the null hypothesis. It is concluded that elevation influences erosivity. This result opens up the need to examine how wind speed influences erosivity. This is addressed in the following Chapter.

: THE INFLUENCE OF WIND SPEED ON RAINFALL EROSIVITY

7.1 Introduction

This chapter addresses the fourth objective of this research. The objective is to compare rainfall erosivity derived from the WFR methods with that computed through the Wind Driven Rain (WDR) methodology. The Universal Soil Loss Equation (USLE) and the Soil Loss Estimation Model for Southern Africa (SLEMSA) are the WFR methods. The comparison aims to establish whether WFR or WDR erosivity is a better representation of reality.

The comparison begins by establishing the deviation between WDR and WFR erosivity values from historical data. This is because one of the factors that influence rainfall measurement is the effect of wind deformation. The WMO (2021) indicate that rainfall measurements are sensitive to, among other elements, wind, and strong winds may alter rain gauge catch. Wind creates localised disturbances that can result in rain gauge catch variations of up to 10% (Yang, 1998; WMO, 2021). Thus, wind affects rainfall intensity as it brings in a horizontal dimension to the vertically falling raindrops. Therefore, basing erosivity computations on rainfall amount and intensity without considering wind speed can be considered a significant oversight. This part, therefore, establishes the extent of differences between the WFR and WDR erosivity values based on 383 erosive storms recorded during the period under review.

The second part establishes the differences between different erosivity values using Multiple Analysis of Variance (MANOVA) (Glen, 2015; Pallant, 2016; Lund and Lund, 2018) where erosivity is the dependent variable while wind speed and rainfall amount are the independent variables. The computed soil loss using different models is eventually compared with data collected from splash cups. Values produced from the models that are closer to collected samples for the same conditions are considered a better representation of reality.

7.2 Rainfall and Wind Co-occurrence

This research considers that the exclusion of wind speed in the wind free rain (WFR) erosivity computation is fundamental oversight. This is because most rainstorms are

accompanied by winds (Reis *et al.*, 2010; Sobel, 2012; Zorn and Komac, 2013). This section uses the 383 erosive storms to statistically establish if the occurrence of rain is accompanied by wind. This is done through linear regression analysis. That establishes if there is a linear relationship between rainfall amount and horizontal wind speed for each of the five automated weather stations and rainfall amount is the independent variable.

A strong correlation between rainfall amount per rainfall event and wind speed would suggest that wind speed is a function of rainfall amount. Therefore, it would be safe to suggest that wind co-occurs with rainfall. Such regression results would mean that excluding wind in WFR erosivity is a fundamental misrepresentation of reality.

Levubu Weather Station data regression results indicate a very weak correlation (multiple r = 0.056) between rainfall and wind speed. The r^2 indicates that virtually no wind speed (r^2 = 0.003) can be explained by rainfall amount. This indicates that wind speeds recorded at Levubu station were not strongly influenced by the occurrence of rainfall. Hence there was no strong co-occurrence of wind and rain. Therefore, wind speed and rainfall amount do not necessarily need to be taken together all the time in assessing erosivity.

However, the p-value indicates that the relationship is not statistically significant (p-value = 0.711). That the correlation between rainfall rates and wind speed is weak and the r^2 is poor reinforces the statistical significance of the relationship. Therefore, though there is statistical indication that the wind speed and the rainfall amount are not correlated, it is statistically insignificant. Therefore, assuming that wind does not co-occur with rainfall is not statistically supported, at least for the data recorded at Levubu Station between January 2000 and November 2019.

The statistics for Mara Weather Station data show a similar characteristic as that of Levubu Weather Station. The correlation between rainfall rates and wind speed is very low at 0.162 while the r^2 is 0.026. Both the p-value and the significance F are larger than 0.05. This again indicates that the record at Mara station supports the existence of a positive relationship between rainfall amount and wind speed. However, the relationship is not statistically significant. Therefore, one may not

conclude that the WFR approach is correct in excluding wind speed in erosivity computations.

The regression results for Thohoyandou Weather Station reveal the same results as the Levubu and Mara data. The correlation between rainfall rates and wind speed is very weak (multiple r = 0.170) while the r^2 is 0.029. Both significance F and p-value are larger than 0.05. In addition to the insignificant relationship, the coefficient is also very low (0.031). This further emphasizes the point that one cannot conclude that wind and rainfall do not co-occur. This statistical result also applies to Tshivhase Weather Station and for the combined data for all the weather stations.

However, Punda Maria station regression results are different. The rainfall amount and the wind speed at Punda Maria have a moderate correlation (Ratner, 2009) of 0.342 while the r^2 is 0.117. This relationship is statistically significant (significance F = 0.020). The p-value is less than 0.05, supporting the notion that wind and rainfall co-occur, implying that the exclusion of wind speed in the WFR model was a serious oversight. However, this data is not conclusive. The following section interrogates how horizontal wind speed relates with rainfall erosivity using historical data.

7.3 Erosivity Variability – Evidence from Historical Data

The Soutpansberg range is a low rainfall region as presented in Chapter 5. A total of 383 erosive storms meeting the 12.5 mm/hr threshold was recorded over the 20 year period in five stations. That gives an average of 19 erosive storms per year. This further gives an average of 4 erosive storms per station per year. The storms are also not evenly balanced. Tshivhase Tea Estate had 140 storms. Thohoyandou follows at 86. Mara is third with 65. Punda Maria and Levubu had 46 apiece. However, valuable information was still derived from the few erosive storms.

The general outlook is that horizontal wind speed significantly increases rainfall erosivity. The differences can be as high as 1400% as in the storm at Tshivhase Estate on 13 February 2019. All the differences are above 100% as shown in Table 7.1 where the least difference 233%. The highest average difference is 441% at Tshivhase Tea Estate. Most cases have higher WDR erosivity.

Table 0.1: Average WDR and WFR Erosivity Differences (%)

Station	Mara	Levubu	Thohoyandou	Tshivhase	Punda Maria
SLEMSA	370.38	394.06	371.46	441.64	405.19
USLE	233.65	247.87	233.96	278.41	256.11

An interesting point to note is the role of both wind speed and total rainfall amount and their differential effects on USLE, SLEMSA and WDR. The USLE seems to respond to both wind speed and rainfall amount while rainfall amount seems to affect SLEMSA more. This stems from the model designs where SLEMSA is directly linked to rainfall amount while USLE includes rainfall intensity. Rainfall intensity is influenced by wind characteristics (Yang, 1998; WMO, 2021). Wind speeds below 3m/h consistently resulted in a WDR erosivity lower than the WFR, irrespective of the rainfall amount. On the other hand, rainfall amounts above 15mm coupled with wind speeds above 3m/hr produced WDR erosivity higher than the WFR for USLE.

On the other hand, all SLEMSA WDR erosivity values are higher than the WFR ones. This questions the representativeness of SLEMSA. The use of the energy constant and rainfall amount only seems to have excluded other important rainfall characteristics such as intensity. Yet rainfall intensity is an important factor in creating energy for erosion (Kinnell, 2010).

The statistical comparison between Wind Driven Rain (WDR) and Wind Free Rain (WFR) erosivity computations was an attempt to reveal the influence of wind speed on rainfall erosivity. It was also an attempt to reveal the model that represents reality better. The statistical analysis was done through MANOVA and verified by a pairwise t-test to statistically compare the different erosivity computing models. The MANOVA begins by establishing the significance of the individual contribution of wind speed and rainfall to erosivity (Pallant, 2016; Lund and Lund, 2018) as computed using both WFR and WDR models. The individual contribution is indicated by the Wilk's Lambda, which points to the amount of erosivity that is not explained by the effect of rainfall amount or wind speed. Hence, a Wilk's Lambda as close to zero as possible

is preferable than one that is far away from zero. The significance of the contribution of wind speed or rainfall amount to erosivity is indicated by a p-value ≤ 0.05. The effect size (influence) of either wind speed or rainfall amount is indicated by the eta squared. Results are presented at both individual station and combined data form. The extent of individual differences is then analysed by t-test.

The multivariate test results for Levubu Weather Station show that 88% of the variance in erosivity in both WFR and WDR models pooled together can be explained by wind speed. The Wilk's Lambda value is close to zero and shows significant interaction between wind speed and erosivity. The interaction is statistically significant (p ≤ 0.05). Results also show that wind speed has a large influence on the erosivity computation (eta squared = 0.876). By the same token, the rainfall amount explains all erosivity (Lambda = 0; p = 0) computed by both WFR and WDR models pooled together. The rainfall amount has total influence (eta squared = 1) on erosivity as shown in Table 7.2.

This result indicates the significance of the exclusion of wind speed in WFR erosivity computation. That rainfall amount explains all erosivity, including the WDR one, should not play down the 88% significant influence of wind speed. Rather, it should be considered as an indication of how rainfall occurrence does not mean the absence of wind. This is what the test between subject effects shows as it indicates how wind speed and rainfall amount each affect erosivity as computed using USLE, SLEMSA or WDR model.

Table 0.2: Multivariate Tests

Station Name	Wind Speed			Rainfall Amount		
	Lambda Value	Significance	Eta	Lambda Value	Significance	Eta
Levubu	0.124	0.000	0.876	0.000	0.000	1.000
Mara	0.163	0.000	0.837	0.000	0.000	1.000
Punda Maria	0.350	0.000	0.650	0.000	0.000	1.000
Thohoyandou	0.245	0.000	0.755	0.000	0.000	1.000
Tshivhase	0.063	0.000	0.937	0.000	0.000	1.000
All Stations	0.317	0.000	0.683	0.000	0.000	1.000

The between-subjects effects for Levubu station reveal the separate effect and significance of rainfall amount and wind speed in the USLE, SLEMSA and WDR calculations of erosivity individually. Results in Table 7.3 indicate that wind speed has an insignificant statistical effect on USLE R and SLEMSA R (p = 0.536 and 0.584, respectively). The effect sizes are also low (0.009 and 0.007, respectively) indicating a very weak association. This should not be surprising since the two models (USLE and SLEMSA) exclude wind in their erosivity computations. However, wind speed does not explain all variance in WDR R (eta squared = 0.874) although the association at 87% is strong.

Another important point to note is that the rainfall total influences a very low percentage (4.3%) of erosivity in the USLE. Although the effect is statistically insignificant (0.173), rainfall amount and USLE R are not strongly related because of the very low effect size. Hence, it can be concluded that WFR erosivity has a significant missing phenomenon in wind speed, at least for Levubu station. However, the Wilk's Lambda indicates that wind speed has a statistically large effect on erosivity computations. The results from Mara weather station give more insight to the wind and rainfall relationship vis-à-vis soil erosion.

Table 0.3: Tests Between Subjects Effects

Source	Dependent Variable	Levubu		Mara		Thohoyandou		Tshivhase		Punda Maria		All Stations	
		Sig.	Eta	Sig.	Eta	Sig.	Eta	Sig.	Eta	Sig.	Eta	Sig.	Eta
Wind Speed	USLE R	0.536	0.009	0.693	0.003	0.539	0.005	0.547	0.003	0.303	0.025	.	.
	SLEMSA R	0.584	0.007	0.000	0.836	0.000	0.631	0.000	0.754	0.000	0.930	0.000	0.683
	WDR R	0.000	0.874	0.796	0.001	0.603	0.003	0.006	0.055	0.216	0.035	0.218	0.004
Rainfall Amount	USLE R	0.173	0.043	0.000	1.000	0.000	1.000	0.000	1.000	0.000	1.000	.	1.000
	SLEMSA R	0.000	1.000	0.001	0.173	0.000	0.196	0.000	0.446	0.000	0.328	0.000	0.220
	WDR R	0.055	0.083	0.000	1.000	0.000	1.000	0.000	1.000	0.000	1.000	0.000	1.000

The Mara Weather Station multivariate test results show that wind speed influences a significant (83.7%) amount of the variance in erosivity. The interaction is statistically significant ($p \leq 0.05$) with wind exerting a large effect on erosivity (eta squared = 0.837). By the same token, the rainfall amount has a significant interaction with erosivity (Lambda = 0; p = 0) and the effect is large (eta squared = 1). Table 7.2 shows the results. However, between subject effects shines more light into the analysis.

The interaction effect overlaps between wind speed and rainfall amount depicted for Levubu Weather Station data are repeated at Mara. The Wilk's Lambda indicates that rainfall amount explains all variances in erosivity. This is despite the treatment of wind speed as a separate variable in WDR erosivity computation and exclusion in WFR. This gives credence to the findings of a weak accounting of wind speed in WFR erosivity computations. Wind speed cannot be accounted for by a variable with which it has a weak statistical link. A further analysis of the influence of wind speed and rainfall amount on erosivity will expose the weak link. The analysis is done by test of between-subjects' effects. This should reveal the effects of rainfall amount and wind speed on each erosivity type.

The between-subjects effects give more information of the effect and significance of rainfall amount and wind speed on individual erosivity type. It is a given that wind speed has an insignificant statistical effect on USLE R and SLEMSA R ($p = 0.693$ and 0.796, respectively). The effect sizes are also low (0.003 and 0.001, respectively) indicating a very weak association as shown in Table 7.3. Therefore, it can be argued that WFR erosivity makes a significant omission by not including wind speed. However, the Wilk's Lambda indicates wind speed's statistically significant large effect on erosivity computation. Therefore, the exclusion of wind speed in WFR is statistically significant. The Thohoyandou weather station also provides more insight to the wind speed and rainfall amount relationship vis-à-vis soil erosion.

Wind speed influences 65% of the variance in erosivity at Thohoyandou Weather Station. The interaction between wind speed and erosivity is significant ($p \leq 0.05$) where wind speed exerts a large effect on erosivity computation (eta squared = 0.650). Similarly, rainfall amount has a large effect, and a significant influence on erosivity, as shown in Table 7.2. However, test between subject effects shines more light into the analysis.

The same interaction effect picture of overlaps between wind speed and rainfall amount depicted for Levubu and Mara Weather Stations data recurs. The Wilk's Lambda indicates that rainfall amount explains all variances in erosivity. It also indicates a strong association of 0.650 between wind speed and erosivity despite

exclusion in WFR erosivity. Therefore, wind speed exclusion in the WFR erosivity is a misrepresentation of reality.

The inclusion of the rainfall intensity aspect for USLE and the constant for rainfall type in SLEMSA may somehow represents the effect of wind speed on rainfall. However, the statistically weak relationship between rainfall amount and wind speed within the WFR model suggests otherwise. A further analysis of the influence of wind speed and rainfall amount on erosivity unravels the challenge further.

The between-subject effects reveal the finer detail of the influence and significance of rainfall amount and wind speed on individual erosivity computations. Considering that wind is excluded in the WFR models, it is not a surprise that wind speed has an insignificant statistical effect on USLE R and SLEMSA R ($p = 0.569$ and 0.603, respectively). The effect sizes are also low (0.005 and 0.003, respectively), indicating a very weak association (Table 7.3). The results reinforce the observation that excluding wind speed in WFR erosivity makes the models inadequately represent reality.

Further analysis indicates that wind speed has a statistically significant influence on erosivity as indicated by Wilk's Lambda. Rainfall amount also has a statistically significant relationship with WDR R. The effect of rainfall amount on WDR R at Thohoyandou is large (eta squared = 0.196). Hence, there is a strong association between rainfall amount and WDR R. This contradicts the weak relationship established in Section 7.2. A shift to look at Tshivhase weather station gives more insight to the horizontal wind speed and rainfall relationship vis-à-vis soil erosion.

The multivariate test results for Tshivhase Weather Station show that 24.5% of the variance in erosivity is not explained by wind speed. The Wilk's Lambda value is statistically significant ($p \leq 0.05$), and wind speed has a large effect on erosivity computation (eta squared = 0.75.5). The same applies with rainfall amount as shown in Table 7.2. However, the test between subjects' effects shines more light into the analysis.

The same interaction effect pattern produced for Levubu, Mara and Thohoyandou Weather Stations data depicting overlaps between wind speed and rainfall amount

recurs. The Wilk's Lambda indicates that rainfall amount explains all variances in erosivity despite its exclusion wind speed. It also indicates a strong association of 0.755 between wind speed and erosivity despite wind's exclusion from SLEMSA and USLE computations. This supports the findings of a weak relationship between wind speed and rainfall amount as applied in WFR erosivity. The statistically weak relationship between rainfall amount and wind speed warrants further analysis of the influence of wind speed and rainfall amount on erosivity. The test of between-subject effects does the analysis.

The tests between-subject effects reveal the finer details of the effect and significance of rainfall amount and wind speed on individual erosivity computations. Tshivhase Weather station data gives different statistical results compared to Levubu, Mara and Thohoyandou Weather Stations. While wind speed has an insignificant statistical effect on SLEMSA R ($p = 0.547$), the effect on USLE R is statistically significant at $p = .006$. However, both effect sizes are low (.003 and .055, respectively) indicating a very weak association (Table 7.3). This reinforces the findings where the correlation between wind speed and rainfall amount is statistically weak. However, the statistically significant effect of wind speed on USLE R needs further probing.

Though the effect size is low, the statistical significance requires some thought. The role of terrain and the inclusion of rainfall intensity in USLE erosivity, among other factors, easily comes to mind. The orographic factor can be factored into the statistically significant effect of wind speed on USLE R. Tshivhase weather station is located on significantly higher elevation (976 m. a. s. l.) than the other weather stations, save for Mara. The station's location in the southern-central high crest of the Soutpansberg range puts it in the very high rainfall zone. The orographic effect of the mountain on rainfall and wind speed (Banta and Cotton, 1981; Beniston, 2003; Barry, 2008; Sun and Sun, 2015) in that section of the mountain is revealed from the results in Chapter 5 in which the spatial temporal characterisation of rainfall on the mountain range was made clear. The conclusion in Chapter 5 was that potentially erosive rainfall distribution is spatially dependent.

Furthermore, rainfall intensity is affected by wind speed. Therefore, one can argue that the wind effect in latent in rainfall intensity. In addition, although the effect size is small, the statistical significance suggests the importance of wind in erosivity. Wilk's Lambda further reinforces the statistical significance of wind on erosivity. Therefore, the view that rainfall total amount infuses wind speed cannot be sustained. A shift to look at Punda Maria weather station data gives more insight to the wind speed and rainfall amount relationship vis-à-vis soil erosion.

The multivariate test results for Punda Maria Weather Station show that 0.970 variance in erosivity is explained by wind speed. This Wilk's Lambda value shows statistically significant ($p \leq 0.05$) interaction between wind speed and erosivity. The test also shows that wind speed has a large effect (eta squared = 0.937) on erosivity. The large effect size implies a strong association between wind speed and erosivity.

By the same token, the rainfall amount recorded at Mara weather station has a significant interaction with erosivity (Lambda = 0; p = 0). The effect of the rainfall amount on erosivity is large (eta squared = 1). Table 7.2 shows that there is a strong association between rainfall amount and erosivity. However, the test between subject effects shines more light into the analysis.

The interaction effect pattern depicting overlaps between wind speed and rainfall amount produced for Levubu, Mara, Thohoyandou and Tshivhase Weather Stations data is also produced at Punda Maria weather station. The Wilk's Lambda indicates that the rainfall amount explains all the variances in erosivity despite the treatment of wind speed independently of rainfall amount in WDR R computation. It also indicates a strong association of 0.937 between wind speed and erosivity despite wind's exclusion from SLEMSA and USLE. Such statistics are in keeping with the findings of a weak relationship between wind speed and rainfall amount as applied in WFR in that rainfall does not always co-occur with wind. The statistically weak relationship between rainfall amount and wind speed for the WFR warrants further analysis of the influence of wind speed and rainfall amount on erosivity. Such analysis is done by test of between-subject effects. This should reveal the effects of rainfall amount and wind speed on each erosivity type.

The tests between-subjects effects probe the finer details of the effect and significance of rainfall amount and wind speed on individual erosivity computations. Like in the other stations, wind speed has an insignificant statistical effect on USLE R and SLEMSA R ($p = 0.303$ and 0.216, respectively). The effect sizes are also low (0.025 and 0.035, respectively) indicating a very weak association (Table 7.2). The statistics reinforce the statistically weak correlation between wind speed and rainfall amount. However, Punda Maria weather station data present an insight regarding WDR R.

The WDR R for Punda Maria has a statistically significant relationship with rainfall amount. The effect size of rainfall amount on WDR R is large (eta squared = 0.328). This indicates an important link between rainfall amount and wind speed. It should be remembered that WDR R considers wind speed independently of rainfall amount, yet the effect of rainfall on WDR is large. Therefore, it can be argued that WFR erosivity ignores a significant natural relationship between rainfall occurrence and wind speed. Wind speed has a statistically significant influence on erosivity as indicated by Wilk's Lambda. Rainfall amount also shows a statistically significant effect on WDR R. The effect size is large (eta squared = 0.328) indicating a strong association.

It is interesting that Punda Maria weather station gives a different picture. Incidentally, it is the station located at the lowest elevation (457 m. a. s. l.). Punda Maria weather station falls in a low elevation area less than 20 km from the Soutpansberg range. Therefore, the orographic effect does impact on the results. Hence, Punda Maria weather station may not be a typical mountain weather station. A look at the combined data for all five weather stations gives more insight to the wind speed and rainfall relationship vis-à-vis soil erosion.

The multivariate test results for all weather stations, considering both WFR and WDR, show that 0.683 of variance in erosivity is explained by wind speed. The Wilk's Lambda value shows statistically significant ($p \leq 0.05$) interaction between wind speed and erosivity. The test also suggests that wind speed has a large effect (eta squared = 0.683) on erosivity. The large effect size implies a strong association between wind speed and erosivity.

However, the rainfall amount also has a significant interaction with erosivity (Lambda = 0; p = 0). The effect of rainfall amount on erosivity is large (eta squared = 1). Table 7.2 shows that there is a strong association between rainfall amount and erosivity. The interaction effect pattern depicting overlaps between wind speed and rainfall amount produced for individual weather stations data are also present for the combined data set.

The Wilk's Lambda indicates that the rainfall amount for the combined data explains all the variances in erosivity despite treatment of wind speed and rainfall amount as separate variables in WDR. It also indicates a strong association between wind speed and erosivity despite wind speed not included in SLEMSA and USLE erosivity computations. A strong association between rainfall amount and wind speed is an indication of the fundamental oversight in SLEMSA and USLE erosivity computations. The statistics support the co-occurrence of wind and rainfall.

Individual weather station data indicate a poor statistical relationship between wind speed and WFR erosivity. The Punda Maria weather station is the only station for which the data suggest some relationship. This aligns with the generalisations of the WFR theory. However, the post hoc t-test sheds light that can lead to a solid conclusion.

A t-test is a pairwise comparison that modifies the p-value for each test. The pairwise comparison produced for this research were: WDR – USLE; WDR – SLEMSA; USLE -SLEMSA. The treatment is for each weather station and a combined data set of all stations. The new pairwise p-value (P (T<=t two tail)) indicates the probability of the groups belonging to the same population. A pairwise p-value ≤0.05 indicates that the members of the pair are different. A p-value indicating a difference suggests the rejection of the view that rainfall total amount adequately represents rainstorm reality in WFR. The conclusion will be that exclusion of wind speed in WFR erosivity is a significant oversight in the model.

The important pairwise comparisons are WDR R versus SLEMSA R and WDR R versus USLE R. The pairing pits WDR and WFR (SLEMSA and USLE) to clarify whether WFR and WDR belong to the same group. The t-test results from all stations, except Levubu, suggest that WDR R does not belong to the same group

with USLE R as indicated in Table 7.4. The combined statistics indicate a difference too. The t-test results conclude that wind speed exclusion in WFR erosivity does not represent rainstorm reality.

Table 0.4: T-test p Values

	Mara	Levubu	Thohoyandou	Tshivhase	Punda Maria	All Stations
WDR-USLE	0.000	**0.075**	0.000	0.000	0.000	0.000
WDR-SLEMSA	0.019	**0.269**	0.000	0.000	0.000	0.000
USLE-SLEMSA	0.000	0.000	0.000	0.000	0.000	0.000

Be that as it may, this section used historical data. Although it has been shown that wind speed is important in erosivity, USLE and SLEMSA models have been tested widely and are scientifically proven to be reliable (Stocking *et al.*, 1988; Renard *et al.*, 1997). Therefore, it is necessary to do an empirical test to prove whether WFR or WDR is a closer representation of natural settings. Therefore, sediment collection equipment was set up at University of Venda Experimental Farm (representing Thohoyandou weather station) and Tshivhase Tea Estate between November 2020 and March 2021. The following section presents the results.

7.4 Erosivity Variability – Evidence from Empirical Data

The aim of this section is to establish the influence of wind speed on erosivity through empirical relationships obtained from observational data. This is juxtaposed such that USLE, SLEMSA and WDR erosivity are statistically compared with WDR erosivity. Section 7.2 established the correlation between rainfall amount and wind speed. The purpose was to establish if the exclusion of wind speed in the WFR erosivity overlooked a statistically significant natural relationship. The results indicate a weak correlation between rainfall occurrence and wind. This means that a firm conclusion cannot be reached regarding the role of wind on erosivity based on a weak statistical relationship. Therefore, further analysis then followed.

Section 7.3 focused on establishing the interaction effect, as well as strength of association between wind speed and erosivity. The same was sought between rainfall amount and erosivity. The analyses revealed a generally significant interaction effect as well as strong association between WDR erosivity and wind speed as well as rainfall amount. However, the WFR models, as expected, produced mainly statistically insignificant interaction effects and weak associations. This necessitated further analysis.

This section moves to further investigate sections 7.2 and 7.3 using empirical data. The sediment data collected by setting up splash cups are significant for this research. The erosive storm frequency in the study area is low because the region is generally dry in most areas (Kabanda, 2004; Nenwiini and Kabanda, 2013; Rapolaki *et al.*, 2019). However, water erosion is still a challenge in the region (Gibson, 2006; Le Roux and Smith, 2014). The first erosive storm was recorded after 6 January 2021. The last was recorded on 22 and 26 February 2021 for Tshivhase and Thohoyandou, respectively. The data are used as empirical evidence to determine the influence of wind speed on erosivity. More crucially, this data assists in identifying the erosivity model that better represents reality.

Before presenting the sediment results, it is prudent to also do statistical analyses on wind speed and rainfall amount as done in sections 7.2 and 7.3. This will be followed by presentation of total soil loss according to each model. Then the same model's R is replaced with WDR R. The outcomes are compared with the sediments collected from the splash cups. This would indicate the influence of wind speed on erosivity. Furthermore, the erosivity computation method that is closer to reality will be revealed.

7.4.1 Wind - Rainfall Correlation and Variability

This section is a mirror of section 7.2. The aim is to establish if wind speed and rainfall amount correlate. This guides in determining if wind and rainfall co-occur. This is tested through a simple linear regression between the observed hourly rainfall amount and wind speed.

Thohoyandou Weather Station data regression results indicate a very weak correlation (multiple r = 0.083) between rainfall amount and wind speed. The r^2 indicates that virtually no wind (r^2 = 0.007) can be explained by rainfall amount. This aligns with the results in section 7.2. However, the statistical basis for a decision on the view is determined by significance F and the p-value.

Both the significance F and p-value are above 0.05. Therefore, based on the two statistics, it can be argued that wind speed is associated rainfall amount. However, the p-value indicates that the association is not statistically significant (p-value = 0.906). That the correlation is weak and the r^2 is poor reinforces the statistical insignificance. Therefore, though there is statistical indication of wind speed association with rainfall amount, it is statistically insignificant. Therefore, this should not be the basis for excluding wind speed in erosivity computations.

Regression results for Tshivhase Weather Station data are the same as those of Thohoyandou weather station. The same outcome is also true in the case of the combination of the two stations. The results confirm the weak correlation that was established by long term data. Therefore, it is logical to now turn to MANOVA. The multivariate analysis for individual as well as combined short term data indicate a slightly different trend from that produced in section 7.3.

Long term data for Thohoyandou in section 7.3 produced multivariate results where wind speed had a statistically significant interaction with erosivity. Short term data indicate an insignificant interaction (Wilk's Lambda = 0.58). The same applies to the test between subject effects. Long term data analysis results presented in section 7.3 produced a significant relationship between WDR R and rainfall amount. The short-term data produced an insignificant relationship (p = 0.057). However, the results are from short term data that may not be fully representative of the interactions. Weather parameters need to be considered for longer periods of time to establish their full signature.

On the other hand, short term data for Tshivhase follow the trend of the long-term data. Therefore, a look at the T-test results would give a clearer picture of whether the erosivity computations are similar. The pairwise comparison gives the statistical

position regarding the erosivity computations. The results of interest are those that include WDR.

The WDR-USLE erosivity are different for individual stations as well as for the combined data ($p \leq 0.05$). However, the WDR-SLEMSA erosivity are different only for Tshivhase. They are the same for Thohoyandou and combined data. The logical explanation for this should be topographic elevation. Tshivhase station is located at a higher elevation where the influence of wind speed would be strong. Therefore, the results suggest that horizontal wind speed influences erosivity. Hence, the following section uses sediments collected from splash cups to establish the erosivity models that is closer to reality.

7.4.2 Wind Driven Rain or Wind Free Rain? A comparison

Regression results have proven that there is a weak statistical correlation between rainfall amount and wind speed. Statistical computations have proven that wind speed is an important element of erosivity. It has been established that wind speed has a significant interaction with erosivity, even that computed from WFR models. Wind speed has a large effect on erosivity, depicting strong association between the two variables. Therefore, using rainfall and sediment data collected from Tshivhase and Thohoyandou stations, a comparison is done to establish the erosivity model that better represents the natural setting.

Potential erosion was calculated using USLE and SLEMSA applying rainfall data collected from Thohoyandou and Tshivhase weather stations. The erosivity for both models was substituted for the WDR R. The outcome of the results was to subtract the sediment collected by splash cups and measured. The lower the difference from the sediment sample collected, the closer to reality the method is.

Indications from data presented in Table 7.5 are that representativeness depends on wind speed. It is evident that winds accompanying rains are sufficient to significantly affect erosivity (Lyles and Allison, 1976; Stroosnijder and Gabriels, 2004a; Reis *et al.*, 2010; Erpul, 2013; Iserloh *et al.*, 2013; Marzen *et al.*, 2015; Marzen, 2017). The influence of wind speed is evident. The 24 February storm at Tshivhase indicates that wind speed is less influential at velocity below 3 m/s. This is also supported by

the historical data as well as by other scholars' findings (for example Blocken and Carmeliet, 2004; Hens, 2010; Sun and Sun, 2015; Uzun *et al.*, 2017).

Results displayed in Table 7.5 confirm the findings in section 7.3. They demonstrate that wind speed influences erosivity. This is confirmed by the comparison for Tshivhase regarding the 24 February 2021 rainfall. The wind speed is low and so is the WDR erosivity. This is because WDR influence increases with wind speed (Hens, 2010). Ultimately, USLE erosivity closely matches the collected sediment for this event.

However, as the wind speed increases, the WDR erosivity becomes the closest to the collected sediment. The WDR output at least doubles the USLE and is extremely not comparable with SLEMSA. The SLEMSA output is too low. Therefore, the observational data confirm that wind speed is important for erosivity computations. Furthermore, it is confirmed that WDR erosivity matched collected sediment more closely than WFR erosivity. Therefore, WDR is a better representative of the natural soil erosion process than the WFR, at for the 5 case studies observed here.

Table 0.5: WFR Comparison with WDR – Empirical Data

				Computed Soil Loss (g)					Computed less Collected Sediment (g)			
Date	Station	Wind Speed (m/s)	Rain (mm)	SLEMSA	USLE	SLEMSA-WDR	USLE-WDR	Collected Sediment (g)	SLEMSA - Sediment	USLE - Sediment	S-WDR - Sediment	U-WDR-Sedmient
05/02/2021	Thohoyandou	5.6	23	0.69	6.89	22.43	25.00	90.56	-89.88	-83.67	**-68.14**	**-65.56**
24/02/2021	Tshivhase	2.0	13	0.49	8.33	2.79	1.18	8.07	-7.58	**0.26**	**-5.28**	-6.89
25/02/2021	Thohoyandou	3.6	25.4	0.98	7.53	15.27	15.90	22.74	-21.77	-15.21	**-7.47**	**-6.84**
05/03/2021	Thohoyandou	3.4	31.8	0.22	5.86	11.92	9.20	16.32	-16.10	-10.46	**-4.40**	**-7.12**
05/03/2021	Tshivhase	3.0	17	0.13	12.92	17.59	17.85	15.58	-15.45	-2.66	**2.01**	**2.27**

7.5 Chapter Summary

This chapter aimed to establish the influence of wind on soil erosion. This was based on the hypothesis that the rainfall amount included in the WFR approaches accounts for the influence of the wind speed in WFR erosivity. The influence was also tested for the WDR, USLE and SLEMSA rainfall erosivity using MANOVA. The hypothesis is tested by simple linear regression, MANOVA, T-test and a direct comparison of observational data.

The regression results indicate that there is a weak statistical correlation between rainfall amount and wind speed. That the statistical relationship is weak leads to the

rejection of the null hypothesis that wind speed is accounted for by rainfall amount and allows this research to conclude that wind speed is not included in WFR erosivity. Further analysis with MANOVA established that wind speed has significant statistical interaction with erosivity in general. Wilk's Lambda confirmed the strong association between wind speed and erosivity.

Tests between subject effects revealed that wind speed has a statistically insignificant effect on erosivity computed through the SLEMSA and USLE models. This further supports the rejection of the null hypothesis that the wind speed is accounted for by rainfall amount. This is followed the Bonferroni post hoc test (the t-test) to compare if WDR and WFR erosivity, through USLE and SLEMSA, are similar. The results confirm differences. The differences are further supported by observational data collected from The University of Venda Experimental Farm and Tshivhase Tea Estate.

The soil loss computed from the models was compared with that from the collected sediment observations. Two computations were done. One using the conventional WFR model and the other where the erosivity value was replaced with the WDR erosivity value. Results indicated that WFR and WDR erosivity are different. Wind Driven Rain computations where wind is above 2 m/s produced results more closely aligned to collected sediments. Therefore, for the 2 stations of the Soutpansberg examined here, the WDR erosivity represents reality better than WFR. However, the results may need further interrogation using more stations and a longer period of observation.

Date	Station	Wind Speed (m/s)	Rain (mm)	SLEMSA	USLE	SLEMSA-WDR	USLE-WDR	Coll Sed (g)
05/02/2021	Thohoyandou	5.6	23	0.69	10.37	25.81	159.74	90.5
24/02/2021	Tshivhase	2.0	13	0.49	11.93	90.80	4.27	8.07

25/02/2021	Thohoyandou	3.6	25.4	0.98	11.45	80.76	41.66	22.7
05/03/2021	Thohoyandou	3.4	31.8	0.22	14.34	11.71	51.77	16.3
05/03/2021	Tshivhase	3.0	17	0.27	15.60	20.45	23.18	15.5

: SYNTHESIS, CONCLUSION AND RECOMMENDATIONS

8.1 Introduction

Soil erosion remains a critical and widespread challenge in the majority of developing countries (Food and Agiculture Organisation, 2015; Borrelli *et al.*, 2017). Global population growth has increased pressure on land for food production. This has put more marginal lands under cultivation, the result of which is an increased threat of soil erosion (Borrelli *et al.*, 2017; Marzen, 2017).

Soil erosion is a natural geomorphic surface process that removes soil and regolith from their primary location on the Earth's crust. Natural agents, primarily water and wind, do the removal. The removal upsets the ecosystem balance and functions. All life on earth directly and or indirectly depends on the soil. Hence, the health status of the soil component of the ecosystem is of paramount importance to organism survival. Consequently, this compels scientists to research and explain soil erosion processes.

Natural processes are always embedded in all erosion processes (Dotterweich, 2013; Zorn and Komac, 2013). This research approached soil erosion from a natural process point of view because soil erosion is a natural process (Borrelli *et al.*, 2017). Therefore, the aim of this research has been to analyse soil erodibility and rainfall erosivity on the Soutpansberg range to establish the characteristics of the varous factors that influence soil erosion.

The aim of the research was based on two hypotheses. The first null hypothesis was that rainfall erosivity is a not function of rainfall only. Its alternative hypotheses are that elevation and wind speed increase rainfall erosivity. The tests of the effect of elevation and wind speed were performed separately which is why they are treated as two alternative hypotheses for the same null hypothesis.

The second null hypothesis was that rainfall total amount accounts for wind speed in wind free rain (WFR) erosivity computations. The alternative hypothesis was that rainfall total amount and wind speed are independent of each other. The hypotheses are based on the two soil erosion models considered for this research.

The models are the Universal Soil Loss Equation (USLE) (Wischmeier and Smith, 1958) and Soil Loss Estimation Model for Southern Africa (SLEMSA) (Stocking *et al.*, 1988), respectively. The models base soil loss estimation on two important factors – soil erodibility and rainfall erosivity (Stocking *et al.*, 1988; Renard *et al.*, 1997; Kinnell, 2010). Soil erodibility is based on both intrinsic and extrinsic soil characteristics. Rainfall erosivity is based on the rainfall intensity, the storm energy (USLE) or kinetic energy, and the mean annual precipitation (SLEMSA). Achieving the following specific objectives allowed for the assessment of the two hypotheses.

The first objective was to classify geomorphic features of the Soutpansberg range. The classification illustrated the erodibility characteristics on the mountain range. The second objective was to characterise the spatial-temporal aspects of potentially erosive rainfall on the Soutpansberg range. The purpose was to reveal the distribution of rainfall risk on the mountain range. The third objective was to assess the influence of topography on wind speed and rainfall erosivity on the mountain range. The final objective was to compare the Universal Soil Loss Equation (USLE) and the Soil Loss Estimation Model for Southern Africa (SLEMSA) rainfall erosivity incorporating wind driven rain (WDR) erosivity to establish the influence of wind on soil erosion. The following section presents the results of the analyses of each objective and hypotheses tests.

8.2 Synthesis

8.2.1 Soil Erodibility on the Soutpansberg Range

A deep comprehension of the components and factors controlling soil erodibility is the foundation of effective erosion control. Such a grasp is achievable through analysis and simplification of the components and factors controlling soil erodibility. That is what the first objective of this research intended to achieve. The result is an illustration of the erosion risk associated with the Soutpansberg mountain range from the soil perspective.

The determinants of soil erodibility guided the data needed to achieve this objective. The two selected soil erosion models, USLE and SLEMSA, are the guiding lights to the factors affecting soil erodibility. The factors that play a controlling role in soil

erosion include rainfall erosivity (R), vegetation cover management factor (C), soil erodibility (K), slope length and steepness (LS), and conservation practices (P) (Wischmeier and Smith, 1958; Stocking, 1980; Renard *et al.*, 1997; O'geen, 2006; Irvem *et al.*, 2007). However, soil erosion is principally determined by rainfall erosivity (R) and soil erodibility (K) (Renard *et al.*, 1997; Kinnell, 2010). Erosivity explains about 80% of variations in erosion (Wischmeier and Smith, 1958). It is the primary driver of erosion with considerable influence from erodibility (Yao *et al.*, 2016). Soil erodibility plays a significant role in determining soil particle detachability (O'geen, 2006; Kusumandari, 2014; Uzun *et al.*, 2017) and represents the effect of soil characteristics and properties on soil erosion (Renard *et al.*, 1997).

The soil erodibility characteristics may be intrinsic or extrinsic. Intrinsic characteristics are innate in the soil, such as grain size. Extrinsic characteristics are the other factors that interact with the soil, such as water, and cause erosion. Therefore, the illustration of soil erodibility on the Soutpansberg range covers both intrinsic as well as extrinsic soil characteristics. The factors used for the geomorphological classification were adapted from SLEMSA and USLE. The result is the GIS based geomorphic classification using five factors representing different aspects of erodibility.

The five factors are soil erodibility, slope, hydrography, land use-land cover and geology. Hydrography was adapted water systems to represent the erosivity factor as indicated by runoff. Slope represents the angle and length. Land use- land cover represented crop practices and vegetation cover and management. Geology emanates from its role in soil formation, vertical ground water movement and slope types.

Different sources provided data for each specific objective. Soil data were obtained from the Harmonised World Soil Database (HWSD v 1.21) layer downloaded from The International Institute for Applied Systems Analysis (IIASA) online database. Additional soil data were obtained from field samples and splash cups. Hydrological data were downloaded from Department of Water Affairs, Forestry and Fisheries (DWAFF). Further data were derived from the DEM. Slope data were derived from

the 30m pixel size SRTM DEM obtained from National Geo-Spatial Information (NGI). The derivations were done in SAGA GIS.

Geological data were downloaded from South African Geosciences online database. Land-use-land-cover were extracted from the South African National Land Cover 2018 dataset accessed online on the Department of Forestry, Fisheries and Environment website. Rainfall and wind speed data were obtained from the South African Weather Services. The data record covered the years from 2000 to 2019.

Except for geology and land-use-land cover factors, data processing and analysis for geomorphic classification followed three stages of GIS analysis as guided by Najwer and Zwoliński (2014) and Zwoliński *et al.* (2019). The first stage of the GIS analysis was the geo-computation and extraction of factor indicator elements from the data source. The geo-computation and extraction included creating the various indicator element field on the attribute table of the various factor maps.

The second stage was the normalisation of each factor indicator element into five classes using Jenk's Natural Breaks. Except for slopes that were derived from a DEM and produced as a raster layer, normalization began with rasterising the factor map using the factor indicator element as the rasterization field. Automatic classification means that the indicator field was geo-computed. Expert classification indicates that the indicator field was created from expert knowledge. The second stage of the GIS analysis produced the factor maps for slope position, landform position, geological setting, soil detachability and erosion exposure.

The third stage of the GIS analysis was the weighting and overlaying of the factor maps to create a final soil erodibility map. The Multi-Criteria Evaluation (MCE) using the Analytic Hierarchy Process (AHP) weighed the relative contribution of each factor. The online MCE using pairwise comparisons. The overlay was done using the raster calculator in ArcGIS.

ArcGIS and SAGA GIS tools were used in the analysis. Most computations were done in ArcGIS. River slopes were computed using the 3D Analyst Functional Surface Tool. Drainage density was produced through the Line to density tool. The Raster Calculator was used for weighted sum overlay of factor maps. The Reclass

tool was used for normalisation to five classes employing Jenks Natural Breaks. In addition, SAGA GIS Wetness Index and TPI tools were also used.

The results produced six factor maps and two erodibility maps, one for USLE and another for SLEMSA. An additional soil type distribution map was produced. The soil distribution map indicates that the mountain range has fourteen soil types belonging to five texture classes. Leptosols, Acrisols, Lixisols and Luvisols are the common soil types of the Soutpansberg range. Leptosols occupy 54% of the range occur in the high elevation areas, above 1200 m.a.s.l. Acrisols occupy 12 % while Lixisols cover 10%. Luvisols cover just over 7%. Acrisols occupy areas between 800 and 1200 m.a.m.s.l. Lixisols and Luvisols occupy areas falling below 600 m.a.s.l. Clay loam is the most common soil texture. Clay loam occupies 56% while sandy clay loam occupies 27%. Sandy Loam is found in 10% of the range, while clay occupies 5% and sand occupies only 2% of the range.

The intrinsic erodibility results present the USLE and SLEMSA erodibility computations for each polygon as well as maps. The numerical results from both USLE and SLEMSA computations indicate generally low erodibility. Few polygons indicate different values. However, Jenks Natural Breaks show significant differences as depicted in the erodibility maps. The impacts of the inclusion of rainfall amount in the SLEMSA formula becomes apparent as the whole western wing of the range has very low SLEMSA erodibility. The western wing of the range is very dry. USLE classified very negligible portions of the whole range as very low erodibility.

In general terms, discounting the western wing of the range (Figure 8.1), there is no major difference between the SLEMSA and the USLE very high and low erodibility classes. Major differences emerge on the low and moderate erodibility classes. While USLE classifies most north facing slopes as mostly moderate, SLEMSA codes them as mostly low erodibility areas. The north facing slopes are dry and, therefore, have low SLEMSA erodibility potential. The interplay of the intrinsic erodibility and extrinsic factors produce the overall erodibility condition of the mountain range.

The extrinsic factors examined are erosion exposure, geological setting, slope position and landform position. These were derived from land use – land cover, geology, slopes and hydrography, respectively. Erosion exposure represents how

the land surface is exposed and susceptible to the impacts of raindrops. The exposure is determined by land use and land cover characteristics. Rocks influence the vertical movement of water hence affect overland flow. Slope position gradient determines overland flow energy (Ban *et al.*, 2020). The landform position is determined by the hydrography through defining areas where water tends to accumulate.

The Multi-Criteria Evaluation (MCE) using the Analytic Hierarchy Process (AHP) ranked the five factors. This is a pairwise comparison of each factor. The factor weighting shows the dominance of intrinsic soil erodibility and rain exposure in determining soil erodibility. Conversely, landform position and geology carry the least weight, respectively. The weighting was important in overlaying the layers using the weighted sum tool in ArcGIS to produce the final erodibility map of the Soutpansberg range.

Two final erodibility maps were produced – one using USLE erodibility and the other from SLEMSA. Therefore, the final erodibility maps indicate the influence of SLEMSA and USLE based erodibility computations. The major difference between the maps is in the distribution of very low erodibility characteristics. The USLE based final map shows minute areas on very low erodibility. The SLEMSA generated one has the large part of the western region of the mountain classified as very low erodibility (Figure 8.1).

Another major difference in the final erodibility maps is on the north facing slopes in the eastern region of the mountain. The SLEMSA map classifies many places as low erodibility, while the USLE low erodibility is more pronounced in elevations above 1000 m.a.s.l. The differences embedded in the intrinsic erodibility are made manifest in the final erodibility map.

There are some similarities between the USLE and SLEMSA maps too. Both maps show high to very high detachability in the south facing slopes in areas including Thohoyandou, Tshakhuma, Tshivhase and Phiphidi areas. The belt stretches eastwards to Makonde and Begwa. Another belt of high to very high erodibility is found along Nzhelele River from Siloam westwards to a pass just after Dzanani. From the pass, the belt stretches westwards. The places have clay (Rhodic Nitisols)

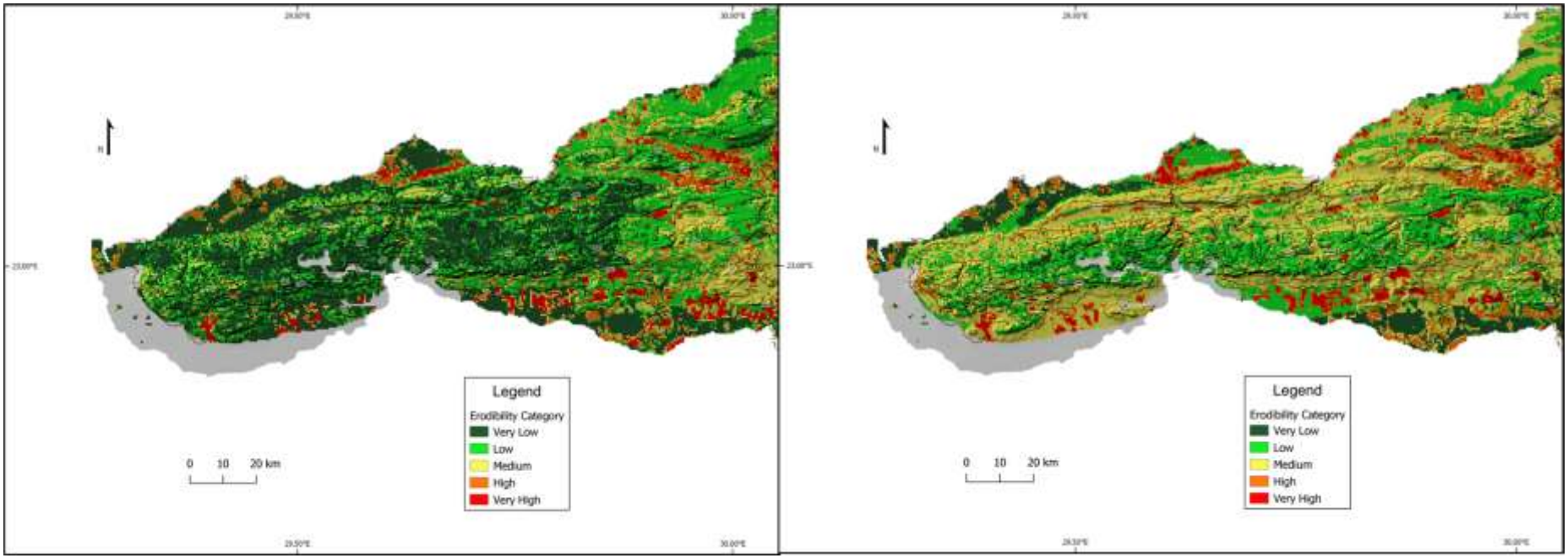

Figure 0.1: Western Region of Soutpansberg. Left – SLEMSA. Right – USLE

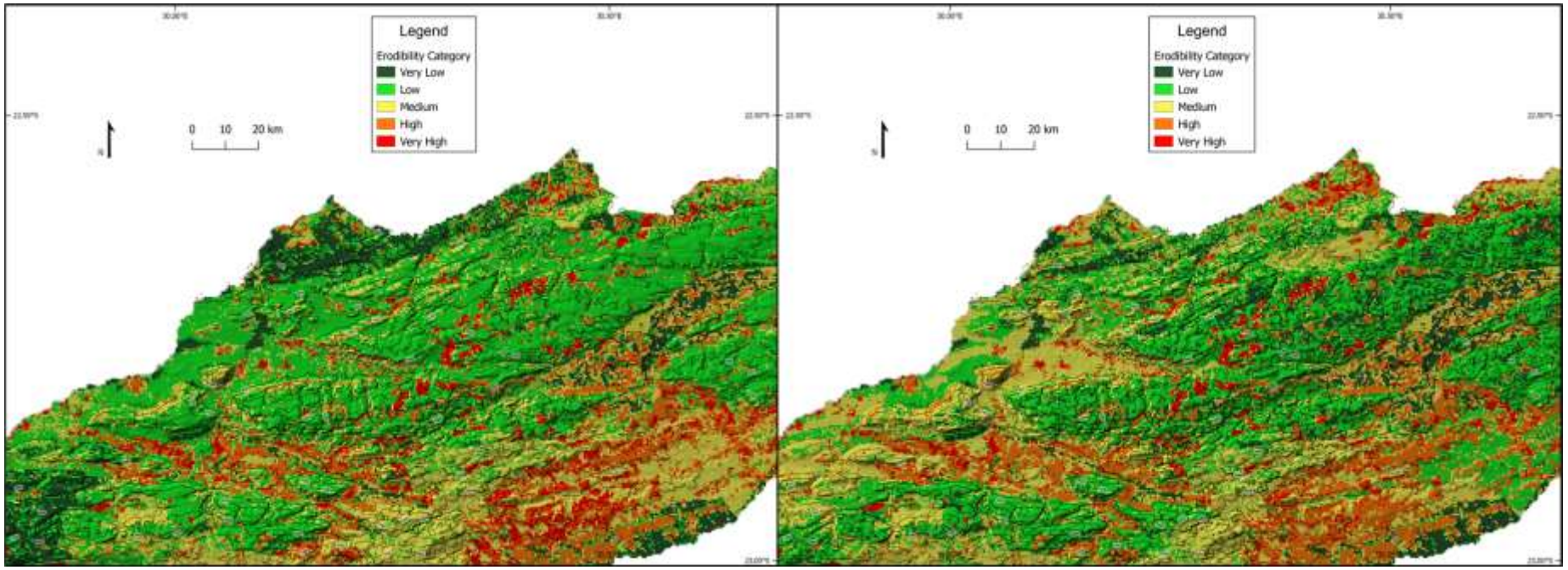

Figure 0.2: North Facing Slopes of Soutpansberg. Left – SLEMSA. Right – USLE

and sand clay loam (Haplic Acrisols and Calcaric Cambisols). That gives the summary of soil erodibility on the Soutpansberg mountain. The following section summarises potentially erosive rain spatial-temporal characteristics.

8.2.2 Soutpansberg Range Potentially Erosive Rain Spatial-temporal Characteristics

The second specific objective of the research is to characterise the spatio-temporal aspects of rainfall to reveal the distribution of rainfall erosive potential on the mountain range. Forty-five stations, some ~30 km out of the mountain range's physical boundary, are used for the research. Five stations, namely Mara, Levubu, Thohoyandou, Tshivhase and Punda Maria, are fully automatic weather stations and record wind as well.

Rainfall data are considered at monthly and at storm timescales. The first part dealt with monthly and annual spatial characteristics while the second part focused on erosive rainstorm spatial-temporal characteristics. This distinction is necessary because only five weather stations could provide rainstorm event data.

Therefore, event analyses were limited to the five stations while monthly and annual analyses covered the whole mountain range. Ordinary co-kriging was used for the spatial interpolation of monthly rainfall. Co-kriging catered for the relationship between potentially erosive rainfall and the landscape on the mountain range. Spatial interpolation generates an estimated surface from a scattered set of points (Gu *et al.*, 2019). Temporal distribution is depicted by the monthly, quarterly and annual averages derived from daily totals over the 20-year period.

Spatial autocorrelation or dependency was indicated by variography created from semi variance (Burgess and Webster, 1980; Paramasivam and Venkatramanan, 2019). Semi variance indicates distance decay. It shows how data are similar or different over space. As distance increases between points, semi variance increases until a point where there is no semi variance. The range, sill and nugget of the semi variogram indicate spatial autocorrelation.

The ratio of nugget to sill indicates the spatial dependency of variables (Al-Omran *et al.*, 2013). There are three classes used for model explanation (Tadayon and Rasekh, 2019). If the ratio is less than 25 %, it shows strong spatial dependence; if the ratio is between 25 and 75 %, it indicates moderate spatial dependence; and if the ratio is more than 75 %, it represents weak spatial dependence.

In addition, hotspot analysis was adopted to indicate the number of rain days each weather station recorded. This is important for identification of potential flash flood prone areas. A station recording high potentially erosive rain in a few days has the potential for flash flood erosion. Such information is critical for soil erosion planning and management. Erosion planning also needs spatial variability information.

A fusion of the Coefficient of Variation (CV) and the Global Moran's I (Zhang and Han, 2017) is employed to indicate spatial variability in 383 erosive storms recorded from five stations as well as for the whole mountain range. The mountain range analyses cater for both rainfall total amount and rain days. Therefore, spatial variability assessment was done for monthly, quarterly, annual and event rainfall. It was also conducted for erosive days and wind. While the monthly, quarterly, annual rainfall and potentially erosive days covered the whole mountain range, event analyses covered the five stations only.

Spatial variability represents the relationship between rainfall figures recorded by nearby stations in terms of clustering or dispersion. It incorporates the influence of topography in the variability. The variability is described as either simple, medium or complex. A simple variability is one where high values cluster, and they are close to the mean. This means the variability is explainable by changes in space as calculated by Moran's I. A medium spatial variability is where high values cluster but are dispersed from the mean. Clustering of low values that are close to the mean is also medium spatial variability. Medium variability has a balance of space and non-space factors controlling rainfall distribution. Clustering of high rainfall values that are dispersed from the mean shows complex spatial variation. Complex variation cannot be explained by space only. Other factors would be at play in the rainfall distribution. The following is the summary of results of the spatial temporal analysis of potentially

erosive rainfall on the Soutpansberg range. The presentation is divided into spatial-temporal distribution and spatial-temporal variability.

8.2.2.1 Rainfall Spatial-temporal Distribution

The first part is spatial temporal interpolation using co-kriging. This is to show spatial autocorrelation or dependency. This is indicated by the variography. The variography results return an inconclusive spatial temporal situation. July and November are the only moths indicating strong spatial dependency. The spatial dependency is also supported by the variography range that falls within the 30 km WMO (2008) meso-meteorological network density standards.

However, January, April and May show weak spatial dependency. A variography range above the 30 km sphere of influence supports the April and May outcomes. However, the January scenario is not supported by its variography range. The variography range for January is within the 30 km sphere of influence. Furthermore, November is the only month in the rainy season that returned strong spatial autocorrelation. Its range is also below 30 km.

Nonetheless, overall, nine months of the year receive rainfall that has spatial dependency. January, April, May and September have a spatial dependency ratio above 75% that indicates weak spatial dependency. April, May, August and September have ranges above 30 km while the range for December is just 0.721 km above the meso-meteorological network density standards. April, May and August have both weak spatial dependency and ranges above 30 km. Hence, it is concluded that topography plays a role in rainfall distribution on the Soutpansberg range. This largely agrees with other researchers (Kabanda, 2003; 2004; Kephe *et al.*, 2016; Rapolaki *et al.*, 2019) that observed the influence of topography on rainfall distribution.

The spatial dependency is more apparent on visual representation. The JFM rainfall distribution shows that high and very high erosive rainfall potential is concentrated in the central south facing slopes of the mountain range. The highest rainfall is found in areas above 1200 m.a.s.l. However, the western wing records the lowest rainfall despite the highest elevation of the mountain range being resident there. This is an

indication of the orographic effect of the mountain range on the south-eastern winds that dominate the area.

The distribution of rain days tells another story. Except for Tshakhuma, Folonhondwe and Dzanani stations are outside the high and very high potentially erosive rain zones. All the stations fall below 1000 m.a.s.l. However, Tshakhuma station is in the windward side of the mountain range. Folonhondwe and Dzanani are in the rain shadow zone. This is an indication that erosion hazard is not limited to high rainfall areas only.

The same rainfall spatial pattern is also exhibited by the AMJ quarter. Rainfall in both April and May indicate weak spatial dependency with spatial ranges of 122 and 47 km, respectively. The high rainfall zone extends north and east. The low rainfall zone significantly extends west. The rain days' hotspots remain in Tshakhuma, Dzanani and Folonondwe, with the addition of Waterpoort weather station.

The JAS spatial distribution sees a large shrinking of the very high rainfall zone. However, it remains in the same location around Tshivhase and Matiwa high elevation areas in the central areas of the south facing slope. The high rainfall region extends northeast. The three months of this quarter have strong, moderate and weak spatial dependency, respectively. Mara joins Folonhondwe and Dzanani in the rain days' hotspot category. Folonhondwe and Mara fall in the very low rainfall category while Dzanani falls into the low rainfall category for this quarter.

The last quarter of the year indicates that November has strong, while October and December have moderate spatial dependency. The very high potentially erosive rain expands slightly from the JAS period. The high and moderate rainfall zones decrease from the northern extend. The high rainfall region extends eastwards while the medium and low rainfall zones shrink from the western side. The very low region then extends eastwards on the northern edge. Rambuda station joins Folonhondwe, Tshakhuma, Waterpoort and Dzanani in the rain days' hotspots group.

The final annual rainfall distribution map indicates the general characteristics of rainfall erosive potential distribution on the Soutpansberg range. It shows the dominance of the first quarter that contributes 49.5% of all erosive potential on the

range. The fourth quarter contributes 28 %. The second and third quarters contribute 14 and 8 %, respectively. Therefore, the rainfall spatial distribution maintains the very high rainfall core fixed in the high elevation areas around Tshivhase, Matiwa and Entabeni in the central south facing slopes of the range (Figure 8.3). The high rainfall zone radiates to the east from the very high rainfall zone. The low rainfall zone touches the periphery of the mountain from the eastern parts creating a ring on the northern edge. The northern low rainfall ring expands southward as it covers Dzanani in the central interior of the mountain range. It touches the southern edge south of Roodewal and then it then extends westwards covering a large part of the range from the east. The rest of the western wing is a region of very low rainfall

Four stations are flagged as rain days' hotspots. The stations are Folonhondwe, Dzanani, Waterpoort and Tshakhuma. Important to note is that Folonhondwe and Dzanani fall in the low rainfall zone. Waterpoort is in the very low rainfall zone. Tshakhuma falls in the high rainfall zone. This indicates places with high flash flood potential. Further characterisation is done using the CV and Moran's I. The following section presents a summary of these results.

8.2.2.2 Rainfall Spatial-temporal Variability

Spatial-temporal variability analysis is conducted using the Coefficient of Variation (CV) and Moran's I. The spatial variability is done for both the whole mountain range and the 383 erosive storms recorded at the five weather stations over the 20 year period. The mountain range analyses cater for both rainfall and rain days. Spatial temporal variability is classified as simple, moderate or complicated (Zhang and Han, 2017).

Hourly erosive storms spatial-temporal variability considered 383 erosive storms recorded at Punda Maria, Mara, Thohoyandou, Tshivhase and Levubu weather stations. Analysis results show that 53% of the erosive storms over the period had simple spatial temporal variability which is an indicator of the significant influence of topography on rainfall spatial distribution. Spatially complex storms, where factors other than topography play a role in rainfall spatial distribution, constituted 26% while the rest were moderate storms. This suggests the influence of factors such as

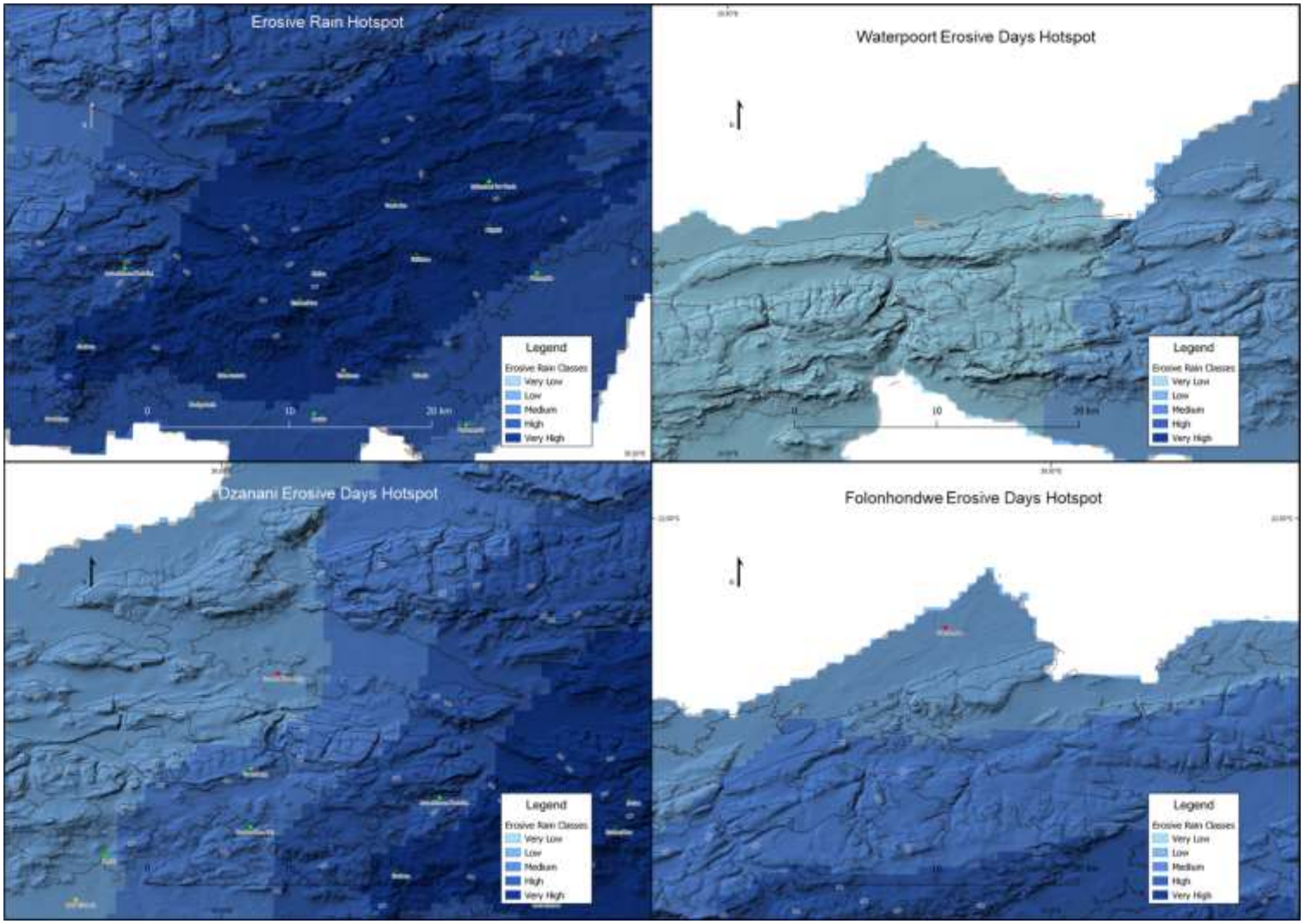

Figure 0.3: Erosivity Hotspots

tropical-temperate troughs, tropical lows, cut-off lows and tropical cyclones (Kundu et al., 2015; Dedekind et al., 2016) on about a quarter of rainstorms recorded during the period under review.

Most complex storms were recorded at Thohoyandou station probably because of the urban heat island as well as Nandoni Dam effect on rainfall in the area. Levubu station recorded one complex storm that became the most complex storm of the period under review.

Monthly potentially erosive rainfall and rain days spatial-temporal variability considered monthly rainfall to compute CV and Moran's I for the forty-five stations over the period under review. The JFM analysis shows that simple rainfall variability constituted 38% while medium and complex variability constituted 36% and 26%, respectively. This implies that there is no clear dominance of either topography or outside factors on rainfall spatial distribution during the JFM quarter. Medium rain days' variability constituted 42% while simple and complex variability constituted 31% and 27%, respectively. A simplistic view shows that the rainfall variability and rain days' variability patterns do not correlate for JFM. However, further analysis shows a correlation between rainfall and rain days' variability.

The AMJ quarter is characterised by a wet April and dry May and June. Simple variability constitutes 60% of the rainfall recorded during the period under review suggesting the strong influence of topography on rainfall spatial distribution. Medium and complex variability constituted 20% each. On the other hand, rain days were moderately variable (50%) with a bias towards complexity (30%) suggesting a slight dominance of other factors of rainfall distribution.

The third quarter is a typical dry period of the climatic region. However, some stations still recorded potentially erosive rainfall. About 40% of the rainfall received during this quarter had simple variability suggesting the impact of topographical relief on rainfall distribution. Complex and medium variability are not far apart at 31% and 29%, respectively. On the other hand, simple variability constituted 20% rain days. Moderate variability had the majority at 50% while complex variability had 30% suggesting a balance between topography and external forces.

The simple variability dominates both rainfall distribution and rain days during the OND quarter. Analysis shows that 51% and 29% of both rainfall and rain days' variability was simple and moderate, respectively, suggesting the influence of topography on rainfall distribution. Complex variability constituted 20% only.

The annual spatial variability therefore depicts different variability characteristics. Rainfall variability is predominantly simple while rain days' variability splits between moderate and complex variability. The general rainfall variability on the mountain range can safely be described as simple which means that the topography plays a major role in rainfall distribution. On the other hand, the low rain days' simple variability indicates the inferior contribution of topography to rainfall variability and highlights the role of other factors to the rainfall variability. No station that experienced extremely complex rainfall variability also experienced the same complexity on rainy days. While all four stations with extremely complex rainfall variability are at a high elevation, the stations with extremely complex rainy days include three from very low elevation areas. This means that the variability of total rainfall and rainy of days do not correlate. While the rainfall spatial distribution is influenced by topography, the rainy days distribution has nothing to do with topography.

It is important to note that rainy days' hotspots are in low and very low rainfall areas. It is also important to note that the rainy days' hotspots fall in high and very high erodibility zones. This indicates that erosion hazard planning should not focus on high rainfall zones only. Waterpoort, Dzanani and Folonhondwe fall in the low rainfall zones but in high erodibility zones. That makes the areas very high erosion risk zones. This now leads to the influence of topography on wind speed and rainfall erosivity.

8.2.3 The Influence of Topography on Wind Speed and Rainfall Erosivity

The third specific objective was to assess the influence of topography on wind speed and rainfall erosivity. The section is in two parts – one focusing on the influence of topography on horizontal wind speed and the other on rainfall erosivity. The focus was on 383 erosive storms recorded from 2000 to 2019 at five weather stations: Levubu, Mara, Punda Maria, Thohoyandou and Tshivhase.

Horizontal winds are classified into calm (<1.5 m/s^{-1}), light (1.6 and 3.0 m/s^{-1}), moderate (3.1 and 4.5 m/s^{-1}), strong (4.6 to 6 m/s^{-1}) and very strong (>6 m/s^{-1}) winds. Results indicate that 44% of the winds during the period under review were light. Thohoyandou station, at 614 m.a.s.l., recorded the strongest winds, stronger than those at Tshivhase station which is at the highest elevation of 976 m.a.m.s.l. While this hints at elevation not influencing wind speed, a closer scrutiny of wind speeds and elevation indicates otherwise.

Levubu and Punda Maria stations are located at a very low elevation (706 and 457 m.a.s.l., respectively). Punda Maria station recorded neither strong nor very strong winds. Levubu station recorded just 2% strong winds and no very strong winds. On the other hand, Mara (914 m.a.s.l.) and Tshivhase (976 m.a.s.l.) stations both recorded strong and very strong winds. The highest speeds at Levubu and Punda Maria were 4.7m/s^{-1} and 3.6m/s^{-1}, respectively. Tshivhase and Mara recorded highest wind speeds of 6.9m/s^{-1} and 7.1m/s^{-1}, respectively. This clearly indicates that wind speed increases with elevation in this small sample of 5 stations on the Soutpansberg range.

A simple linear regression proved that elevation increases rainfall erosivity. This links back to the rainfall spatial distribution and dependency analysis. It was found that the rainfall distribution has spatial dependency, that is, it is influenced by topography. Considering that SLEMSA and USLE erosivity are direct products of rainfall amounts, this makes sense. Therefore, the focus now turns to the influence of wind speed on rainfall erosivity.

8.2.4. The Influence of Wind Speed on Rainfall Erosivity

The fourth objective of the research is to establish the influence of wind speed on rainfall erosivity. The basis for this objective is that the omission of wind speed in the WFR calculations is a fundamental oversight and misrepresentation of the natural setting. Therefore, the starting point is to establish the co-occurrence of rainfall and wind. The influence of wind speed followed and is established through comparing USLE, SLEMSA and WDR erosivity with collected sediments.

The difference between the different erosivity values was assessed through MANOVA. The rainfall amount is the independent variable in the linear regression. Erosivity is the dependent variable, while wind speed and rainfall amount are the independent variables for MANOVA. The MANOVA analysis demonstrated a strong statistical relationship between horizontal wind speed and rainfall erosivity. The Bonferroni post hoc test (t-test) proved that wind free rain (WFR) and wind driven rain (WDR) erosivity are different. Empirical data obtained from observations made in the Soutpansberg region supported the statistical results, although the number of observations made in the field were for only 2 stations and 5 storms, and thus comprise a very small dataset. Erosivity computed using the WDR with wind above $2m/s^{-1}$ produced estimations that are closer to the sediments collected from splash cups. Therefore, the empirical results support the statistical implications that WDR erosivity is different from WFR erosivity and that WDR erosivity represents reality better. Therefore, the research makes following conclusions.

8.3 Conclusion and Contribution to Knowledge

The goal of the research was to analyse soil erodibility and rainfall erosivity on the Soutpansberg range. The analysis was based on four objectives aimed at establishing the characteristics of the factors that influence soil erosion. Soil erodibility and rainfall erosivity are the variables of choice because they are the basis on which soil erosion models are based (Renard *et al.*, 1997; Kinnell, 2010). Thus, the four objectives are to:

1. classify geomorphic features of the Soutpansberg range to illustrate the erodibility characteristics on the mountain;
2. characterise the spatial-temporal aspects of potentially erosive rainfall to reveal the distribution of rainfall erosion risk on the mountain range;
3. assess the influence of topography on
    a. wind speed and
    b. rainfall erosivity to establish the effect of topography on wind speed and erosivity;

4. compare rainfall erosivity derived from the USLE and the SLEMSA incorporating WDR erosivity to establish the influence of wind on rainfall erosivity.

The following conclusions and contributions are made:

1. There are fourteen different soil types on the Soutpansberg range. The soils' intrinsic characteristics and raindrop exposure (represented by land use and land cover) are the most influential soil erodibility factors on the mountain range. The intrinsic soil characteristics are the major difference between USLE and SLEMSA erodibility. The major difference is brought by the inclusion of rainfall kinetic energy in the SLEMSA. That results in the SLEMSA classification of the western wing of the mountain range as predominantly very low. The USLE classification returns a mix of different erodibility categories in the same region. However, the overall erodibility spatial characteristics are not very different between the SLEMSA and USLE models. Medium and low erodibility dominate both SLEMSA and USLE classifications.
2. (Wischmeier and Smith (1958)), the proponents of the USLE, present that erosivity accounts for approximately 80% of variations in soil loss. This research concludes from Multi-Criteria Evaluation (MCE) using the Analytic Hierarchy Process (AHP) that intrinsic soil characteristics and land-use-land-cover are the highest, each explains about 36% of variation in soil loss.
3. Rainfall erosive potential spatial variability is influenced by topography. It was demonstrated that the rainfall distribution has spatial dependency. As such, high potentially erosive rainfall is concentrated on the central south facing slopes at elevations above 1000 m.a.s.l. The very low potentially erosive rain zone is in the western region despite the existence of highest elevation there. This scenario reinforces the influence of topography on rainfall distribution as the orographic effect makes the highest elevation on the mountain lie in a rain shadow zone. Waterpoort, Mara, Dzanani, Folonhondwe and Rambuda are rain days' hotspots during one period of the year or another. This means that the areas are erosion hazard zones. This is despite their location in the very low rainfall zone.

4. Topography increases both wind speed and rainfall erosivity. Rainfall erosivity is not a function of rainfall amount only.
5. Rainfall amount and wind speed are correlated suggestion co-occurrence. Wind speed is correlated with rainfall erosivity. Wind speeds above $2m/s^{-1}$ increases rainfall erosivity. Wind driven rain (WDR) erosivity is a better representation of rainfall energy than wind free rain (WFR) in the Soutpansberg region. Therefore exclusion of wind speed in WFR erosivity is a misrepresentation of the natural setting.

8.4 Recommendations

From the conclusions, the following recommendations are made:

1. This study only utilized 5 automated stations in its analysis. This may significantly impact the statistical analyses and assessments made in this study. Further studies on rainfall spatial distribution need to be done using satellite based rainfall data which cover more extensive regions.
2. Further research on rainfall erosivity considering the rainfall temporal distribution is necessary to identify erosion hazard zones.
3. Further research on incorporating the influence of wind speed in the computation of rainfall erosivity may improve soil erosion estimation models.

REFERENCES

Adhikary, S. K., Muttil, N. and Yilmaz, A. G., 2017. Cokriging for Enhanced Spatial Interpolation of Rainfall in Two Australian Catchments. *Hydrological Processes,* 31(12), pp. 2143-2161.

Al-Omran, A., Al-Wabel, M., El-Maghraby, S., Nadeem, M. and Al-Sharani, S., 2013. Spatial Variability for Some Properties of the Wastewater Irrigated Soils. *Journal of the Saudi Society of Agricultural Sciences,* 12(2), pp. 167-175.

Araujo, A. M. and Pereira, D. Í., 2018. A New Methodological Contribution for the Geodiversity Assessment: Applicability to Ceará State (Brazil). *Geoheritage,* 10(4), pp. 591-605.

Aronow, S., 1982. Shoreline Development Ratio. *Beaches and Coastal Geology, Springer US*, pp. 754-755.

Arsyad, S., 2010. Soil and Water Conservation. *Bogor.[Indonesian]*.

Avwunudiogba, A. and Hudson, P. F., 2014. A Review of Soil Erosion Models with Special Reference to the Needs of Humid Tropical Mountainous Environments. *European Journal of Sustainable Development,* 3(4), pp. 299-310.

Baade, J., Franz, S. and Reichel, A., 2012. Reservoir Siltation and Sediment Yield in the Kruger National Park, South Africa: A First Assessment. *Land degradation & development,* 23(6), pp. 586-600.

Bagalwa, R., Chartin, C., Baumgartner, S., Mercier, S., Syauswa, M., Samba, V., Zabona, M., Karume, K., Cizungu, N. and Barthel, M., 2021. Spatial and Seasonal Patterns of Rainfall Erosivity in the Lake Kivu Region: Insights from a Meteorological Observatory Network. *Progress in Physical Geography: Earth and Environment,* 45(6), pp. 866-884.

Ban, Y., Wang, W. and Lei, T., 2020. Measurement of Rill and Ephemeral Gully Flow Velocities and Their Model Expression Affected by Flow Rate and Slope Gradient. *Journal of Hydrology,* 589, pp. 125172.

Banta, R. and Cotton, W. R., 1981. An Analysis of the Structure of Local Wind Systems in a Broad Mountain Basin. *Journal of Applied Meteorology,* 20(11), pp. 155-1266.

Barry, R. G., 2008. *Mountain Weather and Climate.* 3rd edn. Cambridge: Cambridge University Press.

Batjes, N. H., Ribeiro, E. and Van Oostrum, A., 2020. Standardised Soil Profile Data to Support Global Mapping and Modelling (Wosis Snapshot 2019). *Earth System Science Data,* 12(1), pp. 299-320.

Beasley, D., Huggins, L. and Monke, a., 1980. Answers: A Model for Watershed Planning. *Transactions of the ASAE,* 23(4), pp. 938-0944.

Benavidez, R., Jackson, B., Maxwell, D. and Norton, K., 2018. A Review of the (Revised) Universal Soil Loss Equation ((R) Usle): With a View to Increasing Its Global Applicability and Improving Soil Loss Estimates. *Hydrology and Earth System Sciences,* 22(11), pp. 6059-6086.

Beniston, M., 2003. Climatic Change in Mountain Regions: A Review of Possible Impacts. In Diaz, H. F. (ed.) *Climate Variability and Change in High Elevation Regions: Past, Present & Future: Vol. 15 Advances in Global Change Research*. Amsterdam: Springer, pp. 5-31.

Berger, K., Crafford, J., Gaigher, I., Gaigher, M., Hahn, N. and Macdonald, I. (eds.), 2003. *A First Synthesis of the Environmental, Biological and Cultural Assets of the Soutpansberg*. Leach Printers & Signs, Louis Trichardt, South Africa.

Bijleveld, A. I., van Gils, J. A., van der Meer, J., Dekinga, A., Kraan, C., van der Veer, H. W. and Piersma, T., 2012. Designing a Benthic Monitoring Programme with Multiple Conflicting Objectives. *Methods in Ecology and Evolution,* 3(3), pp. 526-536.

Blanco-Pastor, J. L., Fernández-Mazuecos, M., Coello, A. J., Pastor, J. and Vargas, P., 2019. Topography Explains the Distribution of Genetic Diversity in One of the Most Fragile European Hotspots. *Diversity and Distributions,* 25(1), pp. 74-89.

Blocken, B. and Carmeliet, J., 2004. A Review of Wind-Driven Rain Research in Building Science. *Journal of Wind Engineering and Industrial Aerodynamics,* 92(13), pp. 1079-1130.

Blocken, B. and Carmeliet, J., 2010. Overview of Three State-of-the-Art Wind-Driven Rain Assessment Models and Comparison Based on Model Theory. *Building and Environment,* 45(3), pp. 691-703.

Boardman, J., 2006. Soil Erosion Science: Reflections on the Limitations of Current Approaches. *Catena,* 68(2-3), pp. 73-86.

Böhner, J., Selige, T. and Ringeler, A., 2006. Image Segmentation Using Representativeness Analysis and Region Growing.

Borrelli, P., Robinson, D. A., Fleischer, L. R., Lugato, E., Ballabio, C., Alewell, C., Meusburger, K., Modugno, S., Schütt, B., Ferro, V., Bagarello, V., Oost, K. V., Montanarella, L. and Panagos, P., 2017. An Assessment of the Global Impact of 21st Century Land Use Change on Soil Erosion. *NATURE COMMUNICATIONS,* 8(1), pp. 2013.

Breetzke, G., 2004. *A Critique of Soil Erosion Modelling at a Catchment Scale Using Gis.* Master of Science, Vrije Universiteit, Amsterdam, Amsterdam.

Brodowski, R., 2013. Soil Detachment Caused by Divided Rain Power from Raindrop Parts Splashed Downward on a Sloping Surface. *Catena,* 105, pp. 52-61.

Bryan, R. B., 2000. Soil Erodibility and Processes of Water Erosion on Hillslope. *Geomorphology,* 32(3-4), pp. 385-415.

Burgess, T. and Webster, R., 1980. Optimal Interpolation and Isarithmic and Isarithmic Mapping of Soli Properties. *Soil Sci,* 31, pp. 315-341.

Caon, L. and Vargas, R., 2017. Threats to Soils: Global Trends and Perspectives. In *Global Land Outlook Working Paper* [Online]. Version.

Chakela, Q. and Stocking, M., 1988. An Improved Methodology for Erosion Hazard Mapping Part Ii: Application to Lesotho. *Geografiska Annaler. Series A. Physical Geography*, pp. 181-189.

Chaudhry, F. H., Andrade Filho, A. G. and Calheiros, R. V., 1996. Statistics on Tropical Convective Storms Observed by Radar. *Atmospheric research,* 42(1-4), pp. 217-227.

Choi, E., 2002. Modelling of Wind-Driven Rain and Its Soil Detachment Effect on Hill Slopes. *Journal of Wind Engineering and Industrial Aerodynamics,* 90(9), pp. 1081-1097.

De Roo, A., Offermans, R. and Cremers, N., 1996. Lisem: A Single-Event, Physically Based Hydrological and Soil Erosion Model for Drainage Basins. Ii: Sensitivity Analysis, Validation and Application. *Hydrological Processes,* 10(8), pp. 1119-1126.

De Villiers, M., Nell, J., Barnard, R. and Henning, A., 2003. Salt-Affected Soils: South Africa. *Food agricultural organization contract No. PR,* 26897.

Dedekind, Z., Engelbrecht, F. A. and Van der Merwe, J., 2016. Model Simulations of Rainfall over Southern Africa and Its Eastern Escarpment. *Water SA,* 42(1), pp. 129-143.

Derome, D., Kubilay, A., Defraeye, T., Blocken, B. and Carmeliet, J., 2017. Ten Questions Concerning Modeling of Wind-Driven Rain in the Built Environment. *Building and Environment,* 114, pp. 495-506.

Development Studies Associates (DSA) and Shawel Consult International (SCI), 2006. *Potential Survey, Identification of Opportunities and Preparations of Projects Profiles and Feasibility Studies*, Addis Ababa, Ethiopia: Development Studies Associates (DSA) and Shawel Consult International (SCI),.

Diodato, N., Knight, J. and Bellocchi, G., 2013. Reduced Complexity Model for Assessing Patterns of Rainfall Erosivity in Africa. *Global and Planetary Change,* 100, pp. 183-193.

Doran, M. P., Lennox, M. and Lewis, D., 2020. *Ucce Ranch Water Quality Planning: Instructor's Guide and Lesson Plan.*

Dotterweich, M., 2013. The History of Human-Induced Soil Erosion: Geomorphic Legacies, Early Descriptions and Research, and the Development of Soil Conservation - a Global Synopsis. *Geomorphology,* 201, pp. 1-34.

Du Preez, C. C., Van Huyssteen, C. W. and Mnkeni, P. N., 2011. Land Use and Soil Organic Matter in South Africa 2: A Review on the Influence of Arable Crop Production. *South African Journal of Science,* 107(5), pp. 1-8.

Dušan, Z., 2019. 'What Is a Good R-Squared Value?', *Statology*. Available at: https://www.statology.org/good-r-squared-value/ 2022].

Ebelhar, S. A., Chesworth, W., Paris, Q., Spaargaren, O. and Spaargaren, O., 2008. Lixisols. In Chesworth, W. (ed.) *Encyclopedia of Soil Science*. Dordrecht: Springer Netherlands, pp. 439-440.

Ebhuoma, O., Gebreslasie, M., Ngetar, N. S., Phinzi, K. and Bhattacharjee, S., 2022. Soil Erosion Vulnerability Mapping in Selected Rural Communities of Uthukela Catchment, South Africa, Using the Analytic Hierarchy Process. *Earth Systems and Environment*, pp. 1-14.

El Jazouli, A., Barakat, A., Ghafiri, A., El Moutaki, S., Ettaqy, A. and Khellouk, R., 2017. Soil Erosion Modeled with Usle, Gis, and Remote Sensing: A Case Study of Ikkour Watershed in Middle Atlas (Morocco). *Geoscience Letters,* 4(1), pp. 25.

Elwell, H. A., 1976. Soil Loss Estimator for Southern Africa. *Natal Agricultural Research Bulletin,* No. 7.

Elwell, H. A., 1978. *Soil Loss Estimation: Compiled Works of the Rhodesian Multidisciplinary Team on Soil Loss Estimation.* Salisbury: Institute of Agricultural Engineering.

Encyclopedia Britannica, 2016. Leptosol. In The Editors of Encyclopedia Britannica (ed.) *Encyclopedia Britannica, 6 June 2016*. Online: Encyclopedia Britannica Inc.

Encyclopedia Britannica, 2019. Erosion. In The Editors of Encyclopedia Britannica (ed.) *Encyclopedia Britannica, 20 October 2019*. Online: Encyclopedia Britannica Inc.

Erpul, G., 2013. Wind Driven Rain Erosion Processes, *College on soil Physics: 30th Anniversary (1983 -2013)*, Ankara University, Turkey. International Centre for Theoretical Physics, Ankara University, Turkey: International Centre for Theoretical Physics, Ankara University, Turkey.

Erpul, G., Gabriels, D. and Norton, L., 2005. Sand Detachment by Wind-Driven Raindrops. *Earth Surface Processes and Landforms: The Journal of the British Geomorphological Research Group,* 30(2), pp. 241-250.

Erpul, G., Gabriels, D., Norton, L., Flanagan, D., Huang, C.-F. and Visser, S., 2013. Mechanics of Interill Erosion Erosion with Wind-Driven Rain. *Earth Surface Process and Landforms,* 38, pp. 160-168.

Erpul, G., Norton, L. and Gabriels, D., 2002. Raindrop-Induced and Wind-Driven Soil Particle Transport. *Catena,* 47(3), pp. 227-243.

Erpul, G., Norton, L. and Gabriels, D., 2003. The Effect of Wind on Raindrop Impact and Rainsplash Detachment. *Transactions of the ASAE,* 46(1), pp. 51.

FAO, 2015a. *Soil Is a Non-Renewable Resource*, *2015 International Year of Soils*, Available: FAO. Available at: https://www.fao.org/3/i4373e/i4373e.pdf (Accessed 9 October 2022).

FAO, 2015b. *Soils Are Endangered, but the Degradation Can Be Rolled Back*, Available: FAO. Available at: https://www.fao.org/news/story/en/item/357059/icode/ (Accessed 02/09/2020).

FAO, 2019. *Soil Erosion: The Greatest Challenge to Sustainable Soil Management.* Rome, Italy: FAO.

FAO and ITPS, 2015. *Status of the World's Soil Resources (Swsr): Main Report.* Rome, Italy: Food and Agricultural Organisation of the United Nations and Intergovernmental Technical Panel on Soils.

Fernández-Raga, M., Campo, J., Rodrigo-Comino, J. and Keesstra, S. D., 2019. Comparative Analysis of Splash Erosion Devices for Rainfall Simulation Experiments: A Laboratory Study. *Water,* 11(6), pp. 1228.

Fister, W., Marzen, M., Iserloh, T., Seeger, M., Heckrath, G., Greenwood, P., Kuhn, N. J. and Ries, J. B., The Relevance of Wind-Driven Rain for Future Soil Erosion Research. *EGU General Assembly Conference Abstracts*.

Flanagan, D. and Nearing, M., 1995. Usda-Water Erosion Prediction Project: Hillslope Profile and Watershed Model Documentation. *Nserl Rep,* 10, pp. 1-123.

Food and Agiculture Organisation, 2015. *The Status of the World's Soil Resources (Main Report)*, Rome: Food and Agriculture Organization of the United Nations.

Food and Agriculture Organisation 2019. *Soil Erosion: The Greatest Challenge for Sustainable Soil Management Author Edition, Design & Publication. 2019*. Rome: Food and Agriculture Organisation.

Food and Agriculture Organization for the United Nations, 1998. *World Reference Base for Soil Resources No. 84*, Paris: Food and Agriculture Organisation (9251041415, 84).

Foord, S. H., Gelebe, V. and Prendini, L., 2015. Effects of Aspect and Altitude on Scorpion Diversity Along an Environmental Gradient in the Soutpansberg, South Africa. *Journal of Arid Environments,* 113, pp. 114-120.

Fortin, M.-J. and Dale, M. R., 2009. Spatial Autocorrelation. *The SAGE handbook of spatial analysis*, pp. 89-103.

Fosu-Mensah, B. Y. and Mensah, M., 2016. The Effect of Phosphorus and Nitrogen Fertilizers on Grain Yield, Nutrient Uptake and Use Efficiency of Two Maize (Zea Mays L.) Varieties under Rain Fed Condition on Haplic Lixisol in the Forest-Savannah Transition Zone of Ghana. *Environmental Systems Research,* 5(1), pp. 22.

Fox, N. I., 2004. The Representation of Rainfall Drop-Size Distribution and Kinetic Energy. *Hydrology and Earth System Sciences Discussions,* 8(5), pp. 1001-1007.

Frost, J., 2018. 'How High Does R-Squared Need to Be?', *Statistics by Jim*. Available at: https://statisticsbyjim.com/regression/how-high-r-squared/ 2022].

Fu, Y., Li, G., Wang, D., Zheng, T. and Yang, M., 2019. Raindrop Energy Impact on the Distribution Characteristics of Splash Aggregates of Cultivated Dark Loessial Cores. *Water,* 11(7), pp. 1514.

Gaberšek, S. and Durran, D. R., 2004. Gap Flows through Idealized Topography. Part I: Forcing by Large-Scale Winds in the Nonrotating Limit. *Journal of the atmospheric sciences,* 61(23), pp. 2846-2862.

Gabet, E. J. and Dunne, T., 2003. Sediment Detachment by Rain Power. *Water Resources Research,* 39(1), pp. ESG 1-1-ESG 1-12.

Garland, G., Hoffman, T. and Todd, S., 1999. Soil Degradation. In Hoffman, T., Todd, S., Ntshona, Z. & Turner, S. (eds.) *Land Degradation in South Africa*. Claremont, South Africa: National Botanical Institute, pp. 69–107.

Getis, A., 2010. Spatial Autocorrelation. *Handbook of Applied Spatial Analysis*: Springer, pp. 255-278.

Gibson, D. J., 2006. *Land Degradation in the Limpopo Province, South Africa.* Citeseer.

Gilau, A. N. P., 2015. *The Use of Erosion Models to Predict the Influence of Land Use Changes on Urban Impoundments.* Master of Science in Engineering, Witwatersrand University, Johannesburg.

Glen, S., 2015. 'Wilks: Simple Definition ', *StatisticsHowTo.com*. Available at: https://www.statisticshowto.com/wilks-lambda/.

Global Soil Partnership, 2016. *Global Soil Partnership Endorses Guidelines on Sustainable Soil Management*, *New study of topsoil loss in Malawi is example of tapping knowledge to enable change*, Available: Food and Agriculutural Organisation of the United Nations. Available at: http://www.fao.org/news/story/en/item/416121/icode/ (Accessed 19 August 2018).

Griffith, D. A., 1987. Spatial Autocorrelation. *A Primer (Washington, DC, Association of American Geographers)*.

Gu, Y., Han, C. and Wang, X., A Kriging Based Framework for Rapid Satellite-to-Site Visibility Determination. *2019 IEEE 10th International Conference on Mechanical and Aerospace Engineering (ICMAE)*: IEEE, 262-267.

Guo, J., Niu, T., Rahimy, P., Wang, F., Zhao, H. and Zhang, J., 2013. Assessment of Soil Erosion Susceptibility Using Empirical Modeling. *Acta Meteorologica Sinica,* 27(1), pp. 98-109.

Helming, K., Wind Speed Effects on Rain Erosivity. *Sustaining the global farm-Selected papers from the 10th International Soil Conservation Organization Meeting, held in*, 771-776.

Hengl, T., Heuvelink, G. B. and Stein, A., 2004. A Generic Framework for Spatial Prediction of Soil Variables Based on Regression-Kriging. *Geoderma,* 120(1-2), pp. 75-93.

Hens, H., 2010. Wind-Driven Rain: From Theory to Reality. *Proc. Thermal performance of the exterior envelopes of whole buildings XI, Clearwater, Florida*.

Hill, T., Scott-Shaw, B., Gillham, J., Dickey, M., Duncan, G., Everson, C., Everson, T., Zuma, K. and Birkett, C., 2019. Assessing the Impact of Erosion and Sediment Yield from Farming and Forestry Systems in Selected Catchments of South Africa. *WRC Report,* (TT788/19).

Hirschi, M. C. and Barfield, B. J., 1988. Kyermo—a Physically Based Research Erosion Model Part I. Model Development. *Transactions of the ASAE,* 31(3), pp. 804-0813.

Houshold, I. and Sharples, C., 2008. Geodiversity in the Wilderness: A Brief History of Geoconservation in Tasmania. *Geological Society, London, Special Publications,* 300(1), pp. 257-272.

Huggett, R., 2007. *Fundamentals of Geomorphology.* Routledge.

Hui-Ming, S. and Yang, C. T., 2009. Estimating Overland Flow Erosion Capacity Using Unit Stream Power. *International journal of sediment research,* 24(1), pp. 46-62.

Huler, S., 2007. *Defining the Wind: The Beaufort Scale and How a 19th-Century Admiral Turned Science into Poetry.* Crown.

Ighodaro, I. D., Lategan, F. S. and Yusuf, S. F., 2013. The Impact of Soil Erosion on Agricultural Potential and Performance of Sheshegu Community Farmers in the Eastern Cape of South Africa. *Journal of Agricultural Science,* 5(5), pp. 140.

Ikechukwu, M. N., Ebinne, E., Idorenyin, U. and Raphael, N. I., 2017. Accuracy Assessment and Comparative Analysis of Idw, Spline and Kriging in Spatial Interpolation of Landform (Topography): An Experimental Study. *Journal of Geographic Information System,* 9(03), pp. 354.

International Union of Soil Sciences Working Group, 2006. *World Reference Base for Soil Resources No. 103*, Rome: Food and Agriculture OrganisationNo. 103).

Irvem, A., Topaloğlu, F. and Uygur, V., 2007. Estimating Spatial Distribution of Soil Loss over Seyhan River Basin in Turkey. *Journal of Hydrology,* 336(1-2), pp. 30-37.

Iserloh, T., Fister, W., Marzen, M., Seeger, M., Kuhn, N. and Ries, J., 2013. The Role of Wind-Driven Rain for Soil Erosion–an Experimental Approach. *Zeitschrift für Geomorphologie, Supplementary Issues,* 57(1), pp. 193-201.

Jenks, G. F., 1967. The Data Model Concept in Statistical Mapping. *International yearbook of cartography,* 7, pp. 186-190.

Jenness, J., 2006. Topographic Position Index (Tpi) V. 1.2. *Flagstaff, AZ: Jenness Enterprises*.

Kabanda, T., 2003. *Climate*, Louis Trichardt, South Africa.

Kabanda, T., 2004. *Climatology of Long-Term Drought in the Nothern Region of the Limpopo Province of South Africa.* PhD, University of Venda, University of Venda: South Africa.

Kabanda, T. and Munyati, C., 2010. Anthropogenic-Induced Climate Change and the Resulting Tendency Towards Land Conflict: The Case of the Soutpansberg Region, South Africa. *Climate change and Natural Resources Conflicts in Africa. Monograph,* (170), pp. 139-155.

Kephe, P. N., Petja, B. M. and Kabanda, T. A., 2016. Spatial and Inter-Seasonal Behaviour of Rainfall in the Soutpansberg Region of South Africa as Attributed to the Changing Climate. *Theoretical and applied climatology,* 126(1-2), pp. 233-245.

Kheir, R. B., Abdallah, C. and Khawlie, M., 2008. Assessing Soil Erosion in Mediterranean Karst Landscapes of Lebanon Using Remote Sensing and Gis. *Engineering Geology,* 99(3-4), pp. 239-254.

Kinnel, P., 2016. Determining the Susceptibility of Soils Materials to Erosion by Rain Impacted Flows. *Soil Discuss,* 5, pp. 1-27.

Kinnell, P., 2005. Raindrop-Impact-Induced Erosion Processes and Prediction: A Review. *Hydrological Processes: An International Journal,* 19(14), pp. 2815-2844.

Kinnell, P., 2010. Event Soil Loss, Runoff and the Universal Soil Loss Equation Family of Models: A Review. *Journal of Hydrology,* 385(1-4), pp. 384-397.

Kirchhof, S., Krämer, M., Linden, J. and Richter, K., 2010. The Reptile Species Assemblage of the Soutpansberg (Limpopo Province, South Africa) and Its Characteristics. *Salamandra,* 46(3), pp. 147-166.

Kopecký, M., Macek, M. and Wild, J., 2021. Topographic Wetness Index Calculation Guidelines Based on Measured Soil Moisture and Plant Species Composition. *Science of the Total Environment,* 757, pp. 143785.

Kulikov, M., Schickhoff, U., GrÖNgrÖFt, A. and Borchardt, P., 2020. Modelling Soil Erodibility in Mountain Rangelands of Southern Kyrgyzstan. *Pedosphere,* 30(4), pp. 443-456.

Kumar, P., Singh, V. and Singh, A., 2018. Seabuckthorn (Hippophae Spp.) Conserve Plant Diversity in the Fragile Mountain Ecosystem of Cold Desert Himalaya. *Journal of Biodiversity,* 9(1-2), pp. 53-68.

Kundu, P., Mathivha, F. and Nkuna, T., 2015. *The Use of Gis and Remote Sensing Techniques to Evaluate the Impact of Land Use and Land Cover Change on the Hydrology of Luvuvhu River Catchment in Limpopo Province: Report to the Water Research Commission.* Water Research Commission Pretoria, South Africa.

Kusumandari, A., 2014. Soil Erodibility of Several Types of Green Open Space Areas in Yogyakarta City, Indonesia. *Procedia Environmental Sciences,* 20, pp. 732-736.

Laker, M., 2004. Advances in Soil Erosion, Soil Conservation, Land Suitability Evaluation and Land Use Planning Research in South Africa, 1978-2003. *South African Journal of Plant and Soil,* 21(5), pp. 345-368.

Lal, R., 1990. *Soil Erosion in the Tropics: Principles and Management.* McGraw-Hill Inc.

Lal, R., 1994. *Soil Erosion Research Methods.* CRC Press.

Lal, R., 2001. Soil Degradation by Erosion. *Land degradation & development,* 12(6), pp. 519-539.

Lal, R., 2015. Restoring Soil Quality to Mitigate Soil Degradation. *Sustainability,* 7(5), pp. 5875-5895.

Lal, R. and Elliot, W., 2017. Erodibility and Erosivity. *Soil Erosion Research Methods*: Routledge, pp. 181-210.

Larson, W. E., 1981. Protecting the Soil Resource Base. *Journal of Soil and Water Conservation,* 36(1), pp. 13-16.

Laws, J. O. and Parsons, D. A., 1943. The Relation of Raindrop-Size to Intensity. *Eos, Transactions American Geophysical Union,* 24(2), pp. 452-460.

Le Roux, J., 2011. Monitoring Soil Erosion in South Africa at a Regional Scale. *Agricultural Research Council-Institute for Soil, Climate and Water, Pretoria*.

Le Roux, J., 2012. *Water Erosion Risk Assessment in South Africa: Towards a Methodological Framework.* University of Pretoria.

Le Roux, J., Newby, T. and Sumner, P., 2007. Monitoring Soil Erosion in South Africa at a Regional Scale: Review and Recommendations: Saeon Review. *South African Journal of Science,* 103(7), pp. 329-335.

Le Roux, J. and Smith, H., 2014. *Soil Erosion in South Africa - Its Nature and Distribution*, Available: Grain SA. Available at: https://www.grainsa.co.za/soil-erosion-in-south-africa---its-nature-and-distribution (Accessed 30 September 2018).

le Roux, J. and van der Waal, B., 2020. Gully Erosion Susceptibility Modelling to Support Avoided Degradation Planning. *South African Geographical Journal,* 102(3), pp. 406-420.

Li, L., Du, S., Wu, L. and Liu, G., 2009. An Overview of Soil Loss Tolerance. *Catena,* 78(2), pp. 93-99.

Li, P., Mu, X., Holden, J., Wu, Y., Irvine, B., Wang, F., Gao, P., Zhao, G. and Sun, W., 2017. Comparison of Soil Erosion Models Used to Study the Chinese Loess Plateau. *Earth-Science Reviews,* 170, pp. 17-30.

Lima, C. A. d., Palácio, H. A. d. Q., Andrade, E. M. d., dos Santos, J. C. and Brasil, P. P., 2013. Characteristics of Rainfall and Erosion under Natural Conditions of Land Use in Semiarid Regions. *Revista Brasileira de Engenharia Agrícola e Ambiental,* 17(11), pp. 1222-1229.

Lobo, G. P. and Bonilla, C. A., 2015. Sensitivity Analysis of Kinetic Energy-Intensity Relationships and Maximum Rainfall Intensities on Rainfall Erosivity Using a Long-Term Precipitation Dataset. *Journal of Hydrology,* 527, pp. 788-793.

Lorentz, S. and Schulze, R., 1995. Sediment Yield. *Hydrology and agrohydrology: a text to accompany the ACRU,* 3.

Lu, J., Zheng, F., Li, G., Bian, F. and An, J., 2016. The Effects of Raindrop Impact and Runoff Detachment on Hillslope Soil Erosion and Soil Aggregate Loss in the Mollisol Region of Northeast China. *Soil and Tillage Research,* 161, pp. 79-85.

Lund, A. and Lund, M., 2018. 'One-Way Manova in Spss Statistics', *Laerd Statistics*. Available at: https://statistics.laerd.com/spss-tutorials/one-way-manova-using-spss-statistics-2.php 2021].

Lyles, L., 1977. Soil Detachment and Aggregate Disintegration by Wind-Driven Rain. *SCSA Special Publ,* 21, pp. 152-159.

Lyles, L. and Allison, B. E., 1976. Wind Erosion: The Protective Role of Simulated Standing Stubble. *Transactions of the ASAE,* 19(1), pp. 61-0064.

Makaya, N., 2018. *Remote Sensing of Gully Erosion in the Communal Lands of Okhombe Valley, Drakensberg, South Africa.*

Makaya, N., Dube, T., Seutloali, K., Shoko, C., Mutanga, O. and Masocha, M., 2019. Geospatial Assessment of Soil Erosion Vulnerability in the Upper Umgeni Catchment in Kwazulu Natal, South Africa. *Physics and Chemistry of the Earth, Parts A/B/C,* 112, pp. 50-57.

Malibe, G., 2015. *The Use of Remote Sensing and Gis in Assessing the Impact of Land Use Change on Soil Erosion of Mhlathuze Catchment, South Africa.* Master of Integrated Water Resources Management, Dar es Salaam, Dar es Salaam, Tanzania [Online] Available at: https://www.academia.edu/79012380/THE_USE_OF_REMOTE_SENSING_AND_GIS_IN_ASSESSING_THE_IMPACT_OF_LAND_USE_CHANGE_ON_S

OIL_EROSION_OF_MHLATHUZE_CATCHMENT_SOUTH_AFRICA (Accessed.

Mararakanye, N. and Sumner, P. D., 2017. Gully Erosion: A Comparison of Contributing Factors in Two Catchments in South Africa. *Geomorphology,* 288, pp. 99-110.

Marques, V. S., Ceddia, M. B., Antunes, M. A., Carvalho, D. F., Anache, J. A., Rodrigues, D. B. and Oliveira, P. T. S., 2019. Usle K-Factor Method Selection for a Tropical Catchment. *Sustainability,* 11(7), pp. 1840.

Márquez, A. M., Guevara, E. and Rey, D., 2019. Hybrid Model for Forecasting of Changes in Land Use and Land Cover Using Satellite Techniques. *IEEE Journal of Selected Topics in Applied Earth Observations and Remote Sensing,* 12(1), pp. 252-273.

Martius, O., Pfahl, S. and Chevalier, C., 2016. A Global Quantification of Compound Precipitation and Wind Extremes. *Geophysical Research Letters,* 43(14), pp. 7709-7717.

Marzen, M., 2017. *Wind-Driven Rain: A New Challenge for Soil Erosion Research Wind-Beeinflusster Regen: Eine Neue Herausforderung Für Die Bodenerosionsforschung.* Doctor of Science, The University of Trier, Germany The University of Trier, Germany

Marzen, M., Iserloh, T., Casper, M. C. and Ries, J. B., 2015. Quantification of Particle Detachment by Rain Splash and Wind-Driven Rain Splash. *Catena,* 127, pp. 135-141.

Marzen, M., Iserloh, T., De Lima, J. L. M. P., Fister, W. and Ries, J. B., 2017. Impact of Severe Rain Storms on Soil Erosion: Experimental Evaluation of Wind-Driven Rain and Its Implications for Natural Hazard Management. *Science of the Total Environment,* 590-591, pp. 502-513.

Mathew, S., 2006. *Wind Energy: Fundamentals, Resource Analysis and Economics.* Springer.

Mathews, S., 2018. *Interpreting Regression Output - without All the Statistics Theory.* Online: GraduateTutor.com.

Mattivi, P., Franci, F., Lambertini, A. and Bitelli, G., 2019. Twi Computation: A Comparison of Different Open Source Giss. *Open Geospatial Data, Software and Standards,* 4(1), pp. 1-12.

Meghraoui, M., Habi, M., Morsli, B., Regagba, M. and Seladji, A., 2017. Mapping of Soil Erodibility and Assessment of Soil Losses Using the Rusle Model in the Sebaa Chioukh Mountains (Northwest of Algeria). *Journal of water and land development,* 34(1), pp. 205.

Melelli, L., Vergari, F., Liucci, L. and Del Monte, M., 2017. Geomorphodiversity Index: Quantifying the Diversity of Landforms and Physical Landscape. *Science of the Total Environment,* 584, pp. 701-714.

Mestdagh, M., Pe, M., Pestman, W., Verdonck, S., Kuppens, P. and Tuerlinckx, F., 2018. Sidelining the Mean: The Relative Variability Index as a Generic Mean-Corrected Variability Measure for Bounded Variables. *Psychological Methods,* 23(4), pp. 690.

Mhangara, P., Kakembo, V. and Lim, K. J., 2012. Soil Erosion Risk Assessment of the Keiskamma Catchment, South Africa Using Gis and Remote Sensing. *Environmental Earth Sciences,* 65(7), pp. 2087-2102.

Mitasova, H., Barton, C. M., Ullah, I., Hofierka, J. and Harmon, R., 2013. Gis-Based Soil Erosion Modeling. *Remote Sensing and Giscience in Geomorphology*: Elsevier Inc., pp. 228-258.

Montero-Martínez, G. and García-García, F., 2016. On the Behaviour of Raindrop Fall Speed Due to Wind. *Quarterly Journal of the Royal Meteorological Society,* 142(698), pp. 2013-2020.

Moore, I. D., Gessler, P. E., Nielsen, G. and Peterson, G., 1993. Soil Attribute Prediction Using Terrain Analysis. *Soil science society of america journal,* 57(2), pp. 443-452.

Morales, J. M., Baringo, L., Conejo, A. J. and Mínguez, R., 2010. Probabilistic Power Flow with Correlated Wind Sources. *IET generation, transmission & distribution,* 4(5), pp. 641-651.

Morgan, R., 1981. Field Measurement of Splash Erosion. *IAHS PUBLICATION,* 133, pp. 373-382.

Morgan, R., 1995. *Soil Erosion and Conservation.* London: Longman.

Morgan, R., 2009. *Soil Erosion and Conservation.* John Wiley & Sons.

Morgan, R., Quinton, J., Smith, R., Govers, G., Poesen, J., Auerswald, K., Chisci, G., Torri, D. and Styczen, M., 1998. The European Soil Erosion Model (Eurosem): A Dynamic Approach for Predicting Sediment Transport from Fields and Small Catchments. *Earth Surface Processes and Landforms: The Journal of the British Geomorphological Group,* 23(6), pp. 527-544.

Mostert, T. H. C., 2006. *Vegetation Ecology of the Soutpansberg and Blouberg Area in the Limpopo Province.* University of Pretoria.

Mousazadeh, F. and Salleh, K. O., 2014. Factors Controlling Gully Erosion Development in Toroud Basin–Iran. *Procedia-Social and Behavioral Sciences,* 120, pp. 506-512.

Mughogho, M. T., 1998. *Evaluation of the Revised Universal Soil Loss Equation (Rusle) and the Soil Loss Estimation Model for Southern Africa (Slemsa) under Malawi Conditions: A Case Study of Kamundi Catchment near Mangochi*: University of Malawi.

Muller, C., Yang, D., Craig, G., Cronin, T., Fildier, B., Haerter, J. O., Hohenegger, C., Mapes, B., Randall, D. and Shamekh, S., 2022. Spontaneous Aggregation of Convective Storms. *Annual Review of Fluid Mechanics,* 54, pp. 133-157.

Najwer, A. and Zwoliński, Z., 2014. The Landform Geodiversity Assessment Method–a Comparative Analysis for Polish and Swiss Mountainous Landscape. *IGU 2014 Book of Abstracts,* 1201.

Nciizah, A. D. and Wakindiki, I. I. C., 2015. Physical Indicators of Soil Erosion, Aggregate Stability and Erodibility. *Archives of Agronomy and Soil Science,* 61(6), pp. 827-842.

Nearing, M. A., Foster, G. R., Lane, L. and Finkner, S., 1989. A Process-Based Soil Erosion Model for Usda-Water Erosion Prediction Project Technology. *Transactions of the ASAE,* 32(5), pp. 1587-1593.

Nearing, M. A., Xie, Y., Liu, B. and Ye, Y., 2017. Natural and Anthropogenic Rates of Soil Erosion. *International Soil and Water Conservation Research,* 5(2), pp. 77-84.

Nenwiini, S. and Kabanda, T., 2013. Trends and Variability Assessment of Rainfall in Vhembe South Africa. *J Hum Ecol,* 42(2), pp. 171-176.

O'geen, A. T., 2006. *Erodibility of Agricultural Soils, with Examples in Lake and Mendocino Counties.* UCANR Publications.

Oettli, P. and Camberlin, P., 2005. Influence of Topography on Monthly Rainfall Distribution over East Africa. *Climate Research,* 28(3), pp. 199-212.

Ospina, R. and Marmolejo-Ramos, F., 2019. Performance of Some Estimators of Relative Variability. *Frontiers in Applied Mathematics and Statistics,* 5, pp. 43.

Overton, G. E., 2013. *An Analysis of Wind-Driven Rain in New Zealand.* BRANZ.

Pachauri, A. K., 2009. Terrain Analysis for Landslide Hazard Zonation (Lhz). *IUP Journal of Earth Sciences,* 3(4), pp. 7-35.

Pallant, J., 2016. *A Step by Step Guide to Data Analysis Usinf Ibm Spss. Spss Survival Manual.* 6 edn. Berkshire, England: McGraw Hill Education.

Panagos, P., Ballabio, C., Borrelli, P., Meusburger, K., Klik, A., Rousseva, S., Tadić, M. P., Michaelides, S., Hrabalíková, M. and Olsen, P., 2015. Rainfall Erosivity in Europe. *Science of the Total Environment,* 511, pp. 801-814.

Paramasivam, C. and Venkatramanan, S., 2019. An Introduction to Various Spatial Analysis Techniques. *GIS and geostatistical techniques for groundwater science*, pp. 23-30.

Parwada, C. and Van Tol, J., 2016. The Nature of Soil Erosion and Possible Conservation Strategies in Ntabelanga Area, Eastern Cape Province, South Africa. *Acta Agriculturae Scandinavica, Section B—Soil & Plant Science,* 66(6), pp. 544-552.

Parwada, C. and van Tol, J., 2020. Mapping Soil Erosion Sensitive Areas in Organic Matter Amended Soil Associations in the Ntabelanga Area, Eastern Cape Province, South Africa. *Journal of Applied Sciences and Environmental Management,* 24(9), pp. 1693-1702.

Peattie, R., 2013. *Mountain Geography-a Critique and Field Study.* Read Books Ltd.

Pedersen, H. S. and Hasholt, B., 1995. Influence of Wind Speed on Rainsplash Erosion. *Catena,* 24, pp. 39-54.

Pennock, D. J., Zebarth, B. and De Jong, E., 1987. Landform Classification and Soil Distribution in Hummocky Terrain, Saskatchewan, Canada. *Geoderma,* 40(3), pp. 297-315.

Petrů, J. and Kalibová, J., 2018. Measurement and Computation of Kinetic Energy of Simulated Rainfall in Comparison with Natural Rainfall. *Soil and Water Research,* 13(4), pp. 226-233.

Phinzi, K., Ngetar, N. S. and Ebhuoma, O., 2021. Soil Erosion Risk Assessment in the Umzintlava Catchment (T32e), Eastern Cape, South Africa, Using Rusle and Random Forest Algorithm. *South African Geographical Journal,* 103(2), pp. 139-162.

Poesen, J., 2018. Soil Erosion in the Anthropocene: Research Needs. *Earth Surface Processes and Landforms,* 43(1), pp. 64-84.

Rapolaki, R. S., Blamey, R. C., Hermes, J. C. and Reason, C. J., 2019. A Classification of Synoptic Weather Patterns Linked to Extreme Rainfall over the Limpopo River Basin in Southern Africa. *Climate Dynamics,* 53(3), pp. 2265-2279.

Reis, J., Fister, W., Iserloh, T. and Marzen, M., 2010. Wind-Driven Rain as a New Challenge for in-Situ Rainfall Simulation Experiments. *Geophysics Research Abstracts,* 12.

Renard, K. G., Foster, G. R., Weesies, G. A., McCool, D. K. and Yoder, D. C., 1997. *Predicting Soil Erosion by Water: A Guide to Conservation Planning with the Revised Universal Soil Loss Equation (Rusle). Agriculture Handbook*: U.S. Department of Agriculture.

Rickson, R., 2014. Can Control of Soil Erosion Mitigate Water Pollution by Sediments? *Science of the Total Environment,* 468, pp. 1187-1197.

Ries, J. B., Fister, W., Iserloh, T. and Marzen, M., Wind Driven Rain as a New Challenge for in Situ Rainfall Simulation Experiments. *EGU General Assembly Conference Abstracts*, 2747.

Ritter, J., 2012. *Soil Erosion - Causes and Effects.* Online: Ontario Ministry of Agriculture, Food and Rural Affairs (OMAFRA).

Rodrigues, C. V., Palma, J. M. L. M. and Rodrigues, Á. H., 2016. Atmospheric Flow over a Mountainous Region by a One-Way Coupled Approach Based on Reynolds-Averaged Turbulence Modelling. *Boundary-Layer Meteorol,* 159, pp. 407-437.

Rudra, R., Dickinson, W., Clark, D. and Wall, G., 1986. Games—a Screening Model of Soil Erosion and Fluvial Sedimentation on Agricultural Watershed. *Canadian Water Resources Journal,* 11(4), pp. 58-71.

Saaty, T. L., 2000. *Fundamentals of Decision Making and Priority Theory with the Analytic Hierarchy Process.* RWS publications.

Salles, C., Poesen, J. and Sempere-Torres, D., 2002. Kinetic Energy of Rain and Its Functional Relationship with Intensity. *Journal of Hydrology,* 257(1-4), pp. 256-270.

Scheper, S., Weninger, T., Kitzler, B., Lackóová, L., Cornelis, W., Strauss, P. and Michel, K., 2021. Comparison of the Spatial Wind Erosion Patterns of Erosion Risk Mapping and Quantitative Modeling in Eastern Austria. *Land,* 10(9), pp. 974.

Schmidt, J., Werner, M. and Michael, A., 1999. Application of the Erosion 3d Model to the Catsop Watershed, the Netherlands. *Catena,* 37(3-4), pp. 449-456.

Schönbrodt-Stitt, S., Bosch, A., Behrens, T., Hartmann, H., Shi, X. and Scholten, T., 2013. Approximation and Spatial Regionalization of Rainfall Erosivity Based on Sparse Data in a Mountainous Catchment of the Yangtze River in Central China. *Environmental Science and Pollution Research,* 20(10), pp. 6917-6933.

Sepuru, T. K., 2018. *Assessing the Use of Multispectra Remote Sensing in Mapping the Spatio-Temporal Variations of Soil Erosion in Sekhukhune District, South Africa.*

Seutloali, K. E., Dube, T. and Mutanga, O., 2017. Assessing and Mapping the Severity of Soil Erosion Using the 30-M Landsat Multispectral Satellite Data in the Former South African Homelands of Transkei. *Physics and Chemistry of the Earth, Parts A/B/C,* 100, pp. 296-304.

Shahabi, H., Salari, M., Ahmad, B. B. and Mohammadi, A., 2016. Soil Erosion Hazard Mapping in Central Zab Basin Using Epm Model in Gis Environment. *International Journal of Geography and Geology,* 5(11), pp. 224-235.

Skidmore, E., 1982. Soil Loss Tolerance. *Determinants of soil loss tolerance,* 45, pp. 87-93.

Smith, R. B., 2007. Interacting Mountain Waves and Boundary Layers. *Journal of the atmospheric sciences,* 64(2), pp. 594-607.

Sobel, A. H., 2012. Tropical Weather. *Nature Education Knowledge,* 3 (12)(2).

Sörensen, R., Zinko, U. and Seibert, J., 2006. On the Calculation of the Topographic Wetness Index: Evaluation of Different Methods Based on Field Observations. *Hydrology and Earth System Sciences,* 10(1), pp. 101-112.

Spaargaren, O. and Decker, J., 1995. *The Woreference Base for Soil Resources: An Introduction with Special Reference to Soils of Tropical Forests Ecosystems*, The Netherlands: Internation Soil Reference and Information Centre95/14).

Stanchi, S., Falsone, G. and Bonifacio, E., 2015. Soil Aggregation, Erodibility, and Erosion Rates in Mountain Soils (Nw Alps, Italy). *Solid Earth,* 6(2), pp. 403-414.

Stanchi, S., Freppaz, M., Godone, D. and Zanini, E., 2013. Assessing the Susceptibility of Alpine Soils to Erosion Using Soil Physical and Site Indicators. *Soil Use and Management,* 29(4), pp. 586-596.

Stocking, M., 1980. Soil Loss Estimation for Rural Development: A Position for Geomorphology. *Geomorphology,* 36, pp. 264-273.

Stocking, M., Chakela, Q. and Elwell, H., 1988. An Improved Methodology for Erosion Hazard Mapping Part I: The Technique. *Geografiska Annaler. Series A. Physical Geography*, pp. 169-180.

Stoelinga, M. T., Stewart, R. E., Thompson, G. and Thériault, J. M., 2013. Microphysical Processes within Winter Orographic Cloud and Precipitation Systems. *Mountain Weather Research and Forecasting*. Amsterdam: Springer, pp. 345-408.

Stone, R. P. and Hibron, D., MINISTRY OF AGRICULTURE, FOOD AND RURAL AFFAIRS, 2012. *Universal Soil Loss Equation (Usle) Fact Sheet.* Online: MINISTRY OF AGRICULTURE, FOOD AND RURAL AFFAIRS,.

Stroosnijder, L., 2004. Measurement Options for Water and Wind Erosion. In Visser, S. M. & Cornelis, W. (eds.) *Wind and Rain Interaction in Erosion: Vol. 50 Tropical Resource Management Papers*. The Netherlands: Wageningen UR, pp. 183-193.

Stroosnijder, L. and Gabriels, D., 2004a. Future Work on Wind and Water Interaction in Erosion Models. In Visser, S. M. & Cornells, W. M. (eds.) *Wind and Rain Interaction in Erosion: Vol. 50 Tropical Resource Management Papers*. The Netherlands: Wageningen UR, pp. 226.

Stroosnijder, L. and Gabriels, D., 2004b. Introduction. In Visser, S. M. & Cornells, W. M. (eds.) *Wind and Rain Interaction in Erosion Tropical Resource Management Papers, No. 50*. Wageningen, The Netherlands: Wageningen UR, pp. 9-14.

Stroosnijder, L. and Gabriels, D., 2004c. Introduction. In Visser, S. M. & Cornelis, W. (eds.) *Wind and Rain Interaction in Erosion: Vol. 50 Tropical Resource Managenet Papers*. The Netherlands: Wageningen UR.

Sun, W.-Y. and Sun, O. M., 2015. Bernoulli Equation and Flow over a Mountain. *Geoscience Letters,* 2(1), pp. 7.

Tadayon, V. and Rasekh, A., 2019. Non-Gaussian Covariate-Dependent Spatial Measurement Error Model for Analyzing Big Spatial Data. *Journal of Agricultural, Biological and Environmental Statistics,* 24(1), pp. 49-72.

Torres, D. S., Creutin, D., Salles, C. and Delrieu, G., 1992. Quantification of Soil Detachment by Raindrop Impact: Performance of Classical Formulae of Kinetic Energy in Mediterranean Storms. *IAHS Publ,* (210), pp. 115-124.

Torri, D. and Poesen, J., 2014. A Review of Topographic Threshold Conditions for Gully Head Development in Different Environments. *Earth-Science Reviews,* 130, pp. 73-85.

Toy, T. J., Foster, G. R. and Renard, K. G., 2002. *Soil Erosion: Processes, Prediction, Measurement, and Control.* John Wiley & Sons.

Tse-ring, K., Sharma, E., Chettri, N. and Shrestha, A. B., 2010. *Climate Change Vulnerability of Mountain Ecosystems in the Eastern Himalayas*: International centre for integrated mountain development (ICIMOD).

Ulbrich, C. W., 1983. Natural Variations in the Analytical Form of the Raindrop Size Distribution. *Journal of climate and applied meteorology,* 22(10), pp. 1764-1775.

Underwood, J. S. and Meentemeyer, V., 1998. Climatology of Wind-Driven Rain for the Contiguous United States for the Period 1971 to 1995. *Physical Geography,* 19(6), pp. 445-462.

Uzun, O., Kaplan, S., Basaran, M., Deviren Saygın, S., Youssef, F., Nouri, A., Ozcan, A. U. and Erpul, G., 2017. Spatial Distribution of Wind-Driven Sediment Transport Rate in a Fallow Plot in Central Anatolia, Turkey. *Arid land research and management,* 31(2), pp. 125-139.

Van Dijk, A., Bruijnzeel, L. and Rosewell, C., 2002. Rainfall Intensity–Kinetic Energy Relationships: A Critical Literature Appraisal. *Journal of Hydrology,* 261(1-4), pp. 1-23.

Vantas, K., Sidiropoulos, E. and Evangelides, C., 2019. Rainfall Erosivity and Its Estimation: Conventional and Machine Learning Methods. *Soil Erosion-Rainfall Erosivity and Risk Assessment*: IntechOpen.

Verdugo-Vásquez, N., Acevedo-Opazo, C., Valdés-Gómez, H., Araya-Alman, M., Ingram, B., de Cortázar-Atauri, I. G. and Tisseyre, B., 2016. Spatial Variability of Phenology in Two Irrigated Grapevine Cultivar Growing under Semi-Arid Conditions. *Precision Agriculture,* 17(2), pp. 218-245.

Vetter, S., 2013. Development and Sustainable Management of Rangeland Commons–Aligning Policy with the Realities of South Africa's Rural Landscape. *African journal of range & forage science,* 30(1-2), pp. 1-9.

Visser, S. M. and Cornelis, W., 2004. Wind and Rain Interaction in Erosion.

Wang, B., Zheng, F., Römkens, M. J. and Darboux, F., 2013. Soil Erodibility for Water Erosion: A Perspective and Chinese Experiences. *Geomorphology,* 187, pp. 1-10.

Wei, L., Zhang, B. and Wang, M., 2007. Effects of Antecedent Soil Moisture on Runoff and Soil Erosion in Alley Cropping Systems. *Agricultural Water Management,* 94(1-3), pp. 54-62.

Williams, J., 1989. Epic: The Erosion-Productivity Impact Calculator.

Wischmeier, W. and Smith, D., 1958. Rainfall Energy and Its Relationship to Soil Loss. *Eos, Transactions American Geophysical Union,* 39(2), pp. 285-291.

Wischmeier, W. and Smith, D., 1978. *Predicting Rainfall Erosion Losses - a Guide to Conservation Planning. Agriculture Handbook* USA: Sciences and Education Administration, Agricultural Research: USDA.

Wischmeier, W., Smith, D. and Uhland, R., 1958. Evaluation of Factors in the Soil Loss Equation. *Agricultural Engineering,* 39(8), pp. 458-462.

WMO, 2008. Guide to Hydrological Practices. Volume I: Hydrology—from Measurement to Hydrological Information. *WMO Report No. 168*, pp. 296.

WMO, 2021. *Measurement of Meteorological Variables*, Geneva: WMO (8.

Wu, X., Yuan, T., Qie, K. and Luo, J., 2020. Geographical Distribution of Extreme Deep and Intense Convective Storms on Earth. *Atmospheric research,* 235, pp. 104789.

WWF, 2010a. *Agriculture: Facts & Trends South Africa.* Online: World Wildlife Fund (WWF).

WWF, 2010b. *Agriculture: Facts & Trends South Africa.* Pretoria: WWF South Africa,.

Xanthakis, M. and Pavlopoulos, A., 2009. Soil Erosion. In Evelpidou, N. & de Figueiredo, T. (eds.) *Soil Protection in Sloping Mediterranean Agri-Environments: Lectures and Exercises*. Intituto Politecnic de Braganca, Portugal: Intituto Politecnic de Braganca, Portugal, pp. 45.

Yang, D., 1998. Accuracy of Nws 8 Standard Non-Recording Precipitation Gauge: Results and Application of Wmo Intercomparison. *Journal of Atmospheric and Oceanic Technology,* 15, pp. 54-68.

Yang, X. and Yu, B., 2015. Modelling and Mapping Rainfall Erosivity in New South Wales, Australia. *Soil Research,* 53(2), pp. 178-189.

Yao, X., Yu, J., Jiang, H., Sun, W. and Li, Z., 2016. Roles of Soil Erodibility, Rainfall Erosivity and Land Use in Affecting Soil Erosion at the Basin Scale. *Agricultural Water Management,* 174, pp. 82-92.

Zachar, D., 1982. Soil Erosion: Developments in Soil Science. *New York. Elsivier Scientific. 547p*.

Zardi, D. and Whiteman, C. D., 2013. Diurnal Mountain Wind Systems In Chow, F. K., Wekker, S. F. J. D. & Snyder, B. J. (eds.) *Mountain Weather Research and Forecasting: Recent Progress and Current Challenges*. New York: Springer.

Zeng, C., Wang, S., Bai, X., Li, Y., Tian, Y., Li, Y., Wu, L. and Luo, G., 2017. Soil Erosion Evolution and Spatial Correlation Analysis in a Typical Karst Geomorphology Using Rusle with Gis. *Solid Earth,* 8(4), pp. 721-736.

Zhang, J. and Han, D., 2017. Assessment of Rainfall Spatial Variability and Its Influence on Runoff Modelling: A Case Study in the Brue Catchment, Uk. *Hydrological Processes,* 31(16), pp. 2972-2981.

Zhang, J., Han, D., Song, Y. and Dai, Q., 2018. Study on the Effect of Rainfall Spatial Variability on Runoff Modelling. *Journal of Hydroinformatics,* 20(3), pp. 577-587.

Zhu, B., Zhou, Z. and Li, Z., 2021. Soil Erosion and Controls in the Slope-Gully System of the Loess Plateau of China: A Review. *Frontiers in Environmental Science,* 9, pp. 136.

Zorn, M. and Komac, B., 2013. Erosivity. In Bobrowsky, P. T. (ed.) *Encyclopedia of Natural Hazards*. Dordrecht: Springer Netherlands, pp. 289-290.

Zwoliński, Z., 2004. Geodiversity. In Goudie, A. (ed.) *Encyclopedia of Geomorphology*. London and New York: Routledge.

Zwoliński, Z., Giardino, M. and Najwer, A., 2019. *Geodiversity in Mountain Areas*. Krakow-Zakopane, Poland: Publisher.